


2018

# Smart materials for heated concrete pavement systems

Alireza Sassani  
Iowa State University

Follow this and additional works at: <https://lib.dr.iastate.edu/etd>

 Part of the [Civil Engineering Commons](#), [Materials Science and Engineering Commons](#), [Mechanics of Materials Commons](#), and the [Transportation Commons](#)

## Recommended Citation

Sassani, Alireza, "Smart materials for heated concrete pavement systems" (2018). *Graduate Theses and Dissertations*. 17308.  
<https://lib.dr.iastate.edu/etd/17308>

This Dissertation is brought to you for free and open access by the Iowa State University Capstones, Theses and Dissertations at Iowa State University Digital Repository. It has been accepted for inclusion in Graduate Theses and Dissertations by an authorized administrator of Iowa State University Digital Repository. For more information, please contact [digirep@iastate.edu](mailto:digirep@iastate.edu).

**Smart materials for heated concrete pavement systems**

by

**Alireza Sassani**

A dissertation submitted to the graduate faculty  
in partial fulfillment of the requirements for the degree of

**DOCTOR OF PHILOSOPHY**

Major: Civil Engineering (Civil Engineering Materials)

Program of Study Committee:

Halil Ceylan, Co-major Professor  
Peter C. Taylor, Co-major Professor  
Kasthurirangan Gopalakrishnan  
Sunghwan Kim  
Paul Spry  
Mani Mina

The student author, whose presentation of the scholarship herein was approved by the program of study committee, is solely responsible for the content of this dissertation. The Graduate College will ensure this dissertation is globally accessible and will not permit alterations after a degree is conferred.

Iowa State University

Ames, Iowa

2018

Copyright © Alireza Sassani, 2018. All rights reserved.

**DEDICATION**

I dedicate this dissertation to my lovely wife and best friend *Shadi* who gives me my first billion reasons to live. To my parents who have been through a lot to help me come this far. To my sister and brothers who always make me feel special. To my niece and nephews who are the greatest beauty of this world to me. And to the ever-loving memory of my father-in-law, the most virtuous man I can ever know and is so dearly missed; may his smile shine to all eternity in our hearts and in heaven.

## TABLE OF CONTENTS

|  | Page |
|--|------|
| LIST OF FIGURES .....  | vi   |
| LIST OF TABLES .....   | ix   |
| ACKNOWLEDGMENTS .....  | xi   |
| ABSTRACT .....   | xiii |
| CHAPTER 1. INTRODUCTION .....  | 1    |
| Background.....  | 1    |
| Objective.....   | 4    |
| Dissertation Organization .....  | 5    |
| CHAPTER 2. LITERATURE REVIEW .....   | 8    |
| Smart Materials and Their Application in Civil Engineering Systems .....   | 8    |
| Background .....   | 8    |
| Application in Civil Engineering Systems .....   | 9    |
| Review on Electrically Conductive Portland Cement Concrete Heated Pavement<br>Systems .....  | 12   |
| Applications of Electrically Conductive Portland Cement concrete.....  | 12   |
| Electrical Properties of Plain Portland Cement-based Concrete .....  | 12   |
| ECON: materials, properties, and methods of production .....   | 14   |
| Applications and Methods of Measuring the Electrical Properties of Concrete ....   | 20   |
| Significance of Study on ECON HPS .....  | 23   |
| Literature Review on Electrically Conductive Coating (ECOT) Heated Pavement<br>systems.....  | 24   |
| CHAPTER 3. INFLUENCE OF MIX DESIGN VARIABLES ON ENGINEERING<br>PROPERTIES OF CARBON FIBER-MODIFIED ELECTRICALLY<br>CONDUCTIVE CONCRETE ..... | 30   |
| Abstract.....  | 30   |
| Introduction .....   | 31   |
| Methodology and Materials.....   | 35   |
| Mix Design Variables.....  | 35   |
| Mixture Components.....  | 38   |
| Sample Preparation and Electrical Resistivity Measurement.....   | 40   |
| Data Analysis .....  | 42   |
| Results and Discussion .....   | 43   |
| Effect of Variables on ECON Electrical Resistivity .....   | 46   |
| ECON Electrical Resistivity Response Prediction.....   | 47   |
| Sensitivity Assessment of Variables for ECON Electrical Resistivity<br>Response.....   | 49   |
| Effect of Variables on ECON Strength Properties .....  | 53   |

|  |            |
|--|------------|
| ECON Strength Response Prediction.....   | 54         |
| Sensitivity Assessment of Variables for ECON Strength Property Responses.....  | 55         |
| Discussion .....   | 60         |
| Conclusions .....  | 61         |
| Acknowledgements .....   | 62         |
| References .....   | 63         |
| <br>   |            |
| <b>CHAPTER 4. SALT-FREE DEICING OF PAVEMENTS BY CARBON FIBER-BASED ELECTRICALLY CONDUCTIVE CONCRETE HEATED PAVEMENT SYSTEMS: DESIGN AND QUASI LONG-TERM PERFORMANCE.....</b> | <b>69</b>  |
| Abstract.....  | 69         |
| Introduction .....   | 70         |
| Methodology.....   | 74         |
| Research Approach.....   | 74         |
| Materials.....   | 74         |
| Determination of Optimum Carbon Fiber Dosage Rate.....   | 76         |
| Cementitious paste and mortar.....   | 76         |
| Concrete .....   | 77         |
| System Design and Control with finite Element Evaluation of the ECON HPS Performance.....  | 80         |
| Experimental Evaluation of ECON HPS Performance .....  | 81         |
| Results and Discussion .....   | 84         |
| Conclusions and Recommendations .....  | 94         |
| Acknowledgements .....   | 96         |
| References .....   | 96         |
| <br>   |            |
| <b>CHAPTER 5. DEVELOPMENT OF CARBON FIBER-MODIFIED ELECTRICALLY CONDUCTIVE CONCRETE FOR IMPLEMENTATION IN DES MOINES INTERNATIONAL AIRPORT .....</b>                         | <b>103</b> |
| Abstract.....  | 103        |
| Introduction .....   | 104        |
| Materials and Methodology.....   | 110        |
| Materials.....   | 111        |
| Laboratory-prepared ECON Mix Designs .....   | 113        |
| Mixing and Pouring the ECON in Des Moines International Airport Test Section .....   | 118        |
| Investigation of the Properties and Performance of ECON in Des Moines International Airport.....   | 121        |
| Results and Discussion .....   | 124        |
| Properties of Laboratory-prepared ECON Mixtures .....  | 124        |
| Comparison of Laboratory-Prepared Samples with Field-taken Samples .....   | 126        |
| Heating Performance of Slabs.....  | 130        |
| Conclusions .....  | 134        |
| Acknowledgements .....   | 136        |
| References .....   | 137        |

|  |     |
|--|-----|
| CHAPTER 6. POLYURETHANE-CARBON MICROFIBER COMPOSITE<br>COATING FOR ELECTRICAL HEATING OF CONCRETE PAVEMENT<br>SURFACES .....             | 142 |
| Abstract.....  | 142 |
| Introduction .....   | 143 |
| Experimental.....  | 147 |
| Results and Discussion .....   | 156 |
| Conclusion .....   | 169 |
| Acknowledgements .....   | 171 |
| References .....   | 172 |
| CHAPTER 7. CONCLUSIONS AND RECOMMENDATIONS FOR FUTURE<br>WORK .....  | 181 |
| Summary.....   | 181 |
| Conclusions .....  | 183 |
| Identification of significant Mix Design Variables Influencing the Properties<br>of ECON.....  | 183 |
| The Laboratory-scale Prototype EHPS Using Carbon Fiber-Modified ECON ...   | 184 |
| Developing Carbon Fiber-modified ECON for Application in a Full-scale<br>ECON HPS Test Section in Des Moines International Airport ..... | 186 |
| Developing a Polymer-based Electrically Conductive Coating (ECOT).....   | 187 |
| Recommendations for Future Studies.....  | 188 |
| Recommendations for Studies Related to ECON.....   | 188 |
| Recommendations for Studies Related to ECOT .....  | 189 |
| REFERENCES .....   | 190 |

## LIST OF FIGURES

|  | Page |
|--|------|
| Figure 3-1 Electrical resistivity measurement specimen: (a) schematic of cubic ECON specimens with embedded electrodes, (b) measurement set-up. ....   | 42   |
| Figure 3-2 Predicted-versus-measured values of electrical resistivity at 28-day age. ....  | 49   |
| Figure 3-3 Sensitivity assessment of individual variables for electrical resistivity response. ....  | 51   |
| Figure 3-4 Sensitivity assessment of significant variable interactions on electrical resistivity response: (a) FDA dosage-fiber content coupled effect, (b) CEA dosage-fiber content coupled effect, (c) fiber length-fiber content coupled effect, and (d) fiber length. .... | 52   |
| Figure 3-5 Predicted-versus-measured values of compressive strength. ....  | 54   |
| Figure 3-6 Predicted-versus-measured values of flexural strength. ....   | 55   |
| Figure 3-7 Sensitivity assessment of individual variables on compressive strength responses. ....  | 57   |
| Figure 3-8 Sensitivity assessment of individual variables on flexural strength. ....   | 58   |
| Figure 3-9 Sensitivity assessment of significant variable interactions on strength responses: (a) FDA dosage-fiber content coupled effect on compressive strength, (b) FDA dosage-fiber content coupled effect on flexural strength, (c) fiber length-C/F coupled effect. .... | 59   |
| Figure 4-1 Illustration of an electrically heated concrete pavement system. ....   | 81   |
| Figure 4-2 . Elements of the finite element model of ECON test slab having ECON layer on top and regular concrete on bottom. ....  | 82   |
| Figure 4-3 Schematic presentation of the prototype slab. ....  | 83   |
| Figure 4-4 Variation of electrical conductivity by fiber content in cementitious paste and mortar. ....  | 86   |
| Figure 4-5 Variation of electrical conductivity by fiber content for ECON samples at different ages. ....  | 89   |
| Figure 4-6 Temperature distribution in the ECON HPS computed by FE model. ....   | 90   |

|  |     |
|--|-----|
| Figure 4-7 Temperature profile of ECON system during snow melting at 28-day age.....   | 91  |
| Figure 4-8 Temperature profile of ECON system during snow melting at 460-day age.....  | 92  |
| Figure 4-9 Thermal image of prototype slab after one minute (a) and 60 minutes (b) of electric heating. ....   | 93  |
| Figure 4-10 Predicted and measured temperatures at the center of ECON layer at 28-day age. ....  | 94  |
| Figure 5-1. Gradation curves of aggregate systems used in the mix design groups. ....  | 115 |
| Figure 5-2. System configuration and sensor locations for each slab; a) plan view of slabs; b) the cross section of a slab with embedded sensors. ....   | 119 |
| Figure 5-3. Mixing and placement of ECON; (a) feeding fibers and admixtures into the mixer at concrete plant; (b) fiber bags inside the mixer; (c) pouring and spreading the concrete; (d) consolidation, (e) finishing; and (f) covering the fresh concrete with curing. .... | 123 |
| Figure 5-4. Evolution of electrical resistivity in laboratory-prepared and field samples. ....   | 126 |
| Figure 5-5. SEM image of carbon fiber-cement matrix composite in ECON: (a) laboratory-prepared, and (b) field-taken ECON samples.....  | 129 |
| Figure 5-6. (a) aggregate surface in field-taken ECON; (b) isolated carbon fiber broken piece; and (c) the vicinity of an aggregate, in field-taken ECON. ....   | 130 |
| Figure 5-7. Temperature (a) and current (b) profiles during the first testing of the ECON slab.....  | 132 |
| Figure 5-8. Thermal image of ECON HPS slabs in operation (a, and b), anti-icing operation mode of ECON HPS (c), and deicing on ECON HPS slabs (d). ....  | 133 |
| Figure 6-1. Coated specimens for determination of percolation threshold.....   | 152 |
| Figure 6-2. Concrete specimens coated with PU-CMF composite for resistive heating test.....  | 153 |
| Figure 6-3. Concrete specimens coated with PU-CMF composite and the test set-up for evaluating the (a) effect of loading cycle on mass loss, (b) effect of   |     |



|   |     |
|---|-----|
| loading cycles-induced current flow path deterioration on electrical conductivity, (c) loading cycles-induced.....  | 155 |
| Figure 6-4. Schematic of the coating durability test set-up. ....   | 155 |
| Figure 6-5. Variation of volume conductivity with CMF dosage rate in the PU-CMF composite coatings. ....  | 158 |
| Figure 6-6. Thermal image of different CMF-content coatings on wood substrate after 1 minute of current application. ....   | 159 |
| Figure 6-7. Average surface temperature rise of coatings on wood substrate at CMF dosage rates (a) below and (b) above the lower limit of second percolation transition zone after 1 minute of current application..... | 160 |
| Figure 6-8. Average temperature rise on the surfaces of coated concrete specimens at different durations of electric current application. ....  | 162 |
| Figure 6-9. Selected infrared thermal images of concrete specimens after 3 minutes of electric current application. ....  | 164 |
| Figure 6-10. Mass loss of coatings with different CMF dosage rates. Coatings showing measurable mass loss at (a) all; (b) greater than 500; and (c) greater than 5,000 loading cycles. ....                             | 165 |
| Figure 6-11. The changes in electrical resistance of coatings after 10,000 loading cycles for (a) coatings that experienced resistance increase, and (b) coatings that experienced resistance decrease. ....            | 168 |
| Figure 6-12. PU-CMF coatings with (a) 10%, and (b) 15% CMF dosage rates after 10,000 loading cycles. ....   | 169 |

## LIST OF TABLES

|  | Page |
|--|------|
| Table 2-1 Different electrically conductive cement-based composites found in the literature and their respective characteristics. .... | 16   |
| Table 3-1 Variable description in the screening DOE. ....  | 36   |
| Table 3-2 Combination of variables for ECON mix designs. ....  | 37   |
| Table 3-3 Mix proportions of the basic PCC mixtures. ....  | 39   |
| Table 3-4 Averaged measurement results for each mix design. ....   | 44   |
| Table 3-5 Regression coefficients of the model for the three responses. ....   | 45   |
| Table 3-6 Comparison of measured and predicted responses. ....   | 46   |
| Table 3-7 Effect of the variables on electrical resistivity. ....  | 48   |
| Table 3-8 Effect of the variables on compressive and flexural strengths. ....  | 53   |
| Table 4-1 Physical properties of Cementitious Materials and Aggregates. ....   | 75   |
| Table 4-2 Chemical compositions of cementitious materials. ....  | 76   |
| Table 4-3 Volumetric mixing proportions of carbon fiber-containing paste samples. ....   | 77   |
| Table 4-4 Volumetric mixing proportions of carbon fiber-containing mortar samples. ....  | 78   |
| Table 4-5 Volumetric and mass mixing proportions of carbon ECON samples. ....  | 79   |
| Table 4-6 Mixing Proportions of Plain PCC for heated slab. ....  | 84   |
| Table 4-7 Electrical conductivity of paste and mortar specimens with different carbon fiber dosage rates. ....                         | 85   |
| Table 4-8 Electrical conductivity of concrete specimens at different carbon fiber dosages and ages. ....                               | 88   |
| Table 4-9 Compressive Strength of ECON Samples at Ages of 7 and 28 Days. ....  | 89   |
| Table 4-10 Energy and power requirements for melting 6 cm-thick compacter snow layer. ....   | 93   |

|   |     |
|---|-----|
| Table 5-1. Chemical compositions of cementitious materials. ....  | 112 |
| Table 5-2. Combined aggregate gradations for each mix design group. ....  | 114 |
| Table 5-3. Mixing proportions of laboratory-prepared econ mix designs. ....   | 116 |
| Table 5-4. Properties of all laboratory-prepared econ mixtures. ....  | 125 |
| Table 5-5. Actual fiber dosage in laboratory-prepared and field ECON samples. ....                                    | 127 |
| Table 5-6. Results of pore structure evaluation of hardened laboratory-prepared and<br>field-taken ECON samples. .... | 128 |
| Table 5-7 . Snow melting performance of the slab at different ages. ....  | 134 |
| Table 6-1. Mixing proportions of PU-CMF composite mixtures for determination of<br>percolation transition zone. ....  | 151 |
| Table 6-2. Electrical conductivity of PU-CMF coatings containing different volume<br>fractions of CMF. ....           | 157 |
| Table 6-3. Thermography results for PU-CMF-coated concrete specimens. ....  | 163 |

## ACKNOWLEDGMENTS

Now that I have come to the brink of standing upon another milestone in my life, I would like to express my gratitude to people who have helped me along my path. I am aware that this is not an end to my journey as a student, and I will continue being a “*wide-eyed wanderer*”. However, with thanks to my mentors and the precious people who have given me their kind and generous support, I am now equipped with sharper eyes to see the wonders of “*the brave new world*”.

I would like to express my sincere gratitude to my Co-major professors Dr. Halil Ceylan and Dr. Peter C. Taylor for mentoring me through my Ph.D. studies and being such great professional and moral role models for me. I am also very thankful to Dr. Sunghwan Kim and Dr. Kasthurirangan Gopalakrishnan for their scientific advice and moral support. I would never have been able to go through such difficult times without Dr. Kim and Dr. Gopalakrishnan being there to help me with their kindness, comprehensive knowledge, and excellent recommendations for which I will always be grateful. I would like to thank my committee members, Dr. Mani Mina and Dr. Paul Spry for honoring me by their very presence on my program of study (POS) committee and setting my research and studies on the right path by providing support, insightful comments, motivation, encouragement, and recommendations.

I profusely thank Mr. Robert Frank Steffes, the lab manager at the Portland Cement Concrete Research Laboratory for giving me his support and sharing his widespread knowledge and experience with me. I thank Mr. Paul Kremer for kindly providing access to the laboratory spaces, training, and technical consultation. I express my appreciation to all faculty and staff of ISU CCEE, especially Ms. Kathy Peterson, Ms.

Marva Banks, Ms. Nancy J. Qvale. Ms. Emma J. Estrada, Mr. Paul J. McIntyre, and Mr. Theodore J. Huisman. This study was conducted at Iowa State University (ISU) under the Federal Aviation Administration (FAA) Air Transportation Center of Excellence Cooperative Agreement 12-C-GA-ISU for the Partnership to Enhance General Aviation Safety, Accessibility and Sustainability (PEGASAS); I would like to thank ISU and FAA for this support.

I would like to thank my Friends Ali Arabzadeh and Mehran Ebadollahi who have been no less than brothers to me. They pushed me forward whenever I was tired and their company over the past seven years has been a boon that produced sweet memories out of difficult times. I thank my friend Sharif Gushgari for being such a good and supportive friend to me. I thank my friends Shahram, Kaveh, Amir, Hani, and Nima who filled all the physical distance between us with love. I thank Sue, Danielle, Hannah, Saeed, Yassaman, Ali, Arya, and Shahin for their friendship and moral support. I also thank my imaginary friend, “*me at the end of my life*”, who has motivated me to live in such a way that, when the time comes, I can embrace the final journey with a grin.

I express my love and gratitude to my beloved family who never lost their trust in me and went through a great deal of hardship to support me. And last, but indeed most importantly, I express my gratitude and deepest love to my wife, *Shadi*, who is my guardian angel and has been my patient, loving, and divine soulmate. I can never thank her enough for a lifetime of happiness she has given me, but I will be fortunate enough to spend the rest of my life trying to give her the same.

**ABSTRACT**

Today's predominant pavement de-icing methods rely on mechanical removal and chemical de-icers. The limitations of such approaches include high investment in time/labor, pavement damage, and traffic interruption, and they have given rise to a need for novel alternatives to replace or complement existing traditional methods. This study, inspired by such a need, has approached the problem of pavement deicing from a heated pavement systems (HPS) prospective. The study has sought to investigate the feasibility of using smart materials in electrically heated pavement systems (EHPS). To this end, two types of composite materials: (1) portland cement-based electrically conductive concrete (ECON), and (2) polymer-based electrically conductive coatings (ECOT) were studied.

ECON mix design, using carbon fibers (CF) of micrometer-scale diameter and millimeter-scale length as an electrically conductive additive, was prepared and optimized for pavement applications in accordance with relevant standards and specifications. The optimum carbon fiber dosage rate for achieving desirable electrical conductivity and avoiding excessive fiber use was determined based on fiber percolation phenomenon. The ECON HPS system design and configuration were evaluated by finite element (FE) analysis and laboratory tests, and the feasibility of using ECON was then investigated both at laboratory scale and through a real-size EHPS test section at the Des Moines International Airport. The performance of the ECON HPS was evaluated in terms of energy demand for snow-melting, energy conversion efficiency, and service life.

An electrically conductive composite coating, made with a Polyurethane (PU) binder and micrometer-scale carbon fiber (CMF) filler, was produced and applied as an electrically heated layer on the surface of portland cement concrete (PCC). The CMF dosage rate required to achieve desirable volume conductivity, heating capability, and durability was investigated. Coating durability was evaluated using a loaded cyclic wheel path to simulate coating performance on pavement surfaces. This research has introduced PU-CMF coating as a versatile smart material with application to various fields such as EHPS and self-sensing structures.

## CHAPTER 1. INTRODUCTION

### Background

Operational safety of paved areas, especially in critical infrastructures such as airports, bridges, and highways, is a major concern for public and private sectors, particularly under harsh winter conditions. Pavement surface conditions are influenced by frozen precipitation, i.e. ice, snow, and slush, jeopardizing vehicles and individuals who use pavement. Traditional de-icing methods are based on the application of de-icing chemicals and/or sand on the surface or mechanically removing accumulated frozen objects from the surface. These methods are subject to inadequate effectiveness, long down-time of the paved facilities, high labor demand, environmental concerns, safety problems, and damage to pavement. The drawbacks of conventional ice/snow removal methods include –but are not limited to- ineffectiveness in removing snow under extreme weather conditions, negative impact on the environment because of possible contamination of nearby water bodies, increased labor cost, safety issues, and possible damage to pavement by de-icing chemicals (durability problem) and machinery. These methods are also challenging to implement in congested and small areas such as sidewalks, highway ramps, aprons, taxiways at airports, and stairways. Considering these challenges to commonly-used traditional methods, it seems timely to explore use of active heated pavement systems for addressing such problems.

Because of the urgent nature of these problems, relevant sectors have been seeking new technologies that can more effectively and efficiently remove or prevent formation of ice and snow on paved surfaces. Heated pavement systems (HPS) represent one alternative to traditional methods that has gained considerable attention over the past few years. Application of heated pavement systems has attracted attention as a promising alternative to current ice and snow



removal practices as a practical and economic means of keeping pavements free of ice and snow during winter. When traditional ice/snow removal methods are used, the pavements are a passive component of the system, but application of heated pavements gives an active role to the pavement in the de-icing and anti-icing processes.

Hydronic heated pavement systems (HHPS), the currently dominant form of HPS application, melt ice and snow by circulating heated fluid through an embedded pipe system within the very structure of the pavement. A heat source heats the fluid, the heated fluid is pumped into the pipe system heating the pavement, and the cooled fluid is directed back to the heating source for reheating. Different heating sources can be used in hydronic heated pavement systems including geothermal waters, boiler, and heat exchangers. The disadvantages of hydronic systems include construction difficulties, high installation costs, and challenges associated with fluid leakage or pipe damage. Electrically heated pavement systems (EHPS) are a relatively newer and less common approach of heated pavement systems application. Numerous studies related to electrically heated pavement systems have studied the feasibility of using resistive cables, sheet, or grills embedded inside concrete structures for pavement deicing [1–3]. This approach suffers from high power density requirements, or risk of damages to electrical cables which tends to break down the whole system. To overcome such shortcomings, EHPS application has been steered toward using electrically conductive concrete (ECON) as the heating element of the system. Electrically conductive coatings (ECOT) are another alternative practice of EHPS that –to the best of author’s knowledge- has not been previously studied and will be proposed as a proof of concept in this dissertation.

The problems associated with traditional ice/snow removal methods and hydronic systems have given rise to application of new methods and materials in heated pavement

systems. An alternative to hydronic heated pavements is electrically heated pavement systems (EHPS). The recent boom in the field of smart materials at both research and commercial levels make them an attractive option for production of more efficient, sustainable, and effective HPS. In that regard, electrically conductive cement-based and polymer based composites represent two categories of smart materials that appear to be promising for application in heated pavement systems (HPS). This study investigated the feasibility of applying two types of electrically conductive smart materials in electrically heated pavement systems (EHPS):

- 1) Electrically conductive portland cement concrete (ECON), a cement-based composite
- 2) Electrically conductive coating (ECOT), a polymer-based composite

Electrically heated pavement systems (EHPS), including ECON and ECOT, is based on the concept of joule heating (or resistive heating) by applying an electric potential difference (voltage) across the conductive layer (ECON or ECOT) and converting the electrical energy into thermal energy. The ECON/ECOT layer acts as a resistor, generating heat that increases the concrete temperature and melts ice and snow on the pavement surface. An EHPS can be represented as a combination of resistors and capacitors, representing conductive and non-conductive materials respectively [4].

While the effectiveness of various conductive materials such as steel fiber, carbon fiber, etc., added to conventional concrete to produce ECON with sufficient electrical conductivity (i.e., low electrical resistivity) and engineering properties has been thoroughly investigated in the existing literature [5,6,15,7–14], there is very limited knowledge regarding material selection for electrically heated coatings [16]. To the best of the author's knowledge, there is in fact no available study on the application of electrically heated coatings and associated materials on pavement surfaces. Electrically conductive coatings (ECOT), although already developed and

studied to some extent for use in non-transportation fields and on metallic substrates, have not up to now been studied for use on Portland cement concrete (PCC) surfaces and other forms of pavements.

### **Objective**

The primary objectives of this research include:

- To determine important mix design factors related to electrical conductivity and mechanical properties of carbon fiber-modified electrically conductive concrete (ECON) and optimize the mix design of ECON for application in electrically heated pavement systems (EHPS).
- To produce a prototype electrically conductive heated pavement system (EHPS) using carbon fiber-modified ECON at laboratory-scale and investigate its performance adequacy as a function of age.
- To develop carbon fiber-modified ECON for application in a full-scale ECON HPS test section, and monitor the ECON HPS performance under various levels of cold weather conditions, operational modes, and at different ages. The intent was to evaluate the utilized materials, mixing proportions, and mixing procedures with respect to performance and material characteristics of ECON, such that potential problem sources can be identified and eliminated in future work.
- To develop a polymer-based electrically conductive coating (ECOT) providing a cost-effective, efficient, and durable material to be used on pavement surfaces as an electrically heated pavement at the proof-of-concept level.

The overall goal of this study was to identify, optimize, and design smart materials to be used in production of electrically heated pavement systems (EHPS). To this end, two general

categories of smart composite materials, electrically conductive concrete (ECON) and electrically conductive coating (ECOT), were developed using carbon fibers with size scales at macro (millimeter) and micro (micrometer) levels and tested to evaluate their performance as electrically heated pavement materials. In other words, the materials studied in this research lie within the category of multi-functional, multi-scale smart composites.

### **Dissertation Organization**

This journal paper-based dissertation is organized as follows:

- Chapter 1 includes summarized background, research objectives and dissertation organization.
- Chapter 2 provides a state-of-the-art annotated bibliography including a thorough literature review on Smart materials, electrical conductivity of cementitious composites, heated pavement systems, electrically conductive portland cement concrete, polymer-based coating materials, smart and electrically conductive coatings, and methods for synthesizing and characterizing such materials.
- Chapter 3 presents the first journal article: *Influence of Mix Design Variables on Engineering Properties of Carbon Fiber-Modified Electrically Conductive Concrete* that discusses the most important factors related to mix design of electrically conductive concrete (ECON) that influence its electrical conductivity and strength-related properties. This section provides a concrete basis for determining the mixture components and mixing proportions of ECON to achieve desirable properties for HPS applications.
- Chapter 4 presents the second journal article: *Salt-free Deicing of Pavements by Carbon Fiber-based Electrically Conductive Concrete Heated Pavement Systems: Design and Quasi Long-term Performance* that discusses the performance-based design of materials

and system configurations for ECON HPS. The results presented in Chapter 3 were utilized to develop the experimental plan for this research. The optimum carbon fiber dosage for achieving the most desirable value of electrical conductivity and avoid excessive fiber use was determined by considering percolation threshold phenomena in different carbon fiber-based cementitious composites. The ECON HPS system design and configuration were evaluated by finite element (FE) analysis. The performance sustainability of the ECON HPS in terms of energy demand for snow melting, and energy conversion efficiency were studied by experimental evaluation of a prototype ECON HPS slab.

- Chapter 5 presents the third journal article: *Development of Carbon Fiber-modified Electrically Conductive Concrete for Implementation in Des Moines International Airport*, a case study based on field implementation of a real size electrically conductive concrete (ECON) heated pavement test section at the Des Moines International airport. This paper reports ECON design and production procedures, characteristics of the produced ECON mixture, and system performance under winter conditions. Potential challenges faced in large-scale production of ECON and construction of ECON heated pavement are discussed in this section based on the laboratory tests and field data acquisition.

- Chapter 6 presents the fourth journal article: *Polyurethane-Carbon Microfiber Composite Coating for Electrical Heating of Concrete Pavement Surfaces* that describes a method for synthesizing an electrically conductive polyurethane-carbon-microfiber (PU-CMF) composite coating and its application as a resistive-heating material for portland cement concrete pavement surfaces. This study specifically describes materials treatment and mixture preparation procedures for PU-CMF composite coating for application on portland cement concrete (PCC) substrates. The feasibility of using such coating materials in EHPS was studied through electrical heating and durability tests performed on coated specimens.
- Chapter 7 provides a summary, concluding remarks, and recommendations for future work.

## CHAPTER 2. LITERATURE REVIEW

This chapter provides a state-of-the-art annotated bibliography including the survey of the relevant literature for each topic studied under the framework of this research. The background of smart materials and their application in civil engineering systems is provided referring to the existing literature. A thorough literature review on heated pavement systems and electrically conductive portland cement concrete is presented in this chapter. This chapter also includes a literature review on materials and methods for synthesizing electrically conductive coatings and their application on portland cement concrete pavements to achieve electrically heated pavement systems. In addition to the information provided in this chapter, each journal article included in this study will have its own literature review, specific to its scope.

### Smart Materials and Their Application in Civil Engineering Systems

#### Background

Oxford dictionary of mechanical engineering [17] defines smart materials as:

*“Materials which have one or more properties that can be changed significantly in a controlled fashion by external stimuli such as temperature, stress, electric or magnetic fields.”*

Another definition for smart materials which is more function-based than property-based goes as:

*“Smart or intelligent materials are materials that have the intrinsic and extrinsic capabilities, first, to respond to stimuli and environmental changes and, second, to activate their functions according to these changes.”* [18]

If the above-given definitions are adopted, smart materials have been available since ancient times. For example, “*pyroelectric materials*” which develop spontaneous electric dipole moment when heated -and hence can attract objects- or ceramics that are an important part of

modern smart materials have been known to human since ancient times [19,20]. Nevertheless, the use of the terms “smart” and “intelligent” for describing materials started in 1980’s [21] and it was not before 1992 that smart materials were commercially introduced to the public by being used in snow skis [22]; ever since, the market has been bombarded with a tremendous number of engineered products made with so-called smart materials.

### **Application in Civil Engineering Systems**

Construction sector and, in general, Civil Engineering has taken a relatively small share of the market of smart materials. Since the beginning of the profession of “building”, which dates back to the onset of human settlement [23], the material selection in the design and construction process of built objects has been mainly based on mechanical strength, availability/abundance, and appearance/ornamental qualities. The cost and availability have imposed a limitation on replacing conventional construction materials, as passive members as they are, with newer materials that can take active roles in the intended function of the structure [22]. The vision of smart cities, developed in recent years, includes application of smart materials and structures functioning as an integrated component of the urban system towards a safe, secure, environmentally friendly, and efficient built environment [24]. By application of smart systems, it will be possible to monitor, control, or trigger all critical infrastructures such as roads, sidewalks, buildings, bridges, airports, etc. [24]. The development of smart systems, as so far experienced, is either by developing novel materials capable of assuming certain functions as a response to external stimuli, or applying the existing control and monitoring systems such as sensors; due to cost and difficulty considerations, the latter is currently the predominant approach [24].



Some of the most well-known smart materials are [18,21]:

(1) *Piezoelectric materials*

Materials that exhibit mechanical variations in their structure if they are subjected to a voltage variation or develop a voltage variation when subjected to stress/strain are called piezoelectric.

(2) *Electrostrictive materials*

Piezoelectric materials which always show the variations in the same direction, due to dependence of mechanical properties to the square of electric field, are known as electrostrictive.

(3) *Magnetostrictive materials*

If the material's mechanical properties are altered by exposure to variation of magnetic field, and vice versa, it is called magnetostrictive. These materials are magnetic equivalents of piezoelectric and electrostrictive materials.

(4) *Magneto- and Electro-rheological materials (smart fluids)*

Materials that experience dramatic change in viscosity when subjected to electric current variation or magnetic field variation are called electro-rheological and magneto-rheological materials respectively.

(5) *Shape memory alloys (SMAs)*

Materials that change shape or re-assume previous shape at a certain temperature. If the material can go through this process only once, it is called one-way shape memory alloy.

(6) *Optical fibers*

Fibers that undergo alteration in molecular level is subjected to variation of intensity, phase, frequency, or polarization of modulation.

(7) *Chromic materials*

Materials that change color when subjected to variation of

- Temperature (referred to as thermochromic materials)
- Level of light (referred to as photochromic materials)
- Stress/strain (referred to as piezochromic materials)

There are numerous other smart materials which are either single-component or multi-component, the latter being compounds of different chemicals or mixtures of different materials which may or may not be individually smart. In recent years, smart materials have found their ways to construction materials, mainly in research level. Piezoelectric materials have been extensively used in construction materials as vibration sensors [25].

Composites are among most common multi-component smart materials. Composite materials in which different types of carbon nanotube (CNT) or nanofiber (CNF) are incorporated, have been extensively used as smart materials in the past years [26–32]. CNT/CNF composites have been utilized in construction of smart structures utilizing their electrical conductivity, piezoelectric properties, and magnetoresistance features [33]. Macro-sized carbon fibers (hereinafter referred to as CF) can also be used to produce smart structural material. Incorporating CF in cementitious composites, if adequate dosage rates are used, imparts features such as electrical conductivity [34,35], piezoelectricity (or piezoresistivity) [36], and thermistor characteristics [5,37,38] to the composite. Utilizing such properties, many studies have used CF in production of carbon fiber-modified cementitious composites to be used as electrically conductive self-heating and self-sensing structural members [34,36,37,39]. Also, polymer-based composites comprising of polymer binder matrices and electrically conductive additives such as CF [40], CNT [32], or CNF [41] have been developed and used as smart materials.

## **Review on Electrically Conductive Portland Cement Concrete Heated Pavement Systems**

### **Applications of Electrically Conductive Portland Cement concrete**

ECON is an avant-garde technology which is gaining importance in the context of pavement safety under freezing conditions. Furthermore, previous studies have suggested that ECON provides manifest benefits in multiple applications. Besides electrical heating which has been the most popular application of ECON [42–46], researchers have shown the feasibility of employing ECON for purposes such as; a) as a self-sensing construction material for structural health monitoring practices [47–49]; b) as an electromagnetic radiation reflector for electromagnetic interference (EMI) shielding [11,50,51].

### **Electrical Properties of Plain Portland Cement-based Concrete**

Plain portland cement-based concrete (PCC) is not electrically conductive [52,53]; the electrical resistivity of air-dried normal concrete ranges from  $6 \times 10^5$  to  $10^6$   $\Omega$ -cm [52], oven-dried plain concrete has an electrical resistivity as high as  $10^{11}$   $\Omega$ -cm [54], and the electrical resistivity of moist concrete is about  $10^4$   $\Omega$ -cm and is therefore classified as a semiconductor [54]. Hardened PCC is comprised of three phases [52,53,55]: (1) a vapor phase (pore filled with air) with about  $10^{11}$   $\Omega$ -cm electrical resistivity (that makes it an insulator of electricity); (2) a solid phase (aggregate and hydration products of cementitious materials) with about  $10^{17}$   $\Omega$ -cm electrical resistivity (which is again categorized as an electrical insulator); and (3) a fluid phase (pore filled with liquid solution including water) with about 5 to 100  $\Omega$ -cm of electrical resistivity which is the main conductor of electricity in plain concrete. The aggregates commonly used in PCC production have an electrical resistivity in the range of  $0.3 \times 10^5$   $\Omega$ -cm to  $1.5 \times 10^5$   $\Omega$ -cm [15]; thus, when commonly used aggregates are considered, the aggregate phase can be considered as an electrical insulator phase within the cementitious matrix.

The basic mechanisms of electricity conduction in Cement-based materials include: (a) electrolytic conduction through the motion of ions in pore solution of a fluid phase; and (b) electronic conduction through the motion of free electrons along the continuous or segmented network of conductive or relatively conductive materials in a solid phase [13,15]. Due to the presence of different ionic entities within the pore solution it acts as the primary medium for ion/charge transfer within the concrete; the principal ions in the pore solution that enable the flow of electricity are  $\text{Ca}^{2+}$ ,  $\text{K}^+$ ,  $\text{Na}^+$ ,  $\text{SO}_4^{2-}$ , and  $\text{HO}^-$  [52]. An evidence for the charge transfer through pore solution is the corrosion of reinforcing bars which is essentially associated with the transfer of electrons or charge in the rebar-“pore solution” interface [56]. Conduction of electricity through ion mobility in the pore solution is called “electrolytic conduction”[15]. Cement matrix –without pores- and the aggregates being poor electricity conductors, leaves the pore solution as the dominant phase which contributes to the flow of electric current through the concrete. Hence, the electrical conductivity of PCC can be accredited to the volume percentage [57], degree of saturation [58], and ionic composition [59] of the pore structure.

Despite the pivotal role of pore solution in charge transfer through concrete, it is not a reliable source of conductivity. Evaporation of water from the pores and variation of the ionic composition of pore solution can exert significant changes to its conductivity [60]. Moreover, electricity flow through discontinuous segments of pores does not provide sufficient conductivity for applications such as electrical heating, health monitoring of concrete structures, and electromagnetic shielding [5,38,50]. Due to inadequacy of electrolytic conduction in concrete, a different conduction mechanism should be involved in ECON. Electrolytic conduction in ECON is identical to conventional PCC. The basic difference of the conduction path between ECON and PCC is that in ECON the dominant conduction mechanism is electronic conduction; that is

the motion of electrons –instead of ions- through a conductive medium [15]. Both mechanisms exist in the conventional PCC and the ECON, whereas, in the latter the electronic conduction is boosted by introducing a distinctive conductive phase into the concrete matrix. Conductive materials with electrical resistivity values less than  $10^{-1} \Omega\text{-cm}$  can be used as electrically conductive additives (ECA) materials to impart electrical conductivity to the plain concrete [15].

### **ECON: materials, properties, and methods of production**

The general constituents of ECON are cement, coarse and fine aggregates, water, ECAs, and possibly admixtures. Nevertheless, as mentioned in the above, the main component(s) imparting electrical conductivity to the concrete is/are the ECA(s) phase by creating the path for electricity conduction. Numerous studies [9,15,42,43,61–65] have used various materials such as fibers, powders, and granular solid particles as ECAs to constitute the path of electronic conduction in the concrete. Table 2-1 presents a summary of the electrically conductive cementitious composites and their respective applications provided in the literature.

As seen in the table, fiber materials provide better performance as ECA than granular or powder materials. Furthermore, granular materials are associated with very high ECA dosage requirement (Table 2-1), reduction of concrete strength [66,67], and high cost of materials especially in the case of nanoparticles. Although steel fiber has been found to be more effective in achieving resistive heating [68], addition of steel fiber to concrete mix is associated with drawbacks such as corrosion problem [66,67], high ECA dosage requirement in terms of material weight [69], and prohibitions for use in critical infrastructures such as airfield pavements [70]. Carbon fiber can be used in minor volume and weight dosages. Previous studies have shown the ability of carbon fiber ECA to render cementitious composites electrically conductive while improving the concrete properties such as freeze-thaw durability, compressive

strength, tensile strength, fatigue cracking, shrinkage cracking potential, and expansion cracking susceptibility [71–73].

Using SS as a single-material ECA gave similar results as SF in terms of electrical resistivity values [13,15]. Although the combined use of SS and SF at appropriate dosage rates provided acceptable engineering properties, field experiments revealed several concerns with respect to the use of SF and/or SS in pavements [62]: stains on the pavement surface due to the corrosion of SFs and SSs, potential damage the vehicle tires by exposed SS and SF, and delamination and concrete spalling risk due to corrosion of metallic ECAs. Another problem with SS material is susceptibility to produce electrical charges during the mixing process which makes dispersion more difficult. Also, SS materials obtained from industrial waste are usually contaminated with oil or other impurities.

The combined use of SF and carbon particles in ECON gave acceptable engineering properties, however, the aforementioned issues with the SF materials still prevail [62,69]. Similar results were reported by studies investigating the combined use of SFs and graphite powder [74]. In addition, the use of granular carbon products or graphite powder has been found to cause reduction of mixture workability [69,74]. Lignin-derived conductive fibers are another type of materials that have been investigated for use in electrically conductive cement-based composites and [75].

*Table 2-1 Different electrically conductive cement-based composites found in the literature and their respective characteristics.*

| Reference | No. of ECA Phases | ECA materials | ECA dosage         | Achieved resistivity ( $\Omega$ -cm) | Composite type | Intended application |
|-----------|-------------------|---------------|--------------------|--------------------------------------|----------------|----------------------|
| [67]      | 1                 | CF            | 0.80 *             | 4.00E+03                             | Concrete       | Self-heating         |
| [67]      | 1                 | SF            | 1.00 *             | 2.40E+03                             | Concrete       | Self-heating         |
| [67]      | 2                 | SF, GP        | 1.00, 8.00 *       | 6.40E+02                             | Concrete       | Self-heating         |
| [67]      | 3                 | SF, CF, GP    | 1.00, 0.40, 4.00 * | 3.22E+02                             | concrete       | Self-heating         |
| [8]       | 2                 | SF, SS        | 1.50, 15.00 *      | N.R.                                 | Concrete       | Self-heating         |
| [13,15]   | 2                 | SF, SS        | 1.50, 20.00 *      | N.R                                  | Concrete       | Self-heating         |
| [71]      | 1                 | CF            | 0.35 *             | 0.31 E+06                            | Mortar         | N.S.                 |
| [76]      | 1                 | SF            | 0.05 *             | 1.65 E+06                            | Mortar         | N.S.                 |
| [64]      | 1                 | GP            | 37.00 *            | 4.8 E+02                             | Mortar         | EMI shielding        |
| [64]      | 1                 | SF            | 0.72 *             | 1.60E+01                             | Mortar         | EMI shielding        |
| [77]      | 1                 | CF            | 0.73 *             | 3.80E+01                             | Concrete       | N.S.                 |
| [78]      | 1                 | CNF           | 1.50 *             | N.R.                                 | Concrete       | Sensing              |
| [47]      | 1                 | CNT           | 0.50 *             | N.R.                                 | Paste          | Sensing              |
| [35]      | 1                 | CF            | 0.75 *             | 2.00E+04                             | Concrete       | N.S.                 |
| [74]      | 2                 | SF, GP        | 2.70, 17.20 *      | 6.43E+02                             | Concrete       | Self-heating         |
| [36]      | 1                 | SF            | 0.72 *             | 1.60E+01                             | Paste          | Sensing              |
| [36]      | 1                 | CF            | 0.50 *             | 1.50E+04                             | Paste          | Sensing              |
| [79]      | 1                 | CF            | 0.95 *             | 8.30E+02                             | Paste          | Self-heating         |
| [79]      | 1                 | SF            | 0.20 *             | 3.20E+04                             | Paste          | Self-heating         |
| [37]      | 1                 | CF            | 0.40 *             | 1.92 E+4                             | Paste          | Thermistor           |
| [80]      | 1                 | CF            | 1.16 *             | 5.41 E+02                            | Mortar         | N.S.                 |
| [81]      | 1                 | GP            | 30.00 *            | 6.00E+02                             | Paste          | Anode                |
| [42]      | 1                 | CNT           | 5.00 **            | 2.20E+01                             | Paste          | Self-heating         |
| [42]      | 1                 | CNF           | 5.00 **            | 7.30E+02                             | Paste          | Self-heating         |
| [42]      | 1                 | CFP           | 5.00 **            | 1.60E+03                             | Paste          | Self-heating         |
| [42]      | 1                 | GP            | 5.00 **            | 1.10E+03                             | Paste          | Self-heating         |
| [82]      | 1                 | CF            | 0.50 *             | 1.27E+02                             | Concrete       | Electrical grounding |
| [26]      | 1                 | CF            | 1.00 *             | 3.60E+01                             | Paste          | Self-Heating         |
| [83]      | 1                 | GP            | 50.00 **           | 1.50E+02                             | Paste          | Anode                |
| [84]      | 1                 | CFL           | 1.00 *             | 1.21 E+04                            | Paste          | EMI shielding        |
| [85]      | 2                 | GP, SF        | 5.00 **,40.00 ***  | N.R.                                 | Mortar         | Self-heating         |
| [85]      | 2                 | CP, SF        | 5.00 **,40.00 ***  | N.R.                                 | Mortar         | Self-heating         |
| [7]       | 1                 | SF            | 0.50 *             | 1.4 E+03                             | Paste          | Self-heating         |
| [86]      | 1                 | CF            | 0.22-0.95 *        | 6.04E+05                             | Paste          | N.S.                 |
| [87]      | 1                 | CF            | 2.00**             | 4.00E+01                             | Concrete       | Self-heating         |

*CF-carbon fiber, SF-steel fiber, SS-steel shaving, GP-graphite powder, CP-carbon powder, CNF-carbon nanofiber, CNT-carbon nanotube, CFP-carbon fiber powder, CFL-carbon filament. Mortar and paste respectively refer to cementitious paste and cementitious mortar. \*-% total volume of the mix, \*\*-% weight of cementitious materials, \*\*\*- Kg/m<sup>3</sup> of total mix. N.R.-not reported, N.S.-not specified.*

With any of the materials in the foregoing discussions used as the ECA(s), the conductivity of cementitious systems can be discussed with reference to “percolation phenomenon”, which refers to the volume fraction above which the conductive materials within the matrix touch one another to form a continuous electrical path [34,36,88]. Xie et al. [89] investigated the effect of carbon fiber content on the conductivity of cement paste and mortar systems at different water/cement or sand/cement ratios. They reported that after a certain threshold of carbon fiber concentration, the addition of carbon fibers increases the conductivity of paste and mortar systems only marginally. It was further concluded that this percolation threshold is a function of the geometry of carbon fibers (length and diameter) and that the properties of non-conductive components have little influence on the overall conductivity of the system [89].

The percolation transition zone represents the region in electrical conductivity-ECA dosage rate curve where the abrupt jump in the conductivity takes place. The percolation transition zone typically consists of three critical points; (1) a lower limit which corresponds to partial formation of a conductive network, (2) an upper limit which shows the fiber content at which a complete network of conductive materials is formed, and (3) an intermediate value between lower and upper limits that corresponds to the onset of the formation of a continuous path [88]. The range of fiber content over which electrical conductivity experiences abrupt increase by increasing fiber content is known as percolation transition zone. Generally, the “conductivity-ECA dosage rate” curve assumes an almost S-shaped form; i.e., having small slope in fiber contents below and above percolation transition zone while showing very sharp



slope at the percolation zone [36]. The intermediate point in the percolation transition zone (between the lower and upper limits) can be assumed as minimum ECA volume fraction required to achieve a continuous path for electricity conduction. Different researchers have assumed either of the three values –lower limit or upper limit of percolation transition zone, or a value between them- as percolation threshold. However, it is more common to assume the upper limit as the percolation threshold, such that above the percolation threshold, the addition of ECA does not result in abrupt jump in the electrical conductivity [14,80,89–91].

Generally any aggregate suitable for concrete can be used in electrically conductive concrete as well, and specific requirements or limitations have not been applied to the aggregates in ECON. Most of the studies in the existing literature have used limestone aggregate in their ECON mixtures, mostly because it is an abundant and commonly used aggregate and does not exert significant effects on the electrical properties of concrete [10,63]. Furthermore, limestone because of its low coefficient of thermal expansion, tends to minimize the problems associated with thermal expansion in heated concrete [92]. Few studies experimented with the idea of either partially or fully replacing limestone aggregate with Blast Furnace Slag (BFS) along with smaller amounts of graphite powder, but were not successful in achieving desired conductive properties [74,93]. The most common aggregates used in concrete production, such as Limestone, Granite, Basalt, and Quartzite, have thermal conductivity values that are orders of magnitude higher than cement paste [94]; therefore, the effect of aggregate selection relative to cementitious paste is not significant in the thermal performance of the ECON system. However, using more thermally conductive aggregates can help improving the thermal properties of the concrete for heating purposes. Dehdezi et al. [94] used quartzite in concrete pavement mixtures

to enhance the thermal conductivity of the concrete and therefore improve the energy harvesting properties. So far, quartzite has not been investigated in electrically conductive concrete.

There are studies postulating that percolation transition zone of carbon fiber in mortar was independent of water-to-cement and sand-to-cement ratios [14,89]; whereas, some suggest that increasing sand-to-cement ratio increases the percolation threshold [80]. However, it was suggested that for sand-to-cement ratios between 1 and 3, percolation threshold becomes independent from the variations of sand-to-cement ratio [80].

A handful of previous studies have reported mixing procedures for production of conductive concrete and have identified their procedure as the optimum one to achieve good engineering properties. However, there is no systematic guidance or specification available on the optimal mixing technology for conductive concrete. As mentioned previously, the reported studies do indicate that the ECA should be evenly distributed within the system to achieve high composite conductivity [69,95,96]. The degree of ECA dispersion plays an important role in achieving desirable electrical conductivity, especially at low ECA volume fractions. The significance of ECA dispersion is such that the variance (or standard deviation or any other quantity representing the scattering of data) of electrical resistivity between multiple ECA-doped electrically conductive composite can be used for evaluating the dispersion of ECAs [34]. While the dispersion of fiber-form ECAs is more challenging and has attracted more attention in the literature, Powder-form ECAs like graphite also need to be homogeneously distributed in the concrete mix to provide good conductivity [62,69,74].

Admixtures such as silica fume, polymer particles –such as Latex and Acrylic-, water-based surfactants, methylcellulose, and Silanes/Siloxanes can be used to improve the dispersion of ECAs within the partially conductive or non-conductive matrix [96]. Different materials are

available to improve the dispersion of ECAs in concrete mixtures. Acrylic with or without silica fume, styrene acrylic [76], latex with or without Silica fume [37,63], and methylcellulose [77]. Effective fiber dispersion by using acrylic, styrene acrylic, and latex is associated with high dosages of fiber dispersive agent (FDA) – in the range of 10 to 20% by weight of cementitious materials – [71,96]. On the other hand, the dosage of methylcellulose used as a FDA in carbon fiber-modified concrete/mortar in this study can be as low as 0.4% by weight of cementitious materials [77,97].

### **Applications and Methods of Measuring the Electrical Properties of Concrete**

Utilizing joule heating in a pavement system with electrically conductive concrete (ECON) or electrically conductive coatings (ECOT) calls for electrical resistivity values lower than  $10^3 \Omega\text{-cm}$  that is necessary for deicing applications [13,15]. The resistivity of concrete is dependent on a variety of factors, including age (hydration), moisture content [98], salinity of both mixing water and pore water [99], temperature [100], etc. In addition, since concrete is a heterogeneous material, its resistivity can vary throughout the sample [52]. Therefore, especially when smart materials are used in production of portland cement concrete (PCC) or electrically conductive coatings, the electrical properties of the system can be used for investigating many material and structural properties such as the hydration of the concrete, salinity of the pore solution, the temperature gradient in the pavement cross section, the structural integrity of the pavement or structural member, and the stress or strain [16,32,37,47,48,101,102].

Electrical resistivity, defined as electrical resistance (in Ohms) between the two faces of a unit cube of material, is a property of material independent of its shape and size [52], while, electrical resistance is dependent on the geometry of the testing sample. Most measurement devices provide the value of electrical resistance that can be converted into resistivity. A

common practice for measurement of electrical resistance is applying a certain voltage between two points of a specimen (representing two opposite faces) and measuring the resulting electrical current which passes through the specimen. When direct current (DC) is used, the electrical resistance can be calculated from the simplest form of the Ohm's law (Equation 2-1):

$$R = V/I \quad (\text{Equation 2-1})$$

Where,  $R$  is the electrical resistance in Ohms ( $\Omega$ ),  $V$  is the applied voltage in volts ( $v$ ), and  $I$  is the electrical current in Amperes ( $A$ ). Knowing the dimensions of the specimen, the electrical resistivity can be calculated from the measured value of electrical resistance using equation 2-2:

$$\rho = R \frac{A}{l} \quad (\text{Equation 2-2})$$

Where,  $\rho$  represents the electrical resistivity in ohm-meters ( $\Omega\text{-m}$ ),  $R$  is the electrical resistance in Ohms ( $\Omega$ ),  $A$  is the cross sectional area normal to the current direction, and  $l$  is the distance between the two points with electrical potential difference of  $V$  ( $V$  refers to Equation 2-1). Note that alternative units such as KiloOhms, miliAmperes, Centimeter, etc. can be used in the equations if all units are converted accordingly. When alternating current (AC) is used for measurement of the electrical resistivity, the equivalent form of the Ohm's equation for AC should be used (Equation 2-3):

$$V = ZI \quad (\text{Equation 2-3})$$

In equation 2-3,  $Z$  is electrical impedance, the AC equivalent of electrical resistance. Electrical impedance is comprised of a real and an imaginary component, as shown in Equation 2-4.

$$Z = Z' + jZ'' \quad (\text{Equation 2-4})$$

The real part of equation 2-4 (i.e.,  $Z'$ ) is called resistance and the imaginary part (i.e.,  $Z''$ ) is known as reactance. The imaginary part of Equation 4 can be neutralized by applying the AC with a certain frequency which is specimen-specific and is called cut-off frequency. In the cut-off frequency, the resistance of the resistor when subjected to DC is equal to the impedance of the capacitor (i.e., the same specimen subjected to AC).

Considering the characteristics of resistivity measurements by DC and AC, one might encounter a question as to which technique is more suitable for the goal pursued by this study. Obviously each measurement method has advantages and disadvantages. The problem with resistivity measurements using DC or very low-frequency AC is polarization [99]. Electric polarization is defined as the situation in which the centers of positive and negative charges within a resistance sample placed in an electric field do not coincide [39,103,104]. Electric polarization, when involved in resistivity measurements, results in unrealistically higher measured values of resistance. Polarization is of primary importance in dielectric materials and higher-resistivity materials [105], and electrically-conductive concrete (ECON) - with considerably lower resistivity than the normal PCC- is less susceptible to polarization. Furthermore, electrical polarization within a specimen is dependent on the measurement duration, so its effect on the measurement can be minimized by performing instantaneous resistance measurements.

Since the fluid phase in concrete has orders of magnitude higher conductivity than the vapor and solid phases, the conductivity of concrete is higher when the specimen is wet or saturated with liquid solution. Various factors are involved in the electricity conduction mechanism and/or measurement of electrical resistivity/conductivity of cementitious materials. Spragg et al. [53] postulated that specimen geometry, temperature of the specimen during the

test, specimen storage and conditioning are among key factors that should be considered in studying the electrical resistivity/conductivity of cement-based materials.

The most commonly used methods to characterize electrical conductivity of concrete are the wet and dry methods. The wet method measures the total electric charge that passes through a saturated specimen during a certain period of time upon application of a constant voltage across the specimen. In normal concrete, this charge travel happens primarily in the form of electrolytic conduction. The wet methods have mainly been used to characterize the permeability or the open pore network inside the concrete for indirect evaluation of concrete durability. Standard test procedures that employ the wet method include the rapid chloride permeability test specified in ASTM C 1202 [106], the surface resistivity method by using the Wenner probe [107], the bulk resistivity method by flowing sodium chloride (NaCl) solution in concrete specified in ASTM C 1760 [108], and the bulk resistivity method using plate electrodes [109].

The dry method measures the electrical charge through electrodes embedded in or attached to concrete by applying a constant voltage across the unsaturated specimen. The bulk resistivity method using embedded electrodes has been utilized in most previous studies focusing on conductive concrete for heating applications [45,74]. In the case of conductive concrete, the conduction of electricity during the dry method of the bulk resistivity test is mostly by means of electronic conduction. The dry method, unlike the wet method, can also be used for measurements of electrical properties of electrically conductive coatings.

### **Significance of Study on ECON HPS**

In spite of the popularity of ECON -related topics in research level, this technology has not yet gained considerable industrial/commercial popularity. This can be partially attributed to disadvantages such as inadequate strength, high cost, low workability, and poor functionality of

ECON encountered in previous studies [15]. Different mix designs for production of ECON has been proposed in the literature -such as the mixes proposed in references [11,42,61,63,64,67,77,91]-, however, the studies so far conducted on ECON have failed to provide an optimized mix design based on the applied materials. These studies suggest that optimization of ECON mix design, to achieve high conductivity and at the same time maintain adequate mechanical properties (workability, strength, and durability), is a daunting task warranting detailed experimental investigations. It is also inferred that the use of a single ECA type to achieve well-performing ECON has some limitations and challenges. The use of large quantities of a single ECA material required to achieve electrical conductivity can not only be cost-prohibitive, but can also exert negative effects on the mechanical characteristics in gardened concrete and rheological properties of in fresh/plastic state.

Optimization of ECON mix design is a highly challenging task which seeks to achieve high conductivity and at the same time maintain adequate mechanical properties (workability, strength, and durability). In order to achieve a mix design that can provide all required properties, one needs to have a good understanding of the effect of each mixture component on the characteristics of the final product. This study attempts to investigate the role of major components of an electrically conductive concrete - i.e. cement, aggregates, electrically conductive materials, additives, etc. - in the properties of the final product.

### **Literature Review on Electrically Conductive Coating (ECOT) Heated Pavement systems**

Application of ECOT in EHPS is a new and, to the best of authors' knowledge, unprecedented method for producing electrically heated concrete pavements. Polymer-based and portland cement-based coating on concrete substrates have been studied in previous works. The majority of studies investigating the coating application on portland cement concrete (PCC) and

asphalt concrete have focused on Water-repellence and water-proofing [110–118]. Information about electrically conductive coating on concrete surfaces is, however, scarce in the existing literature. Only some limited studies on application of epoxy resin-based [119] or portland cement-based [120,121] coatings as the anode in corrosion protection and/or chloride extraction practices have been conducted. Elsharkawy et al. [122] reported the feasibility of using water-repellent electrically-heated coatings for metallic surfaces using carbon nanofibers (CNF) dispersed in polymer matrix. Despite the importance of electrically conductive composites [123], they have not been extensively studied in the field of construction materials. The main applications of ECOT has been in circuitry [124], production of conductive papers [125,126], electromagnetic interference (EMI) shielding [127–129], and sensor systems [130–132]. Primary constituents of ECOT are electrically conductive filler materials - such as CB [133], CNT [134], CNF [127,129], or graphene [125,135]-, and polymer matrix [133].

Carbonaceous materials, such as carbon fibers [136,137], CNT/CNF [29,48,138–140], and graphite powders [121,141] are good candidates to be utilized as the electrically conductive filler in ECOT. Application of nano-size materials is limited in pavement applications because of high cost [137] and hazardous nature [142] of nanoparticles. Gong et al. [16] used carbon felt made of micrometer-size carbon fibers in an electrically conductive polymer composite. Ameli et al. [40] studied the feasibility of polyurethane-carbon fiber composite foam for EMI shielding, using carbon fibers with micrometer diameter and millimeter length. Hereinafter, the term carbon microfiber (CMF) is used to refer to carbon fibers with both diameter and length in micrometer scale. CMF materials are relatively inexpensive and do not pose health hazards, and their dispersion is less challenging.



Different nano- and micro-particles have been used to functionalize surface coatings and convert a simple coating into a smart material. Different studies have investigated the challenges and benefits of dispersing micro- and nanoparticles in different binder matrices and have studied the properties of the resultant composite material [111,113,143–150]. Materials such as diatomaceous earth [145], SiO<sub>2</sub> [144,151–156], SiO<sub>2</sub> nano-capsules [157], Zinc oxide (ZnO) [151,158–161], copper oxide (CuO) [162], Polyether ether ketone (PEEK) [145,149], Titanium dioxide (TiO<sub>2</sub>) [147,163], Ta<sub>2</sub>O<sub>5</sub> [164], Indium tin oxide (ITO) [151], carbon nanotube (CNT) and nanofiber (CNF) [29,32,129,138,155,165,166], and graphene particles [163] in micro- and nano-scale sizes are among the materials that have so far been incorporated into partially conductive or non-conductive matrices to alter their properties.

The performance and durability of coatings on a given substrate depends on the chemical composition of the coating materials, resistance to aggressive environmental conditions, and the strength of physical bond between the coating material and the substrate [167,168]. The chemical composition of the coating materials defines the occurrence of crosslinking and the adhesion of the coating to the surface. The morphology of the coating is controlled by both chemical composition of the coating materials and the presence of micro- and nano-scale particles.

The filler materials in a composite are the main components rendering a plain composite a smart material. However, when surface coatings are concerned, the matrix gains more importance because it is responsible for the coating durability and ease of production. The matrix phase in a coating is basically the binder which holds all other components together and adhere to the surface. Some coating applications do not include binder phase [169–172], for example, silane compounds were found to be effective as a binder phase in a superhydrophobic

coating mixture which was sprayed on the substrate [155]. Gao et al. [168] used silanes as a sprayable surface coating on concrete without other binder materials. Silanes and siloxanes have smaller molecular size than epoxy and acrylic that enables them to reach small pores and become more effective [167]. Hunek et al. [172] used methylsilicone resin in potassium hydroxide and alkoxysilane oligomer as two types of water-repellent coating materials that were simply applied on the Portland cement concrete surface by a brush and they did not use any additional binder material. Calabrese et al. [173] showed that silanes can be used as an adherent coating; in their research, they fabricated superhydrophobic composite of zeolite particle filler in a silane matrix for coating aluminum substrates. However, in the case of smart electrically conductive coatings, silanes or siloxanes are not viable materials to be used as the binder phase because they are not suitable for dispersing particles/fibers in them, are expensive for large-scale application, and do not provide the thickness required for a smart pavement coating [125,129,135,147,155].

Different polymers can be used as binder phase in smart electrically conductive coatings [167]. *Epoxy resin* has been used as a binder material on various surfaces such as Portland cement concrete [110,145], asphalt cement concrete [111,113,114], glass [152], and polymers to bind the nano-particles and adhere to the substrate. Fluorinated polymers such as Poly(vinylidene fluoride) (PVDF) have been used in coatings as a matrix to accommodate the nanoparticles in a polymer network [160,161]. Tiwari et al. [160] fabricate large-area sprayable superhydrophobic coatings with PVDF and PTFE as binder and filler respectively. However, because of low strength and weak binding ability of PVDF, it needs to be used in conjunction with other binders. Tiwari et al. [160] and Das et al. [41,129] utilized poly(ethyl 2-cyanoacrylate) (PECA) and Poly(methyl methacrylate) (PMMA) as additional binder materials in combination with PVDF. Bayer et al. [161] coupled PVDF with cyanoacrylate, rosin, and ZnO nanoparticles to fabricate

biocompatible coatings. Das et al. [174] used PVDF-PMMA coupled matrix in carbon nanofiber-polymer superhydrophobic and electrically conductive coating. Poly(methyl methacrylate) (PMMA) (a.k.a. acrylic) is an strong polymer that has been used as the binder phase in numerous coating mixtures [175]. The cross-linking ability of PMMA with other polymers and its potential to be functionalized by chemical compounds (such as fluorinated polymers) makes it a good choice as a binder materials [175]. Polyurethane and Polyurea compounds are a very wide variety of materials that provide superior binding and adhesion properties.

*Polyurethane and Polyurea elastomers* are formed typically by reaction between a diisocyanate (aromatic or aliphatic), a long-chain diol (or “macrodiol”), and a small molecule chain-extender diol or a diamine [176]. Polyurea elastomers are produced by reaction of an isocyanate with an amine compound. Polyurethane and Polyurea are also compatible with carbonaceous particles/fibers that are very frequently used material in fabrication of smart coating materials [32,166] and they can be functionalized with a very wide range of materials with different chemistries and size scales. Polyurethanes-based coatings have been safely used in contact with various chemical compounds that are products, by-products, or contaminations found in gas and oil industry [177]. Polyurethane binders have been used to effectively bind macro-sized [40], and nano-sized carbon fibers (CNT and CNF) [32,166]. Gao et al. [178] functionalized multi-walled carbon nanotubes by various linear or hyperbranched polycondensed polymers including polyureas, polyurethanes, and polyuria-polyurethane copolymers through in situ polycondensation approach. Sardon et al. [179] used (3-aminopropyl)triethoxysilane (APTES) to functionalize waterborne hybrid polyurethanes. Polyurethane/Polyurea compounds are also capable of interlinking with and be functionalized by different chemicals. Fir et al. [180] fabricated coatings for application on aluminum alloy by coupling Urea with

Poly(dimethylsiloxane) in a sol-gel process. Sabzi et al. [147] fabricated polyurethane-TiO<sub>2</sub> composite coating where polyurethane showed a good performance as a binding and surface-adherent material. Golovin et al. [181] studied the durability (wear resistance) of sprayable coating materials made with different combinations of binders and fillers (micr- and nanoparticles); they concluded that the coatings made with fluorinated polyurethane elastomer (FPU) as binder phase and 1H,1H,2H,2H-heptadecafluorodecyl polyhedral oligomeric silsesquioxane (F-POSS) as filler provided the most desirable durability.

Electrical conductive surface coatings are smart materials which provide multiple benefits varying in application from joule heating [122] to sensing [32]. Han et al. [155] applied carbon nanotube (CNT)-silane-silica composite to produce electrically conductive and superhydrophobic coatings. In this research, carbon nanotubes contributed to surface nano-roughness and electrical conductivity, silane acted as both water-repellent material and binder phase in the coating mixture. Silica nanoparticles were used to enhance surface roughness. Carbon nanofiber-polymer composites that provided both superhydrophobicity and electrical conductivity were produced in several studies [41,129,174].

### CHAPTER 3. INFLUENCE OF MIX DESIGN VARIABLES ON ENGINEERING PROPERTIES OF CARBON FIBER-MODIFIED ELECTRICALLY CONDUCTIVE CONCRETE

A journal paper published in the Journal of Construction and Building Materials

Alireza Sassani<sup>1</sup>, Halil Ceylan<sup>2</sup>, Sunghwan Kim<sup>3</sup>, Kasthurirangan Gopalakrishnan<sup>4</sup>, Ali Arabzadeh<sup>5</sup>, and Peter C. Taylor<sup>6</sup>

#### Abstract

This research was inspired by the need to optimize the mix design of electrically conductive concrete (ECON) for field implementation. Carbon fiber was used for producing ECON with different mixing proportions and constituents. Calcium nitrite-based corrosion inhibitor admixture and methylcellulose were used as conductivity-enhancing agent (CEA) and fiber-dispersive agent (FDA) respectively. Five easy-to-change mix design variables were evaluated for their effects on electrical conductivity and strength of ECON: carbon fiber dosage, fiber length, coarse-to-fine aggregate volume ratio (C/F), CEA dosage, and FDA dosage. The results approved the effectiveness of the applied CEA in improving electrical conductivity while positively influencing strength. Conductivity was significantly influenced by: fiber content, C/F, fiber length, and CEA dosage. The dosages of Fiber, CEA, and FDA exerted significant influence on compressive strength. C/F and FDA dosage were significant variables influencing flexural strength.

---

<sup>1</sup> Graduate Research Assistant, Civil, Construction and Environmental Engineering (CCEE), Iowa State University (ISU), Ames, IA, E-mail: [asassani@iastate.edu](mailto:asassani@iastate.edu)

<sup>2</sup> Professor, Director, Program for Sustainable Pavement Engineering and Research (PROSPER), CCEE, ISU, Ames, IA, E-mail: [hceylan@iastate.edu](mailto:hceylan@iastate.edu)

<sup>3</sup> Research Scientist, Institute for Transportation, ISU, Ames, IA, E-mail: [sunghwan@iastate.edu](mailto:sunghwan@iastate.edu)

<sup>4</sup> Research Associate Professor, Iowa State University, Ames, IA. Email: [rangan@iastate.edu](mailto:rangan@iastate.edu)

<sup>5</sup> Graduate Research Assistant, CCEE, ISU, Ames, IA, E-mail: [arab@iastate.edu](mailto:arab@iastate.edu)

<sup>6</sup> Director, National Concrete Pavement Technology Center, SU, Ames, IA, E-mail: [ptaylor@iastate.edu](mailto:ptaylor@iastate.edu)

## Introduction

Electrically conductive concrete (ECON) is a versatile type of concrete with potential benefits in different applications such as: self-sensing construction material for structural health monitoring practices [1–3], electromagnetic radiation reflector for electromagnetic interference (EMI) shielding [4–6], and resistance heating material in self-heating pavement systems [7–10]. Recent attention to ECON is mainly related to self-heating pavement systems [8, 11, 12] because of the inadequacy of common ice and snow removal methods [12–15].

The basic mixture components of ECON are cementitious materials, coarse and fine aggregates, water, electrically conductive additive (ECA), and possibly chemical admixtures [11]. Air-dried normal Portland cement concrete (PCC) has an electrical resistivity in a range between  $6.54 \times 10^5$  and  $11.4 \times 10^5 \Omega\text{-cm}$  [16], while, electrical resistivity of ECON is orders of magnitude lower ( $30 \Omega\text{-cm}$  to  $1.00 \times 10^4 \Omega\text{-cm}$ ) [4,12,17–20]. The primary source of electrical conductivity that renders ECON considerably more conductive than normal concrete is the ECA component that creates a continuous path for electricity conduction. ECA portion of ECON may consist of a single material or a mixture of two or more different materials all possessing high electrical conductivity. Forming a continuous network in concrete matrix by the ECA materials is referred to as percolation phenomenon and the volume content of ECA enabling the percolation is called the percolation threshold [21–23].

Since 1965, when the first patent related to ECON was issued [18], numerous mix designs have been proposed for production of electrically conductive cement paste, mortar, or concrete [4,22,24]. Carbon fiber is a material that has been used and tested as an ECA in production of electrically conductive cementitious composites for different purposes [7, 25, 26]. Moreover, previous research have postulated [27–29] that carbon fiber-reinforced concrete provides better characteristics in terms of freeze-thaw durability, tensile strength, fatigue

cracking, shrinkage cracking potential, and expansion cracking susceptibility. Wu et al. [12] produced carbon fiber-modified ECON with 4,000  $\Omega$ -cm resistivity using 0.8% (Vol.) carbon fiber dosage. While, Kraus and Naik [30] achieved 127  $\Omega$ -cm electrical resistivity with only 0.5% (Vol.) carbon fiber and Galao et al. [31] produced ECON with 40  $\Omega$ -cm resistivity using <0.2 % (Vol.) carbon fiber in the concrete mix. This shows that the electrical resistivity of carbon fiber-modified ECON is dependent on multiple factors and not only the carbon fiber dosage. Speaking of carbon fiber-related factors, in addition to carbon fiber dosage [12], the properties of the fibers such as fiber length [21,22], material origin (e.g. pitch-based or polyacrylonitrile-based) [22,32] , and the surface chemistry of carbon fiber strands [32,33] influence the effectiveness of fibers in modifying the properties of concrete. Percolation of fibers in concrete depends on dispersion level, that is, controlled by fiber properties, mixture constituents, mix proportions, and mixing procedure [21, 28, 34, 35]. Improved fiber dispersion leads to improved fiber-cement paste bond, higher ductility, and reduced electrical resistivity [33]. A variety of chemicals can be used for facilitating the dispersion of fibers in concrete mixture; methylcellulose is a fiber dispersive material that is effective in minor dosages [28, 36].

In both normal concrete and ECON, the mix design variables such as cement content, aggregate-to-cement volume ratio, and coarse-to-fine aggregate volume ratio (C/F) exert a significant influence on the electrical conductivity of the concrete [37–39]. In addition to the conventional applications of chemical admixtures - such as improvement of workability, air entrainment, etc.-, they can be used for engineering the internal environment of concrete to boost electricity conduction; for instance, calcium nitrite-based corrosion inhibitor admixtures can change the electrical conductivity of concrete [40,41]. While, sodium-based corrosion inhibitors tend to decrease the compressive strength of concrete, calcium compounds do not exert any

reducing effect on concrete strength properties; in fact, calcium nitrite, which is an anodic corrosion inhibitor, has been found to increase the 28-day compressive strength of concrete [42]. Due to the presence of different ionic entities within the pore solution, it acts as the primary medium for ion/charge transfer within the concrete. The principal ions in the pore solution that enable the flow of electricity are  $\text{Ca}^{2+}$ ,  $\text{K}^{+}$ ,  $\text{Na}^{+}$ ,  $\text{SO}_4^{2-}$ , and  $\text{HO}^{-}$  [16]. Hence, the ionic composition of pore solution and the ion concentration in the pore solution play an important role in electricity conduction by concrete [43]. It was reported, that when calcium nitrite is added to the mix water of concrete, the concentration of nitrite in the pore solution is comparable to the mix water, i.e. the majority of the nitrite is diffused in the pore solution. Furthermore, at high calcium nitrite contents, hydroxyl ions concentration in the pore solution is increased due to competitive adsorption of nitrite ions on the surface of cement hydration products [44, 45]. Therefore, calcium nitrite admixture tends to enhance electricity conduction by increasing the ion concentration in the pore solution of concrete.

Different materials have been proposed in the literature to improve the dispersion of synthetic and/or natural fibers. Examples are Acrylic with or without Silica fume, Styrene acrylic [28], Latex with or without Silica fume [46, 47], and Methyl cellulose [20]. Effective fiber dispersion by using Acrylic, Styrene Acrylic, and Latex is associated with high dosages of fiber dispersive agent (FDA) – in the range of 10 to 20% by weight of cementitious - [21,28,34]. On the contrary, the dosage of Methyl Cellulose as a FDA in carbon fiber-modified concrete/mortar can be as low as 0.4% by weight of cementitious materials [20, 36].

Developing an ECON mix design with desirable multifunctional behavior calls for adjusting all variables/constituents to achieve required electrical resistivity [39]. Furthermore, the final product should possess desirable mechanical properties. The majority of studies on



electrically conductive cementitious composites have followed a trial–error approach using trial mix batches [12]. Regarding the heterogeneity of concrete and the uncertainty it adds to the evaluation of different variables' effects on concrete properties [48], generalizing the results of such trial-and-error studies is not an efficient and reliable way for development of a mix design; on the other hand, the heterogeneity of concrete continuum is more significant in fiber-containing concrete [49]. There are limited studies investigating the electrical conductivity of ECON in light of the ratio of mixture constituents. Wen and Chung [38] studied the double percolation of carbon fibers and cement paste in mortar. Baeza et al. [39] investigated the double and triple percolation of carbon fibers, cement paste, and mortar within a concrete mixture. Another example is the study by Shi [37] that investigated the effect of cement composition, aggregate content, and mineral admixtures on electrical resistivity of plain concrete.

Application of ECON in a real project calls for developing a project-specific mix design or using a previously proposed mix design. However, most ECON products presented in the existing literature suffer from disadvantages such as inadequate strength, high cost, low workability, and poor functionality [50]. On the other hand, developing a mix design in a timely manner requires knowledge about the effect of each component on the final product's characteristics. The dynamic of modern markets being profit-driven [51], necessitates thorough investigation of any new technology –such as ECON- before it gains wide acceptance by the industries. Therefore, the needs have arisen to investigate the role of each component of ECON in order to enable the producers to tailor the final product to their needs.

The use of statistical design of experiments (DOE) and regression analysis of the results is a powerful means of evaluating the influence of different variables on concrete characteristics [52]. By this method, the main effects of single variables and the interactions can be

quantitatively evaluated with a certain confidence level [53]. ECON mix designs based on such pre-defined, structured DOE will be more rational and universal than those based on trial–error approach.

The primary objective of this study is to identify the effects of easy-to-change mix design variables on electrical conductivity and mechanical properties of ECON. The findings of this paper can provide a basis for developing an optimized ECON mix design that satisfies both electrical conductivity and strength requirements for a given project with efficient amount of ECA materials and admixtures. Therefore, it is worth mentioning that producing high-conductivity ECON samples did not lie within the scope of this research; rather, it was attempted to change different variables to evaluate their respective effects on the product characteristics. Furthermore, this paper -for the first time in the literature- investigates the application of calcium nitrite-based corrosion inhibitor admixtures as a conductivity-enhancing agent in ECON production. A statistical DOE was performed to develop an experimental plan for investigating the effects of five mix design variables on three different responses; then, the measurement results were analyzed by regression analysis.

## **Methodology and Materials**

### **Mix Design Variables**

Selected variables were carbon fiber content, carbon fiber length, Coarse-to-fine aggregate volume ratio (C/F), fiber-dispersive agent (FDA) dosage, and conductivity-enhancing agent (CEA) dosage (Table 3-1). Since electrical conductivity of concrete decreases with increase of aggregate volume [37], C/F ratio was used as a mix design variable instead of total aggregate volume. Methylcellulose and corrosion inhibitor admixture were used as FDA and CEA respectively.

A screening experiment design (a.k.a. 2k design, k being the number of variables) was used for evaluating the effect of each variable at two levels. Screening DOE enables the number of experiments for each variable to be minimized [53]. By applying a fractional factorial design, it was made possible to evaluate variable effects with reduced number of experiments. Nineteen ECON types, including three replicate center points, were produced. Table 3-2 gives the variable combinations for each mix design. The responses of the statistical model were electrical resistivity, compressive strength, and flexural strength. The DOE and analysis of results were performed using a commercial software (JMP®).

*Table 3-1 Variable description in the screening DOE.*

| Variable                    | Unit                           | Levels |      | Variable type |
|-----------------------------|--------------------------------|--------|------|---------------|
| <b>Carbon fiber content</b> | % of total mix volume (% Vol.) | 0.1    | 1.0  | Continuous    |
| <b>Carbon fiber length</b>  | mm                             | 6.0    | 12.0 | Categorical   |
| <b>C/F</b>                  | N.A.                           | 0.7    | 1.2  | Continuous    |
| <b>FDA dosage</b>           | % of the cement weight         | 0.0    | 0.4  | Continuous    |
| <b>CEA dosage</b>           | kg/m <sup>3</sup>              | 0.0    | 15.0 | Continuous    |

Note: N.A - Not Applicable.

The percolation transition zone of carbon fiber in mortar and concrete have been reported in the range of 0.4-1 % (Vol.) [12, 22]. Therefore, the fiber dosages were selected in the proximity of percolation threshold. Carbon fiber was supplied in three nominal lengths of 3, 6, and 12 mm. Because the fiber length added a categorical variable to the experiments and the higher fiber length is desirable for achieving electrical conductivity in concrete [12], the two longer fibers (6- and 12-mm) were used in order to minimize the number of categorical variables and evaluate the length effect in the higher length range. In addition, a previous study have

suggested that carbon fibers with 6-12.7 mm length were more desirable with respect to compressive and flexural strength than shorter fibers [54]. Fiber-dispersive agent was used in the optimum dosage range recommended in the literature [36]. Coarse-to-fine aggregate volume ratio was selected in the ranges recommended by Iowa DOT [55] for Portland cement concretes that can be used for both paving and construction purposes. Conductivity-enhancing agent was used in the manufacturer-recommended dosage range.

Table 3-2 Combination of variables for ECON mix designs.

| Mix design No. | Variable          |                        |      |                         |                                 |
|----------------|-------------------|------------------------|------|-------------------------|---------------------------------|
|                | Fiber length (mm) | Fiber content (% Vol.) | C/F  | FDA dosage (% wt. cem.) | CEA dosage (kg/m <sup>3</sup> ) |
| 1              | 6                 | 0.10                   | 1.20 | 0.4                     | 15.0                            |
| 2              | 12                | 0.10                   | 0.70 | 0.4                     | 15.0                            |
| 3              | 12                | 0.10                   | 1.20 | 0.4                     | 0.0                             |
| 4              | 6                 | 0.10                   | 1.20 | 0.0                     | 0.0                             |
| 5*             | 6                 | 0.55                   | 0.95 | 0.2                     | 7.5                             |
| 6              | 12                | 0.10                   | 1.20 | 0.0                     | 15.0                            |
| 7*             | 6                 | 0.55                   | 0.95 | 0.2                     | 7.5                             |
| 8              | 12                | 1.00                   | 0.70 | 0.4                     | 0.0                             |
| 9              | 6                 | 1.00                   | 0.70 | 0.0                     | 0.0                             |
| 10             | 6                 | 0.10                   | 0.70 | 0.4                     | 0.0                             |
| 11             | 6                 | 1.00                   | 0.70 | 0.4                     | 15.0                            |
| 12             | 12                | 0.10                   | 0.70 | 0.0                     | 0.0                             |
| 13             | 6                 | 1.00                   | 1.20 | 0.4                     | 0.0                             |
| 14             | 12                | 1.00                   | 1.20 | 0.0                     | 0.0                             |
| 15             | 6                 | 0.10                   | 0.70 | 0.0                     | 15.0                            |
| 16*            | 6                 | 0.55                   | 0.95 | 0.2                     | 7.5                             |
| 17             | 6                 | 1.00                   | 1.20 | 0.0                     | 15.0                            |
| 18             | 12                | 1.00                   | 1.20 | 0.4                     | 15.0                            |
| 19             | 12                | 1.00                   | 0.70 | 0.0                     | 15.0                            |

Note: \* sign marks the center points

## Mixture Components

Variation of C/F in a concrete mix requires adjustments to the entire mix proportions. In this study, C/F of the concrete mix design was a variable with two experimental levels and one additional level for center points. Therefore, to maintain the consistency among specimens, three basic normal Portland cement concrete (PCC) mixtures were designed as the basis upon which the ECON mix designs were developed by applying required changes to proportions and/or mixture components. According to the variable combination corresponding to each ECON type, the mix designs were made by replacing given volume fraction of fine aggregate with carbon fiber. In addition to carbon fiber, each ECON mix design had specific admixture requirements. After incorporation of carbon fiber and admixtures into the mix design, the required adjustments to the mix proportions were made in accordance to specific gravity and water absorption capacity of the materials to maintain fixed values of water-to-cement and C/F ratios. The amount of mix water was not changed during mixing; instead, water-reducing agent was used for achieving target slump of 75-100 mm.

Table 3-3 shows the mix proportions of the three PCC mix design types. Materials used in preparation of samples were as follows:

- ASTM C 33 [56] D-57 Coarse aggregate- nominal maximum size 25 mm.
- Fine aggregate conforming to ASTM C 33.
- ASTM C150 [57] type I/II cement manufactured by Holcim.
- ASTM C 494 [58] high-range water reducing – type F- admixture (MasterGlenium 7500 obtained from BASF).

- Methylcellulose in fine powder form as FDA. The FDA was dissolved in the mix water before being added to the batch. The FDA powder was gradually added to the water and hand-mixed in during 30 minutes; blender mixing was not used in order to prevent foaming.
- WR Grace & Co. Derex Corrosion Inhibitor (DCI) admixture used as CEA. Mix designs accounted for the extra water added to the mix by DCI.
- Chopped carbon fiber was polyacrylonitrile(PAN)-based with 7.2  $\mu\text{m}$  diameter, 95% carbon content, and electrical resistivity of  $1.55 \times 10^{-3} \Omega\text{-cm}$ . PAN-based carbon fiber gives better electrical conductivity than pitch-based types [12]. Two different length size classes of the same type carbon fiber were used, namely PX35-0.25 and PX35-0.50 with respectively 6 mm and 12 mm nominal length. Specific gravity and water absorption capacity of the carbon fiber were 1.81 and 7.35 (% wt.) respectively.

Table 3-3 Mix proportions of the basic PCC mixtures.

| Component               | Properties |                  |                    | Mix design C/F ratio |       |       |
|-------------------------|------------|------------------|--------------------|----------------------|-------|-------|
|                         |            |                  |                    | 0.7                  | 0.95  | 1.2   |
|                         | Type       | Specific gravity | Absorption (% wt.) | Volume fraction      |       |       |
| <b>Cement</b>           | Type I/II  | 3.15             | -                  | 0.135                | 0.135 | 0.135 |
| <b>Coarse aggregate</b> | Lime stone | 2.67             | 1.4                | 0.290                | 0.334 | 0.378 |
| <b>Fine aggregate</b>   | River sand | 2.49             | 1.7                | 0.395                | 0.351 | 0.307 |
| <b>Water</b>            | Tap water  | 1.00             | -                  | 0.180                | 0.180 | 0.180 |

## Sample Preparation and Electrical Resistivity Measurement

The ECON mix designs, as explained in the previous section, were used for making concrete samples. The batches were mixed using a 0.5 m<sup>3</sup>-capacity rotating pan mixer. Three batches were prepared with each mix design. From each batch three 100 × 200 mm cylinders, three 75×75×300 mm beams, and three 100×100×100 mm cubic specimens were prepared for compressive strength, flexural strength, and electrical resistivity measurements respectively. All specimens were cured at 100% relative humidity and 23° C temperature during the entire study. Compressive and flexural strength tests were respectively performed according to ASTM C 39 [59] and ASTM C 78 [60]. Electrical resistivity was measured at three ages (3, 7, and 28 days), while, compressive strength, and flexural strength were measured at 28-days.

The electrical resistance of a concrete specimen can be measured using direct current (DC) or alternating current (AC). The use of AC measurement is preferred due to difficulties associated with polarization effect and permanent microstructure changes induced by DC methods [61]. Commonly used techniques for measuring electrical resistivity of concrete are electrode probe method, Wenner probe and rapid chloride permeability test (RCPT). RCPT uses high voltage and DC current that limit each sample to only one measurement at a certain age because of permanent microstructure changes made to the concrete [61, 62]. Wenner probe technique uses low frequency AC that is associated with polarization; on the other hand, Wenner probe is designed to measure surface resistivity and has high dependency on surface texture, surface moisture, and specimen geometry [62]. Using electrode probes with AC measurements can determine the bulk resistivity of concrete specimens in a repeatable manner [62]. Electrode probe method has the advantages of rapid testing, repeatability, and simple geometry factor [62,

63]. Using AC with a frequency of 1,000 Hz eliminates the problems caused by electrode polarization and reactance [61].

The experimental setup for measuring electrical resistivity consisted of two copper mesh electrodes of compatible cross section embedded inside the concrete cubes as shown in Figure 3-1. Ohmic resistance across the concrete was measured on hardened specimens and electrical resistivity was calculated using Equation 3-1:

$$\rho = R (A/l) \quad ( \text{Equation 3-1} )$$

Where,  $\rho$  represents the electrical resistivity in ohm-centimeters ( $\Omega$ -cm),  $R$  is the electrical resistance in Ohms ( $\Omega$ ),  $A$  ( $\text{cm}^2$ ) is the cross sectional area between the electrodes normal to the current direction, and  $l$  (cm) is the electrode spacing measured for each specimen.

Factors affecting the measurement in electrode probe method are: (1) voltage, current, and frequency, (2) specimen geometry, (3) electrode contact, (4) degree of saturation of specimens, and (5) measurement temperature [61–64]. In this research, using low-current and low-voltage AC measurement with 1,000 Hz frequency and applying the required geometry factor ( $A/l$  in Eq. 3-1) maintained measurement consistency and helped avoid the problems associated with polarization, reactance, and microstructure change. Copper mesh electrodes were embedded in fresh concrete and vibration was applied in order to ensure good bond between electrode and cementitious matrix; presence of water in fully saturated specimens ensured full electrical contact between electrodes and concrete matrix. For a concrete specimen, higher degree of saturation and higher temperature lead to lower resistivity [63, 64]. On the other hand, electrolytic conduction (that is an important electricity conduction mechanism in concrete) occurs through capillary water that is present in >40% degree of saturation [63, 64]. Hence, in order to guarantee the consistency of measurements, involvement of electrolytic conduction, and



elimination of surface moisture effect all specimens were tested in saturated surface-dry condition and 23°C ambient temperature. Electrical resistance was measured by an LCR meter (BK Precision® 875B).

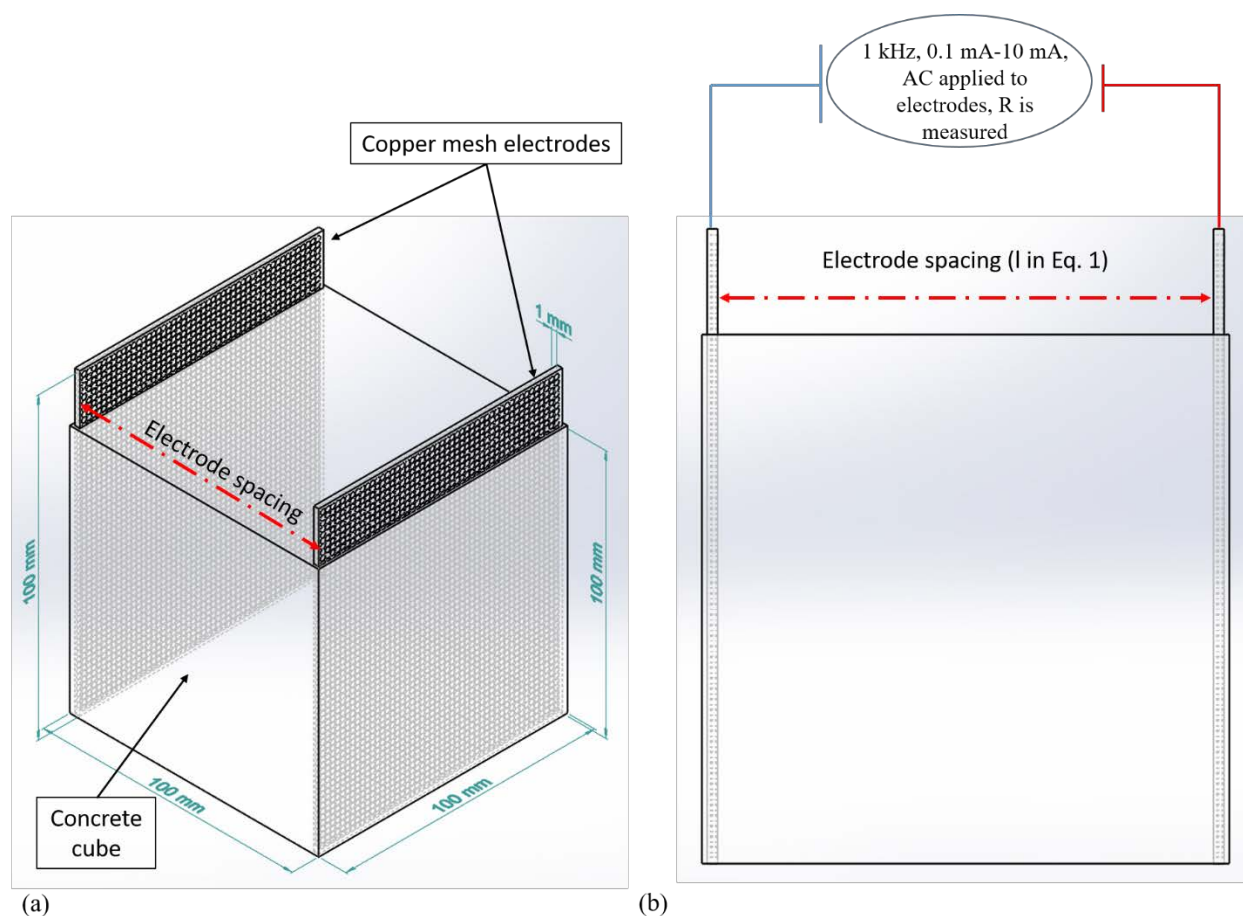


Figure 3-1 Electrical resistivity measurement specimen: (a) schematic of cubic ECON specimens with embedded electrodes, (b) measurement set-up.

### Data Analysis

Variable estimates were derived by standard least square regression analysis of the measured responses. This method applies a separate two-way analysis of variance (2-way ANOVA) on each response to generate a model for a particular response. The significance of each variable's effect on each response is then indicated by the p-value (i.e. probability) parameter. The confidence interval  $(1-\alpha)$  was selected as 0.95. A variable was considered to be

significant if its p-value was smaller than  $\alpha$ ; therefore, the effects corresponding to a p-value smaller than 0.05 would be significant. The smaller the p-value the higher the significance level. The estimates for a variable refer to the coefficients of the model built up by least square analysis [52]. The model feature of the software was used to simulate the effect of individual variables on the responses as well as the coupled variable interactions. For a  $2^k$  experiment design, a regression model is more natural and intuitive [53], therefore, in this research a regression model was used for analyzing the results as given in Equation 3-2 [53]:

$$y = \beta_0 + \sum_{i=1}^k \beta_i x_i + \sum \sum_{i < j} \beta_{ij} x_i x_j + \epsilon \quad (\text{Equation 3-2})$$

Where,  $y$  is the response,  $x_i$  and  $x_j$  are the coded variables,  $k$  is number of variables,  $\beta$ 's are regression coefficients, and  $\epsilon$  is random error. The third term on the right side of the equation shows the interaction between variables  $x_i$  and  $x_j$ ; significant interactions were included in the model.

## Results and Discussion

The test results used to derive the response prediction models are presented in Table 3-4. Considering the number of batches and prepared specimens explained in the previous section, each value in the table is the average of nine measurements. Table 3-5 shows the regression coefficients for each response and the predicted values are given in Table 3-6.

Table 3-4 Averaged measurement results for each mix design.

| Age (days)     |                   | 3                           |     | 7                           |     | 28                          |     | 28                         |     | 28                      |     |
|----------------|-------------------|-----------------------------|-----|-----------------------------|-----|-----------------------------|-----|----------------------------|-----|-------------------------|-----|
| Mix design No. | HRWR (% wt. cem.) | Resistivity ( $\Omega$ -cm) | SD  | Resistivity ( $\Omega$ -cm) | SD  | Resistivity ( $\Omega$ -cm) | SD  | Compressive strength (MPa) | SD  | Flexural strength (MPa) | SD  |
| 1              | 1.0               | 2,543                       | 125 | 3,370                       | 130 | 4,313                       | 326 | 55                         | 1.6 | 6.5                     | 2.2 |
| 2              | 1.0               | 2,263                       | 265 | 2,953                       | 318 | 3,730                       | 361 | 59                         | 2.6 | 5.5                     | 0.1 |
| 3              | 1.0               | 3,193                       | 181 | 4,023                       | 248 | 5,293                       | 320 | 44                         | 1.4 | 7.0                     | 0.4 |
| 4              | 1.0               | 4,197                       | 536 | 4,873                       | 560 | 5,890                       | 541 | 46                         | 0.7 | 6.0                     | 0.6 |
| 5              | 1.0               | 2,583                       | 258 | 2,837                       | 104 | 3,177                       | 281 | 50                         | 1.6 | 8.0                     | 1.5 |
| 6              | 1.0               | 2,963                       | 187 | 3,560                       | 192 | 3,943                       | 264 | 65                         | 3.0 | 8.5                     | 0.5 |
| 7              | 1.0               | 2,457                       | 35  | 2,670                       | 44  | 2,910                       | 167 | 52                         | 1.4 | 6.0                     | 0.8 |
| 8              | 3.0               | 897                         | 38  | 1,087                       | 55  | 1,163                       | 58  | 37                         | 0.4 | 6.5                     | 0.5 |
| 9              | 3.0               | 988                         | 170 | 1,107                       | 237 | 1,563                       | 313 | 22                         | 0.1 | 5.5                     | 0.9 |
| 10             | 3.0               | 2,673                       | 58  | 3,567                       | 104 | 4,093                       | 129 | 45                         | 3.1 | 7.0                     | 0.1 |
| 11             | 2.0               | 1,350                       | 30  | 1,520                       | 30  | 1,753                       | 29  | 53                         | 1.6 | 7.5                     | 0.2 |
| 12             | 1.0               | 3,953                       | 59  | 4,593                       | 60  | 5,373                       | 32  | 52                         | 2.3 | 6.0                     | 0.4 |
| 13             | 2.5               | 1,997                       | 95  | 2,273                       | 127 | 2,643                       | 129 | 39                         | 4.0 | 7.0                     | 0.7 |
| 14             | 3.0               | 600                         | 66  | 647                         | 68  | 800                         | 87  | 20                         | 2.7 | 6.5                     | 0.4 |
| 15             | 1.0               | 2,697                       | 35  | 2,727                       | 21  | 3,297                       | 42  | 66                         | 0.5 | 6.0                     | 0.5 |
| 16             | 1.0               | 2,080                       | 80  | 2,323                       | 32  | 2,750                       | 55  | 53                         | 2.9 | 7.0                     | 1.1 |
| 17             | 2.5               | 1,950                       | 141 | 2,337                       | 180 | 2,653                       | 176 | 31                         | 5.2 | 6.5                     | 0.3 |
| 18             | 2.5               | 1,463                       | 45  | 1,737                       | 67  | 1,983                       | 32  | 60                         | 1.2 | 9.0                     | 0.8 |
| 19             | 3.0               | 780                         | 56  | 870                         | 62  | 1,110                       | 89  | 24                         | 4.5 | 5.5                     | 0.5 |

Note: HRWR=high range water reducing admixture, SD=standard deviation

Table 3-5 Regression coefficients of the model for the three responses.

| Parameters                          | Responses              |                      |                    |
|-------------------------------------|------------------------|----------------------|--------------------|
|                                     | Electrical resistivity | Compressive strength | Modulus of rupture |
| Regression coefficients             |                        |                      |                    |
| Intercept ( $\beta_0$ )             | 3055.2                 | 45.8                 | 6.74               |
| Fiber content                       | -1391.5                | -9.1                 | 0.07               |
| Fiber length                        | 130.6                  | 0.7                  | -0.06              |
| C/F                                 | 339.8                  | 0.3                  | 0.49               |
| CEA dosage                          | -252.3                 | 6.8                  | 0.19               |
| FDA dosage                          | 21.5                   | 4.1                  | 0.32               |
| Fiber content $\times$ CEA dosage   | 418.5                  | -0.5                 | 0.14               |
| Fiber content $\times$ Fiber length | 269.0                  | 0.7                  | 0.06               |
| C/F $\times$ Fiber length           | 259.4                  | -2.0                 | -0.45              |
| Fiber content $\times$ FDA dosage   | 155.6                  | 7.4                  | 0.47               |
| C/F $\times$ FDA dosage             | 96.8                   | 0.3                  | -0.10              |
| CEA dosage $\times$ FDA dosage      | 75.6                   | 1.1                  | -0.04              |
| Fiber length $\times$ FDA dosage    | -96.5                  | -0.9                 | 0.17               |

Table 3-6 Comparison of measured and predicted responses.

| Mix design No. | Electrical resistivity ( $\Omega$ -cm) |           |          | Compressive strength (MPa) |           |          | Modulus of rupture (MPa) |           |          |
|----------------|--|-----------|----------|----------------------------|-----------|----------|--------------------------|-----------|----------|
|                | Measured                               | Predicted | Residual | Measured                   | Predicted | Residual | Measured                 | Predicted | Residual |
| 1              | 4,313                                  | 4,269     | 45       | 55.3                       | 55.9      | -0.5     | 6.6                      | 6.4       | 0.2      |
| 2              | 3,730                                  | 3,775     | -45      | 58.8                       | 58.2      | 0.5      | 5.4                      | 5.6       | -0.2     |
| 3              | 5,293                                  | 5,320     | -26      | 43.9                       | 46.7      | -2.7     | 6.9                      | 7.3       | -0.4     |
| 4              | 5,890                                  | 5,878     | 12       | 46.5                       | 48.9      | -2.5     | 6.2                      | 6.5       | -0.2     |
| 5              | 2,970                                  | 2,946     | 24       | 50.7                       | 51.5      | -0.8     | 6.6                      | 7.0       | -0.4     |
| 6              | 3,943                                  | 3,860     | 84       | 65.1                       | 65.4      | -0.3     | 8.6                      | 8.2       | 0.4      |
| 7              | 3,060                                  | 2,946     | 114      | 50.9                       | 51.5      | -0.6     | 7.2                      | 7.0       | 0.2      |
| 8              | 1,163                                  | 1,119     | 45       | 37.2                       | 37.7      | -0.5     | 6.5                      | 6.3       | 0.2      |
| 9              | 1,563                                  | 1,480     | 84       | 22.2                       | 22.4      | -0.3     | 5.6                      | 5.2       | 0.4      |
| 10             | 4,093                                  | 4,067     | 26       | 44.5                       | 41.8      | 2.7      | 6.9                      | 6.5       | 0.4      |
| 11             | 1,753                                  | 1,780     | -26      | 52.8                       | 55.6      | -2.7     | 7.6                      | 8.0       | -0.4     |
| 12             | 5,373                                  | 5,386     | -12      | 51.7                       | 49.2      | 2.5      | 6.2                      | 6.0       | 0.2      |
| 13             | 2,643                                  | 2,688     | -45      | 38.6                       | 38.1      | 0.5      | 7.1                      | 7.3       | -0.2     |
| 14             | 800                                    | 884       | -84      | 20.0                       | 19.7      | 0.3      | 6.5                      | 6.9       | -0.4     |
| 15             | 3,297                                  | 3,380     | -84      | 65.6                       | 65.4      | 0.3      | 6.0                      | 6.4       | -0.4     |
| 16             | 2,807                                  | 2,946     | -139     | 53.0                       | 51.5      | 1.4      | 7.1                      | 7.0       | 0.1      |
| 17             | 2,653                                  | 2,666     | -12      | 31.0                       | 28.5      | 2.5      | 6.5                      | 6.2       | 0.2      |
| 18             | 1,983                                  | 1,957     | 26       | 60.4                       | 57.7      | 2.7      | 8.9                      | 8.6       | 0.4      |
| 19             | 1,110                                  | 1,098     | 12       | 23.5                       | 26.0      | -2.5     | 5.3                      | 5.5       | -0.2     |

### Effect of Variables on ECON Electrical Resistivity

Table 3-7 presents p-values and the respective values of standard error (SE) for the main and coupled effects of variables on electrical resistivity of ECON. Concerning only main effects, for the selected confidence interval ( $1-\alpha = 0.95$ ) four variables (fiber content, fiber length, C/F, and CEA dosage) were found to be significant at all ages with the p-values smaller than 0.05.

FDA dosage was significant only at the 3-day age. This indicated that variable are likely age-dependent. Variation of FDA effectiveness with cement hydration time can be attributed to the effect of porosity at early ages when fibers are clustered/flocculated in absence of FDA. Nevertheless, as the results showed, the influence of FDA on conductivity was dwarfed by evolution of cement hydration. This is also in agreement with the findings of previous studies of the effect of porosity and hydration on electrical resistivity of normal concrete [37–39, 61]. Therefore, 28-day measurement results would be more reliable than earlier ages because cement has undergone most of its hydration by this age. Considering 28-day results analysis, fiber content and C/F ratio having infinitesimally small p-values were the most significant variables followed by CEA dosage and fiber length.

Although the main effects of variables can reveal the importance of individual variables, the analyses results should also account for any existing interactions between variables. As shown in Table 3-7, some interactions between the studied variables were found to be significant at 28 days with p-values smaller than 0.05. These are the fiber content  $\times$  CEA dosage coupled effect, the fiber content  $\times$  fiber length coupled effect, the C/F  $\times$  fiber length coupled effect, and the fiber content  $\times$  FDA dosage coupled effect.

### **ECON Electrical Resistivity Response Prediction**

Figure 3-2 shows the predicted-versus-measured electrical resistivity values at 28-day age. The standard error of estimate (SEE) for prediction of 28-day electrical resistivity was 4.7 ( $\Omega$ -cm) which is 0.15% of the mean measured resistivity. The SEE and coefficient of determination ( $R^2$ ) showed a strong correlation between the predicted and measured resistivity values (Figure 3-2).

Table 3-7 Effect of the variables on electrical resistivity.

| Variables                           | Age (days) |      |          |      |          |      |
|-------------------------------------|------------|------|----------|------|----------|------|
|                                     | 3          |      | 7        |      | 28       |      |
|                                     | P-value    | SE   | P-value  | SE   | P-value  | SE   |
| <b>Fiber content</b>                | 0.00E+00   | 2.77 | 0.00E+00 | 3.07 | 0.00E+00 | 3.27 |
| <b>Fiber length</b>                 | 5.35E-07   | 2.57 | 5.27E-05 | 2.85 | 3.04E-06 | 3.27 |
| <b>C/F</b>                          | 4.00E-09   | 2.77 | 0.00E+00 | 3.07 | 0.00E+00 | 2.70 |
| <b>CEA dosage</b>                   | 1.51E-06   | 2.50 | 1.58E-07 | 3.07 | 1.20E-09 | 3.27 |
| <b>FDA dosage</b>                   | 3.03E-04   | 2.77 | 7.11E-01 | 3.00 | 5.16E-01 | 2.60 |
| <b>Fiber content × CEA dosage</b>   | 0.00E+00   | 2.77 | 0.00E+00 | 3.07 | 0.00E+00 | 3.27 |
| <b>Fiber content × Fiber length</b> | 1.42E-07   | 2.77 | 1.19E-08 | 3.07 | 2.00E-10 | 3.27 |
| <b>C/F × Fiber length</b>           | 4.52E-07   | 2.77 | 1.32E-08 | 3.00 | 6.00E-10 | 3.20 |
| <b>Fiber content × FDA dosage</b>   | 0.00E+00   | 2.70 | 1.11E-08 | 2.80 | 2.25E-05 | 3.27 |
| <b>C/F × FDA dosage</b>             | 1.11E-01   | 2.77 | 7.51E-01 | 3.07 | 5.89E-02 | 3.27 |
| <b>CEA dosage × FDA dosage</b>      | 6.41E-01   | 2.77 | 4.72E-01 | 3.07 | 1.66E-01 | 3.27 |
| <b>Fiber length × FDA dosage</b>    | 8.25E-02   | 2.77 | 3.72E-01 | 3.07 | 5.52E-02 | 3.27 |

Note: × sign shows interaction between two variables.

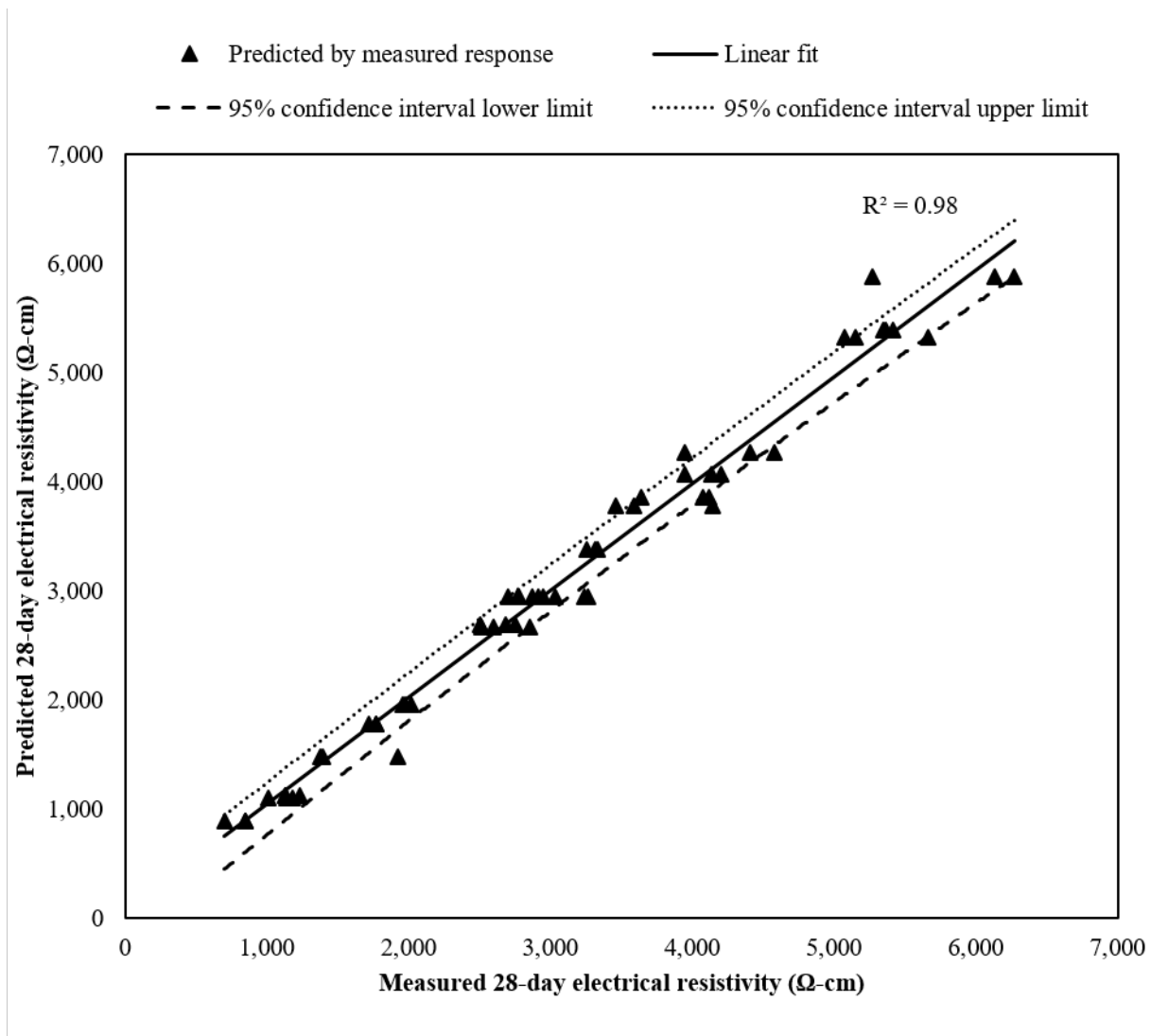


Figure 3-2 Predicted-versus-measured values of electrical resistivity at 28-day age.

### Sensitivity Assessment of Variables for ECON Electrical Resistivity Response

Figure 3-3 shows the prediction profiler for the variation of resistivity with each variable at 28 days. Resistivity decreased with increasing fiber content, fiber length, CEA dosage, and FDA dosage, whereas, higher C/F led to increased resistivity. Electrical resistivity exhibited a decreasing trend by the increase of fiber dosage; however, the rate of resistivity drop by fiber addition was reduced at higher fiber dosages. This is in agreement with the findings of Baeza et al. [39] who showed that the electrical resistivity decreasing rate significantly reduced beyond



fiber dosage of 0.5% (Vol.). It was also suggested by Baeza et al. [39] that higher coarse-to-fine aggregate ratio gives higher electrical resistivity. This effect was also observed and verified in this research as shown in Figure 3-3, where, increasing the C/F resulted in the higher electrical resistivity. As Figure 3-3 reveals, the CEA showed a significant reducing effect on electrical resistivity, however, this effect was dependent on synergic influence of fiber content and CEA dosage as will be discussed later on.

Indicated by the slope of resistivity-FDA dosage line in Figure 3-3, the effect of FDA dosage was negligible that is in agreement with the calculated p-value ( $5.16E-01$  in Table 3-7). Several studies have shown the effectiveness of methylcellulose in improving carbon fiber dispersion [28,47,65,66] and electrical conductivity [65,66] of cementitious composites using mortar or cement paste samples. Methyl cellulose was used for improving carbon fiber dispersion in concrete samples [12], however, the degree of effectiveness was not reported. Using cement paste and mortar test results, it was postulated that methyl cellulose provides desirable effectiveness particularly when used in combination with silica fume [28, 36]. In this study, methylcellulose was used as the only fiber-dispersive material; hence, its low effect on improvement of electrical conductivity comes in agreement with the findings of previous studies. Nevertheless, the effectiveness level of the material in concrete still needs to be more deeply investigated.

Figure 3-4 shows all significant interactions for electrical resistivity response. According to Figure 3-4(a), electrical resistivity decreased with increasing fiber content regardless of whether or not FDA was applied. However, above a certain fiber content (0.55%) the FDA-modified mixes gave higher predictions for electrical resistivity. Figure 3-4(b) reveals that CEA was more effective in low fiber contents. Up to 0.87% fiber content the CEA-modified mixes

showed lower electrical resistivity, however, as fiber content increased the difference between the CEA-modified and non-modified mixes became smaller. Above 0.87% fiber content the predicted resistivity values for CEA-modified mixes exceeded those of non-modified ECON.

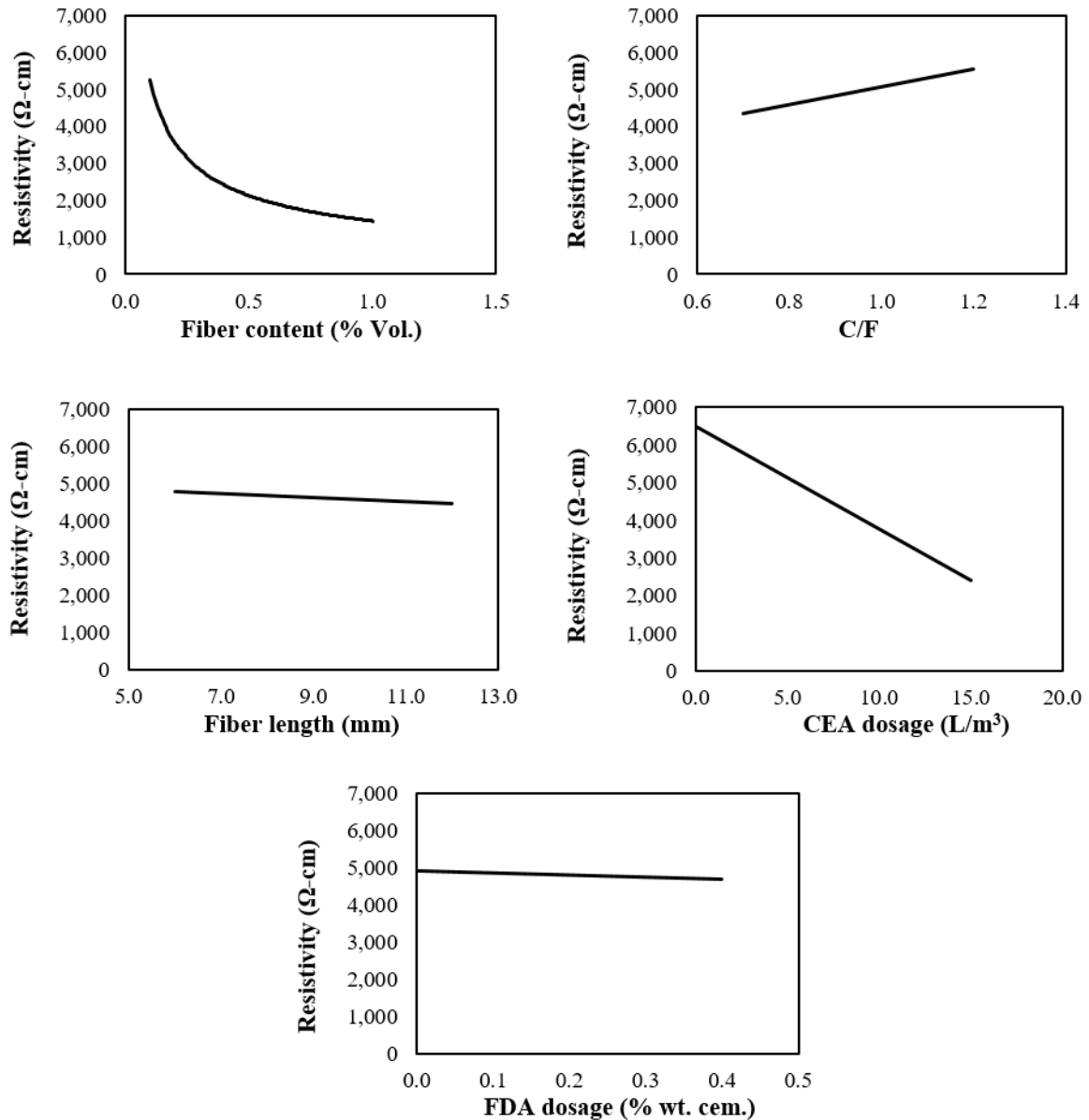


Figure 3-3 Sensitivity assessment of individual variables for electrical resistivity response.

Figure 3-4(c) reveals that with both fiber size classes electrical resistivity decreased by fiber content while the resistivity of ECON was less sensitive to variation of fiber content in the

case of 6-mm fiber. Regarding the coupled effect of fiber length and C/F (Figure 3-4(d)), with 6-mm fiber electrical resistivity dramatically increased by increasing C/F, whereas, it was negligibly increased in the case of 12-mm fiber.

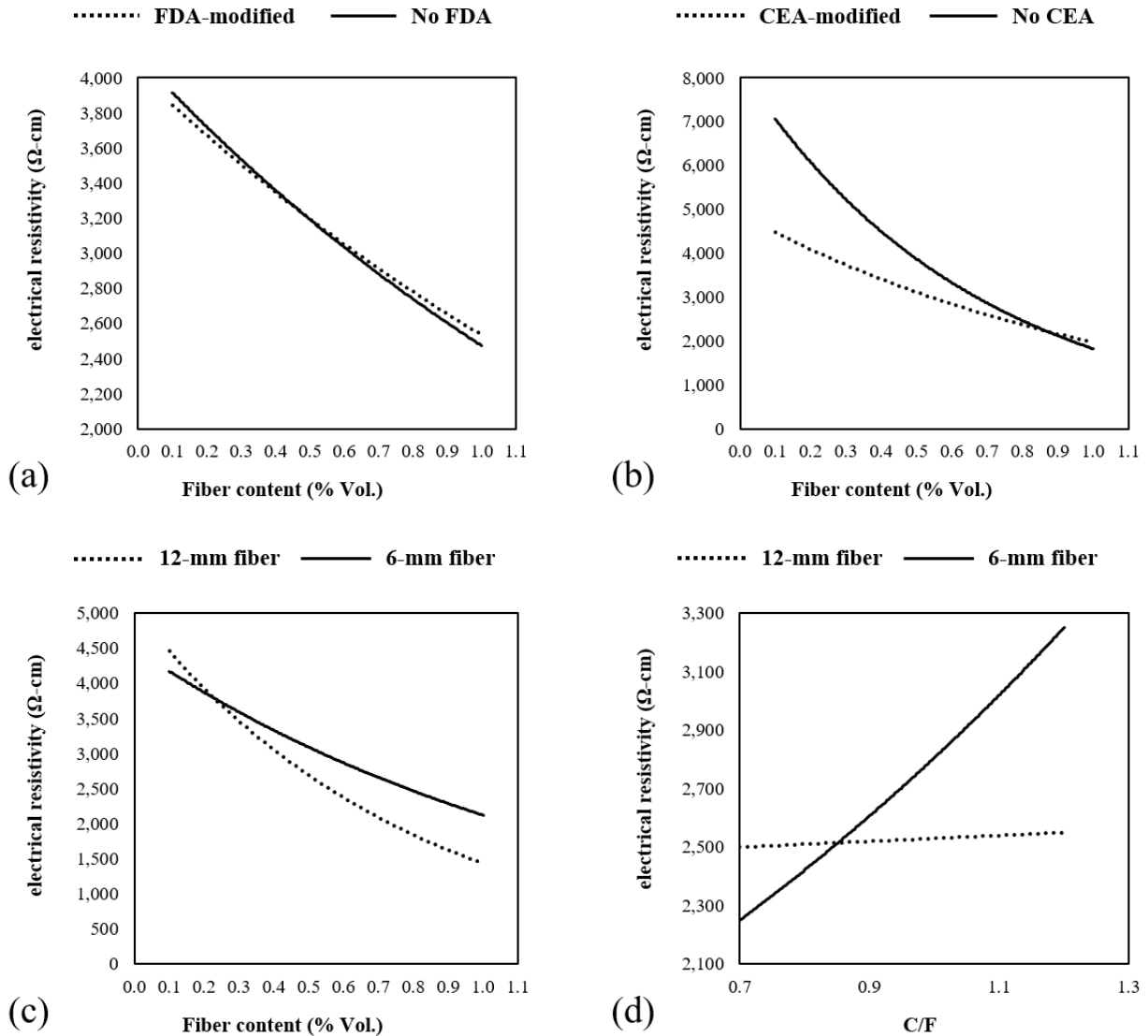


Figure 3-4 Sensitivity assessment of significant variable interactions on electrical resistivity response: (a) FDA dosage-fiber content coupled effect, (b) CEA dosage-fiber content coupled effect, (c) fiber length-fiber content coupled effect, and (d) fiber length.

### Effect of Variables on ECON Strength Properties

Variable effects on strength properties are shown in Table 3-8. Regarding the p-values of main effects, three variables of fiber content, CEA dosage, and FDA dosage were significant with respect to compressive strength, while, only C/F ratio and FDA dosage were significant variables influencing flexural strength. The interactions between the studied variables identified to be significant are the C/F× fiber length coupled effect on compressive strength, the C/F × fiber length coupled effect on flexural strength, the fiber content × FDA dosage coupled effect on compressive strength, and the fiber content × FDA dosage on flexural strength.

Table 3-8 Effect of the variables on compressive and flexural strengths.

| Variables                           | Response             |      |                   |      |
|-------------------------------------|----------------------|------|-------------------|------|
|                                     | Compressive strength |      | Flexural strength |      |
|                                     | P-value              | SE   | P-value           | SE   |
| <b>Fiber content</b>                | 0.00E+00             | 0.45 | 5.79E-01          | 0.12 |
| <b>Fiber length</b>                 | 5.82E-01             | 0.45 | 3.35E-01          | 0.12 |
| <b>C/F</b>                          | 5.41E-01             | 0.41 | 2.79E-04          | 0.13 |
| <b>CEA dosage</b>                   | 0.00E+00             | 0.45 | 1.36E-01          | 0.12 |
| <b>FDA dosage</b>                   | 0.00E+00             | 0.46 | 1.18E-02          | 0.18 |
| <b>Fiber content × CEA dosage</b>   | 2.56E-01             | 0.45 | 2.65E-01          | 0.12 |
| <b>Fiber content × Fiber length</b> | 1.36E-01             | 0.41 | 6.43E-01          | 0.13 |
| <b>C/F × Fiber length</b>           | 7.28E-05             | 0.45 | 6.04E-04          | 0.12 |
| <b>Fiber content × FDA dosage</b>   | 0.00E+00             | 0.45 | 3.98E-04          | 0.12 |
| <b>C/F × FDA dosage</b>             | 4.53E-01             | 0.43 | 4.01E-01          | 0.12 |
| <b>CEA dosage × FDA dosage</b>      | 1.17E-01             | 0.45 | 7.48E-01          | 0.13 |
| <b>Fiber length × FDA dosage</b>    | 6.28E-02             | 0.46 | 1.76E-01          | 0.11 |

### ECON Strength Response Prediction

The predicted versus measured response plots for compressive strength and flexural strength are respectively given in Figure 3-5 and Figure 3-6. Compressive strength predictions gave good convergence for predicted and measured responses with a SEE of 2.7 (6% of measured data mean) and coefficient of determination of 0.96. The accuracy of flexural strength predictions with a SEE of 0.73 (i.e. 11% of measured data mean) and coefficient of determination of 0.58 was not as good as compressive strength predictions.

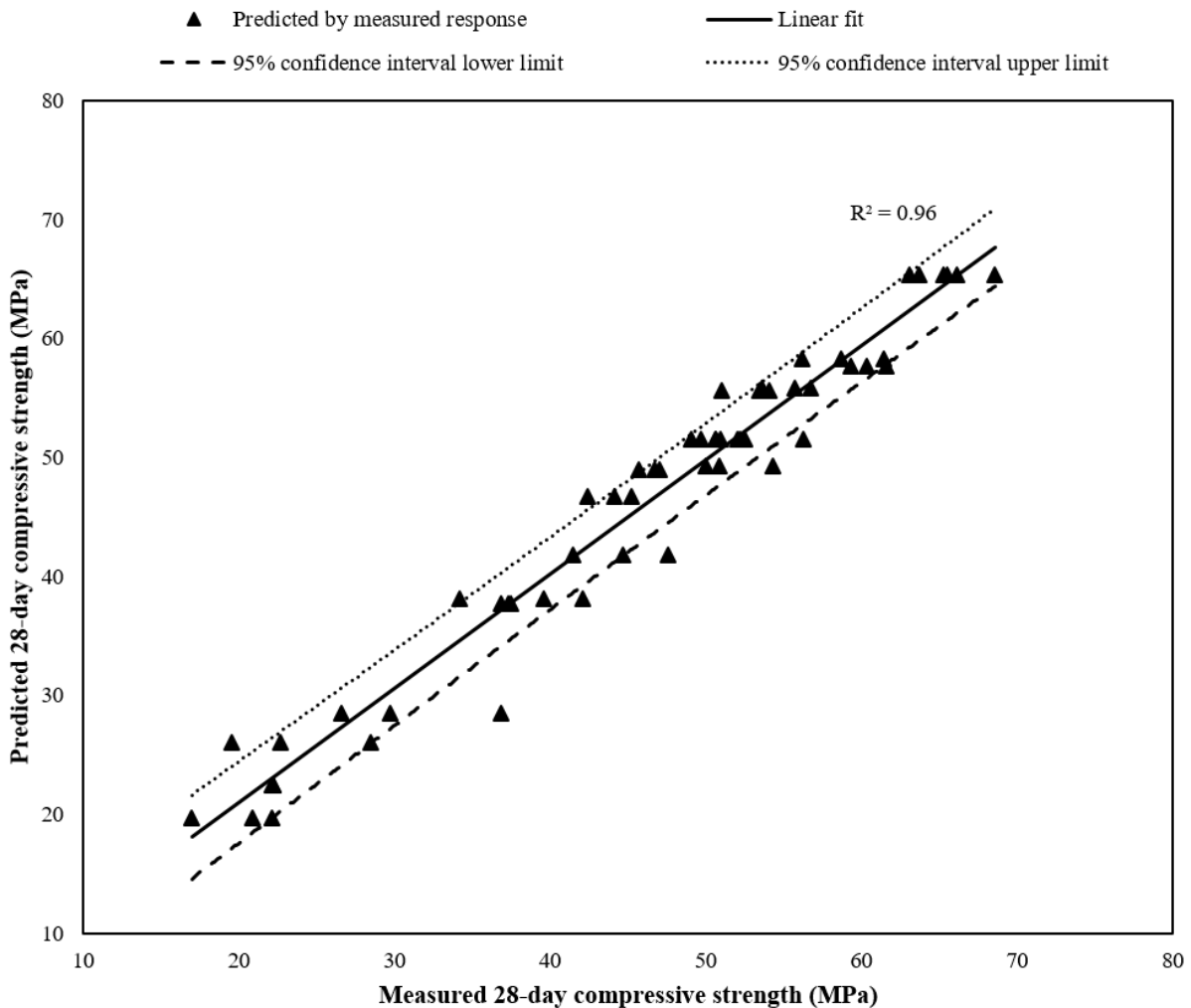


Figure 3-5 Predicted-versus-measured values of compressive strength.

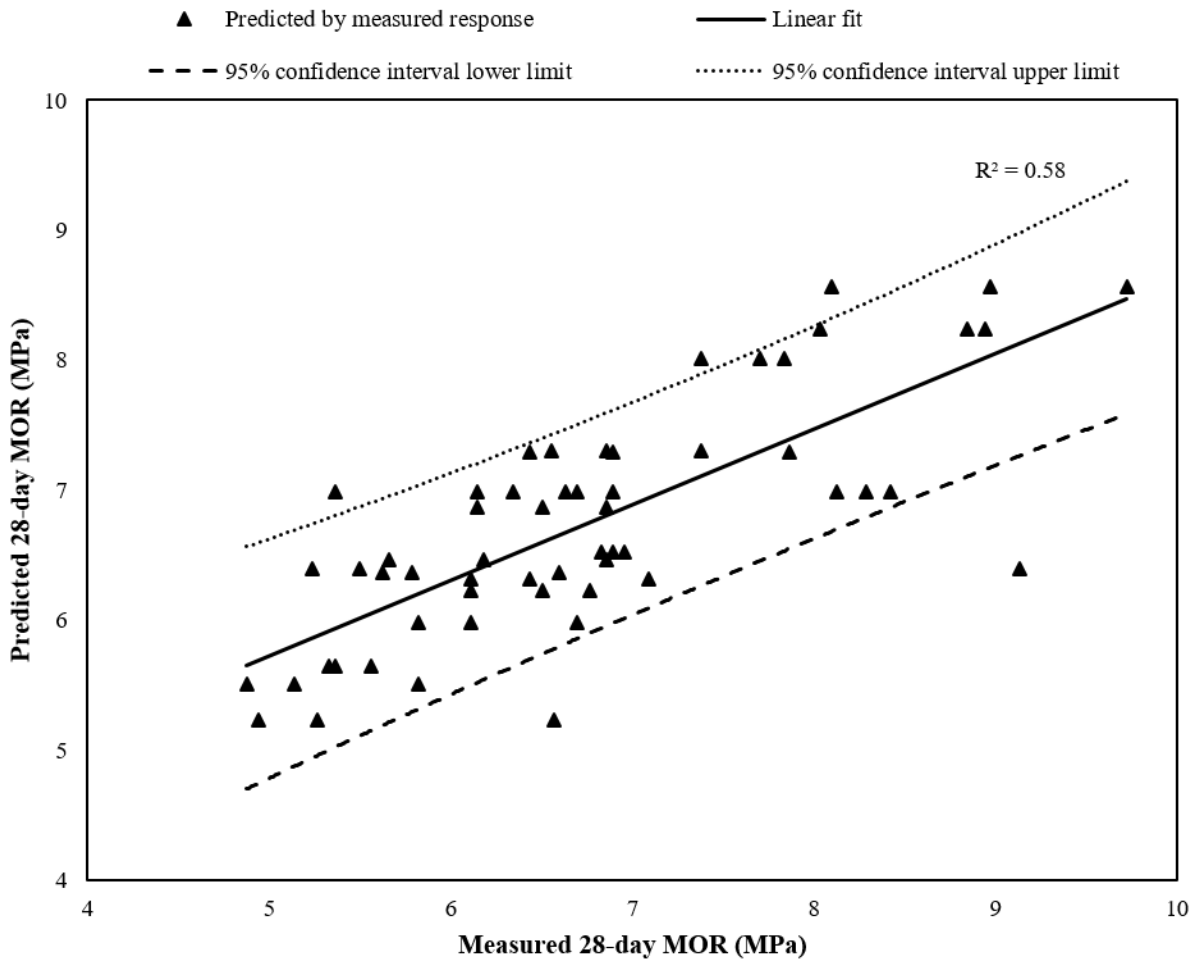


Figure 3-6 Predicted-versus-measured values of flexural strength.

### Sensitivity Assessment of Variables for ECON Strength Property Responses

Figure 3-7 and Figure 3-8 respectively present the prediction profilers for compressive and flexural strengths with respect to each variable. As revealed in Figure 3-7, fibers positively affected compressive strength only to a certain fiber content (0.55%). Unlike compressive strength, flexural strength maintained a constantly increasing trend with increasing fiber content; however, this effect is tied to the coupled effect of variables and needs to be discussed with regard to interaction of fiber content and FDA dosage.

Both compressive and flexural strengths were increased with increasing CEA dosage or using longer fibers. Positive effect of fiber length on compressive strength is in contrast to the findings of Chen and Chung [54] who showed that in mortar samples, compressive strength decreases by fiber length while flexural strength is improved. However, the difference of the behavior of mortar and concrete samples makes it difficult to compare these two conclusions. Increasing fiber dosage up to 0.55% (Vol.) improved compressive strength, while, beyond 0.55% the compressive strength decreased by increasing the fiber dosage. This can be attributed to the higher void content of concrete when fiber dosage passes a certain threshold [67].

Higher C/F or higher FDA dosage resulted in lower compressive and flexural strengths. Xu and Chung [36] postulated that application of methylcellulose up to 0.8% (wt. cem.) improved tensile strength and decreased compressive strength of cement pastes. Also, carbon fiber in dosages up to 4% (Vol.) was used with methylcellulose as dispersive agent to improve flexural strength of carbon fiber-reinforced cement pastes [65]; however, the effect was not compared with fiber-reinforced samples without methylcellulose. The reduction of compressive strength by methylcellulose found in this research is in agreement with the findings of the previous studies, while, the reduction of flexural strength in carbon fiber-reinforced concrete samples has not been reported in the existing literature. On the contrary, Chen and Chung [54] reported slight improvement of flexural strength of carbon fiber-reinforced concrete by application of methyl cellulose; however, they used very low fiber dosage (0.2% Vol.). Note that the effects of fiber length and C/F variables on compressive strength as well as the effects of fiber content, fiber length, and CEA dosage on flexural strength were non-significant.

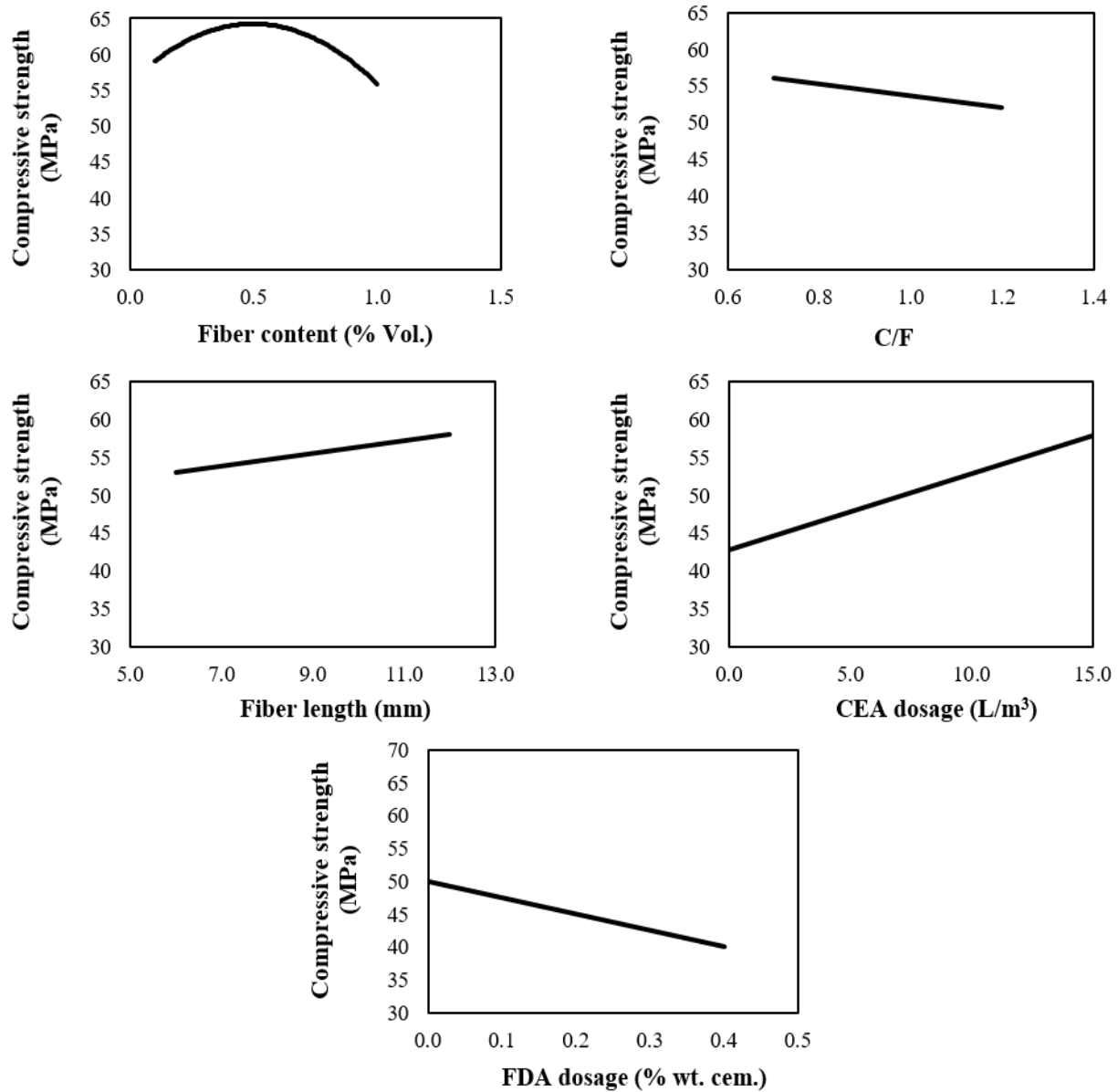


Figure 3-7 Sensitivity assessment of individual variables on compressive strength responses.

Figure 3-9 shows all significant interactions for strength property responses. Figure 3-9 (a) and (b) show the interaction of FDA and fiber content in the case of compressive and flexural strengths respectively. In absence of FDA, compressive strength followed a decreasing trend with increasing fiber content. The variation of compressive strength with fiber content was not steady in presence of FDA. Up to 0.55% fiber content, FDA application led to increased



compressive strength. Beyond this percentage, compressive strength experienced a falling trend with increase of fiber content. Without FDA addition, increasing fiber content resulted in lower flexural strength.

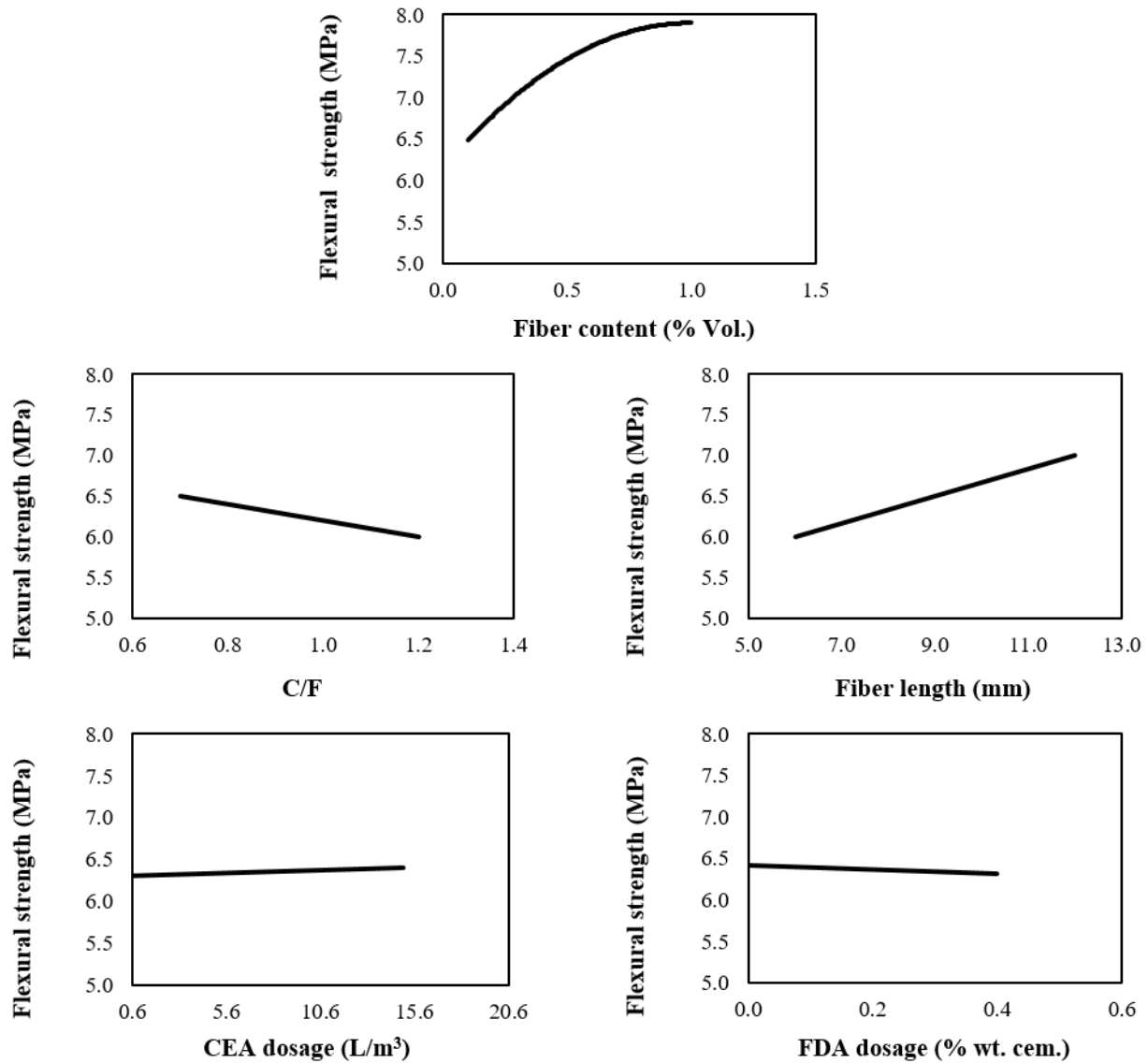


Figure 3-8 Sensitivity assessment of individual variables on flexural strength.

However, when FDA was present, the flexural strength increased with increasing fiber content. Carbon fiber-reinforced concrete is expected to exhibit better flexural behavior than normal PCC [68]. The results of this research do not contradict this statement; rather, it shows

that in carbon fiber-reinforced concrete in absence of FDA increasing the amount of fiber led to flexural strength reduction. On the contrary, when FDA was used to enhance the dispersion of fibers, a higher efficiency was observed in improving flexural behavior. Based on this observation, higher fiber content leads to higher flexural strength.

As seen in Figure 3-9(c), the effect of C/F on compressive strength was different between the ECONs containing 6-mm and 12-mm fibers. Simulations showed that when the ECON was made with 6-mm fibers, compressive strength decreased with increasing C/F, whereas, it followed an opposite trend with 12-mm fiber. When 6-mm fiber was used, flexural strength slightly decreased by increasing C/F; on the contrary, higher C/F resulted in considerably higher flexural strength upon application of 12-mm fiber (Figure 3-9(d)).

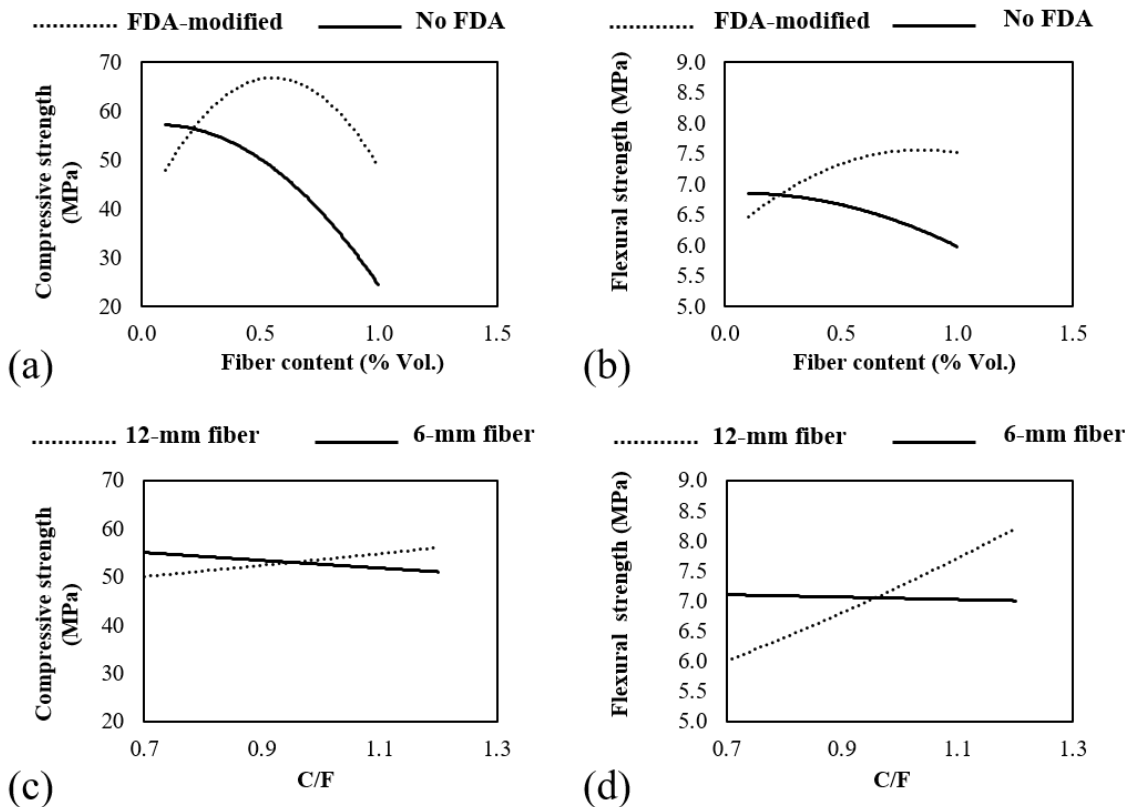


Figure 3-9 Sensitivity assessment of significant variable interactions on strength responses: (a) FDA dosage-fiber content coupled effect on compressive strength, (b) FDA dosage-fiber content coupled effect on flexural strength, (c) fiber length-C/F coupled effect.

## Discussion

The foregoing results suggest that use of fiber in a volume fraction that lies within the 0.4 to 0.8% (Vol.) range was desirable with respect to the electrical resistivity and strength properties of ECON. This is in agreement with the results of previous studies that reported percolation threshold of carbon fibers with fiber dosages of 0.55-0.8 Vol. % in cement paste [38,69], 0.4-1 Vol% in mortar [22,67], and between 0.5 and 0.6 Vol.% in concrete[39]. It is not recommended to consider carbon fiber contents higher than the amounts required for achieving the intended performance. It was revealed that longer fiber resulted in lower resistivity and higher strength values; however, the effects of fiber length on the responses were either moderate or non-significant.

Using 6-mm fiber rendered the mixture very sensitive to variation of C/F with electrical resistivity dramatically increased with increasing C/F. Furthermore, mixtures with low (0.7) or moderate (0.95) C/F values exhibited considerably better workability and cohesiveness. Hence, practical considerations and C/F effect on all responses suggest reducing C/F as much as allowed by the relevant specifications and/or application-induced requirements.

The effect of FDA on electrical resistivity was found to be non-significant. However, when fiber content is in the percolation threshold range (as reported in the literature), minor dosages of FDA can result in improvement of both compressive and flexural strengths. CEA exerted a significant reducing effect on electrical resistivity as long as fiber content did not exceed percolation threshold. Moreover, CEA helped improve compressive and flexural strengths.

## Conclusions

The effects of five variables on the electrical resistivity and mechanical properties of electrically conductive concrete (ECON) were investigated. The responses were electrical resistivity, compressive strength, and flexural strength. Statistical analysis provided the significance levels of each variable and/or interaction of variables in terms of p-value and prediction profiler provided the trend of responses with change in each variable. The results can be summarized in the following statements:

- Calcium nitrite-based corrosion inhibitor admixture was successfully used as conductivity-enhancing agent (CEA) for improving the electrical conductivity of ECON samples. However, the prediction profiler showed that CEA was effective in conductivity improvement up to fiber dosage of 0.87% (Vol.). CEA improved electrical conductivity and compressive strength, especially at low fiber contents. Although CEA improved flexural strength, its effect was not significant.
- Significance of variables varied by hydration time (age) becoming almost steady after 7 days. It is recommended to use 28-day or later age measurement results for analyses.
- Four significant variables affecting electrical resistivity -arranged from most to least significant- were fiber content, coarse-to-fine aggregate volume ratio (C/F), fiber length, and conductivity-enhancing agent (CEA) dosage.
- Compressive strength was significantly influenced by fiber content, CEA dosage, and fiber-dispersive agent (FDA) dosage.
- Two variables showed significant effect on flexural strength, namely, C/F and FDA dosage.
- Interactions between different variables resulted in coupled effects on the responses.

- In addition to main effects and coupled effects of variables, the ECON mix design should account for practical and implementation considerations.
- Although using 12-mm fiber exerted positive effect on the responses, the effect was moderate in case of electrical resistivity and non-significant on strength properties. Therefore, regarding mixing and implementation considerations it is recommended to use 6-mm fiber in production of ECON.

Future studies can use the results of this research to develop an experimental plan for investigating the discussed effects with more levels of the significant variables. A full factorial DOE with the significant variables can be used to obtain predictions that are more accurate. A variety of admixtures and electrically conductive materials still need to be evaluated for improvement of electrical conductivity of ECON. Developing three-phase electrically conductive composites [12] is a viable method that can be integrated with the methods proposed in this study to expand the functionality of ECON beyond the levels so far achieved.

### **Acknowledgements**

This paper was prepared from a study conducted at Iowa State University under Federal Aviation Administration (FAA) Air Transportation Center of Excellence Cooperative Agreement 12-C-GA-ISU for the Partnership to Enhance General Aviation Safety, Accessibility and Sustainability (PEGASAS). The authors would like to thank the current project Technical Monitor, Mr. Benjamin J. Mahaffay, and the former project Technical Monitors, Mr. Jeffrey S. Gagnon (interim), Mr. Donald Barbagallo, and Dr. Charles A. Ishee for their invaluable guidance on this study. The authors would like to express their sincere gratitude to Mr. Robert F. Steffes, Iowa State University (ISU), CCEE (Civil, Construction, and Environmental Engineering Department), Portland cement concrete (PCC) Lab Manager for his significant assistance with

the lab investigations. Special thanks are expressed to Zoltek, the Candlemakers Store (TCS), and WR Grace & Co for providing carbon fiber, methylcellulose, and corrosion inhibitor admixture, respectively. Although the FAA has sponsored this project, it neither endorses nor rejects the findings of this research. The presentation of this information is in the interest of invoking comments by the technical community on the results and conclusions of the research.

### References

- [1] X. Yu, E. Kwon, Carbon Nanotube Based Self-sensing Concrete for Pavement Structural Health Monitoring, Research report–Contract Number: US DOT: DTFH61-10-C-00011, Duluth, Minnesota, 2012. <http://ntl.bts.gov/lib/45000/45000/45066/3789.pdf>.
- [2] R.N. Howser, H.B. Dhonde, Y.L. Mo, Self-sensing of carbon nanofiber concrete columns subjected to reversed cyclic loading, *Smart Mater. Struct.* 20 (2011). doi:10.1088/0964-1726/20/8/085031.
- [3] S. Mingqing, L. Zhuoqiu, M. Qizhao, S. Darong, A study on thermal self-monitoring of carbon fiber reinforced concrete, *Cem. Concr. Res.* 29 (1999) 769–771.
- [4] R. McCormack, Method of making concrete electrically conductive for electromagnetic shielding purposes, US Pat. 5,346,547. (1994). <https://www.google.com/patents/US5346547> (accessed August 2, 2015).
- [5] S. When, D. Chung, Electromagnetic interference shielding reaching 70 dB in steel fiber cement, *Cem. Concr. Res.* 34 (2004) 329–332. doi:10.1016/j.cemconres.2003.08.014.
- [6] M.F.L. De Volder, S.H. Tawfick, R.H. Baughman, and J. Hart, Carbon nanotubes: present and future commercial applications., *Science.* 339 (2013) 535–9. doi:10.1126/science.1222453.
- [7] Y. Lai, Y. Liu, D. Ma, Automatically melting snow on airport cement concrete pavement with carbon fiber grille, *Cold Reg. Sci. Technol.* 103 (2014) 57–62. doi:10.1016/j.coldregions.2014.03.008.
- [8] J. Gomis, O. Galao, V. Gomis, E. Zornoza, P. Garcés, Self-heating and deicing conductive cement. Experimental study and modeling, *Constr. Build. Mater.* 75 (2015) 442–449. doi:10.1016/j.conbuildmat.2014.11.042.
- [9] H. Ceylan, K. Gopalakrishnan, S. Kim, Heated Transportation Infrastructure Systems: Existing and Emerging Technologies, in: Prague, 2014.

- [10] Gopalakrishnan, Kasthurirangan, H. Ceylan, S. Kim, S. Yang, H. Abdulla, Electrically Conductive Mortar Characterization for Self-Heating Airfield Concrete Pavement Mix Design, *Int. J. Pavement Res. Technol.* 8 (2015).
- [11] K. Gopalakrishnan, H. Ceylan, S. Kim, S. Yang, H. Abdulla, Self-Heating Electrically Conductive Concrete for Pavement Deicing: A Revisit, in: *Transp. Res. Board 94th Annu. Meet.*, 2015: p. No. 15-4764.
- [12] J. Wu, J. Liu, F. Yang, Three-phase composite conductive concrete for pavement deicing, *Constr. Build. Mater.* 75 (2015) 129–135. doi:10.1016/j.conbuildmat.2014.11.004.
- [13] A. Arabzadeh, H. Ceylan, S. Kim, K. Gopalakrishnan, A. Sassani, Fabrication of Polytetrafluoroethylene Coated Asphalt Concrete Biomimetic Surfaces: A Nanomaterials Based Pavement Winter Maintenance Approach, in: *ASCE Int. Conf. Transp. Dev.*, ASCE, Houston, Texas, 2016.
- [14] A. Arabzadeh, H. Ceylan, S. Kim, K. Gopalakrishnan, A. Sassani, Superhydrophobic Coatings on Asphalt Concrete Surfaces, *Transp. Res. Rec. J. Transp. Res. Board.* No. 2551 (2016).
- [15] A. Arabzadeh, H. Ceylan, S. Kim, K. Gopalakrishnan, A. Sassani, S. Sundararajan, P.C. Taylor, Superhydrophobic coatings on Portland cement concrete surfaces, *Constr. Build. Mater.* in press (2017).
- [16] M.C. Forde, J. McCarter, H.W. Whittington, The conduction of electricity through concrete, *Mag. Concr. Res.* 33 (1981) 48–60. doi:10.1680/macr.1981.33.114.48.
- [17] D.D.L. Chung, Electrically conductive cement-based materials, *Adv. Cem. Res.* 4 (2004) 167–176.
- [18] E.H. Barnard, Electrically Conductive Cement and Concrete, US3166518 A, 1965.
- [19] J. Farrar, Electrically conductive concrete, *GEC J. Sci. Technol.* (1978). <http://trid.trb.org/view.aspx?id=87575>.
- [20] Z. Hou, Z. Li, J. Wang, Electrical conductivity of the carbon fiber conductive concrete, *J. Wuhan Univ. Technol. Sci. Ed.* 22 (2007) 346–349. doi:10.1007/s11595-005-2346-x.
- [21] D.D. Chung, Dispersion of Short Fibers in Cement, *J. Mater. Civ. Eng.* 17 (2005) 379–383. doi:10.1061/(ASCE)0899-1561(2005)17:4(379).
- [22] B. Chen, K. Wu, W. Yao, Conductivity of carbon fiber reinforced cement-based composites, *Cem. Concr. Compos.* 26 (2004) 291–297. doi:10.1016/S0958-9465(02)00138-5.
- [23] S.C. van der Marck, Calculation of percolation thresholds in high dimensions for fcc, bcc, and diamond lattices, *Int. J. Mod. Phys.* 9 (1998) 529–540. doi:10.1142/S0129183198000431.

- [24] Cao, Jingyao, D.D.L. Chung, Electric polarization and depolarization in cement-based materials, studied by apparent electrical resistance measurement, *Cem. Concr. Res.* 34 (2004) 481–485. doi:10.1016/j.cemconres.2003.09.003.
- [25] C. Chang, M. Ho, G. Song, Y.-L. Mo, H. Li, A feasibility study of self-heating concrete utilizing carbon nanofiber heating elements, *Smart Mater. Struct.* 18 (2009) 127001. doi:10.1088/0964-1726/18/12/127001.
- [26] Z.J. Yang, T. Yang, *Experimental Study on an Electrical Deicing Technology Utilizing Carbon Fiber Tape*, 2012.
- [27] A. Peyvandi, P. Soroushian, A.M. Balachandra, K. Sobolev, Enhancement of the durability characteristics of concrete nanocomposite pipes with modified graphite nanoplatelets, *Constr. Build. Mater.* 47 (2013) 111–117. doi:10.1016/j.conbuildmat.2013.05.002.
- [28] J. Cao, D.D.L. Chung, Carbon fiber reinforced cement mortar improved by using acrylic dispersion as an admixture, *Cem. Concr. Res.* 31 (2001) 1633–1637. doi:10.1016/S0008-8846(01)00599-3.
- [29] B. Chen, J. Liu, Effect of fibers on expansion of concrete with a large amount of high f-CaO fly ash, *Cem. Concr. Compos.* 33 (2003) 1549–1552. doi:10.1016/S0008-8846(03)00098-X.
- [30] R.N. Kraus, T.R. Naik, *Testing and Evaluation of Concrete Using High- Carbon Fly Ash and Carbon Fibers*, Milwaukee, Wisconsin, 2006.
- [31] O. Galao, L. Bañón, F.J. Baeza, J. Carmona, P. Garcés, Highly Conductive Carbon Fiber Reinforced Concrete for Icing Prevention and Curing, *Materials (Basel)*. 9 (2016) 281. doi:10.3390/ma9040281.
- [32] S. Wen, D.D.L. Chung, Effect of carbon fiber grade on the electrical behavior of carbon fiber reinforced cement, *Carbon N. Y.* 39 (2001) 369–373. doi:10.1016/S0008-6223(00)00127-5.
- [33] X. Fu, W. Lu, D.D.L. Chung, Ozone treatment of carbon fiber for reinforcing cement, *Carbon N. Y.* 36 (1998) 1337–1345. doi:10.1016/S0008-6223(98)00115-8.
- [34] J. Cao, D.D.L. Chung, Improving the dispersion of steel fibers in cement mortar by the addition of silane, *Cem. Concr. Res.* 31 (2001) 309–311. doi:10.1016/S0008-8846(00)00470-1.
- [35] C. Chang, G. Song, D. Gao, Y.L. Mo, Temperature and mixing effects on electrical resistivity of carbon fiber enhanced concrete, *Smart Mater. Struct.* 22 (2013) 35021. doi:10.1088/0964-1726/22/3/035021.
- [36] X. Fu, D.D.L. Chung, Effect of methylcellulose admixture on the mechanical properties of cement, *Cem. Concr. Res.* 26 (1996) 535–538. doi:10.1016/0008-8846(96)00028-2.



- [37] C. Shi, Effect of mixing proportions of concrete on its electrical conductivity and the rapid chloride permeability test (ASTM C1202 or ASSHTO T277) results, *Cem. Concr. Res.* 34 (2004) 537–545. doi:10.1016/j.cemconres.2003.09.007.
- [38] S. Wen, D.D.L. Chung, Double percolation in the electrical conduction in carbon fiber reinforced cement-based materials, *Carbon N. Y.* 45 (2007) 263–267. doi:10.1016/j.carbon.2006.09.031.
- [39] F. Javier Baeza, D.D.L. Chung, E. Zornoza, L.G. Andión, P. Garcés, Triple percolation in concrete reinforced with carbon fiber, *ACI Mater. J.* 107 (2010) 396–402.
- [40] T. a. Söylev, M.G. Richardson, Corrosion inhibitors for steel in concrete: State-of-the-art report, *Constr. Build. Mater.* 22 (2008) 609–622. doi:10.1016/j.conbuildmat.2006.10.013.
- [41] ACI committee 350, Letter Ballot 350-A-11-01: Fibers and Corrosion Inhibiting Admixtures, 2011.
- [42] C.M. Hansson, L. Mammoliti, B.B. Hope, Corrosion Inhibitors in Concrete-PART I: the Principles, *Cem. Concr. Res.* 28 (1998) 1775–1781.
- [43] K. Snyder, X. Feng, B. Keen, T. Mason, Estimating the electrical conductivity of cement paste pore solutions from OH<sup>-</sup>, K<sup>+</sup> and Na<sup>+</sup> concentrations, *Cem. Concr. Res.* 33 (2003) 793–798.
- [44] H. Liang, L. Li, N. D. Poor, A.A. Sagu, Nitrite diffusivity in calcium nitrite-admixed hardened concrete, *Cem. Concr. Res.* 33 (2003) 139–146.
- [45] J. Tritthart, P.F.G. Banfill, Nitrite binding in cement, *Cem. Concr. Res.* 31 (2001) 1093–1100.
- [46] P. Xie, P. Gu, Y. Fu, J.J. Beaudoin, Conductive cement-based compositions, US005447564A, 1995.
- [47] S. Wen, D.D.L. Chung, Carbon fiber-reinforced cement as a thermistor, *Cem. Concr. Res.* 29 (1999) 961–965. doi:10.1016/S0008-8846(99)00075-7.
- [48] P. Rossi, S. Rischer, Numerical modelling of concrete cracking based on a stochastic approach, *Mater. Struct.* 20 (1987) 334–337.
- [49] J.F. Lataste, M. Behloul, D. Breyse, Characterisation of fibres distribution in a steel fibre reinforced concrete with electrical resistivity measurements, *NDT E Int.* 41 (2008) 638–647. doi:10.1016/j.ndteint.2008.03.008.
- [50] S. Yehia, C.Y. Tuan, Thin Conductive Concrete Overlay for Bridge Deck Deicing and Anti-Icing, *Transp. Res. Rec. J. Transp. Res. Board.* 1698 (2000) 45–53.
- [51] R. Flynn, P. Bellbay, Risk and the public acceptance of new technologies, 1st ed., UK, 2007.

- [52] M. Sonebi, Medium strength self-compacting concrete containing fly ash: Modelling using factorial experimental plans, *Cem. Concr. Res.* 34 (2004) 1199–1208. doi:10.1016/j.cemconres.2003.12.022.
- [53] D.C. Montgomery, *Design and Analysis of Experiments*, 4th ed., Wiley, New York, 1996.
- [54] P.-W. Chen, D.D.L. Chung, Concrete Reinforced with up to 0.2 Vol% of Short Carbon Fibres, *Composites.* 24 (1993) 33–52.
- [55] Iowa DOT Office of Materials, Iowa DOT Materials IM 529: Portland Cement (PC) Concrete Proportions, 2011.
- [56] ASTM C33/C33M-13, Standard Specification for Concrete aggregates, West Conshohocken, PA, 2010. doi:10.1520/C0033.
- [57] ASTM C 150, Standard Specification for Portland Cement, West Conshohocken, PA, 2007. doi:10.1520/C0150.
- [58] ASTM C494/C494M-16-Standard Specification for Chemical Admixtures for Concrete, West Conshohocken, PA., 2016.
- [59] ASTM C 39, Standard Test Method for Compressive Strength of Cylindrical Concrete Specimens, West Conshohocken, PA, 2016. doi:10.1520/C0039.
- [60] ASTM C 78-02, Standard Test Method for Flexural Strength of Concrete ( Using Simple Beam with Third-Point Loading), West Conshohocken, PA, 2002.
- [61] K. Wang, J.K. Cable, G. Zhi, Investigation Into Improved Pavement Curing Materials And Techniques : Part 1 ( Phases I And II), Ames, Iowa, USA, 2002.
- [62] R.P. Spragg, J. Castro, T. Nantung, M. Paredes, J. Weiss, Variability Analysis of the Bulk Resistivity Measured Using Concrete Cylinders, *Adv. Civ. Eng. Mater.* 1 (2012) 104596. doi:10.1520/ACEM104596.
- [63] M.D. Newlands, M.R. Jones, S. Kandasami, T.A. Harrison, Sensitivity of electrode contact solutions and contact pressure in assessing electrical resistivity of concrete, *Mater. Struct.* 41 (2008) 621–632. doi:10.1617/s11527-007-9257-6.
- [64] M. Nokken, A. Boddy, X. Wu, R.D. Hooton, Effects of Temperature, Chemical, and Mineral Admixtures on the Electrical Conductivity of Concrete, *J. ASTM Int.* 5 (2015) 1–9.
- [65] P.-W. Chen, X. Fu, D.D.L. Chung, Microstructural and mechanical effects of latex, methylcellulose, and silica fume on carbon fiber reinforced cement, *ACI Mater. J.* 94 (1997) 147–155.

- [66] S. Wen, D.D.L. Chung, Seebeck effect in carbon fiber-reinforced cement, *Cem. Concr. Res.* 29 (1999) 1989–1993. doi:10.1016/S0008-8846(99)00185-4.
- [67] D.D.L. Chung, Cement reinforced with short carbon fibers : a multifunctional material, *Compos. Part B Eng.* 31 (2000) 511–526.
- [68] Z.Q. Shi, D.D.L. Chung, Carbon fiber-reinforced concrete for traffic monitoring and weighing in motion, *Cem. Concr. Res.* 29 (1999) 435–439. doi:10.1016/S0008-8846(98)00204-X.
- [69] M. Sun, Z. Li, Q. Mao, D. Shen, Thermoelectric Percolation Phenomena in Carbon Fiber-Reinforced Concrete, *Cem. Concr. Res.* 28 (1998) 1707–1712.

## CHAPTER 4. SALT-FREE DEICING OF PAVEMENTS BY CARBON FIBER-BASED ELECTRICALLY CONDUCTIVE CONCRETE HEATED PAVEMENT SYSTEMS: DESIGN AND QUASI LONG-TERM PERFORMANCE

A paper submitted to Journal of Cleaner Production

Alireza Sassani<sup>1</sup>, Halil Ceylan<sup>2</sup>, Sunghwan Kim<sup>3</sup>, Ali Arabzadeh<sup>4</sup>, S.M. Sajed Sadati<sup>5</sup>, Kasthurirangan Gopalakrishnan<sup>6</sup> and Peter C. Taylor<sup>7</sup>

### Abstract

Traditional methods of removing snow/ice from pavement surfaces involve application of deicing salts and mechanical removal that carry serious environmental concerns. In this study, the feasibility of applying carbon fiber-based electrically conductive concrete (ECON) in heated pavement systems (HPS) as an alternative to traditional methods was investigated. The optimum carbon fiber dosage to achieve desirable electrical conductivity and avoid excessive fiber use was determined based on percolation threshold phenomenon in different carbon fiber-based cementitious composites. The ECON HPS system design and configuration were evaluated by finite element (FE) analysis. The performance sustainability of the ECON HPS in terms of energy demand for snow melting, and energy conversion efficiency were studied by experimental evaluation of a prototype ECON HPS slab. The critical issues related to ECON mix design, system design, and service life were identified and discussed based on a quasi long-term (460 days) experimental study.

<sup>1</sup> Graduate Research Assistant, Civil, Construction and Environmental Engineering (CCEE), Iowa State University (ISU), Ames, IA, E-mail: [asassani@iastate.edu](mailto:asassani@iastate.edu)

<sup>2</sup> Professor, Director, Program for Sustainable Pavement Engineering and Research (PROSPER), CCEE, ISU, Ames, IA, E-mail: [hceylan@iastate.edu](mailto:hceylan@iastate.edu)

<sup>3</sup> Research Scientist, Institute for Transportation, ISU, Ames, IA, E-mail: [sunghwan@iastate.edu](mailto:sunghwan@iastate.edu)

<sup>4</sup> Graduate Research Assistant, CCEE, ISU, Ames, IA, E-mail: [arab@iastate.edu](mailto:arab@iastate.edu)

<sup>5</sup> Graduate Research Assistant, CCEE, ISU, Ames, IA, E-mail: [ssadati@iastate.edu](mailto:ssadati@iastate.edu)

<sup>6</sup> Research Associate Professor, Iowa State University, Ames, IA. Email: [rangan@iastate.edu](mailto:rangan@iastate.edu)

<sup>7</sup> Director, National Concrete Pavement Technology Center, SU, Ames, IA, E-mail: [ptaylor@iastate.edu](mailto:ptaylor@iastate.edu)

The percolation transition zone of carbon fiber in paste, mortar, and concrete composites were respectively 0.25-1% (Vol.), and 0.6-1% (Vol.), and 0.5-0.75% (Vol.). Optimum carbon fiber volume fraction in ECON, to achieve desired heating performance with minimum fiber content, was 0.75%. The electrical conductivity of ECON with optimum fiber dosage was  $1.86 \times 10^{-2}$  S/cm at 28 days and  $1.22 \times 10^{-2}$  S/cm at 460 days of age. The power density of the operating ECON slab was measured as 1.08 kW/m<sup>2</sup> and 1.27 kW/m<sup>2</sup> at 28 and 460 days respectively. Electrical-energy-to-heat-energy conversion efficiency decreased from 66% at 28 days to 50% at 460-day age. The results showed that the studied technology could be effectively applied for ice/snow melting on the pavement surfaces and provide a feasible alternative to traditional methods if the ECON mixing proportions and system configurations are made with necessary precautions.

### **Introduction**

Traditional methods of ice/snow removal from pavements are using deicing chemicals combined with mechanical removal that are associated with large manpower, sophisticated machinery, environmentally harmful chemicals, and damage to pavement [1–6]. Application of deicing chemicals is especially associated with negative environmental impacts [7–12]. The salty runoff from pavement deicing operations is responsible for soil and water contamination [7–9, 11] and adverse health effects on plant life, aquatic life, and human societies [9–13]. Deicing chemicals constitute the majority of greenhouse gas emission associated with traditional deicing methods [14, 15]. An increasing trend of global consumption of deicing chemicals has been reported over the past years making the already existing environmental concern even more challenging [16].

Driven by the economic, safety, and environmental concerns of using deicing chemicals, numerous research efforts have been devoted to finding cleaner and more sustainable ways for safely removing ice and snow from pavements. Some of the emerging techniques for this purpose involve the application of superhydrophobic coatings on pavement surfaces [17–20], embedding electrically heating sheet/grille elements inside the pavement [4, 21]; and application of heated pavement systems (HPS) [22–27]. Previous studies have confirmed higher effectiveness and lower carbon footprint achieved by HPS, particularly in critical horizontal infrastructure systems such as airports [6, 14, 22]. Application of electrically conductive concrete (ECON) is an approach to heated pavements [22, 24, 28] which has so far been predominantly implemented using hydronic systems [25]. Sustainability and viability of an ECON HPS is governed by multiple factors that include, but are not limited to, materials selection, optimum material dosage rates, system design, service life, and energy consumption regime.

Portland cement concrete (PCC) can be engineered by various materials to produce smart cementitious composites that exhibit certain non-structural performances, such as electrical conductivity, photocatalysis, and self-sensing properties [29–34]. ECON is a smart cementitious composite which is produced by modification of plain PCC [35]. Unlike plain cementitious composites in which electricity is mainly conducted through electrolytic conduction, the dominant conduction mechanism in ECON is the motion of electrons instead of ions [36] which is boosted by introducing an electrically conductive additives phase into the cementitious matrix. Previous studies have used various electrically conductive materials such as carbon-based and metallic fibers, powders, and granular solid particles to form the path of electronic conduction in cementitious composites, and suggested that carbonaceous fiber-shaped materials with micrometer-scale diameter and 3-15 mm length provide superior performance [23, 30, 31, 37–

47]. Powder and granular materials are associated with high dosage, reduction of cementitious composite's strength [48], and high cost especially in the case of nano-particles. Although steel fiber is more effective in achieving resistive heating [49], addition of steel fiber to concrete mix is associated with drawbacks such as corrosion [48], high dosage [24], and prohibitions in critical infrastructures such as airports [50,51]. Also, modification of PCC with carbon fiber provides benefits in terms of mechanical performance and durability [38, 52–55], and hence reduces the contribution of maintenance operations to the carbon footprint of the pavement [15]. Industrial-scale production of recycled carbon fiber from waste carbon fiber composites in recent years [56, 57] has provided environmental and economic incentives for its application in construction sector.

Achieving high electrical conductivity in cementitious composites requires fiber percolation through the cementitious matrix; meaning that the volume fraction of fibers should be equal to or greater than the value which forms a continuous path of fibers touching one another [58–63]. The range of fiber content at which electrical conductivity abruptly increases is known as the percolation transition zone (or percolation threshold) [64]. However, using electrically conductive additives beyond the percolation threshold is costly without added benefit, while higher carbon fiber consumption adds to carbon footprint of ECON production. Therefore, knowing the percolation threshold is critical to designing an ECON HPS [41]. Percolation threshold of carbon fiber with different aspect ratios have been investigated by numerous studies [59, 60, 65–68]. The percolation threshold –and consequently the optimum carbon fiber volume fraction- varies by the type of cementitious composite (cement paste, mortar, or concrete), fiber aspect ratio, cementitious system, and aggregate system [59, 65, 68].

In this study, the performance sustainability of a carbon fiber-based ECON HPS is defined as the ability to melt ice and snow with as low energy consumption as possible over a reasonable service life, while the carbon fiber consumption in the production of ECON is minimized. The performance sustainability of an HPS depends on the specific system design used, i.e. electrode configuration, pavement depth, achieved conductivity level, and applied power [69]. Computer modeling is a powerful means to verify the feasibility of an HPS with a specific design under given circumstances [25, 70]. However, given an optimized material and system design, the time-dependent properties of ECON is still a factor that affects long-term performance. There is very limited information on the long-term electrical behavior of ECON systems. Regarding changes in electrical resistivity of concrete with age [65, 71, 72], this is a decisive factor with respect to the time-dependent serviceability of the ECON HPS. Environmental and economic life cycle assessment (LCA) of the ECON HPS application, as encountered by the authors, requires knowledge of the long-term performance of the system and how its energy consumption varies over service life.

This research aimed to investigate the quasi long-term changes of electrical conductivity and heating performance of carbon fiber-based electrically conductive concrete (ECON) for application in heated pavement system (HPS). To minimize carbon fiber consumption, the optimum dosage of carbon fiber was determined by investigating the percolation threshold in different types of cementitious composites. The ECON HPS configuration was designed based on a finite element (FE) model analysis. To evaluate the energy consumption of the ECON HPS for snow melting, the heating performance of ECON HPS was examined through a prototype laboratory-scale ECON HPS slab.



## Methodology

### Research Approach

Optimum carbon fiber dosage is defined as a carbon fiber volume above which additional fiber does not exert significant improvement on conductivity. This optimum fiber content is known as the percolation threshold. In this work, the percolation threshold of carbon fibers was determined in cementitious paste, mortar, and concrete. Once the material dosage rate was determined, an electrically conductive concrete (ECON) heated pavement system (HPS) design previously developed by the authors [51, 69, 70] was analyzed by a finite element (FE) model and evaluated experimentally for performance sustainability over time according to US standards. Performance was assessed by the ability to melt ice on a pavement surface with an acceptable energy demand [73]. Electrical resistivity measurements were performed using 1 kHz AC with embedded copper mesh electrodes in saturated surface-dry (SSD) condition as described in [74]. Electrical conductivity [in S/cm] was calculated as reciprocal of resistivity [in  $\Omega$ -cm].

### Materials

The electrically conductive cementitious composite studied in this research is intended to be used in heated pavement systems (HPS), particularly in horizontal systems such as airfields, highways, and bridges. Therefore, all mixture proportions and materials conformed to Iowa Department of Transportation (Iowa DOT) Materials I.M. 529 specification and Federal Aviation Administration (FAA) advisory circular 150-5370-10G. The properties of the aggregates and cementitious materials are presented in Table 4-1 and the chemical compositions of cementitious materials are given in Table 4-2. High-range water reducing admixture was type F conforming to ASTM C 494. Methylcellulose in fine powder form was used as a fiber dispersive agent (FDA)

at a dosage of 0.4 % by weight of cementitious materials; the FDA was dissolved in the mix water before being added to the batch as explained in [75].

Chopped carbon fiber was polyacrylonitrile (PAN)-based with 7.2  $\mu\text{m}$  diameter, 6 mm nominal length, 95% carbon content, and electrical resistivity of  $1.55 \times 10^{-3} \Omega\text{-cm}$ . Previous studies [68] have shown that in fiber dosage rates below 1% (Vol.), carbon fibers with aspect ratio about 800-900 provide superior performance in terms of electrical percolation. In previous work by the authors [75], it was verified that, although carbon fibers with aspect ratio greater than 900 are more effective in improving electrical conductivity of the cementitious composite, they reduce the workability and surface finishability of the composite. Therefore, a carbon fiber with nominal aspect ratio of 833 was used in this study to ensure performance adequacy and mixture workability.

*Table 4-1 Physical properties of Cementitious Materials and Aggregates.*

| Component        | Properties       |                          |                             |   |           |
|------------------|------------------|--------------------------|-----------------------------|---|-----------|
|                  | Specific gravity | Water absorption (% wt.) | Manufacturer/Supplier       | Specification                                     | Standard  |
| Cement           | 3.15             | N.A.                     | Holcim                      | Type I/II   | ASTM C150 |
| Fly ash          | 2.5              | N.A.                     | Holcim                      | Class F, Average particle size 19.5 $\mu\text{m}$ | ASTM C618 |
| Coarse aggregate | 2.67             | 1.4                      | Martin Marietta, Ames, Iowa | Lime stone, D-57 gradation                        | ASTM C33  |
| Fine aggregate   | 2.62             | 1.7                      | Martin Marietta, Ames, Iowa | Natural sand                                      | ASTM C33  |

Note: N.A.= does not apply

Table 4-2 Chemical compositions of cementitious materials.

| Oxides                         | Portland Cement | Class F Fly ash |
|--------------------------------|-----------------|-----------------|
|                                | % mass          |                 |
| SiO <sub>2</sub>               | 20.10           | 52.10           |
| Al <sub>2</sub> O <sub>3</sub> | 4.44            | 16.00           |
| Fe <sub>2</sub> O <sub>3</sub> | 3.09            | 6.41            |
| CaO                            | 62.94           | 14.10           |
| MgO                            | 2.88            | 4.75            |
| SO <sub>3</sub>                | 3.18            | 0.59            |
| K <sub>2</sub> O               | 0.61            | 2.36            |
| Na <sub>2</sub> O              | 0.10            | 1.72            |
| <b>Loss on ignition</b>        | 2.55            | 0.09            |

### Determination of Optimum Carbon Fiber Dosage Rate

#### Cementitious paste and mortar

Carbon fiber-based cement paste samples were prepared using the proportions in Table 4-3. The mortar mixtures were made using the proportions given in Table 4-4. Water-to-cementitious mass ratio (W/C) of 0.42 was maintained in all paste and mortar mixtures. Sand-to-cementitious ratio was fixed at 1.1; while carbon fiber dosage rate was selected as the variable mix component in mortar samples. The volume of paste was defined as the volume of carbon

fiber-cementitious matrix composite, i.e. the total volume of carbon fibers, cementitious materials, and water. Because the fibers were replacing a portion of sand, the sand-to-paste volume ratios (Sand/Paste) of mixtures were subject to small variations as seen in Table 4-4. Six 50-mm cubic specimens with embedded copper mesh electrodes were obtained from each paste and mortar mix. The cubes were cured in the mold for one day and then cured in moist room at 23°C for seven days.

*Table 4-3 Volumetric mixing proportions of carbon fiber-containing paste samples.*

| Mix component          | Volumetric mixing proportions ( % total volume of the mix) |       |       |       |       |       |       |       |       |       |       |       |       |       |
|------------------------|--|-------|-------|-------|-------|-------|-------|-------|-------|-------|-------|-------|-------|-------|
| <b>Carbon fiber</b>    | 0.00   | 0.25  | 0.40  | 0.50  | 0.60  | 0.75  | 0.90  | 1.00  | 1.25  | 1.50  | 1.75  | 2.00  | 2.50  | 3.00  |
| <b>Portland Cement</b> | 33.52  | 33.44 | 33.39 | 33.36 | 33.32 | 33.27 | 33.22 | 33.19 | 33.10 | 33.02 | 32.94 | 32.85 | 32.69 | 32.52 |
| <b>Fly ash</b>         | 10.56  | 10.53 | 10.52 | 10.51 | 10.50 | 10.48 | 10.46 | 10.45 | 10.43 | 10.40 | 10.38 | 10.35 | 10.30 | 10.24 |
| <b>water</b>           | 55.92  | 55.78 | 55.69 | 55.64 | 55.58 | 55.50 | 55.41 | 55.36 | 55.22 | 55.08 | 54.94 | 54.80 | 54.52 | 54.24 |

### Concrete

To investigate the percolation threshold of carbon fiber in concrete and long-term change of resistivity, ECON samples were prepared at different volume fractions of carbon fiber. Table 4-5 shows the mixing proportions of ECON samples. The sand-to-paste volume ratio (sand/paste) was kept as close to that used in the mortar mixtures as possible. With addition of carbon fiber into the mix design, the C/F and sand/paste ratios varied between mixtures, because carbon fiber was replacing a portion of fine aggregate. The fiber-dispersive agent was also included in the zero-fiber mixture for consistency. High range water reducer (HRWR) in a

dosage of 0.5% by weight of cementitious materials was used in all mixtures to achieve a slump of 38-50 mm. Concrete mixtures were prepared in a 0.08 m<sup>3</sup> drum mixer.

Three batches were prepared with each mixture design, and six cylindrical and three cubic specimens, as shown in [75], were prepared for each batch. Ambient conditions during sample preparation, curing and testing were the same as the paste and mortar tests. Electrical resistivity measurements were performed at 3, 7, 28, 56, 90, 150, 209, and 460 days of age. Compressive strength was measured at 7- and 28-day ages in accordance with ASTM C 39.

*Table 4-4 Volumetric mixing proportions of carbon fiber-containing mortar samples.*

| Mix component                        | Volumetric mixing proportions ( % total volume of the mix) |       |       |       |       |       |       |       |       |       |       |       |       |       |
|--------------------------------------|--|-------|-------|-------|-------|-------|-------|-------|-------|-------|-------|-------|-------|-------|
| <b>Carbon fiber</b>                  | 0.00   | 0.25  | 0.40  | 0.50  | 0.60  | 0.75  | 0.90  | 1.00  | 1.25  | 1.50  | 1.75  | 2.00  | 2.50  | 3.00  |
| <b>Sand</b>                          | 52.38  | 52.25 | 52.17 | 52.12 | 52.07 | 51.99 | 51.91 | 51.86 | 51.73 | 51.60 | 51.46 | 51.33 | 51.07 | 50.81 |
| <b>Cement</b>                        | 15.96  | 15.92 | 15.90 | 15.88 | 15.87 | 15.84 | 15.82 | 15.80 | 15.76 | 15.72 | 15.68 | 15.64 | 15.56 | 15.48 |
| <b>Fly ash</b>                       | 5.03   | 5.02  | 5.01  | 5.00  | 5.00  | 4.99  | 4.98  | 4.98  | 4.97  | 4.95  | 4.94  | 4.93  | 4.90  | 4.88  |
| <b>Water</b>                         | 26.63  | 26.56 | 26.52 | 26.49 | 26.47 | 26.43 | 26.39 | 26.36 | 26.29 | 26.23 | 26.16 | 26.09 | 25.96 | 25.83 |
| <b>Sand/Paste (Vol.)</b>             | 1.10   | 1.09  | 1.09  | 1.09  | 1.09  | 1.08  | 1.08  | 1.08  | 1.07  | 1.07  | 1.06  | 1.05  | 1.04  | 1.03  |
| <b>HRWR (% mass of cementitious)</b> | 0.00   | 0.00  | 0.00  | 1.00  | 1.00  | 1.50  | 1.50  | 2.50  | 2.50  | 3.50  | 4.50  | 6.00  | 6.00  | 6.50  |

Table 4-5 Volumetric and mass mixing proportions of carbon ECON samples.

| Mix component          | Volumetric fraction ( % total volume of the mix) |       |       |       |       |
|------------------------|--|-------|-------|-------|-------|
|                        |  |       |       |       |       |
| Coarse aggregate       | 40.04  | 40.04 | 40.04 | 40.04 | 40.04 |
| Fine aggregate         | 32.16  | 31.99 | 31.78 | 31.49 | 31.37 |
| Cement                 | 9.28   | 9.28  | 9.28  | 9.28  | 9.28  |
| Fly ash                | 2.92   | 2.92  | 2.92  | 2.92  | 2.92  |
| Water                  | 15.47  | 15.47 | 15.47 | 15.47 | 15.47 |
| Carbon fiber           | 0.00   | 0.25  | 0.50  | 0.75  | 1.00  |
| Fiber-dispersive agent | 0.06   | 0.06  | 0.06  | 0.06  | 0.06  |
| sand/paste (Vol.)      | 1.16   | 1.14  | 1.13  | 1.11  | 1.09  |
| Coarse/Fine (Vol.)     | 1.25   | 1.25  | 1.26  | 1.27  | 1.28  |
| Mix component          | Mass proportions (Kg/m <sup>3</sup> )            |       |       |       |       |
|                        |  |       |       |       |       |
| Coarse aggregate       | 1,069  | 1,069 | 1,069 | 1,069 | 1,069 |
| Fine aggregate         | 843  | 838   | 833   | 825   | 822   |
| Cement                 | 292  | 292   | 292   | 292   | 292   |
| Fly ash                | 73   | 73    | 73    | 73    | 73    |
| Water                  | 155  | 155   | 155   | 155   | 155   |
| Carbon fiber           | 0  | 5     | 9     | 14    | 18    |
| Fiber-dispersive agent | 2  | 2     | 2     | 2     | 2     |
| W/C (mass)             | 0.42   | 0.42  | 0.42  | 0.42  | 0.42  |

## **System Design and Control with finite Element Evaluation of the ECON HPS Performance**

System design of an ECON HPS encompasses the electrode shape/type, electrode location, material and number of layers, layer thickness, power source (AC/DC), and electrical and thermal properties of the ECON. A schematic of a typical ECON heated pavement system is presented in Figure 4-1. To estimate the performance of the system before building the actual experimental setup, a finite element (FE) model of the designed slab was built in ANSYS 18.2. SOLID5 elements were used to model the regular concrete and ECON layers and PLANE13 elements were used to model the electrodes. These elements are capable of handling thermoelectric loads and responses. Since all sides of the slab other than the surface were isolated, it was assumed that heat transfer is negligible from all sides except the slab's top surface. A convection load was applied to the surface of ECON layer to account for the heat loss from the surface to the ambient. Material properties including electrical resistivity, heat capacity and thermal conductivity were considered in this analysis. Weather conditions applied to the model included ambient temperature and wind speed. Elements of the developed FE model are shown in Figure 4-2.

A transient solution was performed to find the trend of temperature increase over time. The time step used for this solution was 5 minutes, which was considered to be sufficiently small for this case. Note that, although developing a 2D model would be sufficient for the purpose of current study, a 3D model was developed to be used in future studies by applying asymmetric loads.

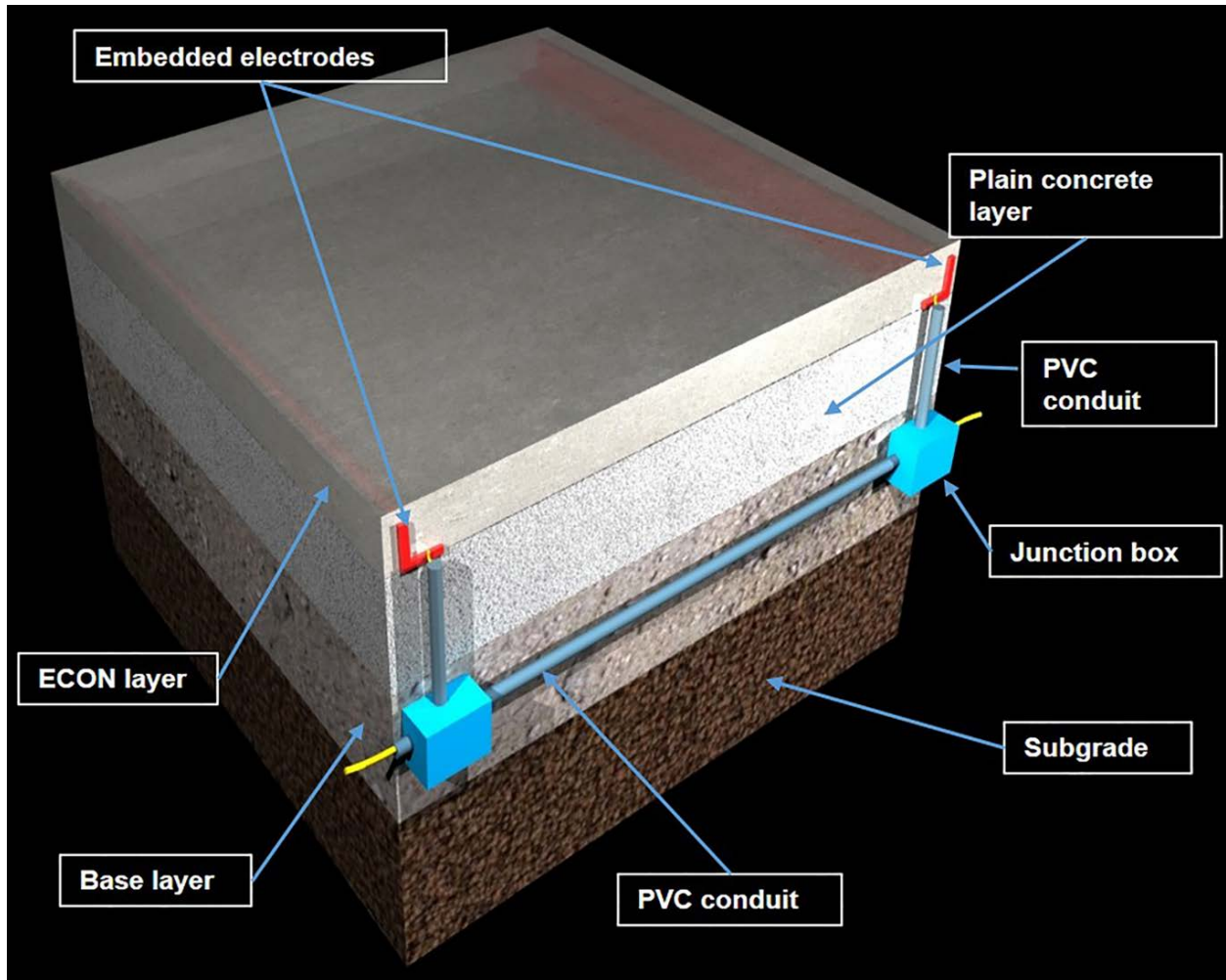


Figure 4-1 Illustration of an electrically heated concrete pavement system.

### Experimental Evaluation of ECON HPS Performance

After verification of the system design by FE modeling, a prototype ECON HPS slab was built and tested to evaluate the performance and validate the modeling approach. Fiber dosage was based on the percolation threshold value. A mixture containing 0.75% (by volume) carbon fiber was used to prepare a prototype slab with embedded electrodes and temperature sensors as illustrated in Figure 4-3. The electrode configuration and materials were selected as described in [76]. The slab was prepared in two lifts: the bottom lift was placed using plain portland cement concrete (PCC) using proportions given in Table 4-6, and the top half was cast using ECON. The



lifts were placed in a wet-on-wet process and the surface of the first layer was tined before placing the second to ensure a good bond between the two layers.

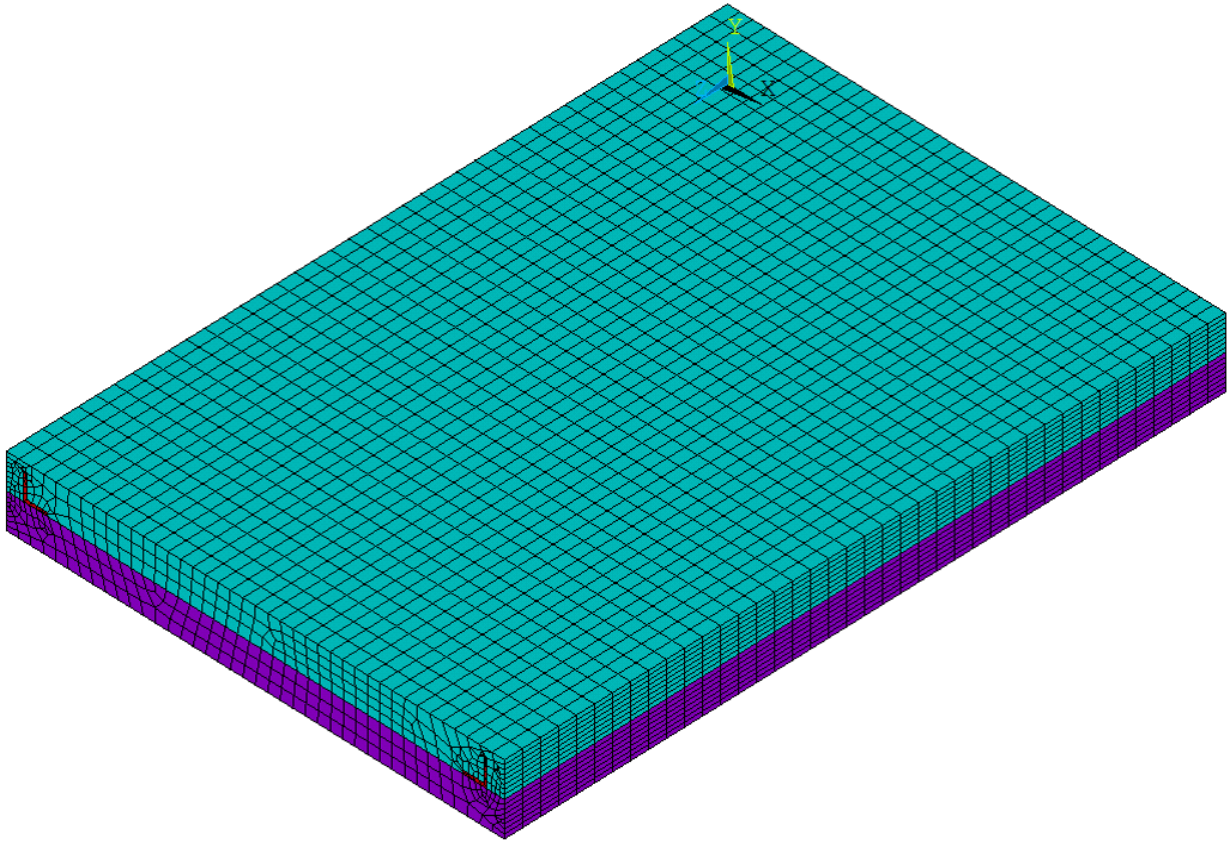


*Figure 4-2 . Elements of the finite element model of ECON test slab having ECON layer on top and regular concrete on bottom.*

As seen in Figure 4-3, temperature sensors were embedded within both ECON and plain concrete layers of the test slab. Sensor locations are shown as S1, S2, and S3 in Figure 3; at each of the three locations, one sensor was placed in the mid-depth of each layer. To test the snow melting ability, the slab was placed in a temperature control chamber at sub-zero (Celsius) temperatures and uniformly covered with a 6-cm layer of compacted snow. 60 Hz AC was then applied to the electrodes. The power absorption, defined as energy dissipated per unit time, was calculated by multiplying voltage and current. Power density, defined as power absorption per unit area of the slab, was also calculated. The efficiency of the conversion of electrical energy to

heat in the ECON layer, i.e. output heat energy as a percentage of the input electrical energy, was calculated using unit weight and the specific heat capacity of the mixture. The amount of energy converted into heat was obtained from time-temperature data according to Equation 4-1:

$$Q = MC(\sum_{i=1}^t(T_i - T_{i-1})) \quad (\text{Equation 4-1})$$

Where, Q is the energy in Joules, M is the mass of the conductive layer in kg, C is the specific heat capacity of ECON in J/kg.K, t is the total duration of snow melting in minutes, and T is the temperature in Kelvin. The heat distribution on the slab surface was monitored with a thermal imaging system over a one-hour heating test.

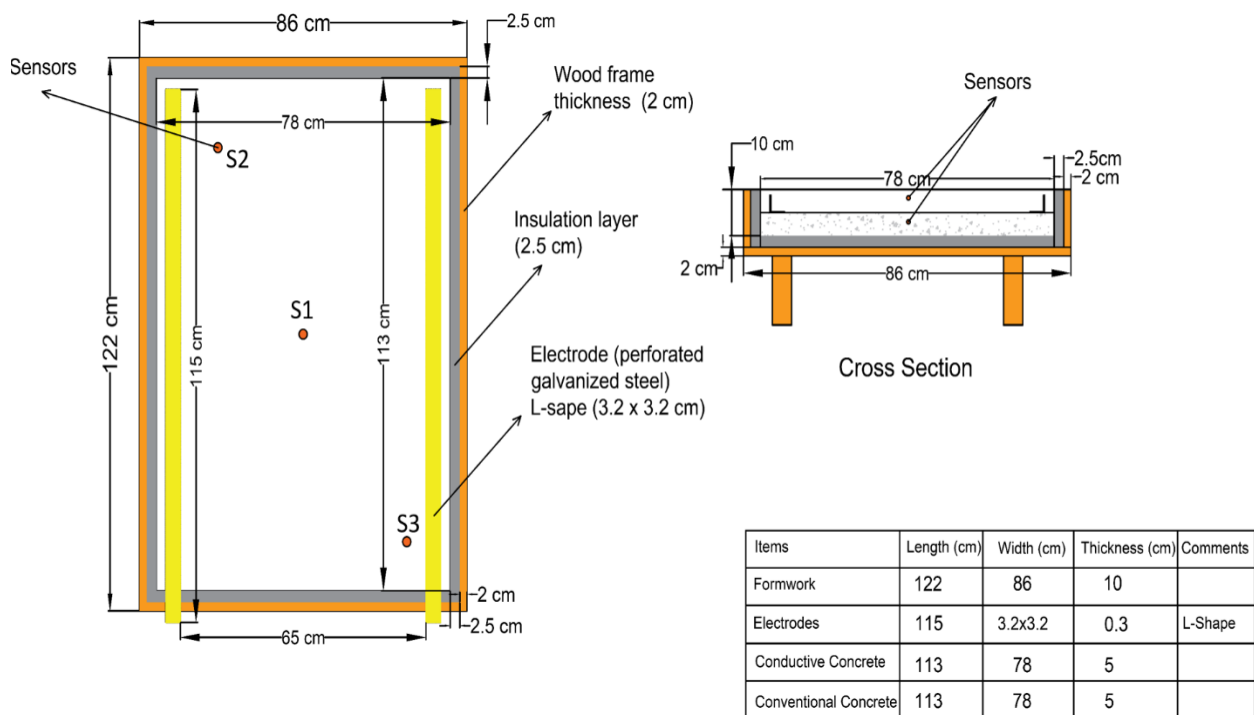


Figure 4-3 Schematic presentation of the prototype slab.

Table 4-6 Mixing Proportions of Plain PCC for heated slab.

| Materials        | Description        | Kg/m <sup>3</sup> |
|------------------|--------------------|-------------------|
| Coarse aggregate | Limestone (SSD)    | 1,022             |
| Fine aggregate   | Natural sand (SSD) | 653               |
| Fly ash          | Class F            | 72                |
| Cement           | type I/II          | 289               |
| Water            | Tap water          | 164               |
| <b>Total</b>     |                    | <b>2,200</b>      |

### Results and Discussion

The results of electrical conductivity ( $\sigma$ ) measurements in cementitious paste and mortar specimens are given in Table 4-7 and Figure 4-4. As seen in the figure, the data exhibited a so-called S-curve for both composites. The upper limit of percolation transition zone, or the top of the S-curve, is identified as the optimum fiber dosage rate [37, 75, 77]. Note that the lower limit of percolation transition zone was shifted upward by addition of sand to the mixture. This can be attributed to double percolation effect in that fiber needs to form a continuous path between the cement and the sand particles [59]. Based on the mix proportions (Table 4-4) and Figure 4-4, the percolation of the paste-fiber composite within the mortar matrix requires a sand-to-paste volume ratio smaller than 1.09 which corresponds to fiber volume dosage rates higher than 0.60%. As seen in Figure 4-4, 1.00 % fiber content in both paste and mortar composites corresponds to percolated system.

*Table 4-7 Electrical conductivity of paste and mortar specimens with different carbon fiber dosage rates.*

| Carbon fiber dosage<br>(% total Vol.) | Paste           |          | Mortar          |          |
|---------------------------------------|-----------------|----------|-----------------|----------|
|                                       | $\sigma$ (S/cm) | SD       | $\sigma$ (S/cm) | SD       |
| <b>0.00</b>                           | 9.15E-03        | 2.12E-04 | 8.81E-04        | 1.94E-05 |
| <b>0.25</b>                           | 2.38E-02        | 2.51E-03 | 1.80E-03        | 2.62E-04 |
| <b>0.40</b>                           | 5.41E-02        | 4.59E-03 | 1.83E-03        | 2.50E-04 |
| <b>0.50</b>                           | 8.15E-02        | 8.12E-03 | 1.89E-03        | 2.50E-04 |
| <b>0.60</b>                           | 1.04E-01        | 4.94E-03 | 2.02E-03        | 2.81E-04 |
| <b>0.75</b>                           | 1.34E-01        | 5.70E-03 | 3.88E-03        | 3.42E-04 |
| <b>0.90</b>                           | 1.70E-01        | 2.07E-03 | 6.54E-03        | 3.16E-04 |
| <b>1.00</b>                           | 1.91E-01        | 6.47E-03 | 7.93E-03        | 4.62E-04 |
| <b>1.25</b>                           | 2.21E-01        | 1.59E-02 | 9.48E-03        | 3.53E-04 |
| <b>1.50</b>                           | 2.37E-01        | 1.26E-02 | 1.00E-02        | 4.15E-04 |
| <b>1.75</b>                           | 2.40E-01        | 5.24E-03 | 1.09E-02        | 4.44E-04 |
| <b>2.00</b>                           | 2.41E-01        | 5.49E-03 | 1.13E-02        | 4.76E-04 |
| <b>2.50</b>                           | 2.43E-01        | 2.61E-02 | 1.23E-02        | 5.62E-04 |
| <b>3.00</b>                           | 2.45E-01        | 1.84E-02 | 1.33E-02        | 5.21E-04 |

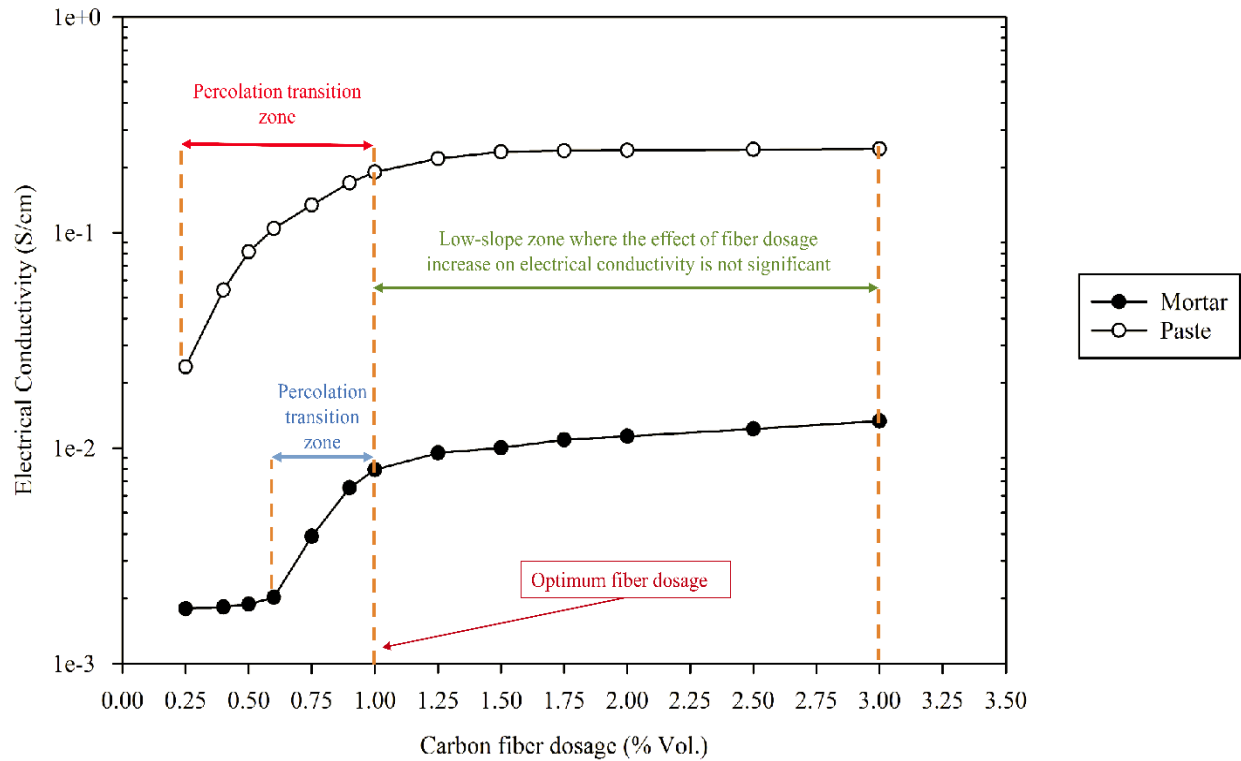


Figure 4-4 Variation of electrical conductivity by fiber content in cementitious paste and mortar.

The results of the percolation determination tests in concrete are presented in Table 4-8 and Figure 4-5. It was found that using early-age measurement results for determination of optimum or required fiber dosage in concrete would be misleading and would result in unduly excessive consumption of carbon fiber. Due to sustainability considerations, excessive carbon fiber consumption is not desirable [28, 37, 75]. Therefore, care must be taken to determine the optimum carbon fiber dosage at a mature age.

It can be observed in Figure 4-5, that the curve is dependent on sample age in that electrical conductivity becomes less sensitive to variation of fiber content as the concrete gets older. This reveals that electrical conductivity of carbon fiber-based concrete at early ages is a poor indicator of the fiber network formation due to the influence of pore structure on conductivity at early hydration ages [75]. As seen in Figure 4-5 the percolation transition zone in

concrete cannot be determined using early-age results, since the conductivity continues to increase with fiber dosage without exhibiting the low-slope zone. While, at ages later than 28 days the curves start to acquire the S-shape until they exhibit a well-defined percolation transition zone between 0.5% and 0.75% and optimum fiber dosage at 0.75%. The percolation threshold in concrete experienced a slight downward shift compared to the percolation range derived from paste and mortar tests. This can be attributed to increased fiber concentration within cement paste matrix and mortar matrices by incorporation of coarse aggregates [65].

As indicated in Figure 4-5 with increasing hydration, the curves became closer to each other. This conveys the important message that the rate of conductivity decrease slows with time. Therefore, if the ECON provides acceptable resistive heating performance over a quasi long-term period (460 days age in this research), the risk of inadequate performance of HPS at later ages is reduced.

Compressive strength measurements of cylindrical ECON specimens (Table 4-9) showed that all specimens satisfied the design compressive strength requirements. ECON samples that contained carbon fiber in the percolation range gave better strength performance especially at 7 days. When fiber content was equal to the lower limit of percolation transition zone, the concrete showed the highest compressive strength. This can be ascribed to the strengthening role of fibers when they start to form a network but the fiber concentration is not yet high enough to introduce defects within the concrete. Strength increased by 23-31% between 7 and 28 days. Unlike normal concrete in which electrical resistivity has a direct relation to compressive strength [78], no relationship between electrical resistivity and strength could be made. Strength is largely controlled by the void system while pore chemistry and percolation of fibers have more significant effects on electrical resistivity.

Table 4-8 Electrical conductivity of concrete specimens at different carbon fiber dosages and ages.

| Age (days) | Parameter       | Carbon fiber dosage (% Vol.) |          |          |          |          |
|------------|-----------------|------------------------------|----------|----------|----------|----------|
|            |                 | 0.00                         | 0.25     | 0.50     | 0.75     | 1.00     |
| 3          | $\sigma$ (S/cm) | 5.00E-04                     | 3.77E-03 | 5.08E-03 | 2.63E-02 | 6.85E-02 |
|            | SD              | 7.45E-05                     | 9.90E-04 | 9.70E-04 | 1.47E-03 | 1.48E-03 |
| 7          | $\sigma$ (S/cm) | 4.51E-04                     | 3.45E-03 | 4.33E-03 | 2.04E-02 | 5.56E-02 |
|            | SD              | 5.74E-05                     | 9.11E-04 | 9.81E-04 | 8.14E-04 | 7.14E-04 |
| 28         | $\sigma$ (S/cm) | 1.32E-04                     | 3.37E-03 | 4.19E-03 | 1.86E-02 | 3.80E-02 |
|            | SD              | 4.92E-05                     | 1.11E-03 | 1.11E-03 | 7.03E-04 | 7.18E-04 |
| 56         | $\sigma$ (S/cm) | 7.89E-05                     | 2.97E-03 | 3.83E-03 | 1.77E-02 | 3.03E-02 |
|            | SD              | 5.24E-05                     | 1.05E-03 | 1.07E-03 | 2.34E-03 | 2.34E-03 |
| 90         | $\sigma$ (S/cm) | 5.07E-05                     | 2.90E-03 | 3.58E-03 | 1.67E-02 | 2.38E-02 |
|            | SD              | 5.88E-06                     | 1.20E-03 | 1.16E-03 | 2.15E-03 | 2.15E-03 |
| 150        | $\sigma$ (S/cm) | 3.77E-05                     | 2.15E-03 | 2.70E-03 | 1.43E-02 | 1.63E-02 |
|            | SD              | 5.88E-06                     | 9.72E-04 | 9.59E-04 | 2.23E-03 | 2.24E-03 |
| 209        | $\sigma$ (S/cm) | 3.13E-05                     | 1.75E-03 | 2.17E-03 | 1.32E-02 | 1.39E-02 |
|            | SD              | 1.24E-06                     | 1.08E-03 | 1.06E-03 | 2.75E-03 | 2.76E-03 |
| 460        | $\sigma$ (S/cm) | 1.35E-05                     | 1.59E-03 | 1.88E-03 | 1.22E-02 | 1.25E-02 |
|            | SD              | 1.74E-06                     | 9.62E-04 | 9.92E-04 | 1.25E-03 | 1.27E-03 |

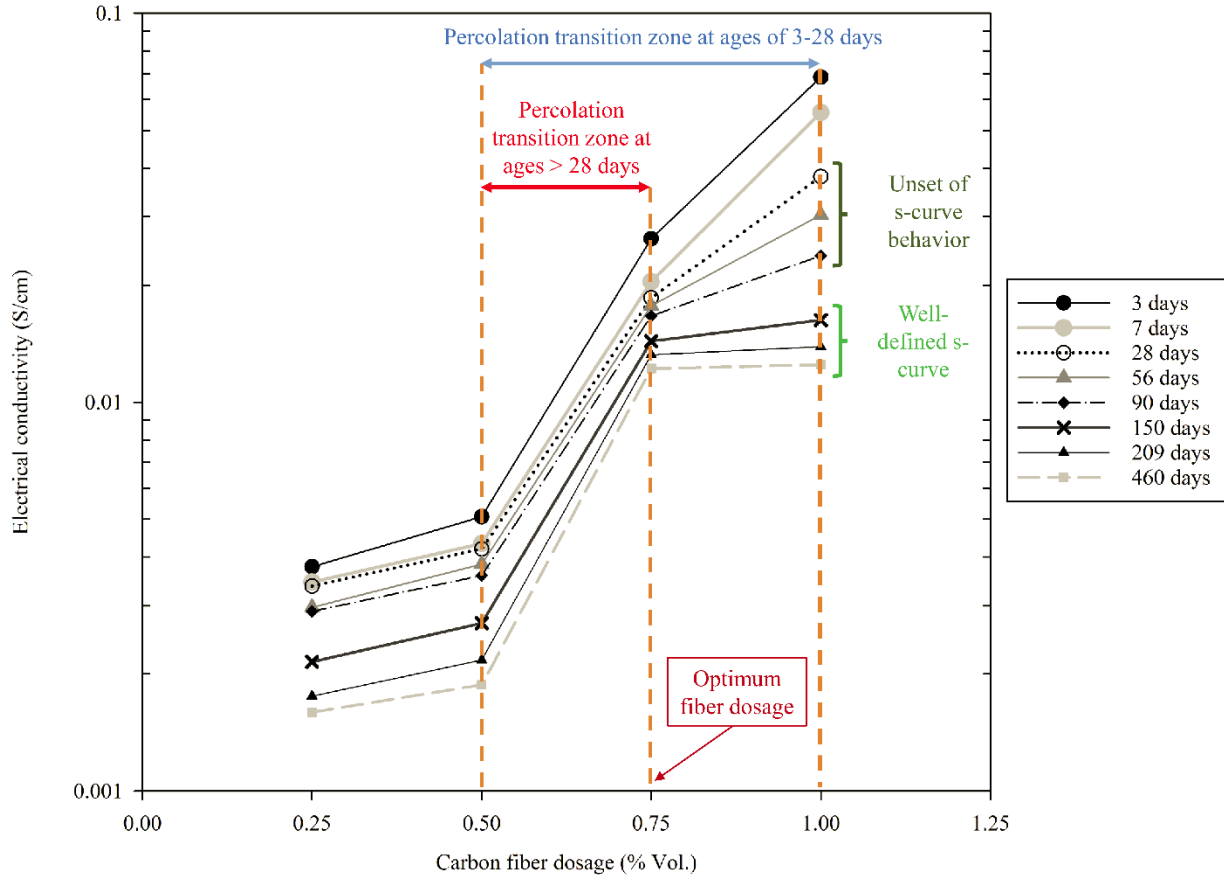


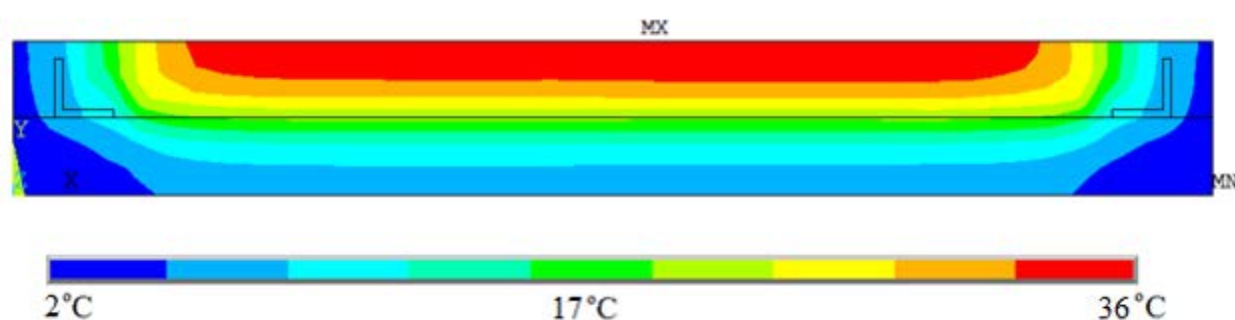
Figure 4-5 Variation of electrical conductivity by fiber content for ECON samples at different ages.

Table 4-9 Compressive Strength of ECON Samples at Ages of 7 and 28 Days.

| CF content (% Vol.) | Compressive strength (MPa) |    |
|---------------------|----------------------------|----|
|                     | Age (days)                 |    |
|                     | 7                          | 28 |
| 0.00                | 24                         | 35 |
| 0.25                | 26                         | 37 |
| 0.50                | 30                         | 39 |
| 0.75                | 30                         | 38 |
| 1.00                | 26                         | 38 |



Figure 4-6 shows the temperature distribution in both ECON and PCC layers obtained from the model. As revealed by the figure, higher temperatures were achieved at the center of the slab. The temperature distribution given by the model is important because it addresses the concern about heat concentration at the electrodes and shows that the temperature distribution over the surface is likely to be uniform with this system design. This could be considered as an advantage of ECON HPS over the use of heating elements embedded inside the concrete, which may be prone to non-uniform heating.



*Figure 4-6 Temperature distribution in the ECON HPS computed by FE model.*

Figure 4-7 and Figure 4-8 respectively present the time-temperature profiles during melting tests at 28 and 460 days of age. As the figures reveal, at 460 days, it took 1.25 times longer to melt the snow layer. While the applied voltage in the 460-day test (118 V) was higher than that used in the 28-day age (81.2 V), the electric current through the slab was still smaller (see Table 4-10). This behavior could be attributed to the increased electrical resistivity of ECON. As shown in Table 4-10, power absorption and power density at the slab surface were increased by 18% from 28 to 460 days which indicates higher energy demand to raise the surface temperature. As seen in the table, energy conversion efficiency decreased from 66% at 28 days to 50% at 460 days of age.

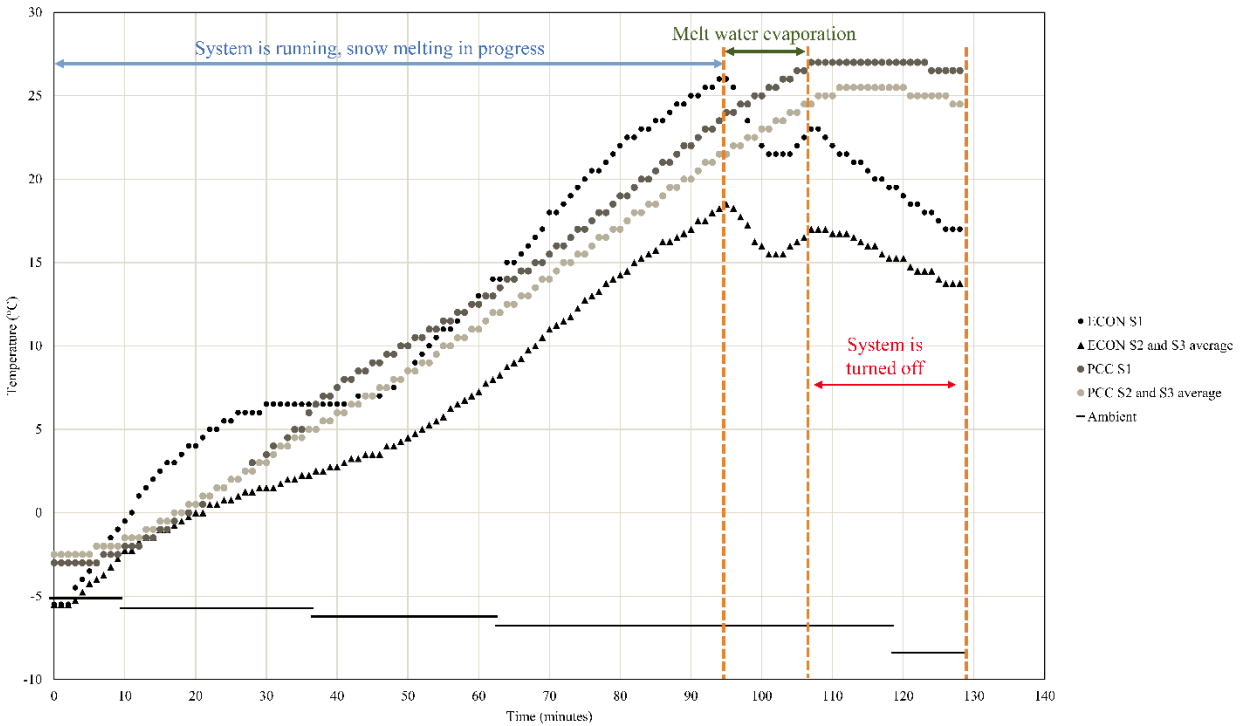


Figure 4-7 Temperature profile of ECON system during snow melting at 28-day age.

The increase of energy requirement for snow melting with concrete age causes a concern about the long-term performance of the system. The American Society of Heating, Refrigerating and Air Conditioning Engineers (ASHRAE) has specified an upper limit of 1.3 kW/m<sup>2</sup> for power density on heated pavement systems for snow melting [73]. While the power density at both ages still lay below this maximum limit, the power density at 460 days (1.27 kW/m<sup>2</sup>) was only marginally lower than that. Therefore, there is a concern that energy consumption grows above acceptable limits during the service life. Such performance deficiencies can be caused by age-dependent conductivity change, cracking in the ECON layer, and electrode corrosion. Note that the optimum carbon fiber volume fraction determined as the upper limit of percolation transition zone is a conductivity-based measurement, while, the heating performance-based carbon fiber dosage rate may be higher to ensure that energy consumption for snow melting stays sufficiently lower than the specification limits during the entire service life.

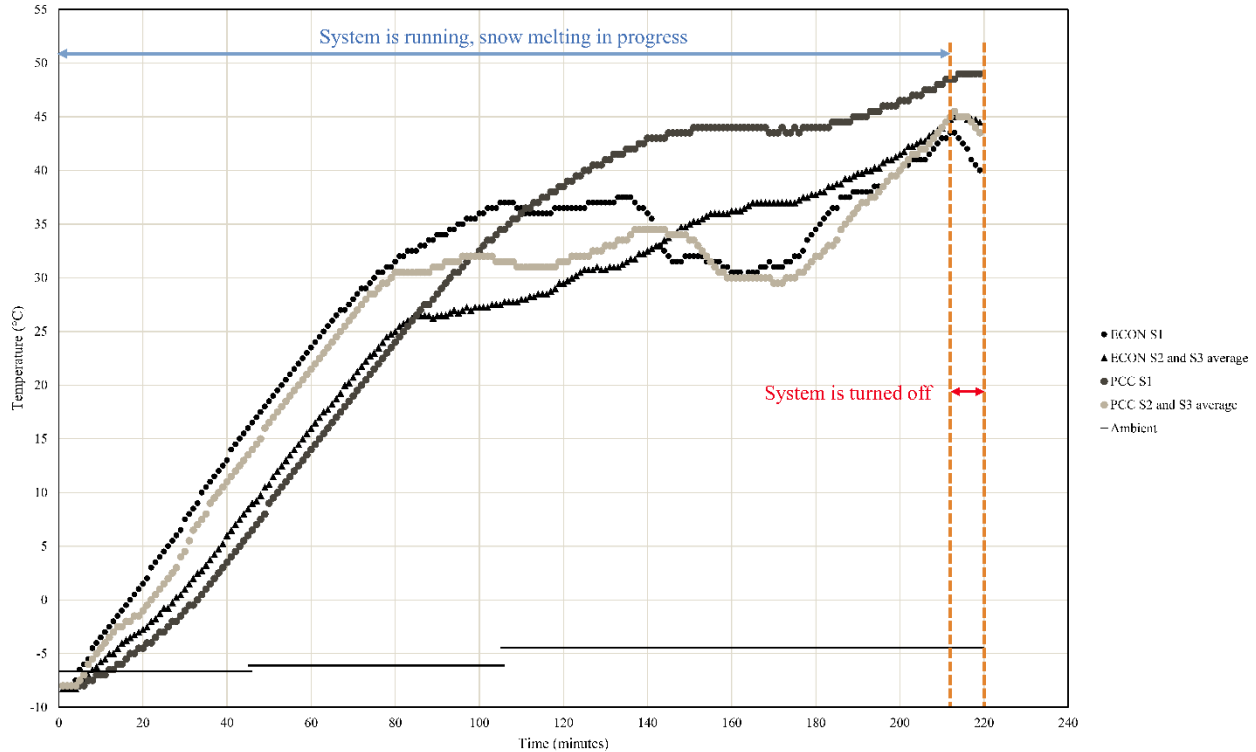


Figure 4-8 Temperature profile of ECON system during snow melting at 460-day age.

It is inferred from temperature profiles that a heat flux occurs between ECON layer and PCC layer, as the temperature change in the PCC and ECON layers followed the same overall trend. Hence, a portion of the heat loss that is responsible for the decrease of electrical energy conversion efficiency may be attributed to the heat flux between the ECON and the underlying PCC layer. The temperature distribution on the slab surface from the thermal imaging system (Figure 4-9) validates the FE model predicting that the highest temperatures were expected at the mid-span of the slab between the two electrodes. Figure 4-10 presents the comparison of FE model-predicted and measured temperatures at the center of ECON layer at the age of 28 days. The acceptable match between the predicted and measured values of temperature indicates the validity of the modeling approach for evaluation of system design. The divergence between the

model and the measurements around the 95th minute can be attributed to the evaporation of the melt water on the slab (discussed in the above) which was not accounted for by the model.

*Table 4-10 Energy and power requirements for melting 6 cm-thick compacter snow layer.*

| Concrete age (days) | Energy consumption |             |                       |                                    | Snow melting performance  |   |                              |                               |  |
|---------------------|--------------------|-------------|-----------------------|------------------------------------|---------------------------|---|------------------------------|-------------------------------|--|
|                     | Voltage (V)        | Current (A) | Power absorption (kW) | Power density (kW/m <sup>2</sup> ) | Snow melting duration (h) | Energy density for snow melting (kWh/m <sup>2</sup> ) | Input electrical energy (kJ) | Energy converted to heat (kJ) | Energy conversion efficiency in ECON (%) |
| 28                  | 81.20              | 11.70       | 0.95                  | 1.08                               | 1.60                      | 1.72  | 5472                         | 3610                          | 66                                       |
| 460                 | 118.00             | 9.50        | 1.12                  | 1.27                               | 3.56                      | 4.53  | 14367                        | 7152                          | 50                                       |

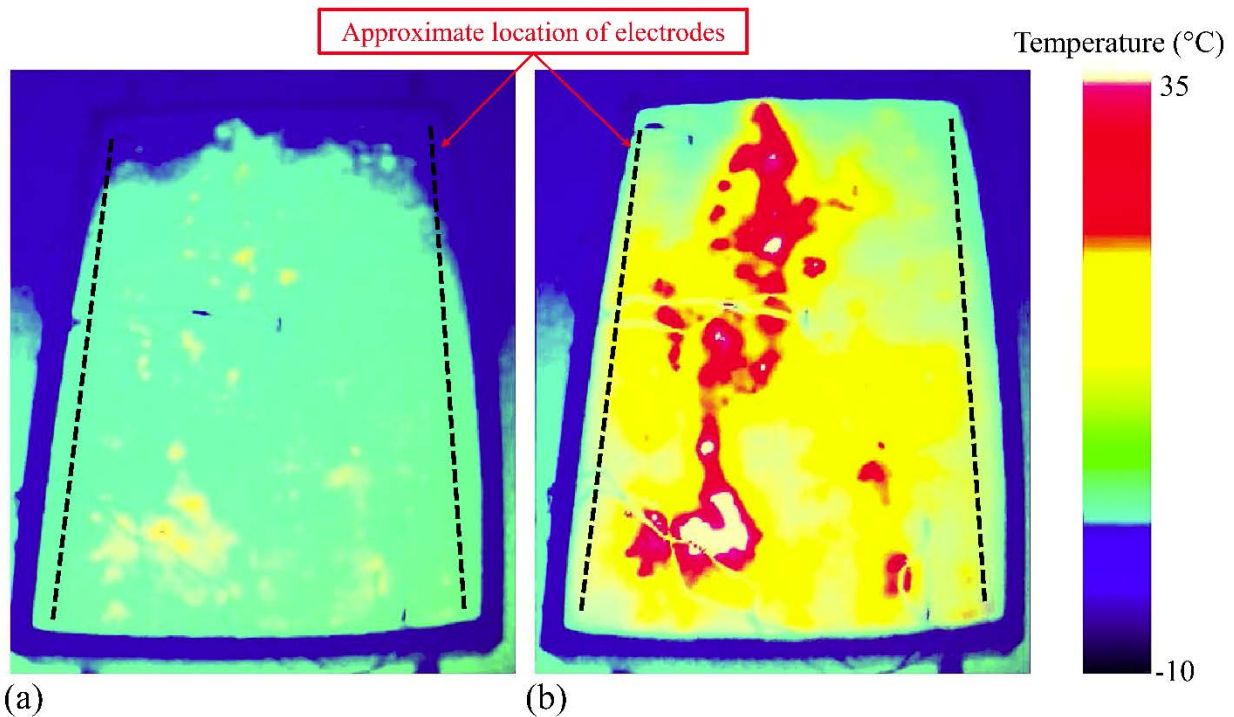


*Figure 4-9 Thermal image of prototype slab after one minute (a) and 60 minutes (b) of electric heating.*

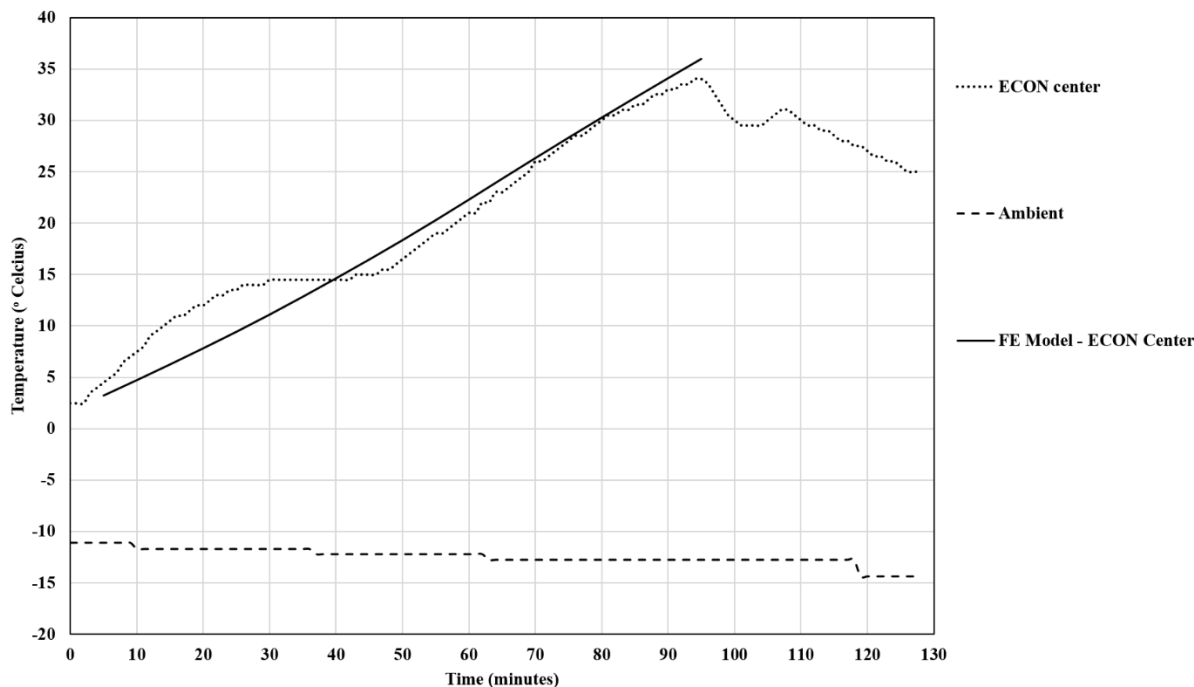


Figure 4-10 Predicted and measured temperatures at the center of ECON layer at 28-day age.

### Conclusions and Recommendations

Carbon fiber was incorporated into the concrete to prepare electrically conductive concrete (ECON) for heated pavement systems (HPS) application. Quasi long-term electrical conductivity evolution and heating performance variation were studied to determine the optimum carbon fiber dosage and investigate the energy consumption efficiency of the ECON HPS. The system design was evaluated with finite element (FE) modeling approach and the ice/snow melting ability of the produced ECON was experimentally studied. The key findings of the study were as follows:

- Measurement of the variation of electrical conductivity with fiber content in different types of cementitious composites (paste, mortar, and concrete) showed that percolation transition occurred when fiber volume dosage was between 0.25% and 1% in paste, 0.6% and 1% in mortar, and 0.5% and 0.75% in concrete.

- Electrical conductivity of ECON decreases dramatically with age up to 150 days. The rate slows down after 150 days and is almost stabilized at later ages.
- The study of the effect of carbon fiber dosage on electrical conductivity of cementitious composites showed that optimum carbon fiber volume fraction to avoid excessive fiber consumption is equal to the upper limit of percolation transition zone. However, based on the results of quasi long-term performance evaluation of ECON HPS, using carbon fibers in a dosage rate which is equal to the optimum volume fraction may not be sufficient to ensure that the energy consumption remains below the specification limits throughout the entire service life.
- The finite element model (FE) was found to be a viable means of evaluating the ECON HPS system design and configurations. The predicted results were similar to the experimental results. Both the FE model and experimental results showed that the heat distribution was acceptably uniform at the slab surface.
- Energy conversion efficiency exhibited a reduction from 66% at 28-day age to 50% at 460 days. At both ages the prototype ECON heated pavement system provided acceptable power density demand for snow melting.
- A considerable heat flux was observed from the ECON layer towards the underlying PCC layer. Insulating the ECON-PCC interface or using PCC with low thermal conductivity (e.g. light weight concrete) is recommended to improve energy consumption efficiency.

Future studies can consider the application of recycled carbon fibers to make the production of ECON environmentally and economically more attractive. It is recommended to perform life cycle assessment (LCA) analyses to investigate the carbon footprint of the ECON HPS under various combinations of production and operation scenarios. LCA analyses can compare ECON HPS with hydronic systems and traditional pavement deicing methods or

compare the recycled fiber-based with virgin fiber-based ECON. Furthermore, optimum scenarios for production and application of each deicing method can be identified by LCA analyses.

### Acknowledgements

This paper was prepared from a study conducted at Iowa State University under Federal Aviation Administration (FAA) Air Transportation Center of Excellence Cooperative Agreement 12-C-GA-ISU for the Partnership to Enhance General Aviation Safety, Accessibility and Sustainability (PEGASAS). The authors would like to thank the current project Technical Monitor, Mr. Benjamin J. Mahaffay, and the former project Technical Monitors, Mr. Jeffrey S. Gagnon (interim), Mr. Donald Barbagallo, and Dr. Charles A. Ishee for their invaluable guidance on this study. Special thanks are expressed to Zoltek, the Candlemakers Store (TCS), WR Grace and Co. for providing carbon fiber, methyl cellulose, and corrosion inhibitor admixture, respectively. Although the FAA has sponsored this project, it neither endorses nor rejects the findings of this research. The presentation of this information is in the interest of invoking comments by the technical community on the results and conclusions of the research.

### References

- [1] A. Sassani, H. Ceylan, S. Kim, K. Gopalakrishnan, A. Arabzadeh, P.C. Taylor, Factorial Study on Electrically Conductive Concrete Mix Design for Heated Pavement Systems, in: Transp. Res. Board 96th Annu. Meet., Washington DC, 2017: pp. 17–05347.
- [2] A. Arabzadeh, H. Ceylan, S. Kim, K. Gopalakrishnan, A. Sassani, S. Sundararajan, P.C. Taylor, Influence of Deicing Salts on the Water-Repellency of Portland Cement Concrete Coated with Polytetrafluoroethylene and Polyetheretherketone, in: ASCE Int. Conf. Highw. Pavements Airf. Technol., Philadelphia, Pennsylvania, 2017.
- [3] A. Arabzadeh, H. Ceylan, S. Kim, K. Gopalakrishnan, A. Sassani, Superhydrophobic Coatings on Asphalt Concrete Surfaces, Transp. Res. Rec. J. Transp. Res. Board. No. 2551 (2016).

- [4] Y. Lai, Y. Liu, D. Ma, Automatically melting snow on airport cement concrete pavement with carbon fiber grille, *Cold Reg. Sci. Technol.* 103 (2014) 57–62.
- [5] T. Yang, Z.J. Yang, M. Singla, G. Song, Q. Li, Experimental Study on Carbon Fiber Tape-Based Deicing Technology, *J. Cold Reg. Eng.* 26 (2012) 55–70.
- [6] H. Ceylan, K. Gopalakrishnan, S. Kim, W. Cord, Heated Transportation Infrastructure Systems : Existing and Emerging Technologies, in: *Civil, Constr. Environ. Eng. Conf. Present. Proceedings.23.*, Iowa State University, 2014.
- [7] A. Christopher, J.E. Strong, P.A. Mosher, Effect of Deicing Salts on Metal and Organic Matter Mobilization in Roadside Soils, *Environ. Sci. Technol.* 26 (1992) 703–709.
- [8] M. Bäckström, S. Karlsson, L. Bäckman, L. Folkesson, B. Lind, Mobilisation of heavy metals by deicing salts in a roadside environment, *Water Res.* 38 (2004) 720–732.
- [9] M.A. Cunningham, E. Snyder, D. Yonkin, M. Ross, T. Elsen, Accumulation of deicing salts in soils in an urban environment, *Urban Ecosyst.* 11 (2008) 17–31.
- [10] D. Sanzo, S.J. Hecnar, Effects of road de-icing salt (NaCl) on larval wood frogs (*Rana sylvatica*), *Environ. Pollut.* 140 (2006) 247–256.
- [11] I. Czerniawska-Kusza, G. Kusza, M. Dużyński, Effect of deicing salts on urban soils and health status of roadside trees in the Opole Region, *Environ. Toxicol.* 19 (2004) 296–301.
- [12] J.R. Karraker, Nancy E., Gibbs, James P., And Vonesh, Impacts of Road Deicing Salt on the Demography of Vernal Pool-Breeding Amphibians, *Ecol. Appl.* 18 (2016) 724–734.
- [13] D.M. Ramakrishna, T. Viraraghavan, Environmental impact of chemical deicers - A review, *Water. Air. Soil Pollut.* 166 (2005) 49–63.
- [14] W. Shen, H. Ceylan, K. Gopalakrishnan, S. Kim, P.C. Taylor, C.R. Rehmman, Life cycle assessment of heated apron pavement system operations, *Transp. Res. Part D Transp. Environ.* 48 (2016) 316–331.
- [15] H. Wang, C. Thakkar, X. Chen, S. Murrel, Life-cycle assessment of airport pavement design alternatives for energy and environmental impacts, *J. Clean. Prod.* 133 (2016) 163–171.
- [16] H. Xu, Y. Tan, Modeling and operation strategy of pavement snow melting systems utilizing low-temperature heating fluids, *Energy.* 80 (2015) 666–676.
- [17] A. Arabzadeh, H. Ceylan, S. Kim, K. Gopalakrishnan, A. Sassani, Superhydrophobic coatings on asphalt concrete surfaces: Toward smart solutions for winter pavement maintenance, 2016.



- [18] A. Arabzadeh, H. Ceylan, S. Kim, K. Gopalakrishnan, A. Sassani, Fabrication of Polytetrafluoroethylene Coated Asphalt Concrete Biomimetic Surfaces: A Nanomaterials Based Pavement Winter Maintenance Approach, in: ASCE Int. Conf. Transp. Dev., ASCE, Houston, Texas, 2016.
- [19] H. Ceylan, A. Arabzadeh, A. Sassani, S. Kim, K. Gopalakrishnan, Innovative nano-engineered asphalt concrete for ice and snow controls in pavement systems, in: 6th Eurasphalt & Eurobitume Congr., Prague, Czech Republic, 2016.
- [20] A. Arabzadeh, H. Ceylan, S. Kim, K. Gopalakrishnan, A. Sassani, S. Sundararajan, P.C. Taylor, Superhydrophobic coatings on Portland cement concrete surfaces, *Constr. Build. Mater.* 141 (2017) 393–401.
- [21] C. Chang, M. Ho, G. Song, Y.-L. Mo, H. Li, A feasibility study of self-heating concrete utilizing carbon nanofiber heating elements, *Smart Mater. Struct.* 18 (2009) 127001.
- [22] K. Gopalakrishnan, H. Ceylan, S. Kim, S. Yang, H. Abdulla, Self-Heating Electrically Conductive Concrete for Pavement Deicing: A Revisit, in: *Transp. Res. Board 94th Annu. Meet.*, 2015: p. No. 15-4764.
- [23] J. Gomis, O. Galao, V. Gomis, E. Zornoza, P. Garcés, Self-heating and deicing conductive cement. Experimental study and modeling, *Constr. Build. Mater.* 75 (2015) 442–449.
- [24] C.Y. Tuan, *Implementation of Conductive Concrete For Deicing*, Omaha, NE, 2008.
- [25] H. Xu, D. Wang, Y. Tan, J. Zhou, M. Oeser, Investigation of design alternatives for hydronic snow melting pavement systems in China, *J. Clean. Prod.* 170 (2018) 1413–1422.
- [26] H. Wang, L. Liu, Z. Chen, Experimental investigation of hydronic snow melting process on the inclined pavement, *Cold Reg. Sci. Technol.* 63 (2010) 44–49.
- [27] P. Pan, S. Wu, Y. Xiao, G. Liu, A review on hydronic asphalt pavement for energy harvesting and snow melting, *Renew. Sustain. Energy Rev.* 48 (2015) 624–634.
- [28] A. Sassani, H. Ceylan, S. Kim, A. Arabzadeh, P.C. Taylor, K. Gopalakrishnan, Development of Carbon Fiber-modified Electrically Conductive Concrete for Implementation in Des Moines International Airport, *Case Stud. Constr. Mater.* 8 (2018) 277–291.
- [29] D. Feng, N. Xie, C. Gong, Z. Leng, H. Xiao, H. Li, X. Shi, Portland Cement Paste Modified by TiO<sub>2</sub> Nanoparticles: A Microstructure Perspective, *Ind. Eng. Chem. Res.* 52 (2013) 11575–11582.
- [30] X. Yu, E. Kwon, Carbon Nanotube Based Self-sensing Concrete for Pavement Structural Health Monitoring, Research report—Contract Number: US DOT: DTFH61-10-C-00011, Duluth, Minnesota, 2012.

- [31] D. Gao, M. Sturm, Y.L. Mo, Electrical resistance of carbon-nanofiber concrete, *Smart Mater. Struct.* 20 (2011) 49501.
- [32] X. Fu, D.D.L. Chung, Self-monitoring of fatigue damage in carbon fiber reinforced cement, *Cem. Concr. Res.* 26 (1996) 15–20.
- [33] S. Wen, D.D.L. Chung, Seebeck effect in steel fiber reinforced cement, *Cem. Concr. Res.* 30 (2000) 661–664.
- [34] L. Pourzahedi, P. Zhai, J.A. Isaacs, M.J. Eckelman, Life cycle energy benefits of carbon nanotubes for electromagnetic interference (EMI) shielding applications, *J. Clean. Prod.* 142 (2017) 1971–1978.
- [35] P. Xie, P. Gu, Y. Fu, J.J. Beaudoin, Conductive cement-based compositions, US005447564A, 1995.
- [36] S. Yehia, C.Y. Tuan, Thin Conductive Concrete Overlay for Bridge Deck Deicing and Anti-Icing, *Transp. Res. Rec. J. Transp. Res. Board.* 1698 (2000) 45–53.
- [37] J. Wu, J. Liu, F. Yang, Three-phase composite conductive concrete for pavement deicing, *Constr. Build. Mater.* 75 (2015) 129–135.
- [38] J. Cao, D.D.L. Chung, Carbon fiber reinforced cement mortar improved by using acrylic dispersion as an admixture, *Cem. Concr. Res.* 31 (2001) 1633–1637.
- [39] D.D.L. Chung, Electrically conductive cement-based materials, *Adv. Cem. Res.* 4 (2004) 167–176.
- [40] Z. Hou, Z. Li, J. Wang, Electrical conductivity of the carbon fiber conductive concrete, *J. Wuhan Univ. Technol. Sci. Ed.* 22 (2007) 346–349.
- [41] C. Chang, G. Song, D. Gao, Y.L. Mo, Temperature and mixing effects on electrical resistivity of carbon fiber enhanced concrete, *Smart Mater. Struct.* 22 (2013) 35021.
- [42] S. Wen, D.D.L. Chung, A Comparative Study of Steel- and Carbon-Fiber Cement as Piezoresistive Strain Sensors, *Adv. Cem. Res.* 15 (2003) 119–128.
- [43] A. Pérez, M.A. Climent, P. Garcés, Electrochemical extraction of chlorides from reinforced concrete using a conductive cement paste as the anode, *Corros. Sci.* 52 (2010) 1576–1581.
- [44] R.N. Kraus, T.R. Naik, *Testing and Evaluation of Concrete Using High- Carbon Fly Ash and Carbon Fibers*, Milwaukee, Wisconsin, 2006.
- [45] J. Carmona, P. Garcés, M.A. Climent, Efficiency of a conductive cement-based anodic system for the application of cathodic protection, cathodic prevention and electrochemical chloride extraction to control corrosion in reinforced concrete structures, *Corros. Sci.* 96 (2015) 102–111.

- [46] X. Fu, D.D.L. Chung, Submicron-diameter-carbon-filament cement-matrix composites, *Carbon N. Y.* 36 (1998) 459–462.
- [47] O. Galao, L. Bañón, F.J. Baeza, J. Carmona, P. Garcés, Highly Conductive Carbon Fiber Reinforced Concrete for Icing Prevention and Curing, *Materials (Basel)*. 9 (2016) 281.
- [48] J. Wu, J. Liu, F. Yang, Study on Three-phase Composite Conductive Concrete for Pavement Deicing, in: *Transp. Res. Board 93rd Annu. Meet.*, 2014: p. No. 14-2684.
- [49] S. Wang, S. Wen, D.D.L. Chung, Resistance heating using electrically conductive cements, *Adv. Cem. Res.* 16 (2004) 161–166.
- [50] Standards for Specifying Construction of Airports, FAA Advisory circular No.150/5370-10G, (2014).
- [51] A. Sassani, H. Ceylan, S. Kim, A. Arabzadeh, P.C. Taylor, K. Gopalakrishnan, Development of Carbon Fiber-modified Electrically Conductive Concrete for Implementation in Des Moines International Airport, *Case Stud. Constr. Mater.* 8 (2018).
- [52] B. Chen, J. Liu, Effect of fibers on expansion of concrete with a large amount of high f-CaO fly ash, *Cem. Concr. Compos.* 33 (2003) 1549–1552.
- [53] A. Peyvandi, P. Soroushian, A.M. Balachandra, K. Sobolev, Enhancement of the durability characteristics of concrete nanocomposite pipes with modified graphite nanoplatelets, *Constr. Build. Mater.* 47 (2013) 111–117.
- [54] X. Shu, R.K. Graham, B. Huang, E.G. Burdette, Hybrid effects of carbon fibers on mechanical properties of Portland cement mortar, *Mater. Des.* 65 (2015) 1222–1228.
- [55] R.K. Graham, B. Huang, X. Shu, E.G. Burdette, Laboratory evaluation of tensile strength and energy absorbing properties of cement mortar reinforced with micro- and meso-sized carbon fibers, *Constr. Build. Mater.* 44 (2013) 751–756.
- [56] J. Howarth, S.S.R. Mareddy, P.T. Mativenga, Energy intensity and environmental analysis of mechanical recycling of carbon fibre composite, *J. Clean. Prod.* 81 (2014) 46–50.
- [57] X. Li, R. Bai, J. McKechnie, Environmental and financial performance of mechanical recycling of carbon fibre reinforced polymers and comparison with conventional disposal routes, *J. Clean. Prod.* 127 (2016) 451–460.
- [58] P. Chen, D.D.L. Chung, Improving the Electrical Conductivity of Composites Comprised of Short Conducting Fibers in a Nonconducting Matrix: The Addition of a Nonconducting Particulate Filler, in: *MRS Proc.*, 1995: pp. 141–146.
- [59] S. Wen, D.D.L. Chung, Double percolation in the electrical conduction in carbon fiber reinforced cement-based materials, *Carbon N. Y.* 45 (2007) 263–267.

- [60] P. Xie, G. Ping, J.J. Beaudoin, Electrical Percolation Phenomena in Cement Composites Containing Conductive Fibers, *J. Mater. Sci.* 31 (1996) 4093–4097.
- [61] Cao, Jingyao, D.D.L. Chung, Electric polarization and depolarization in cement-based materials, studied by apparent electrical resistance measurement, *Cem. Concr. Res.* 34 (2004) 481–485.
- [62] M. Sun, Z. Li, Q. Mao, D. Shen, Study on the Hole Conduction Phenomenon in Carbon Fiber-Reinforced Concrete, *Cem. Concr. Res.* 28 (1998) 549–554.
- [63] S. Wen, D.D.L. Chung, Seebeck effect in carbon fiber-reinforced cement, *Cem. Concr. Res.* 29 (1999) 1989–1993.
- [64] F. Vossoughi, *Electrical Resistivity of Carbon Fiber Reinforced Concrete*, Berkeley, CA, 2004.
- [65] F. Javier Baeza, D.D.L. Chung, E. Zornoza, L.G. Andión, P. Garcés, Triple percolation in concrete reinforced with carbon fiber, *ACI Mater. J.* 107 (2010) 396–402.
- [66] M. Sun, Z. Li, Q. Mao, D. Shen, Thermoelectric Percolation Phenomena in Carbon Fiber-Reinforced Concrete, *Cem. Concr. Res.* 28 (1998) 1707–1712.
- [67] D.D. Chung, Dispersion of Short Fibers in Cement, *J. Mater. Civ. Eng.* 17 (2005) 379–383.
- [68] M. Hambach, H. Moller, T. Neumann, D. Volkmer, Carbon fibre reinforced cement-based composites as smart floor heating materials, *Compos. Part B Eng.* 90 (2016) 465–470.
- [69] H. Abdulla, H. Ceylan, S. Kim, K. Gopalakrishnan, P.C. Taylor, Y. Turkan, System requirements for electrically conductive concrete heated pavements, *Transp. Res. Rec.* 2569 (2016) 70–79.
- [70] H. Abdulla, K. Gopalakrishnan, H. Ceylan, S. Kim, M. Mina, P. Taylor, K.S. Cetin, Development of A Finite Element Model for Electrically Conductive Concrete Heated Pavements, in: the 96th Annual meeting of Transportation Research Board, January 8-12, 2017, Washington, D.C., 2017: pp. 1–18.
- [71] C. Shi, Effect of mixing proportions of concrete on its electrical conductivity and the rapid chloride permeability test (ASTM C1202 or ASSHTO T277) results, *Cem. Concr. Res.* 34 (2004) 537–545.
- [72] K. Wang, J.K. Cable, G. Zhi, *Investigation Into Improved Pavement Curing Materials And Techniques : Part 1 ( Phases I And II)*, Ames, Iowa, USA, 2002.
- [73] SNOW MELTING AND FREEZE PROTECTION, in: *ASHRAE Handb. Fundam.*, 15th ed., American Society of Heating, Refrigerating and Air-Conditioning Engineers, Atlanta, GA, 2009.

- [74] A. Sassani, H. Ceylan, S. Kim, K. Gopalakrishnan, A. Arabzadeh, P.C. Taylor, Influence of mix design variables on engineering properties of carbon fiber-modified electrically conductive concrete, *Constr. Build. Mater.* 152 (2017).
- [75] A. Sassani, H. Ceylan, S. Kim, K. Gopalakrishnan, A. Arabzadeh, P.C. Taylor, Influence of mix design variables on engineering properties of carbon fiber-modified electrically conductive concrete, *Constr. Build. Mater.* 152 (2017) 168–181.
- [76] H. Abdulla, H. Ceylan, S. Kim, M. Mina, K. Gopalakrishnan, A. Sassani, P.C. Taylor, K.S. Cetin, Configuration of Electrodes for Electrically Conductive Concrete Heated Pavement, in *ASCE Int. Conf. Highw. Pavements Airf. Technol.*, Philadelphia, Pennsylvania, USA, 2017.
- [77] B. Chen, K. Wu, W. Yao, Conductivity of carbon fiber reinforced cement-based composites, *Cem. Concr. Compos.* 26 (2004) 291–297.
- [78] A.A. Ramezani pour, A. Pilvar, M. Mahdikhani, F. Moodi, Practical evaluation of relationship between concrete resistivity, water penetration, rapid chloride penetration and compressive strength, *Constr. Build. Mater.* 25 (2011) 2472–2479.

## CHAPTER 5. DEVELOPMENT OF CARBON FIBER-MODIFIED ELECTRICALLY CONDUCTIVE CONCRETE FOR IMPLEMENTATION IN DES MOINES INTERNATIONAL AIRPORT

A paper published in the Journal of Case Studies in Construction Materials

Alireza Sassani<sup>1</sup>, Halil Ceylan<sup>2</sup>, Sunghwan Kim<sup>3</sup>, Ali Arabzadeh<sup>4</sup>, Peter C. Taylor<sup>5</sup>, and Kasthurirangan Gopalakrishnan<sup>6</sup>

### Abstract

This paper reports on the procedures of mix design preparation, production, placement, and performance evaluation of the first electrically conductive concrete (ECON) heated-pavement system (HPS) implemented at a U.S. airport. While ECON has drawn considerable attention as a paving material for multi-functional pavements, including HPS, the majority of ECON HPS applications and studies have been limited to laboratory scale or include materials/methods that do not conform to regulations enforced by airfield construction practices. Carbon fiber-reinforced ECON provides a promising prospective for application in airfield pavements. In this study, ECON mixtures were prepared in the laboratory using varying cementitious materials, aggregate systems, water-to-cementitious ratios, carbon fiber dosages, and admixtures. The results of tests on laboratory-prepared mixes were utilized to find the most suitable ECON mix design for application in an HPS test section at the Des Moines International Airport. The properties of the ECON produced at the concrete plant were measured and

---

<sup>1</sup> Ph.D. Candidate, Civil, Construction and Environmental Engineering (CCEE), Iowa State University (ISU), Ames, IA, E-mail: [asassani@iastate.edu](mailto:asassani@iastate.edu) (Corresponding author)

<sup>2</sup> Professor, Director, Program for Sustainable Pavement Engineering and Research (PROSPER), CCEE, ISU, Ames, IA, E-mail: [hceylan@iastate.edu](mailto:hceylan@iastate.edu)

<sup>3</sup> Research Scientist, Iowa State University, ISU, Ames, IA, E-mail: [sunghwan@iastate.edu](mailto:sunghwan@iastate.edu)

<sup>4</sup> Ph.D. Candidate, CCEE, ISU, Ames, IA, E-mail: [arab@iastate.edu](mailto:arab@iastate.edu)

<sup>5</sup> Director, National Concrete Pavement Technology Center, SU, Ames, IA, E-mail: [ptaylor@iastate.edu](mailto:ptaylor@iastate.edu)

<sup>6</sup> Research Associate Professor, Iowa State University, Ames, IA. Email: [rangan@iastate.edu](mailto:rangan@iastate.edu)

compared with equivalent laboratory-prepared samples. The final mix design exhibited electrical resistivity of 115  $\Omega$ -cm in the laboratory and 992  $\Omega$ -cm in the field, while completely meeting strength and workability requirements. Despite the higher ECON resistivity obtained in large-scale production, the fabricated HPS exhibited desirable performance with respect to deicing and anti-icing operations. The test section was able to generate a 300-350 W/m<sup>2</sup> power density and to effectively melt ice/snow with this level of energy.

### Introduction

Surface conditions of paved areas during harsh winter weather conditions play a crucial role in airport operations. Bad weather conditions are responsible for about 29% of total airplane incidents and accidents, the majority of which occur during take-off and landing [1]. Ice/snow accumulation on paved surfaces of runways, aprons, and taxiways annually causes thousands of flight cancellations or delays [2]. Therefore, airlines and airports incur millions of dollars of expenditure to remove ice and snow from airport pavements. Traditional ice/snow removal methods are using deicing chemicals and mechanical removal that are associated with flight delays, large number of manpower, sophisticated machinery, environmentally harmful chemicals, and damage to pavement [3–8]. Furthermore, the common deicing methods have not shown effectiveness in extreme weather conditions. The machinery can face operational difficulty in freezing weather conditions. The effective temperature range for most deicing chemicals such as sodium chloride, calcium magnesium acetate, and urea does not fall below -10 °C (14°F); only calcium chloride-based deicers –that cause chloride ingress risk for concrete pavements- are effective below -17°C (1.4°F) [9].

The shortcomings and drawbacks of current ice/snow removal practices have steered researchers toward seeking new methods. Factors such as geographical location, environmental

conditions, material availability, and design specifications all influence selection of a deicing method, so no single solution for replacing current methods is available [10]. Many alternative methods have been proposed and tested for this purpose; among them are water-repellent coatings [2, 11, 12], heated pavements with embedded resistive heating elements [6], heated hydronic pavement systems [13, 14], and self-heating electrically conductive concrete (ECON) [9,15–20]. Heated-pavement systems (HPS) combine two basic strategies of anti-icing and deicing for controlling snow and ice on pavement surfaces [10]. ECON-based HPS has proven to be an efficient approach in many locations [21]. The general constituents of ECON are cement, aggregates, water, electrically conductive additives (ECAs), and possibly admixtures, however, the primary source of electrical conductivity is the ECA phase that creates a continuous path for electrical conduction [3].

Carbon fibers can be used as an ECA in minor volume and weight dosages [22–26]. Previous studies have shown the ability of carbon fiber to render cementitious composites electrically conductive while improving the concrete properties such as freeze-thaw durability, compressive strength, tensile strength, fatigue cracking, shrinkage cracking potential, and expansion cracking susceptibility [3, 27–30]. While carbon fiber has shown its effectiveness as an ECA in low volume dosages (0.4-1% Vol.), the optimum carbon fiber dosage in an electrically conductive cementitious composite is defined by multiple factors, the most important of which are so-called percolation phenomenon, the concrete workability requirements, and the economic considerations.

Forming a continuous network within the cementitious composite by the ECA materials is referred to as percolation phenomenon and the volume content of ECA enabling the percolation is called the percolation threshold [30–32]. With respect to percolative behavior, the



effective carbon fiber dosage for producing electrically conductive cementitious composites is between 0.5% and 1% (Vol.) [27, 30, 33–42] which depends on the type of composite (paste, mortar, or concrete), fiber aspect ratio, and fiber length [25]. In short carbon fibers (represented by approximately 7-15  $\mu\text{m}$  nominal diameter and 1-10 mm length), increasing fiber length decreases percolation threshold [25], but increasing the fiber length results in fiber dispersion difficulty [26], and loss of concrete workability [30]. Excessive carbon fiber content reduces the workability of the mixture and, since carbon fiber is the most expensive component of ECON, is not economically justified. So the carbon fiber dosage should be maintained in the vicinity of percolation threshold, such that sufficient electrical conductivity is achieved with minimum negative effects on workability and cost.

Polyacrylonitrile (PAN)-based carbon fibers [33] with diameters between 7 and 15  $\mu\text{m}$  and nominal lengths of 3-6 mm provided superior effectiveness in improving mechanical properties of concrete and imparting high electrical conductivity to cementitious composites [24,25]. In this paper, carbon fiber and carbon microfiber are used interchangeably to refer to carbon fibers with  $\mu\text{m}$ -scale diameter and mm-scale length. Shown by previous studies [8, 18, 19, 22, 24, 33, 43], the carbon microfiber is the most effective carbon product for improving electrical conductivity. For example, carbon nano- fibers (CNF) are less effective than carbon microfibers which have length ranges between 3 and 15 mm [25]. Likewise, powder materials such as graphite powder or coke powder exert less effect on electrical resistivity improvement [25]. On the other hand, the most effective carbonaceous fibers for structural enhancement of concrete are carbon microfibers and microfibers work better than macro- and nano-fibers for structural reinforcement [26]. However, the smaller the fiber diameter, the more difficult is its dispersion in a concrete mixture and, given the same fiber material and diameter, shorter fibers

are easier to disperse [26]. For volume dosages below 1%, and approximately 7 $\mu$ m diameter, carbon fibers with aspect ratios of about 860 provided performance superior to either longer or shorter fiber types in improving electrical conductivity of concrete, but high aspect ratio fibers are more difficult to disperse in concrete and adversely affect the workability of the mixture [26]. Shorter length and lower aspect ratio carbon fibers are easier to disperse, and they contribute a smaller effect on workability, so, despite being otherwise inferior to the 860-aspect ratio-fibers, carbon fibers with an aspect ratio of about 430 have been found to exhibit good performance in improving electrical conductivity of ECON [41].

Wen and Chung [36, 38] reported electrical resistivity values between  $1.50 \times 10^4 \Omega\text{-cm}$  and  $1.92 \times 10^4 \Omega\text{-cm}$  in cement pastes doped with carbon microfibers in dosages of 0.4-0.5% Vol.; they reached electrical resistivity as low as  $8.30 \times 10^2 \Omega\text{-cm}$  in cement pastes when the carbon fiber dosage in cement paste was increased to 0.95% Vol. of the mixture [37]. Wen and chung [38] also suggested that electrically conductive cement paste behaves as a thermistor, i.e. its electrical resistivity decreases with increasing temperature. Baeza et al. [42] produced electrically conductive cement paste by adding carbon fiber to cement paste in dosages of 0.22-0.95% Vol. and reported the lowest resistivity of  $6.04 \times 10^5 \Omega\text{-cm}$  achieved with 0.95% Vol. carbon fiber dosage. Hambach et al. [41] used cement paste modified with 1% Vol. carbon fiber and electrical resistivity as low as  $3.6 \times 10^1 \Omega\text{-cm}$  for resistive heating of a small laboratory-scale slab. Having fine aggregates (sand) included in the carbon fiber-modified cementitious composites, electrically conductive mortar were produced. However, electrical resistivity of  $5.41 \times 10^2 \Omega\text{-cm}$  was achieved only when carbon fiber dosage was increased up to 1.16% Vol. [27, 39].

While mortar tests showed less success than cement paste, it was found that carbon fiber-modified concrete which essentially consists of cementitious materials, fine aggregate, coarse aggregate, water, carbon fiber, and admixtures, provides a promising perspective to attain low electrical resistivity with relatively low dosages of ECA [22,33–35,40]. Wu et al. [33] and Chang et al. [35] reported  $4.00 \times 10^3 \Omega\text{-cm}$  and  $2.00 \times 10^4 \Omega\text{-cm}$  resistivities in ECON with 0.8% (Vol.) and 0.75% (Vol.) carbon fiber dosages respectively. While, using 0.73% (Vol.) carbon fiber content in ECON, Hou et al. [34] achieved  $3.8 \times 10^1 \Omega\text{-cm}$  resistivity. Also, Kraus and Naik [40] produced ECON with  $1.27 \times 10^2 \Omega\text{-cm}$  resistivity using only 0.5% Vol. carbon fiber content. These observations lead to the conclusion that carbon fiber dosage is not the only important factor in electrical conductivity/resistivity of ECON, such that the mixing proportions and mixture components -such as cementitious system, aggregates, and admixtures- also play an important role in defining the electrical characteristics of ECON. For example, Kraus and Naik [40] used high-carbon fly ash to boost the electricity conduction in the concrete matrix and Chang et al. [35] improved fiber dispersion and electrical conductivity by adjusting the mixing proportions of carbon fiber-containing concrete making it similar to self-consolidating concrete. Hou et al. [34] utilized silica fume to enhance the fiber dispersion and enable the use of longer fibers which are more effective in rendering the concrete matrix electrically conductive. Therefore, investigating different mixing proportions and mixture components gain even more importance in production of carbon fiber-modified ECON than in regular/plain concrete.

In the United States, two field implementations of ECON HPS have been previously reported: the Roca Spur Bridge deck project in Nebraska [44], and bridge 17-75R on the Castle Peak Undercrossing in California [43]. The former used ECON containing 1.5% (Vol.) steel fiber and 25% (Vol.) graphite, while the latter used polymer concrete as a blend of polyester

resin, mineral aggregates, and coke breeze. Numerous studies have tested ECON HPS with various ECON recipes at laboratory scale. Heymsfield et al. [45] tested a 1.2×3 m HPS using ECON containing 17.2% (Vol.) graphite powder and 2.7% (Vol.) steel fiber ECAs. Piskunov et al. [46] investigated application of different electrically conductive materials in electrically conductive concrete overlay for deicing of roads and airfield pavements; they used 70 mm cubic specimens. Hou et al. [34] used carbon fiber-reinforced ECON including silica fume for laboratory-scale deicing tests. Chang et al. [16] applied a new approach by mixing carbon fiber ECA in a self-consolidating concrete mixture. Galao et al. [22] used carbon fiber-reinforced conductive concrete for deicing on 30×30×2 cm specimens. Won et al. [19] made an ECON HPS laboratory-scale prototype by incorporating graphite, coke powder, metal fiber, aluminum powder, and steel fiber in concrete mix. Deicing tests were conducted by Sun et al. [17] on a 200×50×5 cm light-weight ECON HPS specimen made with carbon fiber-carbon black ECA. Chen and Gao [18] proposed double-layered stainless steel fiber reinforcement of concrete for making self-heating ECON; they tested the performance on 30×30×6 cm specimens. Wu et al. [33] proposed a three-phase composite conductive concrete with the carbon and steel fibers, as well as graphite for pavement deicing.

Implementation of ECON HPS requires project- and location-specific guidelines to address material selection, mixing proportions, mixing procedure, and various other challenges. A mix design provided for an airport ECON HPS in the United States should meet specifications enforced by the Federal Aviation Administration (FAA). Among the ECON recipes provided in the literature, only a few have undergone large-scale field tests, and most of the aforementioned mix designs cannot be applied to airport rigid pavements. For example, the FAA prohibits using steel fiber and silica fume due to risks of foreign object debris damage to aircraft [47]. High

dosage of ECA materials (as in above-mentioned references) can cause strength reduction, loss of workability, and cost problems. Since, to the best of authors' knowledge, field implementation of ECON in an airport and field implementation of carbon fiber-reinforced ECON are unprecedented, such problems have so far not been addressed.

The objective of this research was to design and produce ECON for implementation of an ECON HPS test section at the Des Moines International Airport (DSM) and test the adequacy of the mix design provided for this purpose. The fabricated section included two adjacent slabs located in a general aviation apron area. Numerous different ECON mixtures were made and tested in the laboratory to seek a suitable ECON mix design. Finally, based on evaluation of the laboratory-prepared mixes, an ECON mix design was provided for use in the ECON slabs. The properties of the ECON (both in the laboratory and in the field), and the slab performances were monitored and evaluated under winter conditions.

### **Materials and Methodology**

This research was motivated by the project supported by Federal Aviation Administration (FAA) for implementation of an ECON HPS test section in Des Moines International Airport (DSM). The selected location was a general aviation apron, where, two pavement slabs were dedicated to testing ECON HPS. The results of previous studies by the authors [3, 21, 30, 48] showed that maintaining an acceptable balance between electrical conductivity and workability of an ECON mixture is a challenging task, particularly when the mixture is meant to be produced in large scale. Therefore, a total of 36 Electrically Conductive Concrete (ECON) mix designs were designed, prepared in the laboratory, and evaluated with respect to workability, consistency, strength, electrical resistivity, and conformance to FAA specifications. The standard specifications used for evaluating the materials were FAA AC 5370-10G [47], FAA AC 5370-17

[49], and the relevant standards mentioned therein. The laboratory-prepared ECON mixes were used to find a combination of carbon fiber dosage, aggregate system, and cementitious system that provides required workability and electrical conductivity to tailor the ECON mix design to the project requirements. The electrically conductive additive (ECA) used for ECON preparation was carbon fiber. Selection of carbon fiber as an ECA and specific sizes and types of carbon fiber were based on the findings of the existing literature (given in introduction) and the previous studies by the authors [3, 21, 30, 48, 50, 51].

### Materials

- Coarse aggregate (CA)- ASTM C 33 D-67, nominal maximum size 19 mm.
- Intermediate aggregate (IA)- ASTM C 33 #8-gradation, nominal maximum size 9.5 mm.
- Fine aggregate (FA) conforming to ASTM C 33.
- ASTM C150 type I/II Portland cement (PC).
- ASTM C 618 class F fly ash (FF).
- ASTM C989 Grade 120 slag cement (SC). Table 5-1 provides the chemical compositions of PC, FF, and SC used in this research.
- ASTM C 494 high-range water reducing – type F- admixture (HRWR). MasterGlenium 7500 obtained from BASF.
- Methylcellulose powder as fiber-dispersive agent (FDA). Methylcellulose was used as explained in [30].
- WR Grace & Co. Derex Corrosion Inhibitor (DCI) admixture as conductivity-enhancing agent (CEA). The CEA was utilized according to Sassani et al. [30].
- Air entraining agent (AEA), conforming to ASTM C 260. MasterAir VR-10 by BASF.

- Chopped carbon fiber (CF) was PAN-based with 7.2  $\mu\text{m}$  diameter, 95% carbon content, and electrical resistivity of  $1.55 \times 10^{-3} \Omega\text{-cm}$ . Two different length size classes of the same type carbon fiber were used, PX35-0.125 and PX35-0.25, with nominal lengths of 3 mm and 6 mm, respectively. Specific gravity and water absorption capacity of the carbon fibers were 1.81 and 7.35 (% wt.), respectively. These carbon fibers were selected based on the aforementioned suggestions made by existing literature and the results of previous studies by the authors [3, 21, 30, 48].

*Table 5-1. Chemical compositions of cementitious materials.*

| <b>Oxides</b>                      | <b>PC</b> | <b>FF</b> | <b>SC</b> |
|------------------------------------|-----------|-----------|-----------|
| <b>SiO<sub>2</sub></b>             | 20.10     | 52.10     | 37.60     |
| <b>Al<sub>2</sub>O<sub>3</sub></b> | 4.44      | 16.00     | 9.53      |
| <b>Fe<sub>2</sub>O<sub>3</sub></b> | 3.09      | 6.41      | 0.44      |
| <b>CaO</b>                         | 62.94     | 14.10     | 40.20     |
| <b>MgO</b>                         | 2.88      | 4.75      | 11.00     |
| <b>SO<sub>3</sub></b>              | 3.18      | 0.59      | 1.14      |
| <b>K<sub>2</sub>O</b>              | 0.61      | 2.36      | 0.44      |
| <b>Na<sub>2</sub>O</b>             | 0.10      | 1.72      | 0.45      |
| <b>Loss on ignition</b>            | 2.55      | 0.09      | 0.01      |

### Laboratory-prepared ECON Mix Designs

The optimum dosage of the carbon fiber used in this research for ECON HPS was 0.75-1% (Vol.) [3, 30]. The coarse-to-fine aggregate and aggregate-to-cementitious ratios, cementitious materials, aggregate gradation, water-to-cementitious ratio (W/C), and fiber dispersive admixtures all influence the electrical conductivity of concrete and also significantly affect the fresh and hardened properties of the carbon fiber-reinforced concrete mixture, so particular combinations of these factors provide ECON mixtures with different electrical conductivity, workability, and strength. Twelve mix design groups were established using different combinations of aggregate system, carbon fiber dosage, HRWR dosage, and W/C. Table 5-2 provides the gradations of the aggregate system for each mix design group. A total of nine different aggregate systems (combined FA, CA, and IA) were used in the 12 mix design groups; the aggregate systems of mix design groups 2 and 3 were similar; as were those for groups 4, 5, and 12; the gradation curves of aggregate systems are presented in Figure 5-1.

Each mix design group was repeated three times, with three different cementitious systems: (C) 100% PC; (F) 80% PC-20% FF (wt.); and (S) 75% PC-25% SC (wt.), to make a total of 36 ECON mixtures. Table 5-3 gives the mixing proportions of all laboratory-prepared ECON mixes with each mixture defined by a number and a letter that respectively refer to mix design group and cementitious system. FDA dosage in all mixtures was 0.2% (wt. cementitious) and CEA was used in a fixed amount in all mixtures. The HRWR dosage (% wt. cementitious) varied by mix design group and the AEA dosage was 262 ml per 100 kg of cementitious.



Table 5-2. Combined aggregate gradations for each mix design group.

| Sieve<br>size<br>(mm) | Mix Design Group      |        |        |        |        |        |        |       |        |        |        |        |
|-----------------------|-----------------------|--------|--------|--------|--------|--------|--------|-------|--------|--------|--------|--------|
|                       | 1                     | 2      | 3      | 4      | 5      | 6      | 7      | 8     | 9      | 10     | 11     | 12     |
|                       | Percent (wt.) passing |        |        |        |        |        |        |       |        |        |        |        |
| <b>50.000</b>         | 100.00                | 100.00 | 100.00 | 100.00 | 100.00 | 100.00 | 100.00 | 99.99 | 100.00 | 100.00 | 100.00 | 100.00 |
| <b>37.500</b>         | 100.00                | 100.00 | 100.00 | 100.00 | 100.00 | 100.00 | 100.00 | 99.99 | 100.00 | 100.00 | 100.00 | 100.00 |
| <b>25.000</b>         | 100.00                | 100.00 | 100.00 | 100.00 | 100.00 | 100.00 | 100.00 | 99.99 | 100.00 | 100.00 | 100.00 | 100.00 |
| <b>19.500</b>         | 100.00                | 100.00 | 100.00 | 99.62  | 99.62  | 99.70  | 99.70  | 99.69 | 99.57  | 99.57  | 99.70  | 99.62  |
| <b>12.500</b>         | 100.00                | 100.00 | 100.00 | 84.81  | 84.81  | 87.90  | 87.94  | 87.80 | 82.67  | 82.91  | 88.16  | 84.81  |
| <b>9.500</b>          | 97.14                 | 95.40  | 95.40  | 74.56  | 74.56  | 79.14  | 79.21  | 78.96 | 71.29  | 71.68  | 80.38  | 74.56  |
| <b>4.750</b>          | 76.83                 | 62.75  | 62.75  | 48.45  | 48.45  | 54.08  | 54.23  | 53.70 | 43.68  | 44.44  | 61.51  | 48.45  |
| <b>2.360</b>          | 67.74                 | 51.78  | 51.78  | 41.73  | 41.73  | 46.86  | 47.01  | 46.47 | 37.19  | 37.96  | 55.18  | 41.73  |
| <b>1.180</b>          | 55.49                 | 42.42  | 42.42  | 34.18  | 34.18  | 38.39  | 38.51  | 38.06 | 30.47  | 31.09  | 45.20  | 34.18  |
| <b>0.600</b>          | 33.93                 | 25.98  | 25.98  | 20.98  | 20.98  | 23.53  | 23.61  | 23.34 | 18.72  | 19.10  | 27.67  | 20.98  |
| <b>0.300</b>          | 5.83                  | 4.63   | 4.63   | 3.87   | 3.87   | 4.26   | 4.27   | 4.23  | 3.53   | 3.59   | 4.88   | 3.87   |
| <b>0.150</b>          | 0.40                  | 0.40   | 0.40   | 0.40   | 0.40   | 0.40   | 0.40   | 0.40  | 0.40   | 0.40   | 0.40   | 0.40   |
| <b>0.075</b>          | 0.21                  | 0.16   | 0.16   | 0.13   | 0.13   | 0.15   | 0.15   | 0.14  | 0.11   | 0.12   | 0.17   | 0.13   |

In this research, the carbon fiber fraction of the ECON mixtures consisted of 70% 6mm-long (aspect ratio $\approx$ 860) and 30% 3mm-long (aspect ratio $\approx$ 430) carbon fibers. Replacing 30% of the total carbon fiber content with shorter fibers helps in improving the ECON workability, while electrical conductivity is not significantly compromised.

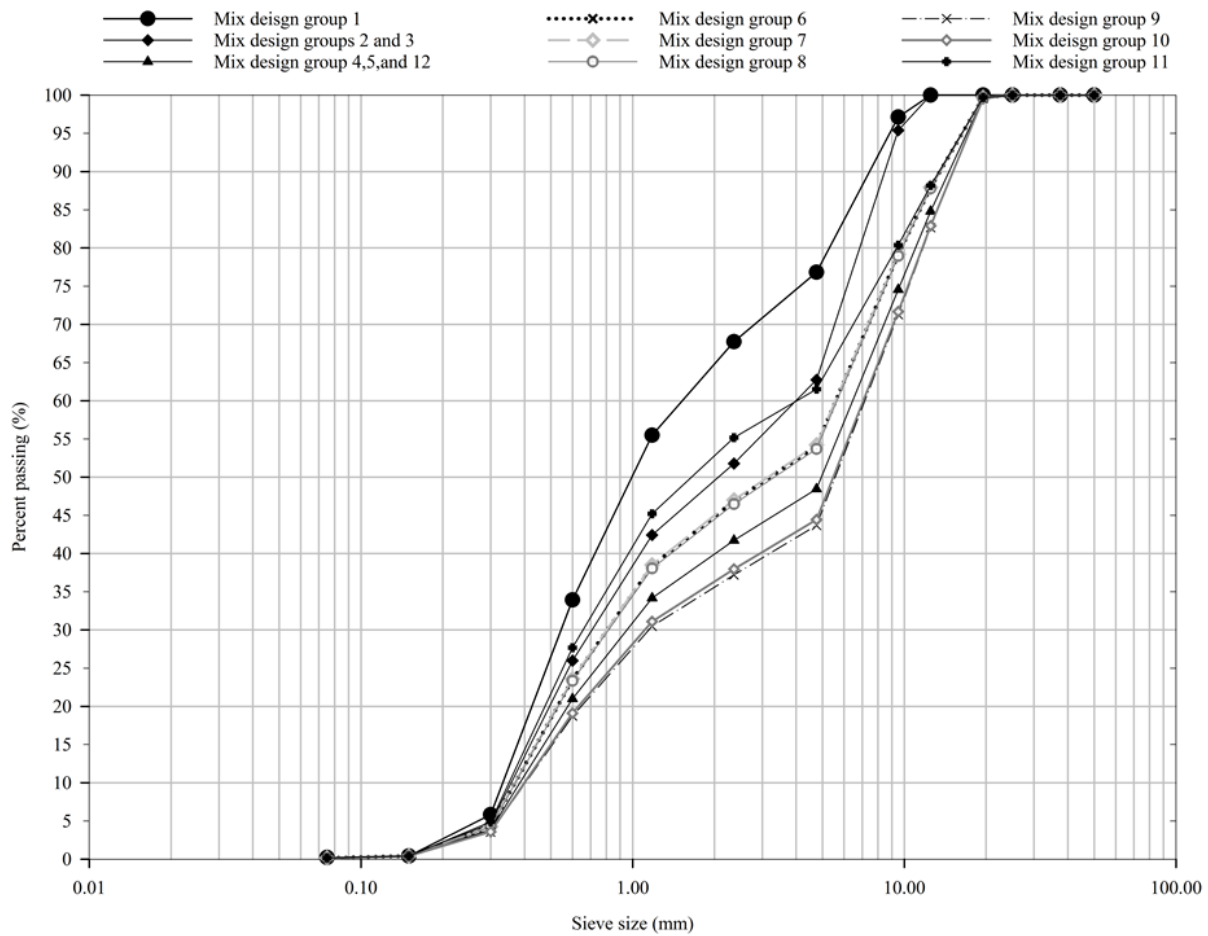


Figure 5-1. Gradation curves of aggregate systems used in the mix design groups.

The aforementioned mix designs were used for preparing samples in a 0.08 m<sup>3</sup> drum mixer using the following mixing procedure:

Table 5-3. Mixing proportions of laboratory-prepared econ mix designs.

| Mix ID | Content (Kg/m <sup>3</sup> ) |     |       |     |     |     |       |    |     |     | W/C  | CF (% Vol.) | HRWR (% wt. cem.) |
|--------|------------------------------|-----|-------|-----|-----|-----|-------|----|-----|-----|------|-------------|-------------------|
|        | CA                           | IA  | FA    | PC  | FC  | SC  | Water | CF | FDA | CEA |      |             |                   |
| 1C     | 0                            | 419 | 1,046 | 529 | 0   | 0   | 208   | 17 | 1.1 | 25  | 0.39 | 0.96        | 2.00              |
| 1F     | 0                            | 419 | 1,046 | 423 | 106 | 0   | 208   | 17 | 1.1 | 25  | 0.39 | 0.96        | 2.00              |
| 1S     | 0                            | 419 | 1,046 | 397 | 0   | 132 | 208   | 17 | 1.1 | 25  | 0.39 | 0.96        | 2.00              |
| 2C     | 0                            | 721 | 847   | 534 | 0   | 0   | 205   | 16 | 1.1 | 25  | 0.38 | 0.88        | 2.00              |
| 2F     | 0                            | 721 | 847   | 427 | 107 | 0   | 205   | 16 | 1.1 | 25  | 0.38 | 0.88        | 2.00              |
| 2S     | 0                            | 721 | 847   | 401 | 0   | 134 | 205   | 16 | 1.1 | 25  | 0.38 | 0.88        | 2.00              |
| 3C     | 0                            | 721 | 847   | 534 | 0   | 0   | 205   | 18 | 1.1 | 25  | 0.38 | 1.00        | 2.00              |
| 3F     | 0                            | 721 | 847   | 427 | 107 | 0   | 205   | 18 | 1.1 | 25  | 0.38 | 1.00        | 2.00              |
| 3S     | 0                            | 721 | 847   | 400 | 0   | 133 | 205   | 18 | 1.1 | 25  | 0.38 | 1.00        | 2.00              |
| 4C     | 594                          | 296 | 673   | 475 | 0   | 0   | 200   | 14 | 0.9 | 25  | 0.42 | 0.77        | 1.00              |
| 4F     | 594                          | 296 | 673   | 380 | 95  | 0   | 200   | 14 | 0.9 | 25  | 0.42 | 0.77        | 1.00              |
| 4S     | 594                          | 296 | 673   | 356 | 0   | 119 | 200   | 14 | 0.9 | 25  | 0.42 | 0.77        | 1.00              |
| 5C     | 594                          | 296 | 673   | 475 | 0   | 0   | 200   | 18 | 1.0 | 25  | 0.42 | 0.98        | 1.00              |
| 5F     | 594                          | 296 | 673   | 380 | 95  | 0   | 200   | 18 | 1.0 | 25  | 0.42 | 0.98        | 1.00              |
| 5S     | 594                          | 296 | 673   | 356 | 0   | 119 | 200   | 18 | 1.0 | 25  | 0.42 | 0.98        | 1.00              |
| 6C     | 489                          | 341 | 787   | 400 | 0   | 0   | 175   | 17 | 0.8 | 25  | 0.44 | 0.96        | 1.00              |
| 6F     | 489                          | 341 | 787   | 320 | 80  | 0   | 175   | 17 | 0.8 | 25  | 0.44 | 0.96        | 1.00              |
| 6S     | 489                          | 341 | 787   | 300 | 0   | 100 | 175   | 17 | 0.8 | 25  | 0.44 | 0.96        | 1.00              |
| 7C     | 489                          | 341 | 792   | 530 | 0   | 0   | 228   | 14 | 1.1 | 25  | 0.43 | 0.75        | 1.00              |
| 7F     | 489                          | 341 | 792   | 424 | 106 | 0   | 228   | 14 | 1.1 | 25  | 0.43 | 0.75        | 1.00              |
| 7S     | 489                          | 341 | 792   | 398 | 0   | 133 | 228   | 14 | 1.1 | 25  | 0.43 | 0.75        | 1.00              |
| 8C     | 489                          | 341 | 773   | 530 | 0   | 0   | 228   | 27 | 1.1 | 25  | 0.43 | 1.50        | 1.00              |
| 8F     | 489                          | 341 | 773   | 424 | 106 | 0   | 228   | 27 | 1.1 | 25  | 0.43 | 1.50        | 1.00              |
| 8S     | 489                          | 341 | 773   | 398 | 0   | 133 | 228   | 27 | 1.1 | 25  | 0.43 | 1.50        | 0.75              |
| 9C     | 708                          | 303 | 623   | 416 | 0   | 0   | 170   | 14 | 0.8 | 25  | 0.41 | 0.75        | 0.75              |
| 9F     | 708                          | 303 | 623   | 333 | 83  | 0   | 170   | 14 | 0.8 | 25  | 0.41 | 0.75        | 0.75              |
| 9S     | 708                          | 303 | 623   | 312 | 0   | 104 | 170   | 14 | 0.8 | 25  | 0.41 | 0.75        | 0.75              |
| 10C    | 708                          | 303 | 645   | 400 | 0   | 0   | 166   | 18 | 0.8 | 25  | 0.42 | 1.00        | 0.75              |
| 10F    | 708                          | 303 | 645   | 320 | 80  | 0   | 166   | 18 | 0.8 | 25  | 0.42 | 1.00        | 0.75              |
| 10S    | 708                          | 303 | 645   | 300 | 0   | 100 | 166   | 18 | 0.8 | 25  | 0.42 | 1.00        | 0.75              |
| 11C    | 486                          | 208 | 947   | 399 | 0   | 0   | 163   | 17 | 0.8 | 25  | 0.41 | 0.96        | 1.00              |
| 11F    | 486                          | 208 | 947   | 319 | 80  | 0   | 163   | 17 | 0.8 | 25  | 0.41 | 0.96        | 1.00              |
| 11S    | 486                          | 208 | 947   | 299 | 0   | 100 | 163   | 17 | 0.8 | 25  | 0.41 | 0.96        | 1.00              |
| 12C    | 594                          | 296 | 673   | 475 | 0   | 0   | 200   | 18 | 1.0 | 25  | 0.42 | 1.00        | 1.00              |
| 12F    | 594                          | 296 | 673   | 380 | 95  | 0   | 200   | 18 | 1.0 | 25  | 0.42 | 1.00        | 1.00              |
| 12S    | 594                          | 296 | 673   | 356 | 0   | 119 | 200   | 18 | 1.0 | 25  | 0.42 | 1.00        | 1.00              |

- 1) Carbon fibers were dried in an oven for 24 hours at 115°C.
- 2) Dried carbon fibers were manually mixed with methyl cellulose powder.
- 3) The inside of the concrete mixer was sprayed with water and then drained.
- 4) CA, IA, and carbon fibers were placed in the drum mixer and mixed for 1 minute.
- 5) ½ of mix water with AEA were added to the mixture and mixed until it foamed.
- 6) FA was added to the mixture and mixed for 3 minutes.
- 7) Cementitious materials were gradually fed into the mixer while it was running.

When the entire cementitious had been added, the mixer was stopped.

8) CEA was added to the mixer. The mixer was then started and mixing occurred for 1 minute, after which the mixer was stopped.

9) The rest of the mix water with HRWR were added to the mixture, the mixer was turned on, and the whole mixture was mixed for 10 minutes.

Three batches were prepared for each mix design. From each batch three 100×200 mm cylinders, three 75×75×300 mm beams, and three 100×100×100 mm cubic specimens with embedded copper mesh electrodes, as described in [30], were prepared for compressive strength, flexural strength, and electrical resistivity measurements, respectively. The specimens were consolidated by rodding and then vibration on a vibrating table according to ASTM C 192 standard practice. All specimens were cured in the moist room at 23°C temperature during the entire study and tested under saturated-surface-dry conditions. Compressive and flexural strength tests, fresh concrete air content measurement, and slump test were performed in conformance with ASTM C39, ASTM C78, ASTM C231, and ASTM C143 respectively. Electrical resistivity was measured at 1 KHz AC using two-probe method and embedded copper mesh electrodes, as

described in [30]. Electrical resistivity was measured at three ages (3, 28, and 90 days), while, compressive strength, and flexural strength were measured at 28 days.

A slump test is not a good indicator of the workability and consistency of a fiber-reinforced concrete, because a mixture can show low slump while still possessing sufficient workability and consistency, or vice versa. However, in this research, slump measurement was one of the requirements enforced by the project contractor. Since carbon fibers introduce excessive surface area into the mixture, a higher amount of paste is required to coat all fibers and aggregates, so if the paste:aggregate:fiber ratio is not appropriate, there would be insufficient cementitious paste to coat all particles and the mixture would present poor consistency. For example, some mixtures in this study crumbled during slump testing, therefore producing no measurable slump value, so two primary criteria were set upon the mixes in terms of slump measurement: 1) sufficient consistency for measurable slump (i.e. the sample does not crumble upon lifting the slump cone); 2) slump value  $\geq 38$  mm.

### **Mixing and Pouring the ECON in Des Moines International Airport Test Section**

Mix design 12C was selected as the final design for ECON HPS implementation at the airport. The test slabs, located in the general aviation apron area, consisted of a 10 cm-thick layer of regular concrete at the bottom and a 9cm-thick ECON layer on top. The structural and system designs were as given in [50, 51]. Figure 5-2 shows a schematic of the two slabs and the sensor locations. The regular concrete layer was placed one month prior to the placement of the ECON layer, and surface of the regular concrete was roughened by broom during placement to enable a good bond between the bottom hardened concrete and the later-placed ECON layer. While two adjacent slabs were made with ECON, in this study the data from only one slab (slab 1) was used

for performance evaluation. Custom-made Arduino temperature sensors were placed in both regular concrete and ECON layers to monitor temperature variations during snow-melting tests.

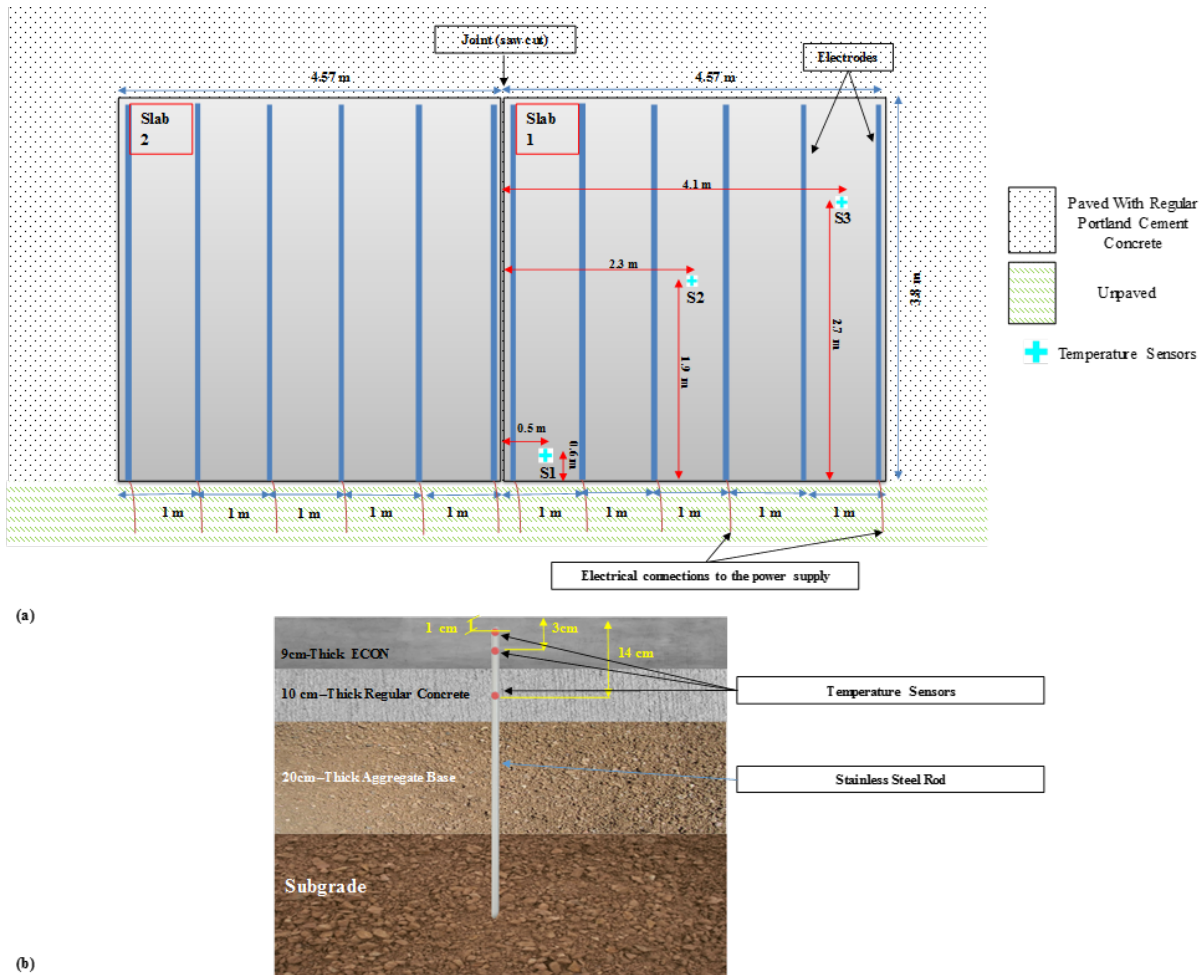


Figure 5-2. System configuration and sensor locations for each slab; a) plan view of slabs; b) the cross section of a slab with embedded sensors.

For the two slabs, 5 m<sup>3</sup> of ECON was produced by Iowa State Ready Mix (ISRM) in a drum mixer using a wet-batch process and transported to the job site by a 10m<sup>3</sup>-capacity truck mixer. Carbon fibers in the required amount were dried in an oven at 115°C for 24 hours and sealed in water-soluble 0.5 Kg bags. Methylcellulose powder was also poured into each bag in conformance with the mix design (about 30 g for each bag). Fibers were packed in water-soluble bags to prevent material loss during transportation and handling, and to expedite the process of

feeding fibers into the mixer. The ECON mixing and placing procedure followed in the concrete plant and at the job site was as follows:

- 1) Five hours prior to concrete placement, the regular concrete layer and electrodes were cleaned by air pump and washed by water to remove dust and debris, because presence of dust and dirt on the electrodes can weaken the electrode-concrete bond. Then water was poured on the bottom layer to nearly saturate it and thereby prevent absorption of the fresh ECON's water by the bottom layer.
- 2) At the concrete plant, the drum mixer was washed clean and drained before batching the ECON.
- 3) Coarse and fine aggregate and AEA with a portion of the mix water were fed into the drum mixer and mixed for 30 seconds; about 10% of the mix water was saved to be added on the job site. Because of the high cement content, a 20-minute distance between the concrete plant and the job site, along with relatively undesirable weather conditions (sunny with about 28°C temperature), there were concerns that flash setting and loss of workability could occur, so this practice was chosen to improve mixture workability at the job site.
- 4) The mixer was then stopped and the carbon fiber bags, ECA, and HRWR were manually fed into the mixer.
- 5) Cement was fed into the mixer and the whole mixture was mixed for 3 minutes and loaded into the truck mixer, with mixing continued during transportation.
- 6) The remaining mix water was added on the job site and mixed for 1 minute.
- 7) The concrete was poured in the slabs, spread manually, consolidated by a vibrating screed, and finished, as shown in Figure 5-3.

- 8) When the ECON layer was sufficiently consolidated and finished, curing agent was sprayed on the slab surface.

### **Investigation of the Properties and Performance of ECON in Des Moines International Airport**

As previously explained, a sufficient number of cube, cylinder, and beam samples were taken from the ECON mix at the job site, and the slump and air content were also measured. Thirty 100×200 mm cylinders, six 100×100×356 mm beams, six 76×76×305 mm beams, six 100-mm cubes with embedded copper mesh electrodes, and six 100×100×356 mm beams with embedded copper mesh electrodes were taken from the concrete in the field. The field sampling was performed in accordance with ASTM C31/31M-15a standard and relevant standards were followed for each specific test. The specimens were used for measurements of compressive strength, flexural strength, and electrical resistivity, and microscopic investigations. The properties of the ECON made in the concrete plant were compared with the properties of the equivalent ECON mixture (12C) prepared in the laboratory. ECON specimens of both field concrete and laboratory-prepared mixture 12C that were continuously cured for one year were used to prepare required test specimens for microscopic investigations. The air content of hardened ECON specimens were determined based on the linear traverse method according to ASTM C 457 Standard; this was accomplished by using an optic microscope with coupled image analysis system (RapidAir test set-up). Microstructure of the ECON samples were analyzed by scanning electron microscope (SEM) on multiple specimens. Also, the carbon fiber content in the laboratory-prepared and field ECON samples were measured and compared. For this purpose, sections with nominal dimensions of 100×100×10 mm were cut from beam specimens with precision saw, then, dried in the oven for 24 hours at 110°C, weighed, measured for actual dimensions, broken into smaller pieces (for ease of dissolving) and dissolved in Hydrochloric



acid. Once each specimen was fully dissolved, the remaining material was washed with deionized water and acetone on a 5- $\mu\text{m}$  sieve, dried in oven for 24 hours at 110°C and weighed. The carbon fiber content as a weight and volume percentage was calculated for each specimen. This test was performed on 18 rectangular specimens for each of laboratory-prepared and field ECON samples. The rectangles were taken from three different beams for each concrete type.

The ECON slabs were not operated for 32 days. At the age of 32 days, the slab instrumented for data acquisition (Figure 5-2) was powered by a 210V AC voltage to test the heat generation capability of the ECON. The temperature data and the total current flowing through the slab were recorded. In addition, for evaluation of operation safety, the measurable electric current on the slab surface was measured by installing current probes on the surface. The current probes were attached to the surface by conductive gel to ensure that sufficient electrical contact is attained.

The first snow event occurred when the slab was 43 days old, and it was followed by snow precipitations at 89, 103, 119, and 136-day ages. The slab performance in snow events was evaluated at two operational modes: anti-icing, and deicing. At the 43-day age, the system was turned on prior to the snow event and remained running until precipitation ended (anti-icing test). In deicing operation tests, the system was turned on after precipitation ended to melt the snow accumulated on the surface. Performance was evaluated in terms of average ambient temperature, wind speed, snow thickness, operation time, average power density, and energy required to fully melt the snow and dry the surface. The heat generation on slab surfaces was also monitored by thermal imaging system. The energy calculation methods, and specific heat capacity were derived from previous works by the authors [50, 51].

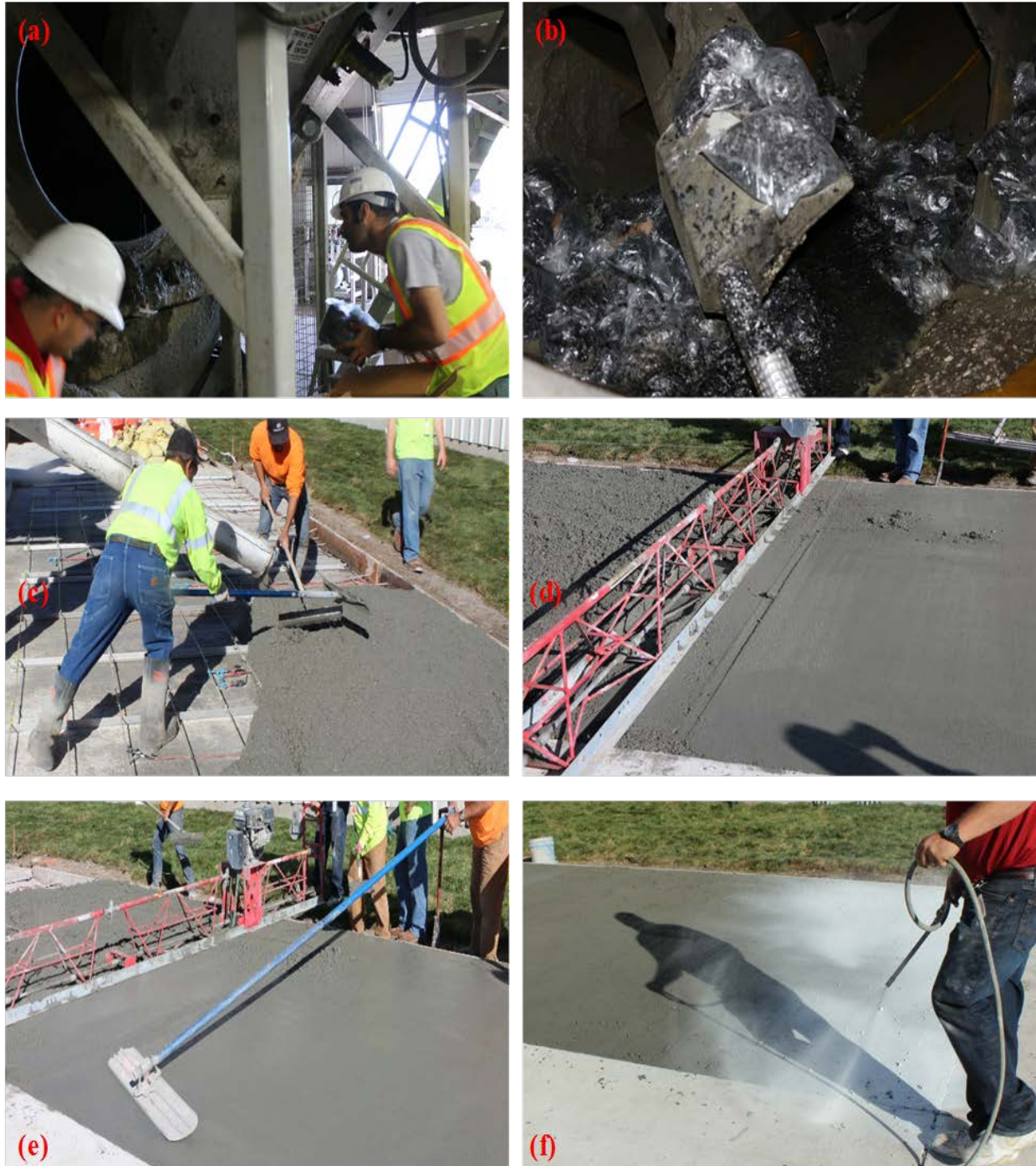


*Figure 5-3. Mixing and placement of ECON; (a) feeding fibers and admixtures into the mixer at concrete plant; (b) fiber bags inside the mixer; (c) pouring and spreading the concrete; (d) consolidation, (e) finishing; and (f) covering the fresh concrete with curing.*

## Results and Discussion

### Properties of Laboratory-prepared ECON Mixtures

The test results of electrical resistivity at three ages (3, 28, and 90 days), compressive strength, flexural strength, and slump for the laboratory-prepared ECON mixtures are provided in Table 5-4, where it can be seen that some mixtures had no measureable slump; this refers to the mixtures that crumbled immediately after lifting the slump cone. This can be attributed to cementitious paste inadequacy with respect to coating and binding all aggregates and fibers together, and such mixtures lacked sufficient consistency. Also, since they also did not possess flowability and passing ability like that observed in self-consolidating concrete, such mix designs were ruled out as candidate mix designs for ECON HPS. The air content of all samples fell within the required values (i.e. 5.5-6.5%). Since all mixes satisfied compressive and flexural strength requirements, electrical resistivity and workability were the decisive factors.

In all mix design groups except for groups 8 and 9, replacing a portion of PC with FF and SC increased electrical resistivity at all ages. Mixtures 8C and 8F exhibited similar average electrical resistivity values at 3 days of age, but at later ages mixture 8F showed higher resistivity than 8C. Mixture 9F showed lower electrical resistivity than 9C at three days of age, but this effect was reversed at later ages. On the other hand, FF and SC replacement did not help improve workability. In mix groups 6 and 11, PC replacement with FF slightly increased the slump, while in the other cases it either reduced the slump or did not affect it. PC replacement with SC showed a negative effect on slump and workability with the exception of mix group 1, where the same slump was obtained for mixtures 1C and 1S. As seen in the table, mix 12C provided a desirable combination of electrical resistivity, strength, and slump value, so it was selected for application in the ECON HPS test section.

Table 5-4. Properties of all laboratory-prepared econ mixtures.

| Mix ID | electrical resistivity ( $\Omega$ -cm) |      |            |      |            |      | Strength (MPa) |     |          | slump |      |      |
|--------|--|------|------------|------|------------|------|----------------|-----|----------|-------|------|------|
|        | 3-day age                              | SD   | 28-day age | SD   | 90-day age | SD   | Compressive    | SD  | Flexural | SD    | mm   | inch |
| 1C     | 240                                    | 31.7 | 477        | 26.5 | 903        | 25.6 | 54.0           | 1.1 | 8.1      | 0.1   | 64   | 2.50 |
| 1F     | 280                                    | 35.1 | 546        | 29.3 | 941        | 33.7 | 49.0           | 2.2 | 7.0      | 0.1   | 38   | 1.50 |
| 1S     | 340                                    | 31.1 | 663        | 26.2 | 1,003      | 48.9 | 58.0           | 0.9 | 8.7      | 1.0   | 64   | 2.50 |
| 2C     | 310                                    | 52.7 | 670        | 43.8 | 1,204      | 45.7 | 64.0           | 0.5 | 7.9      | 0.8   | N.A  | N.A  |
| 2F     | 330                                    | 27.3 | 700        | 23.1 | 1,300      | 50.7 | 62.0           | 0.9 | 9.9      | 1.9   | N.A  | N.A  |
| 2S     | 425                                    | 25.7 | 780        | 21.8 | 1,560      | 60.0 | 64.0           | 1.6 | 10.4     | 0.5   | N.A  | N.A  |
| 3C     | 220                                    | 16.2 | 446        | 13.8 | 833        | 22.1 | 51.0           | 1.1 | 7.5      | 0.8   | N.A. | N.A. |
| 3F     | 315                                    | 5.6  | 500        | 5.1  | 860        | 34.5 | 51.0           | 0.2 | 8.0      | 0.7   | N.A. | N.A. |
| 3S     | 410                                    | 30.5 | 520        | 25.5 | 900        | 46.2 | 54.0           | 0.2 | 7.1      | 1.7   | N.A. | N.A. |
| 4C     | 54                                     | 12.5 | 122        | 10.4 | 160        | 13.7 | 55.0           | 2.0 | 8.7      | 0.1   | 38   | 1.50 |
| 4F     | 75                                     | 2.8  | 142        | 2.4  | 200        | 6.6  | 54.0           | 1.0 | 9.1      | 0.2   | 38   | 1.50 |
| 4S     | 140                                    | 3.1  | 206        | 2.8  | 406        | 6.8  | 59.0           | 1.7 | 7.8      | 0.5   | N.A. | N.A. |
| 5C     | 37                                     | 12.6 | 78         | 10.4 | 113        | 8.8  | 44.0           | 2.6 | 8.3      | 0.8   | 38   | 1.50 |
| 5F     | 65                                     | 8.4  | 87         | 7.0  | 150        | 1.5  | 46.0           | 1.9 | 7.9      | 0.8   | 38   | 1.50 |
| 5S     | 100                                    | 4.1  | 126        | 3.4  | 196        | 3.0  | 50.0           | 0.3 | 7.5      | 0.4   | N.A. | N.A. |
| 6C     | 98                                     | 5.4  | 133        | 4.5  | 177        | 3.1  | 58.0           | 1.9 | 8.7      | 1.2   | 13   | 0.50 |
| 6F     | 120                                    | 17.1 | 180        | 14.2 | 304        | 5.1  | 43.0           | 3.7 | 7.8      | 0.5   | 19   | 0.75 |
| 6S     | 224                                    | 3.1  | 310        | 2.9  | 417        | 15.3 | 50.0           | 0.6 | 10.5     | 0.7   | N.A. | N.A. |
| 7C     | 70                                     | 8.6  | 103        | 7.2  | 134        | 11.8 | 65.0           | 3.8 | 7.5      | 1.3   | 13   | 0.50 |
| 7F     | 98                                     | 3.7  | 125        | 3.1  | 170        | 2.9  | 52.0           | 2.7 | 7.3      | 1.2   | 13   | 0.50 |
| 7S     | 170                                    | 16.6 | 230        | 13.8 | 250        | 8.6  | 37.0           | 0.2 | 6.1      | 0.1   | N.A. | N.A. |
| 8C     | 65                                     | 5.6  | 98         | 4.7  | 115        | 8.5  | 28.0           | 0.5 | 7.4      | 0.3   | N.A. | N.A. |
| 8F     | 65                                     | 3.0  | 100        | 2.5  | 130        | 1.6  | 29.0           | 0.7 | 6.5      | 0.4   | N.A. | N.A. |
| 8S     | 112                                    | 5.7  | 218        | 4.9  | 300        | 5.7  | 31.0           | 1.8 | 8.5      | 0.9   | N.A. | N.A. |
| 9C     | 70                                     | 9.3  | 165        | 7.7  | 210        | 2.8  | 52.0           | 0.7 | 9.3      | 0.4   | 25   | 1.00 |
| 9F     | 61                                     | 6.4  | 206        | 5.4  | 288        | 3.2  | 49.0           | 1.0 | 6.8      | 0.7   | 25   | 1.00 |
| 9S     | 110                                    | 3.4  | 287        | 3.1  | 360        | 7.3  | 52.0           | 0.5 | 7.3      | 0.7   | 13   | 0.50 |
| 10C    | 55                                     | 7.7  | 91         | 6.4  | 117        | 9.3  | 35.0           | 0.9 | 6.1      | 1.4   | 13   | 0.50 |
| 10F    | 75                                     | 13.7 | 115        | 11.4 | 160        | 2.1  | 36.0           | 0.1 | 7.6      | 0.1   | 13   | 0.50 |
| 10S    | 103                                    | 4.4  | 155        | 3.8  | 213        | 3.7  | 39.0           | 0.3 | 8.1      | 0.2   | N.A. | N.A. |
| 11C    | 245                                    | 5.4  | 491        | 4.9  | 979        | 27.0 | 45.0           | 0.6 | 6.7      | 0.4   | 30   | 1.20 |
| 11F    | 325                                    | 18.6 | 670        | 15.9 | 1,120      | 47.6 | 40.0           | 1.2 | 7.6      | 0.7   | 38   | 1.50 |
| 11S    | 380                                    | 4.2  | 700        | 4.2  | 1,500      | 58.4 | 44.0           | 0.5 | 7.2      | 0.8   | 25   | 1.00 |
| 12C    | 36                                     | 5.4  | 78         | 4.5  | 115        | 6.8  | 39.0           | 0.6 | 7.6      | 0.3   | 38   | 1.50 |
| 12F    | 57                                     | 23.0 | 108        | 19.0 | 141        | 11.5 | 37.0           | 1.6 | 7.6      | 0.8   | 38   | 1.50 |
| 12S    | 98                                     | 10.1 | 150        | 8.4  | 318        | 7.7  | 41.0           | 0.6 | 7.2      | 0.4   | 33   | 1.30 |

NOTE: SD=Standard Deviation, N.A.=Not Available.

### Comparison of Laboratory-Prepared Samples with Field-taken Samples

Figure 5-4 shows the electrical resistivity values (and standard deviations) of the same mix design measured both on laboratory-prepared and field-taken specimens. The average 28-day compressive and flexural strengths of the field samples, 37 MPa and 7.7 MPa, were comparable to the results obtained from laboratory-prepared samples. Air content measured for fresh ECON in the field was 5.5% and the slump measured on the job site was 76 mm, two times greater than that of lab samples (38 mm, Table 4). While the laboratory-prepared samples showed slower growth in electrical resistivity with age, for both sample types, the electrical resistivity growth rate was reduced at later ages and changed at a significantly slower pace after 28 days.

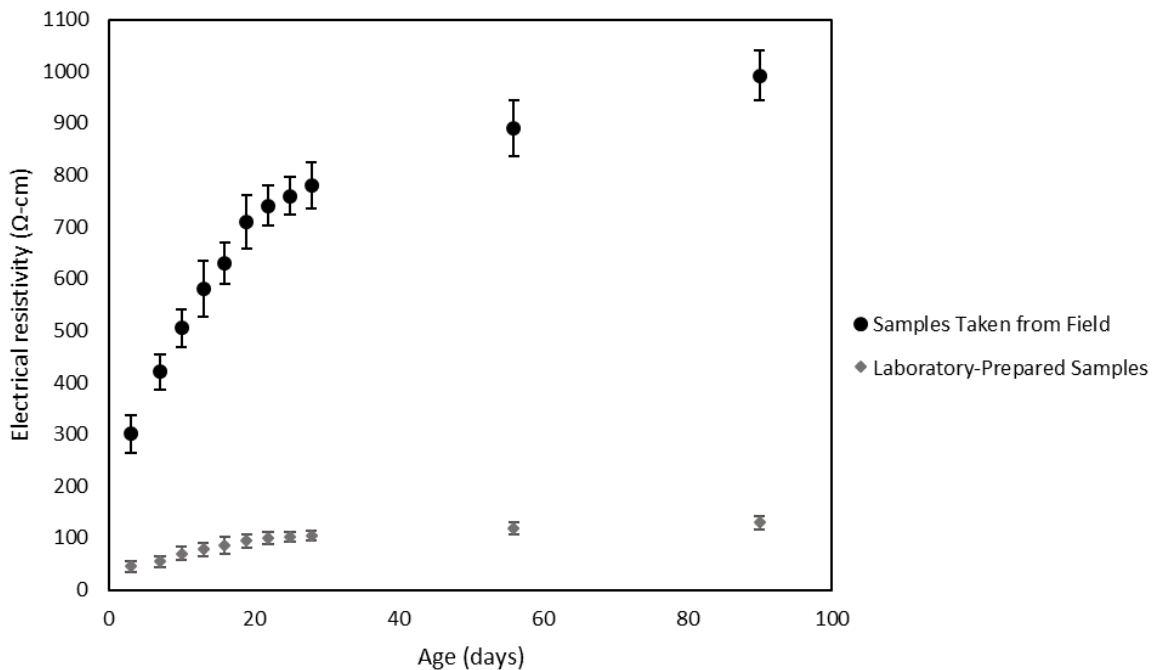


Figure 5-4. Evolution of electrical resistivity in laboratory-prepared and field samples.

As seen in the figure and table, there was a significant difference between the two batches with respect to electrical resistivity and slump, with the field samples exhibiting significantly

higher electrical resistivity, almost eight times higher than the lab samples at 90-day age. This difference can be primarily attributed to a loss of carbon fibers at the concrete plant during mixing. As seen in Table 5-5, the actual fiber dosage was lower in the field than it was designed to be. The big standard deviation values seen in Table 5-5 are due to the nature of the specimens that were thin cuts of concrete which is essentially non-homogeneous in terms of aggregate distribution and fiber dispersion. Because of the presence of an opening at the top of the mixer, a portion of mix carbon fiber was carried out of the drum mixer by air flow during mixing. Furthermore, the mixture was mixed in the truck mixer for a longer time than planned, and longer mixing results in fiber degradation due to excessive wearing of fibers by aggregates [33]. In the laboratory-prepared samples, because of the higher carbon fiber content and presence of a better conductive network, the effect of carbon fibers dominated the effect of void structure and hydration age and resulted in slower growth in electrical resistivity with age [30].

*Table 5-5. Actual fiber dosage in laboratory-prepared and field ECON samples.*

| Specimen type           | Laboratory-prepared |          | Field-taken |          |
|-------------------------|---------------------|----------|-------------|----------|
|                         | Weight %            | Volume % | Weight %    | Volume % |
| Average                 | 0.74                | 0.98     | 0.55        | 0.75     |
| Standard deviation (SD) | 0.27                | 0.42     | 0.25        | 0.34     |

The role of pore content and pore structure should also be taken into account when comparing the field-taken and laboratory-prepared ECON samples with respect to electrical conductivity. Table 5-6 shows the pore structure characteristics of the two type of ECON samples. As seen in the table, the field-taken samples showed higher air content, smaller air void

spacing factor, and smaller paste-to-void ratio. For both laboratory-prepared and field-taken samples, the air contents measured using hardened specimens (ASTM C 457) was higher than air content measured using fresh concrete (ASTM C 231). According to the literature, this type of discrepancy between the two methods is not uncommon [52]; Ram et al. [53], by testing various pavement concrete samples in-situ and in the laboratory, concluded that the pressure method tends to underestimate the air content. Regarding that the main medium for electricity conduction in ECON is the ECA network, the electrical conductivity decreases with the increase of air void content [54]. Furthermore, the smaller spacing factor and greater void frequency in field-taken ECON results in more frequent blocking of the conduction path which dwarfs the conductive function of the carbon fiber-cement composite matrix. This is also in agreement with the smaller paste-to-void ratio of the field ECON.

*Table 5-6. Results of pore structure evaluation of hardened laboratory-prepared and field-taken ECON samples.*

| Specimen type       | Air content (%) |       | void frequency (mm-1) |       | Specific surface (mm-1) |        | Spacing factor (mm) |       | paste to void ratio |       |
|---------------------|-----------------|-------|-----------------------|-------|-------------------------|--------|---------------------|-------|---------------------|-------|
|                     | Average         | SD    | Average               | SD    | Average                 | SD     | Average             | SD    | Average             | SD    |
| Laboratory-prepared | 6.004           | 1.649 | 1.433                 | 0.302 | 96.021                  | 11.844 | 0.053               | 0.004 | 6.273               | 2.210 |
| Field-taken         | 7.189           | 0.514 | 1.678                 | 0.179 | 95.278                  | 5.242  | 0.049               | 0.004 | 4.968               | 0.285 |

SEM investigation of various zones in ECON samples showed that the fibers, are primarily present within a carbon fiber-cement matrix composite. As seen in Figure 5-5, laboratory-prepared samples showed a better distribution of fibers, higher fiber concentration, and more frequent fiber-to-fiber contacts, while, in the field-taken samples the fibers were not as

uniformly distributed and in many spots (such as Figure 5-5(b)) the fiber-matrix composite was segmented into fiber-abundant (right side of Figure 5-5(b)) and fiber-less (left side of Figure 5-5(b)) zones. In all fractured surfaces studied for both ECON sample types, the fiber network was observed only within the cementitious matrix and fiber tangling around the aggregates was not observed. Figure 5-6(a) shows an example of aggregate surface in field-taken samples, where, the surface of aggregate is free of tangled fiber network and only one isolated broken fiber is observed. The short isolated pieces of carbon fiber (Figure 5-6(b)) observed in the field-taken samples on the aggregate surfaces or in the vicinity of aggregates (Figure 5-6(c)) are likely the result of excessive fiber wear by aggregates. The comparative study showed that the discrepancy between the electrical resistivity of the laboratory-prepared and field-taken ECON is caused primarily by lower carbon fiber content and higher void fraction in the ECON which was prepared in large-scale.

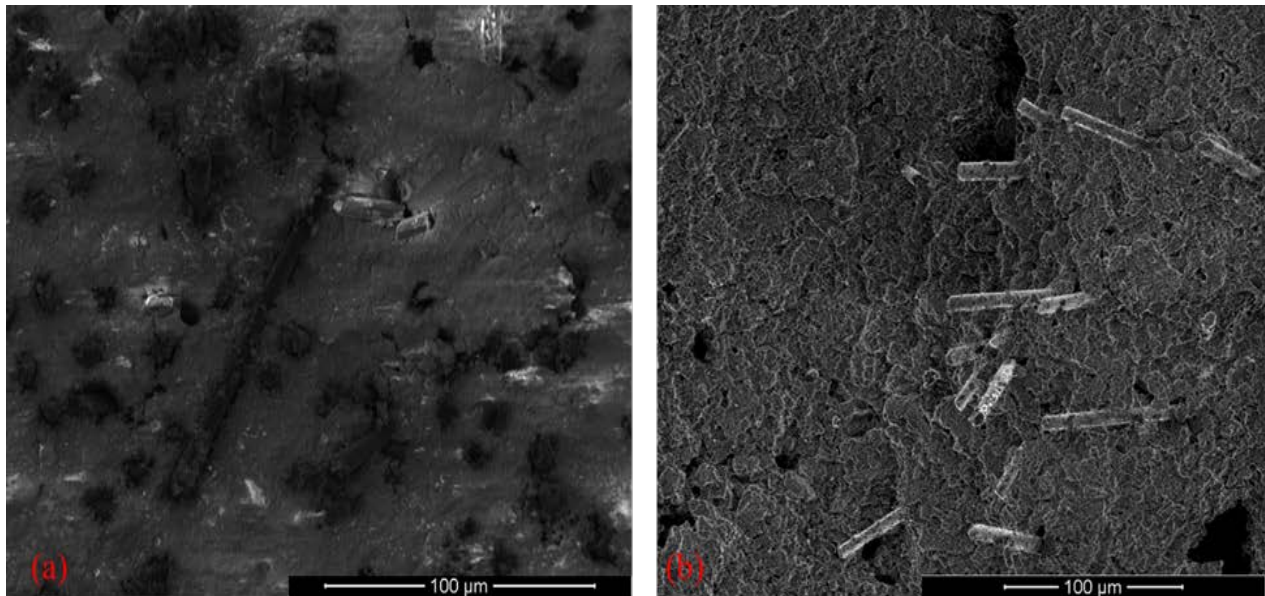


*Figure 5-5. SEM image of carbon fiber-cement matrix composite in ECON: (a) laboratory-prepared, and (b) field-taken ECON samples.*



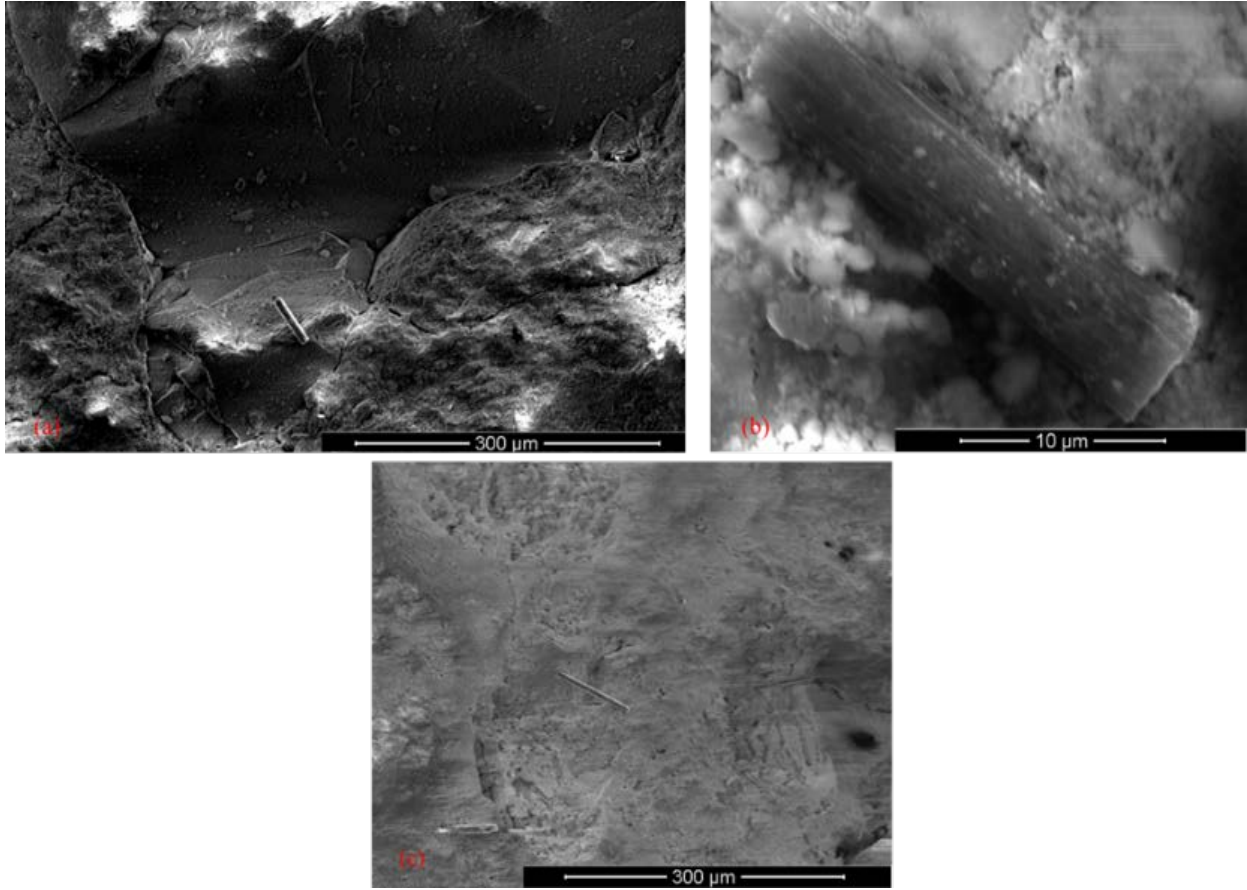


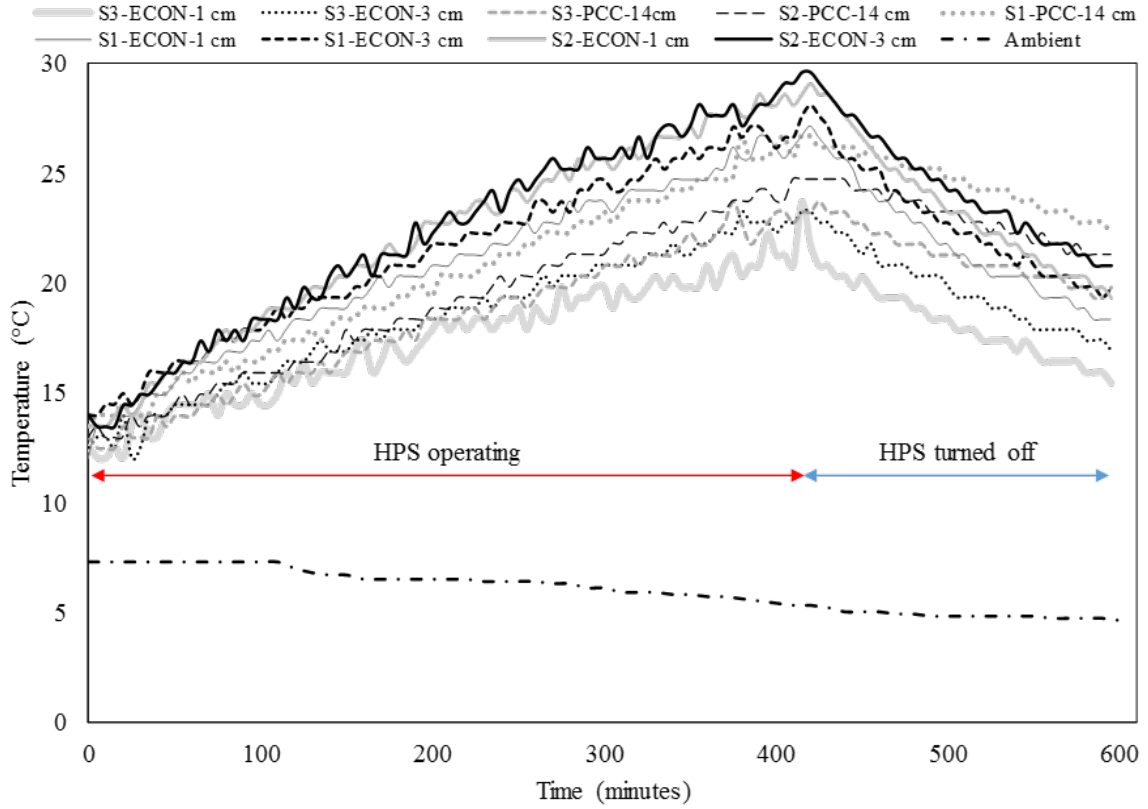
Figure 5-6. (a) aggregate surface in field-taken ECON; (b) isolated carbon fiber broken piece; and (c) the vicinity of an aggregate, in field-taken ECON.

### Heating Performance of Slabs

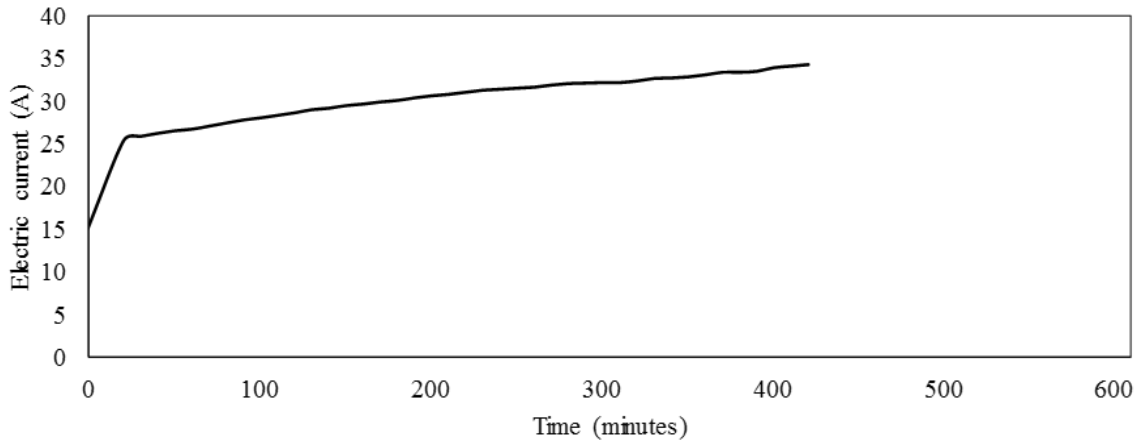
Figure 5-7(a) shows the temperature profile in the ECON slab at three different locations (Figure 5-2(a)) and three different depths (Figure 5-2(b)) during the first performance test at 32 days of age. In the figure, each curves is designated with a code, where S1, S2, and S3 show the sensor number, ECON and PCC show the concrete layer where sensor is placed, and 1 cm, 3 cm, and 14 cm are the depth where sensor is located. Despite some fluctuations in the temperature profiles due to sensor performance, the sequence of temperature can be sorted from highest to lowest, based on the general trends of the temperature profiles, as follows: S2-ECON-3cm > S2-ECON-1cm > S1-ECON-3cm > S1-ECON-1cm > S1-PCC-14cm > S2-PCC-14cm > S3-PCC-14cm ≥ S3-ECON-3cm > S3-ECON-1cm.

The highest value of heat generation was achieved at the center of the slab, shown by the S2 sensor. At both S1 and S2 locations, the lower portion of the ECON layer (3cm-deep) showed the highest temperature followed by the top portion of the ECON layer (1cm-deep). The lowest temperatures were measured at the regular concrete (PCC) layer (14cm-deep). This trend is promising for ice and snow melting purposes, since it shows an absence of considerable heat flux from the ECON layer towards the underlying regular concrete. However, the lowest temperatures throughout the slab were measured at a location represented by sensor S3 that was adjacent to two regular concrete slabs. At the S3 spot, the temperature profile of the underlying PCC layer and the lower portion of the ECON layer were very similar, with the PCC being slightly higher. The top portion of the ECON at S3 spot (1cm-deep) gave the lowest temperature readings that can be attributed to the heat flux between the ECON and the adjacent regular concrete slabs at this spot.

Figure 5-7(b) presents the current variation during the HPS operating time. The figure clearly shows that electric current increases over the time of HPS operation. Since the voltage is constant, this trend shows that the electrical resistivity of ECON is decreased by increasing temperature. This effect was more significant during the first 20 minutes of power application. After 20 minutes, the current increase rate slowed while the rising trend of current with time (temperature) was maintained until the end of the experiment. This is in agreement with the findings of previous studies, where electrical resistivity of a cementitious composite was found to decrease with temperature [16]. In this test, the overall resistance of the slab dropped by 57% during 421 minutes of operation.



(a)



(b)

Figure 5-7. Temperature (a) and current (b) profiles during the first testing of the ECON slab.

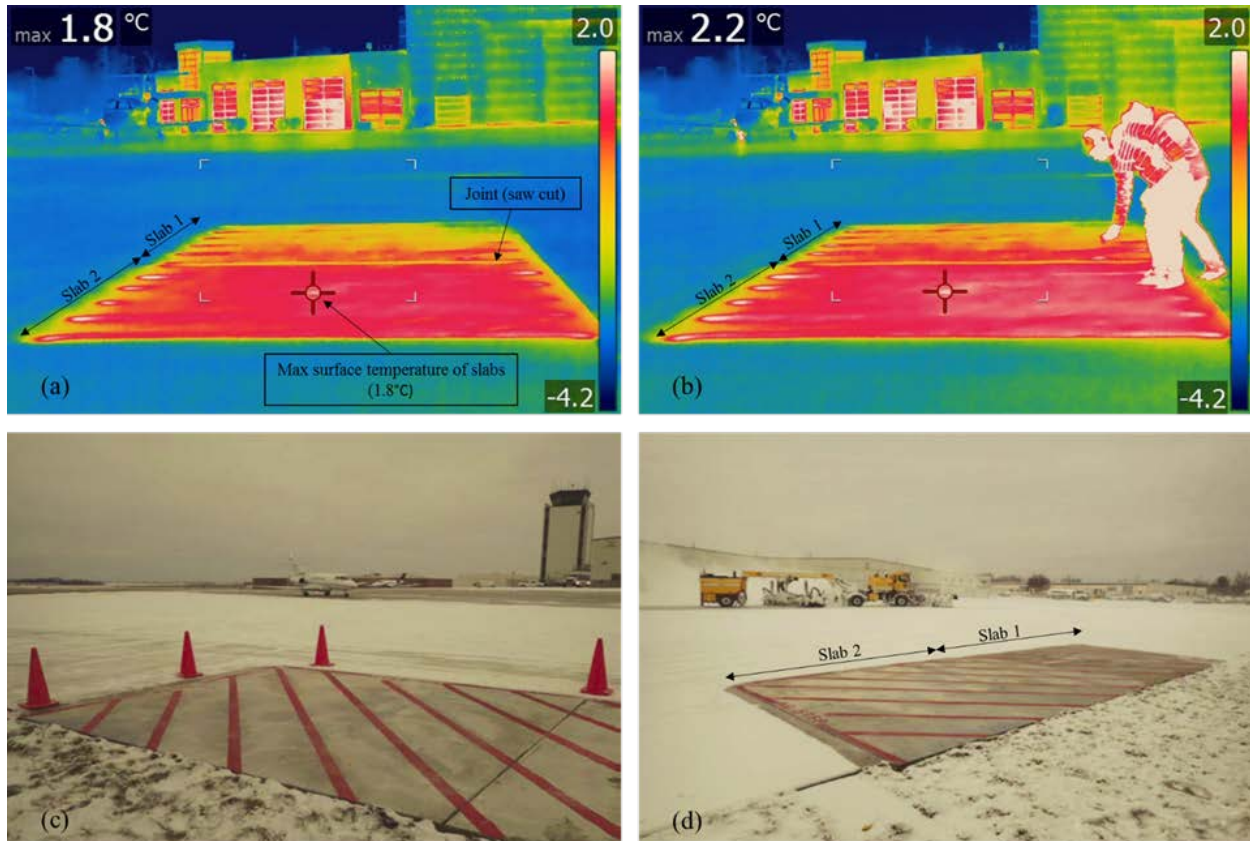


Figure 5-8. Thermal image of ECON HPS slabs in operation (a, and b), anti-icing operation mode of ECON HPS (c), and deicing on ECON HPS slabs (d).

Figure 5-8(a) and (b), when compared with the temperature profiles in Figure 5-7(a), show that the temperature on the slab surfaces is considerably lower than the temperature inside the slabs. This happens because of the heat convection from the surface, and latent heat of fusion (a.k.a. enthalpy of fusion) of ice and water as they absorb excessive thermal energy upon phase change from solid to liquid and evaporation. However, as seen in Figure 5-8(b) and (c), the ECON HPS slabs were able to effectively keep the pavement surface free of ice and snow in both anti-icing and deicing modes. Snow melting tests at different ages showed that the ECON slab was capable of increasing surface temperature to a level sufficient for snow removal at freezing temperatures. The results of the anti-icing and deicing tests are given in Table 5-7. The power density at both operational modes conformed to the ASHRAE handbook limit of a

maximum of 1.3 kW/m<sup>2</sup> [55]. While high current amount between 15 and 35 A was flowing through the slabs, the electric current on the surface of slabs while operating with 210 V AC was measured as 0.4 mA. The threshold of electric current to be perceptible by human body is 1mA [56], therefore the current amount on the surface of slabs, that is an order of magnitude lower than perception threshold, does not cause safety concerns.

*Table 5-7. Snow melting performance of the slab at different ages.*

| <b>age<br/>(days)</b>  | <b>Average<br/>Air Temp.<br/>(°C)</b> | <b>Wind speed<br/>(kmh)</b> | <b>Snow<br/>thickness<br/>(mm)</b> | <b>Average<br/>Power Density<br/>(W/m2)</b> | <b>Operation<br/>time<br/>(hrs.)</b> | <b>Energy<br/>Consumption<br/>(kW-h/m2)</b> |
|------------------------|---------------------------------------|-----------------------------|------------------------------------|---|--------------------------------------|---|
| <b>43<sup>a</sup></b>  | -4                                    | 13                          | 30                                 | 334   | 7.0                                  | 2.37  |
| <b>89<sup>d</sup></b>  | -10                                   | 23                          | 13                                 | 344   | 1.5                                  | 0.54  |
| <b>103<sup>d</sup></b> | -10                                   | 21                          | 38                                 | 312   | 3.5                                  | 1.08  |
| <b>119<sup>d</sup></b> | -6                                    | 27                          | 20                                 | 355   | 2.5                                  | 0.86  |
| <b>136<sup>d</sup></b> | -6                                    | 21                          | 33                                 | 334   | 2.0                                  | 0.65  |

*Note: “<sup>a</sup>” denotes anti-icing experiment, “<sup>d</sup>” denotes deicing experiment.*

### **Conclusions**

The design and production process of an airport electrically conductive concrete (ECON) heated pavement system (HPS) implementation has been reported in this study. To the best of authors' knowledge, this was the first implementation of ECON HPS in a U.S. airport and probably the first in the world. ECON design was based on laboratory experiments using

different ECON mix designs. The final product was compared with the laboratory samples and tested for its anti-icing and deicing performance. The key points of the study are as follows:

- Adequacy of cementitious paste content should be ensured in a carbon fiber-reinforced ECON mix design to ensure sufficient workability.
- Replacement of portland cement with fly ash and slag cement results in higher electrical resistivity, while, not providing workability advantages.
- A significant difference was observed with respect to electrical resistivity and slump between the laboratory-prepared and field samples, with the field samples showing electrical resistivity almost eight times higher than the lab samples at a 90-day age. This can be attributed to the lower carbon fiber content and higher void content of the ECON which was prepared in large-scale.
- Lower carbon fiber content in the field ECON was caused by loss of carbon fibers during mixing and fiber degradation due to excessive wear by aggregates.
- The highest temperature was achieved at the bottom of the ECON layer in the mid-span of the slab.
- The heat flux between the ECON layer and underlying PCC layer was inconsiderable.
- The heat convection on the slabs surface is a crucial factor with respect to effective temperature on slab surface.
- The lowest temperature was observed at the slab corners in contact with the adjacent regular concrete slabs.
- Electrical resistivity of the ECON layer was significantly decreased by temperature.
- The test section was able to generate a power density of 300-350 W/m<sup>2</sup> and effectively melt ice/snow with this amount of energy.

### Acknowledgements

This paper was prepared from a study conducted at Iowa State University under the Federal Aviation Administration (FAA) Air Transportation Center of Excellence Cooperative Agreement 12-C-GA-ISU for the Partnership to Enhance General Aviation Safety, Accessibility and Sustainability (PEGASAS). The authors would like to thank the current project Technical Monitor, Mr. Benjamin J. Mahaffay, and the former project Technical Monitors, Mr. Jeffrey S. Gagnon (interim), Mr. Donald Barbagallo, and Dr. Charles A. Ishee, for their invaluable guidance on this study. The authors also thank Gary L. Mitchell at the American Concrete Pavement Association, and Mr. Gordon Smith and Mr. Dan King in ICPA for valuable discussions and comments on concrete pavement construction. The authors also would like to thank the PEGASAS Industry Advisory Board members for their valuable support. The authors also would like to thank Mr. Bryan Belt, Mr. Mark Duffy, Mr. William Konkol at the Des Moines International Airport (DSM), and Mr. Adam Wilhelm and Mr. Andrew Gettler, Foth infrastructure and environmental, LLC, Mr. Dan Hutton of Kingston Services, LLC, for their full support during construction. Special thanks are expressed to Zoltek, the Candlemakers Store (TCS), and WR Grace & Co for providing carbon fiber, methyl cellulose, and corrosion inhibitor admixture, respectively. The authors would like to express their sincere gratitude to Mr. Robert F. Steffes, ISU CCEE PCC Lab Manager, for his significant assistance with the lab and field investigations, and other ISU graduate and undergraduate student research assistants: Sajed Sadati, Bo Yang, Sharif Gushgar, Jordan Schlak, Colin Heinrichs, and Collin Smith. Although the FAA has sponsored this project, it neither endorses nor rejects the findings of this research. The presentation of this information is in the interest of invoking comments by the technical community with respect to the results and conclusions of the research.

### References

- [1] A. Benedetto, A decision support system for the safety of airport runways : the case of heavy rainstorms, *Transp. Res. Part A*. 36 (2002) 665–682.
- [2] A. Arabzadeh, H. Ceylan, S. Kim, K. Gopalakrishnan, A. Sassani, Fabrication of Polytetrafluoroethylene-Coated Asphalt Concrete Biomimetic Surfaces: A Nanomaterials-Based Pavement Winter Maintenance Approach, in: *ASCE Int. Conf. Transp. Dev.*, ASCE, Houston, Texas, 2016.
- [3] A. Sassani, H. Ceylan, S. Kim, K. Gopalakrishnan, A. Arabzadeh, P.C. Taylor, Factorial Study on Electrically Conductive Concrete Mix Design for Heated Pavement Systems, in: *Transp. Res. Board 96th Annu. Meet.*, Washington DC, 2017: pp. 17–05347.
- [4] A. Arabzadeh, H. Ceylan, S. Kim, K. Gopalakrishnan, A. Sassani, S. Sundararajan, P.C. Taylor, Influence of Deicing Salts on the Water-Repellency of Portland Cement Concrete Coated with Polytetrafluoroethylene and Polyetheretherketone, in: *ASCE Int. Conf. Highw. Pavements Airf. Technol.*, Philadelphia, Pennsylvania, 2017.
- [5] A. Arabzadeh, H. Ceylan, S. Kim, K. Gopalakrishnan, A. Sassani, Superhydrophobic Coatings on Asphalt Concrete Surfaces, *Transp. Res. Rec. J. Transp. Res. Board*. No. 2551 (2016).
- [6] Y. Lai, Y. Liu, D. Ma, Automatically melting snow on airport cement concrete pavement with carbon fiber grille, *Cold Reg. Sci. Technol.* 103 (2014) 57–62.  
doi:10.1016/j.coldregions.2014.03.008.
- [7] T. Yang, Z.J. Yang, M. Singla, G. Song, Q. Li, Experimental Study on Carbon Fiber Tape-Based Deicing Technology, *J. Cold Reg. Eng.* 26 (2012) 55–70.  
doi:10.1061/(ASCE)CR.1943-5495.0000038.
- [8] H. Ceylan, K. Gopalakrishnan, S. Kim, W. Cord, Heated Transportation Infrastructure Systems : Existing and Emerging Technologies, in: *Civil, Constr. Environ. Eng. Conf. Present. Proceedings.23.*, Iowa State University, 2014.
- [9] S. Yehia, C.Y. Tuan, Thin Conductive Concrete Overlay for Bridge Deck Deicing and Anti-Icing, *Transp. Res. Rec. J. Transp. Res. Board*. 1698 (2000) 45–53.
- [10] J. Zhang, D.K. Das, R. Peterson, Selection of Effective and Efficient Snow Removal and Ice Control Technologies for Cold- Region Bridges, *J. Civil, Environ. Archit. Eng.* 3 (2014) 1–14.
- [11] A. Arabzadeh, H. Ceylan, S. Kim, K. Gopalakrishnan, A. Sassani, Superhydrophobic coatings on asphalt concrete surfaces: Toward smart solutions for winter pavement maintenance, 2016. doi:10.3141/2551-02.



- [12] A. Arabzadeh, H. Ceylan, S. Kim, K. Gopalakrishnan, A. Sassani, S. Sundararajan, P.C. Taylor, Superhydrophobic coatings on Portland cement concrete surfaces, *Constr. Build. Mater.* 141 (2017) 393–401.
- [13] H. Wang, L. Liu, Z. Chen, Experimental investigation of hydronic snow melting process on the inclined pavement, *Cold Reg. Sci. Technol.* 63 (2010) 44–49. doi:10.1016/j.coldregions.2010.04.007.
- [14] P. Pan, S. Wu, Y. Xiao, G. Liu, A review on hydronic asphalt pavement for energy harvesting and snow melting, *Renew. Sustain. Energy Rev.* 48 (2015) 624–634. doi:10.1016/j.rser.2015.04.029.
- [15] C.Y. Tuan, S. Yehia, Airfield Pavement Deicing With Conductive Concrete Overlay, in: *Civ. Eng. Fac. Proc. Present.*, 2002: p. paper 2. <http://digitalcommons.unomaha.edu/civilengfacproc/2>.
- [16] C. Chang, M. Ho, G. Song, Y.L. Mo, H. Li, Improvement of Electrical Conductivity in Carbon Fiber-Concrete Composites using Self Consolidating Technology, in: *Earth Sp. 2010 Eng. Sci. Constr. Oper. Challenging Environ.* ASCE, 2010: pp. 3553–3558.
- [17] M. Sun, W. Ying, L. Bin, X. Zhang, Deicing Concrete Pavement Containing Carbon Black/Carbon Fiber Conductive Lightweight concrete Composites, in: *ICTIS 2011 Multimodal Approach to Sustain. Transp. Syst. Dev. Information, Technol. Implement.*, 2011: pp. 662–668.
- [18] W. Chen, P. Gao, Performances of Electrically Conductive Concrete with Layered Stainless Steel Fibers, *Sustain. Constr. Mater.* (2012) 163–171.
- [19] J.P. Won, C.K. Kim, S.J. Lee, J.H. Lee, R.W. Kim, Thermal characteristics of a conductive cement-based composite for a snow-melting heated pavement system, *Compos. Struct.* 118 (2014) 106–111. doi:10.1016/j.compstruct.2014.07.021.
- [20] P.J. Tumidajski, P. Xie, M. Arnott, J.J. Beaudoin, Overlay current in a conductive concrete snow melting system, *Cem. Concr. Compos.* 33 (2003) 1807–1809. doi:10.1016/S0008-8846(03)00198-4.
- [21] K. Gopalakrishnan, H. Ceylan, S. Kim, S. Yang, H. Abdulla, Self-Heating Electrically Conductive Concrete for Pavement Deicing: A Revisit, in: *Transp. Res. Board 94th Annu. Meet.*, 2015: p. No. 15-4764.
- [22] O. Galao, L. Bañón, F.J. Baeza, J. Carmona, P. Garcés, Highly Conductive Carbon Fiber Reinforced Concrete for Icing Prevention and Curing, *Materials (Basel)*. 9 (2016) 281. doi:10.3390/ma9040281.
- [23] J. Gomis, O. Galao, V. Gomis, E. Zornoza, P. Garcés, Self-heating and deicing conductive cement. Experimental study and modeling, *Constr. Build. Mater.* 75 (2015) 442–449. doi:10.1016/j.conbuildmat.2014.11.042.

- [24] N. Banthia, S. Djeridane, M. Pigeon, Electrical resistivity of carbon and steel micro-fiber reinforced cements, *Cem. Concr. Res.* 22 (1992) 804–814. doi:10.1017/CBO9781107415324.004.
- [25] D.D.L. Chung, Electrically conductive cement-based materials, *Adv. Cem. Res.* 4 (2004) 167–176.
- [26] D.D. Chung, Dispersion of Short Fibers in Cement, *J. Mater. Civ. Eng.* 17 (2005) 379–383. doi:10.1061/(ASCE)0899-1561(2005)17:4(379).
- [27] J. Cao, D.D.L. Chung, Carbon fiber reinforced cement mortar improved by using acrylic dispersion as an admixture, *Cem. Concr. Res.* 31 (2001) 1633–1637. doi:10.1016/S0008-8846(01)00599-3.
- [28] B. Chen, J. Liu, Effect of fibers on expansion of concrete with a large amount of high f-CaO fly ash, *Cem. Concr. Compos.* 33 (2003) 1549–1552. doi:10.1016/S0008-8846(03)00098-X.
- [29] A. Peyvandi, P. Soroushian, A.M. Balachandra, K. Sobolev, Enhancement of the durability characteristics of concrete nanocomposite pipes with modified graphite nanoplatelets, *Constr. Build. Mater.* 47 (2013) 111–117. doi:10.1016/j.conbuildmat.2013.05.002.
- [30] A. Sassani, H. Ceylan, S. Kim, K. Gopalakrishnan, A. Arabzadeh, P.C. Taylor, Influence of mix design variables on engineering properties of carbon fiber-modified electrically conductive concrete, *Constr. Build. Mater.* 152 (2017) 168–181. doi:10.1016/j.conbuildmat.2017.06.172.
- [31] N. Xie, X. Shi, D. Feng, B. Kuang, H. Li, Percolation backbone structure analysis in electrically conductive carbon fiber reinforced cement composites, *Compos. Part B Eng.* 43 (2012) 3270–3275. doi:10.1016/j.compositesb.2012.02.032.
- [32] P.-W. Chen, D.D.L. Chung, Concrete as a new strain/stress sensor, *Compos. Part B Eng.* 27B (1996) 11–23.
- [33] J. Wu, J. Liu, F. Yang, Three-phase composite conductive concrete for pavement deicing, *Constr. Build. Mater.* 75 (2015) 129–135. doi:10.1016/j.conbuildmat.2014.11.004.
- [34] Z. Hou, Z. Li, J. Wang, Electrical conductivity of the carbon fiber conductive concrete, *J. Wuhan Univ. Technol. Sci. Ed.* 22 (2007) 346–349. doi:10.1007/s11595-005-2346-x.
- [35] C. Chang, G. Song, D. Gao, Y.L. Mo, Temperature and mixing effects on electrical resistivity of carbon fiber enhanced concrete, *Smart Mater. Struct.* 22 (2013) 35021. doi:10.1088/0964-1726/22/3/035021.
- [36] S. Wen, D.D.L. Chung, A Comparative Study of Steel- and Carbon-Fiber Cement as Piezoresistive Strain Sensors, *Adv. Cem. Res.* 15 (2003) 119–128.

- [37] S. Wen, D.D.L. Chung, Cement as a Thermoelectric Material, *J. Mater. Res.* 15 (2000) 2844–2848.
- [38] S. Wen, D.D.L. Chung, Carbon fiber-reinforced cement as a thermistor, *Cem. Concr. Res.* 29 (1999) 961–965. doi:10.1016/S0008-8846(99)00075-7.
- [39] S. Wen, D.D.L. Chung, Double percolation in the electrical conduction in carbon fiber reinforced cement-based materials, *Carbon N. Y.* 45 (2007) 263–267. doi:10.1016/j.carbon.2006.09.031.
- [40] R.N. Kraus, T.R. Naik, *Testing and Evaluation of Concrete Using High- Carbon Fly Ash and Carbon Fibers*, Milwaukee, Wisconsin, 2006.
- [41] M. Hambach, H. Moller, T. Neumann, D. Volkmer, Carbon fibre reinforced cement-based composites as smart floor heating materials, *Compos. Part B Eng.* 90 (2016) 465–470. doi:10.1016/j.compositesb.2016.01.043.
- [42] F. Javier Baeza, D.D.L. Chung, E. Zornoza, L.G. Andión, P. Garcés, Triple percolation in concrete reinforced with carbon fiber, *ACI Mater. J.* 107 (2010) 396–402.
- [43] R. Maggenti, R. Carter, R. Meline, Development of Conductive Polyester Concrete for Bridge-Deck Cathodic Protection and Ice Control, *Transp. Res. Rec. J. Transp. Res. Board.* (1996) 61–69.
- [44] C.Y. Tuan, Roca Spur Bridge: The Implementation of an Innovative Deicing Technology, *J. Cold Reg. Eng.* 22 (2008) 1–15. doi:10.1061/(ASCE)0887-381X(2008)22:1(1).
- [45] E. Heymsfield, A.B. Osweiler, R.P. Selvam, M. Kuss, *Feasibility of Anti-Icing Airfield Pavements Using Conductive Concrete and Renewable Solar Energy*, Fayetteville, Arkansas, 2013.
- [46] V. Piskunov, O. Volod'ko, A. Porhunov, Composite Materials for Building Heated coverings for Roads and Runways of Airdromes, *Mech. Compos. Mater.* 44 (2008) 215–220.
- [47] *Standards for Specifying Construction of Airports*, FAA Advisory circular No.150/5370-10G, (2014).
- [48] Gopalakrishnan, Kasthurirangan, H. Ceylan, S. Kim, S. Yang, H. Abdulla, Electrically Conductive Mortar Characterization for Self-Heating Airfield Concrete Pavement Mix Design, *Int. J. Pavement Res. Technol.* 8 (2015).
- [49] *Airside use of heated pavement systems*, FAA Advisory Circular No. 150/5370-17, Fedearl Aviat. Adm. (2011).

- [50] H. Abdulla, H. Ceylan, S. Kim, K. Gopalakrishnan, P.C. Taylor, Y. Turkan, System requirements for electrically conductive concrete heated pavements, *Transp. Res. Rec. J. Transp. Res. Board.* No. 2569 (2016) 70–79.
- [51] H. Abdulla, H. Ceylan, S. Kim, M. Mina, K. Gopalakrishnan, A. Sassani, P.C. Taylor, K.S. Cetin, Configuration of Electrodes for Electrically Conductive Concrete Heated Pavement, in: *ASCE Int. Conf. Highw. Pavements Airf. Technol.*, n.d.
- [52] T. Murotani, H. Koto, S. Igarashi, Monitoring of Early-Age Characteristics of Concrete using EMI based Embedded PZT Transducers on Varying Plate Thickness, in: *71st RILEM Annu. Week ICACMS, 2017*: pp. 383–392.
- [53] P. Ram, T. Van Dam, L. Sutter, G. Anzalone, K. Smith, Field Study of Air Content Stability in the Slipform Paving Process, *Transp. Res. Rec. J. Transp. Res. Board.* 2408 (2014) 55–65. doi:10.3141/2408-07.
- [54] Y. Yang, Methods study on dispersion of fibers in CFRC, *Cem. Concr. Res.* 32 (2002) 747–750. doi:10.1016/S0008-8846(01)00759-1.
- [55] Snow melting and freeze protection, in: *ASHRAE Handb. Fundam.*, 15th ed., American Society of Heating, Refrigerating and Air-Conditioning Engineers, Atlanta, GA, 2009. <http://app.knovel.com/hotlink/toc/id:kpASHRAE37/2009-ashrae-handbook>.
- [56] R.M. Fish, L. a Geddes, Conduction of electrical current to and through the human body: a review, *Eplasty.* 9 (2009) e44.

## CHAPTER 6. POLYURETHANE-CARBON MICROFIBER COMPOSITE COATING FOR ELECTRICAL HEATING OF CONCRETE PAVEMENT SURFACES

A journal paper to be submitted to the Journal of Composite Structures

Alireza Sassani<sup>1</sup>, Ali Arabzadeh<sup>2</sup>, Halil Ceylan<sup>3</sup>, Sunghwan Kim<sup>4</sup>, Kasthurirangan Gopalakrishnan<sup>5</sup>, and Peter C. Taylor<sup>6</sup>

### Abstract

The problems associated with traditional ice/snow removal methods have given rise to application of new methods and materials for keeping the surfaces of paved areas free of ice and snow under harsh winter conditions. Electrically heated pavement systems (HPS) have attracted attention as alternatives to the traditional ice/snow removal practices. The recent boom in the field of composite materials at research and commercial levels makes them an attractive option for production of more efficient, sustainable, and effective HPS. Electrically conductive polymer-based composites provide promising properties for this application. Based on the concept of joule heating (or resistive heating), the conductive

<sup>1</sup> Ph.D. Candidate, 497 Town Engineering Building, Department of Civil, Construction, and Environmental Engineering, Iowa State University, Ames, IA 50011, USA, Phone: +1-515-708-6021, E-mail:

[asassani@iastate.edu](mailto:asassani@iastate.edu)

<sup>2</sup> Ph.D. Candidate, 497 Town Engineering Building, Department of Civil, Construction, and Environmental Engineering, Iowa State University, Ames, IA 50011, USA, Phone: +1-515-708-7244, E-mail: [arab@iastate.edu](mailto:arab@iastate.edu)

<sup>3</sup> Professor, Director, Program for Sustainable Pavement Engineering and Research (PROSPER), 406 Town Engineering Building, Department of Civil, Construction, and Environmental Engineering, Iowa State University, Ames, IA 50011-3232, USA, Phone: +1-515-294-8051, E-mail: [hceylan@iastate.edu](mailto:hceylan@iastate.edu) (Corresponding Author).

<sup>4</sup> Research Scientist, 24 Town Engineering Building, Department of Civil, Construction, and Environmental Engineering, Iowa State University, Ames, IA 50011-3232, USA, Phone: 1-515-294-4698, Fax: 1-515-294-8216, E-mail : [sunghwan@iastate.edu](mailto:sunghwan@iastate.edu)

<sup>5</sup> Research Associate Professor, 354 Town Engineering Building, Department of Civil, Construction, and Environmental Engineering, Iowa State University, Ames, IA 50011-3232, USA, Phone: +1-515-294-3044, E-mail: [rangan@iastate.edu](mailto:rangan@iastate.edu)

<sup>6</sup> Director, National Concrete Pavement Technology Center, 2711 South Loop Drive, Suite 4700, Iowa State University, Ames, IA 50011-8664, USA, E-mail: [ptaylor@iastate.edu](mailto:ptaylor@iastate.edu)

coating layer can be utilized as a resistor that when subjected to electric current generates heat to increase the surface temperature and melt the ice and snow on the pavement surface.

This research investigates the feasibility of applying an electrically conductive composite coating made with a Polyurethane (PU) binder and micrometer-scale carbon fiber (CMF) filler as the electrical heating materials on the surface of portland cement concrete (PCC) pavements. PU-CMF composite coatings were prepared using different volume fractions of CMF, applied on the PCC surfaces, and evaluated for their volume conductivity, resistive heating ability, and durability at proof-of-concept level. The percolative behavior of CMF in PU matrix was captured and the desirable CMF dosage rates in terms of each performance parameter were investigated. Two percolation transition zones were identified for CMF in PU matrix at dosage rate ranges of 0.25-1% and 4-10%. The composites exhibited their most desirable performance and properties at CMF dosage rates greater than 10% and smaller than 15%.

### **Introduction**

Keeping the surface of paved areas free of ice and snow is a major challenge during harsh winter conditions. Traditional methods of ice/snow removal from pavements that use deicing chemicals and mechanical removal are associated with large manpower, sophisticated machinery, environmentally harmful chemicals, damage to pavement, and inadequate effectiveness in extreme weather conditions [1–7]. Most deicing chemicals are not effective at temperatures below  $-10\text{ }^{\circ}\text{C}$  ( $14^{\circ}\text{F}$ ); only calcium chloride-based deicers –that cause chloride ingress risk for concrete pavements– can be used at temperatures colder than  $-17^{\circ}\text{C}$  ( $1.4^{\circ}\text{F}$ ) [7]. Application of deicing chemicals is especially associated with negative environmental impacts [8–16]. In recent years many alternative methods have been proposed

and tested for removing ice and snow from paved surfaces; among them are the application of superhydrophobic coatings on pavement surfaces [17–20] and application of Electrically heated pavement systems (EHPS) [4,21–38]. Electrically heated-pavement systems (EHPS) have gained recent attention as an alternative to traditional methods to overcome the pavements' winter maintenance related problems [32, 39]. Two approaches to EHPS have so far been adopted in the existing literature, (a) embedding electrically heating sheet/grille elements inside the pavement [4,21], and (b) application of electrically conductive concrete/asphalt pavements [22–38]. Application of electrically conductive coating in EHPS is a new and, to the best of authors' knowledge, unprecedented method for producing electrically heated concrete pavements.

Numerous studies have investigated the feasibility and benefits of the application of different polymer-based and portland cement-based coating on concrete substrates. Water-repellent and water-proofing coatings on portland cement concrete (PCC) and asphalt concrete materials have been extensively studied [2, 17, 18, 20, 40–44]; on the contrary, there is very limited information regarding electrically conductive coating on concrete surfaces. The only application of electrically conductive coatings on concrete surfaces, in the relevant literature, involve using epoxy resin-based [45] or portland cement-based [46, 47] coatings as the anode in corrosion protection and/or chloride extraction practices. Elsharkawy et al. [48] produced water-repellent and electrically-heated coatings for metallic surfaces using carbon nanofibers (CNF) dispersed in fluoroacrylic copolymer (PMC) matrix. Electrically conductive composites are an important group of versatile materials with various engineering applications [49]. Electrically conductive coatings and thin films have been developed, mainly for application in circuitry [50], production of conductive papers [51, 52],

electromagnetic interference (EMI) shielding [53–55], and sensor systems [56–59]. The electrically conductive thin films and coatings are, typically, produced through dispersing a filler material such as CB [60], CNT [61], CNF [53, 55], or graphene [51,62], in a polymer matrix and casting the mixture on the substrate [60].

Different polymers can be used as binder phase in coatings. Epoxy resin has been used as a binder material on various surfaces such as Portland cement concrete [2, 19], asphalt cement concrete [17,18,20], and glass [63] to bind the nano-particles and adhere to the substrate. Fluorinated polymers such as Poly(vinylidene fluoride) (PVDF) have been used in superhydrophobic coatings as a matrix [55,64,65]. Tiwari et al. [64] and Das et al. [55] fabricated large-area sprayable superhydrophobic coatings with PVDF as binder. However, because of low strength and weak binding ability of PVDF, it needs to be used in conjunction with other binders. Poly(ethyl 2-cyanoacrylate) (PECA) and Poly(methyl methacrylate) (PMMA or acrylic resin) are commonly used as the additional binder materials with PVDF or used alone as the binder phase [55,64,66,67]. A group of polymers gaining increasing attention in the field of coating materials are Polyurethane (PU) compounds, a wide variety of materials that provide superior binding and adhesion properties. Polyurethane elastomers are thermally stable [68], compatible with carbonaceous materials which are a major component of electrically conductive composites [69–72], require no or minimal amount of volatile organic solvents [60, 73], and provide high adhesion and durability [74] on a most substrates including concrete [75].

Carbonaceous materials, especially carbon fibers [76, 77], CNT/CNF [78–82], and graphite powders [47, 83] have been extensively utilized in construction materials. Using nano-size materials in electrically conductive coatings which are meant for pavement



applications is challenging, particularly because of high cost [77] and hazardous nature [84] of nanoparticles. Gong et al. [85] used carbon felt made of micrometer-size carbon fibers in an electrically conductive polymer composite. Ameli et al. [86] studied the feasibility of polyurethane-carbon fiber composite foam for EMI shielding, using carbon fibers with micrometer diameter and millimeter length. In this paper, the term carbon microfiber (CMF) is used to refer to carbon fibers with both diameter and length in micrometer scale. CMF materials are orders of magnitude less expensive than nanomaterials, do not pose health hazards, and are easier to disperse in a given matrix (e.g. polymers or cement paste). However, the literature related to the application of such materials in coating mixtures is scarce and, to the best of authors' knowledge, there is no previous report on using PU-CMF composites for electrical heating (a.k.a. resistive heating or joule heating). On the other hand, there is no report of the application of PU-CMF composite coating on concrete structures and pavements in the existing literature.

This research investigates the feasibility of using PU-CMF composite coating, made with polyurethane elastomer as binder and milled carbon fiber with micrometer diameter and length as conductive filler, for electrical heating (resistive or joule heating) of portland cement concrete (PCC) pavement surfaces. The combination of materials and the application of such coatings on PCC pavements are, to the best of authors' knowledge, unprecedented in the existing literature. The required and/or optimum dosage rate of CMF was determined based on the concept of percolation threshold. Heating capability of the composite coating was studied by active infrared thermography (IRT) in temperature-controlled conditions. The durability of the coating materials was investigated by applying cyclic wheel load on the

coatings and measuring its effect on the mass and electrical resistance of the coating material on concrete surface.

### Experimental

Carbon microfiber (CMF) was milled carbon fiber with 7.2 $\mu$ m nominal diameter and 100 $\mu$ m nominal length, specific gravity of 1.75, 99% carbon content, and electrical resistivity (volume resistivity) of  $1.4 \times 10^{-3} \Omega\text{-cm}$ . A one-component fast-drying thermoplastic polyurethane (PU) (by Minwax®) with a kinematic viscosity ( at 40°C) smaller than  $2.05 \times 10^{-1} \text{ cm}^2/\text{s}$  (<20.5 cSt), specific gravity of 0.86, and boiling point of 148°C was used as the polymer component. The methods to enhance the dispersion of carbon fibers in cementitious matrices are based on improving the wettability of the fibers [87], therefore, they are not useful in polymer-fiber composites which do not have water or other solvents, as is the case in this study. To improve the dispersion of fibers, the treatment method developed by Xiong et al. for dispersing carbon nanotubes (CNT) in polyurethane matrix was adopted with some modifications [88]. The as-received CMF was first heat-treated for 4 hours at 400°C while gently blown with air flow. Then, the CMF was dispersed in a 3:1 mixture of Sulfuric acid and Nitric acid by sonication for 10 minutes in a bath sonicator at 80°C. The suspension was then poured on grade 3 filter paper (6  $\mu$ m pore size), drained off the acid solution, and gently washed with deionized water until the PH of the filtered fluid became close to the PH of the deionized water. Finally, the fibers were collected off the filter paper and desiccated in a vacuum desiccator for 72 hours. It should be mentioned that the effect of fiber treatment on the surface chemistry (and dispersion) of CMF is likely different than CNT, because the properties of materials in nano-scale tend to differ from their macro- and micro-scale characteristics. However, previous studies have shown adequate effectiveness of

such methods in improving the dispersion of carbon fibers with micrometer-scale diameters and millimeter-scale length [87].

The PU-CMF composite suspension was prepared without incorporation of any solvents in the mixture. Because the intended application substrate of this composite coating is pavement surfaces, this approach was adopted to increase the setting rate of the composite, eliminate the time needed for evaporation of the solvent phase, and thus shorten the closing time of the paved facility. In the absence of a solvents, and because of thermo-stability of polyurethanes [68], it was possible to prepare the PU-CMF composite at high temperatures that are above the boiling point of the PU and lower than its degradation temperatures. Thermal degradation of thermoplastic PU takes place above 200°C [73]. Reduction of the viscosity of PU at higher temperatures [89, 90] facilitates the dispersion of CMF in the PU matrix. The treated CMF were added to the PU component of the composite and the mixture was magnetically stirred at 360 rpm speed and 150°C temperature for three minutes. Then, the mixture was placed in bath sonicator at 80°C and sonicated for 10 minutes, followed by another three minutes of magnetic stirring at the aforementioned speed and temperature. Once the PU-CMF mixture was prepared, it was applied on the specimen surfaces using a brush. The weight of the coating material applied on each specimen was determined by measuring weights of the mixture and brush before and after coating application.

Percolation concept is a useful tool for explaining the electrical behavior and determining optimum or required dosage rate of the conductive filler in the composite coatings which consist of an electrically insulating matrix and an electrically conductive filler [49]. Achieving high electrical conductivity in such a composite material requires electrically conductive filler's percolation through the insulating matrix (PU in this study); meaning that

the volume fraction of the filler (CMF in this study) should be equal to or greater than the value which forms a continuous path of fibers touching one another [58–63]. The range of fiber content at which electrical conductivity abruptly increases is known as the percolation transition zone (or percolation threshold) [64]. Within the percolation transition range, by increasing the volume fraction of the conductive filler, the electrical conductivity of the composite rises several orders of magnitude. Above percolation threshold, increasing the conductive filler dosage rate continues to improve the conductivity of the composite, but does not lead to abrupt increase of conductivity because the network of conductive filler is already saturated [49]. Excessive amount of conductive filler increases the mixture viscosity and makes it difficult to be uniformly applied on the substrate [49]. Therefore, the percolation transition zone of the CMF-PU composite was investigated through mixtures containing different volume fractions of CMF as shown in Table 6-1. Using the mixture proportions given in the table, two types of coated specimens on wood and PCC substrates were prepared for measurement of electrical conductivity as shown in Figure 6-1.

Wood substrate was used because the electrical conductivity of dry wood is low enough to ensure the absence of measurable conductivity interferences with the measurements. Oven-dried PCC substrate was used to simulate the real conditions in the intended application of these coating materials on PCC pavements. Since the results of the measurements on the two groups of specimens were comparable, the final electrical conductivity was taken as the average of the measurement results on both substrates (each specimen with three replicates).

Silver paste was applied to the two ends of specimens to be used as electrodes in measurement of resistance. Because the CMF, especially at low dosage rates, may not be

exposed on the surface -reducing the electrical contact of the silver paste with the coating- the two ends of specimens were roughened with scrub pad before applying the silver paste to improve the electrode-specimen contact. Two-probe method [91, 92], a reliable and accurate approach for resistance measurement, was utilized in this study, and the reason for reliability and accuracy of this method is thoroughly explained in the authors' previous studies [1,93]. A FLIR DM62 digital multimeter was used for measuring the resistance values. It is worth noting that the resistivity measurements were conducted using DC current at a very short time (virtually 1 second) to avoid polarization [94]. All the measurements were performed at +20°C, in an environmental chamber, using the silver paste electrodes (Figure 6-1). The environmental chamber, equipped with fans and a dehumidifier unit, ensured a uniform temperature distribution and a minimum and constant amount of humidity in the air.

The thickness of coatings were measured with a thickness gauge (PosiTector® dry film thickness gauge with precision of 13-1000µm); for each specimen, the thickness was measured on several spots and averaged to obtain the coating layer thickness. The width and length of each specimen between the electrodes were also measured with 0.01 mm precision. The dimensions of the coatings were used to calculate the volume resistivity in Ω-cm and volume conductivity (which is the reciprocal of resistivity) in S/cm according to Equation 6-1:

$$\rho = R \cdot A/l \quad (\text{Equation 6-1})$$

Where,  $\rho$  represents the electrical (volume) resistivity in ohm-centimeters (Ω-cm),  $R$  is the electrical resistance in Ohms (Ω),  $A$  is the cross sectional area normal to the current direction, and  $l$  is the distance between the two points with electrical potential difference of  $V$ . The electrical conductivity was plotted against the CMF dosage rate to determine the

percolation transition zone. To relate the percolation results to resistive heating capability of the coatings, a heating test was performed on the wood-substrate specimens. An AC voltage of 5 V at a frequency of 64 Hz was applied to each specimen for the duration of 1 minute. Meanwhile, the surface temperature of the specimen was measured and recorded using a FLIR T650sc Infrared camera, with a resolution of  $640 \times 480$  pixels. The acquired radiometric data were then analyzed using the ResearchIR Max® software package, and the heat generation on the surface of each specimen during one minute was quantified.

*Table 6-1. Mixing proportions of PU-CMF composite mixtures for determination of percolation transition zone.*

| CMF dosage rate (% Vol.) | CMF content (g) | PU content (g) |
|--------------------------|-----------------|----------------|
| 0.25                     | 0.15            | 30.02          |
| 0.50                     | 0.31            | 29.95          |
| 0.75                     | 0.46            | 29.87          |
| 1.00                     | 0.61            | 29.80          |
| 1.50                     | 0.92            | 29.65          |
| 2.00                     | 1.23            | 29.50          |
| 2.50                     | 1.53            | 29.35          |
| 3.00                     | 1.84            | 29.20          |
| 3.50                     | 2.14            | 29.05          |
| 4.00                     | 2.45            | 28.90          |
| 5.00                     | 3.06            | 28.60          |
| 6.00                     | 3.68            | 28.29          |
| 7.50                     | 4.59            | 27.84          |
| 10.00                    | 6.13            | 27.09          |
| 12.50                    | 7.66            | 26.34          |
| 15.00                    | 9.19            | 25.59          |
| 17.50                    | 10.72           | 24.83          |
| 20.00                    | 12.25           | 24.08          |

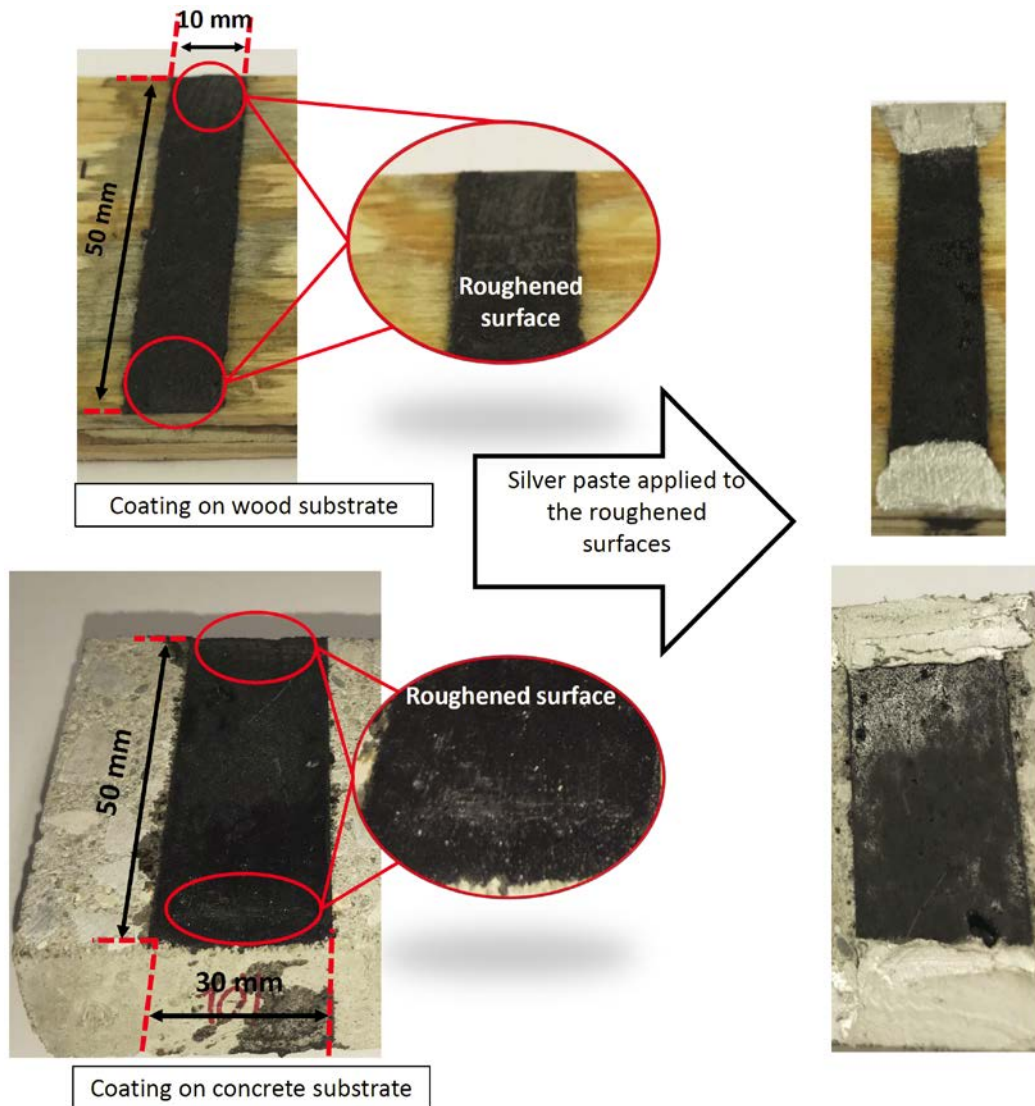


Figure 6-1. Coated specimens for determination of percolation threshold.

To evaluate the performance of the composite coating on concrete substrate in terms of resistive heating and durability, concrete specimens were coated with the PU-CMF composite at different CMF dosage rates which were selected based on the results of percolation threshold tests. The CMF dosage rates were selected such that the whole range of percolation transition zone and its vicinity were covered. The PU-CMF composite coatings used at this stage included 3, 4, 5, 6, 7.5, 10, 12.5, 15, 17.5, and 20% CMF by total volume of the composite. Each specimen was made in three replicates.

To evaluate the heating capability of the composites, rectangular concrete specimens with copper tape electrodes glued to the surface were prepared and coated as shown in Figure 6-2. Heat generation efficiency of the composite-coated specimens were characterized through performing active IRT [95] at a temperature below the freezing temperature of water. To this end, all the specimens were preconditioned at  $-20\text{ }^{\circ}\text{C}$  for at least three hours so they could achieve thermal equilibrium [96]. An AC voltage of 20 V at a frequency of 64 Hz was applied to each specimen through the copper tape electrodes for the duration of 3 minutes. The surface temperature of each specimen was measured and recorded as explained in the above.

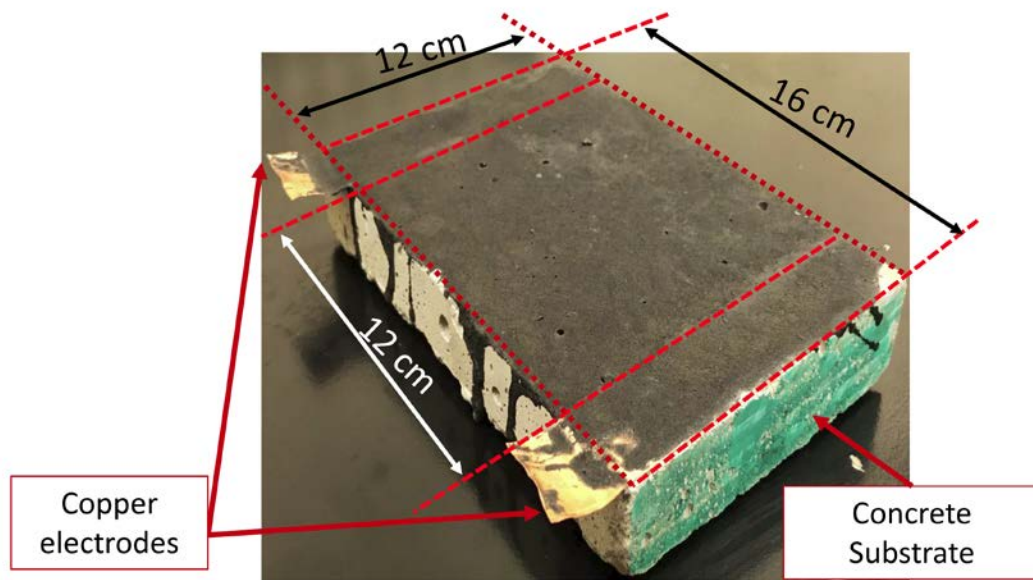


Figure 6-2. Concrete specimens coated with PU-CMF composite for resistive heating test.

The durability of PU-CMF composite in PCC pavement surfaces was studied by applying cyclic rotating wheel path at 250 rpm speed with 196 N force (1.66 MPa stress) vertical load under each wheel on three types of coated specimens as shown in Figure 6-3. The test set-up (Figure 6-4) used in this study was similar to the testing method developed by Hawkins et al. [95] for studying the durability of pavement markings; this method is based on



the abrasion resistance test (ASTM C944/C944M-12 standard) with some modifications that included using higher load magnitude, applying the cyclic load by a different abrading tip (solid rubber wheels instead of rotating cutter), and using different specimen types. The mass loss of the coating materials, as a percentage of the mass of coating, was measured after 500, 1000, 5000, and 10000 cycles. Two types of specimens were used for investigation of the effect of cyclic loading on the electrical conductivity (electrical resistance) of coatings. Because of the changes made to the thickness and coverage area of coatings as the result of cyclic loading, the total electrical resistance of the coatings (instead of volume conductivity) before the test and after 10000 loading cycles were used as the indicator of electrical durability. This approach helps eliminate the complications caused by cross sectional variations and evaluates the actual performance of the coating under load. The specimens shown in Figure 6-3(b), were used to simulate the situation where the entire width of the electric current flow path lies under the loading wheels. Figure 6-3(c) shows the specimens that represent the case where the loading wheels travel on a fraction of the flow path between the electrodes; this approach was taken to investigate the effect of localized damage on the electrical conductivity of the whole coated surface. The change of electrical resistance after the loading was calculated by averaging the results obtained from the two types of specimens for each coating. The electrical resistance of the specimens shown in Figure 6-3(c) were determined by making resistance measurements between each two diagonally opposite silver paste electrodes, repeating each measurement for three times on the same specimen, and taking the average of all readings as the electrical resistance of the specimen.

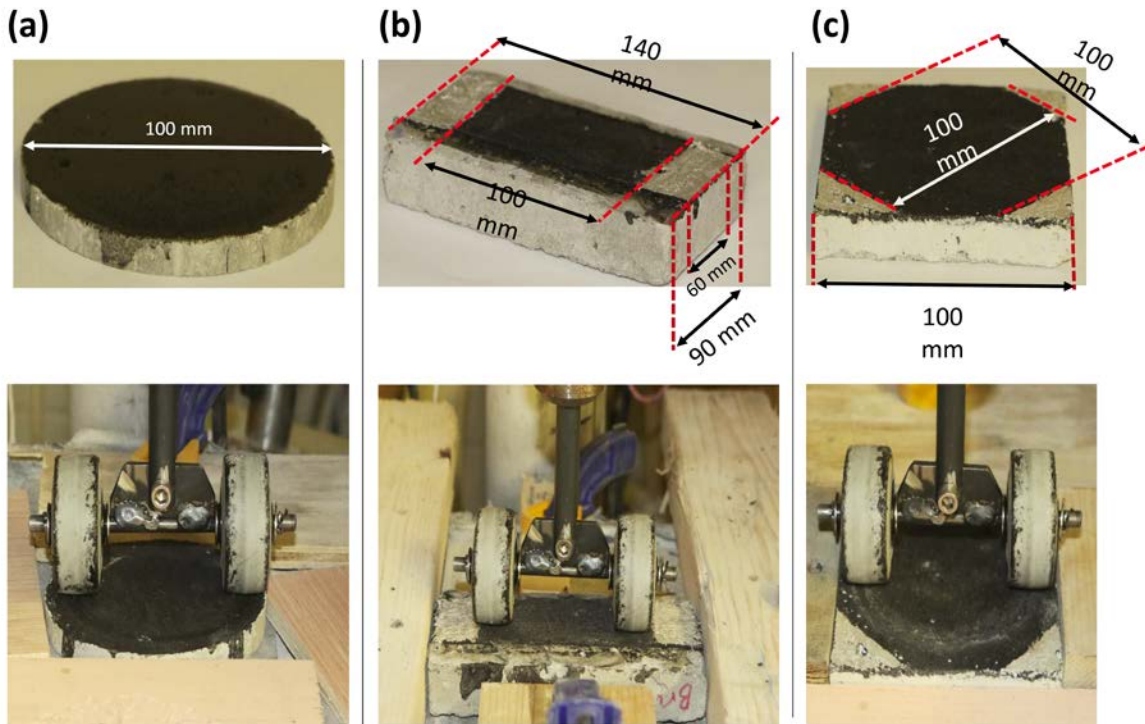


Figure 6-3. Concrete specimens coated with PU-CMF composite and the test set-up for evaluating the (a) effect of loading cycle on mass loss, (b) effect of loading cycles-induced current flow path deterioration on electrical conductivity, (c) loading cycles-induced.

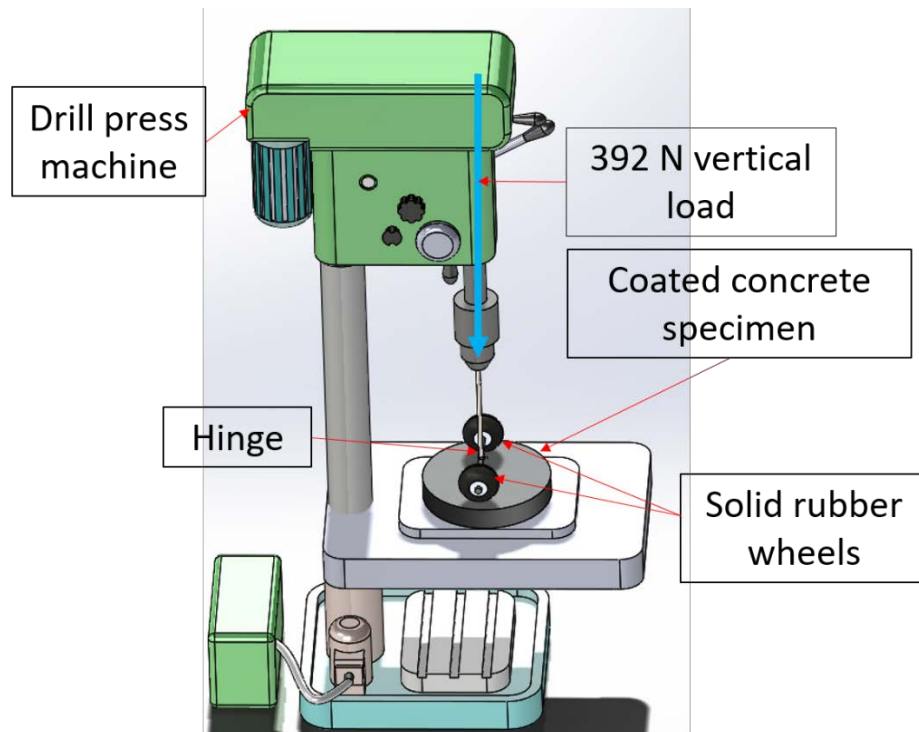


Figure 6-4. Schematic of the coating durability test set-up.

## Results and Discussion

Table 6-2 shows the volume conductivity of PU-CMF coatings with different volume fractions of CMF and the results are visualized in Figure 6-5. As seen in Figure 6-5, the selected range of CMF content resulted in fully capturing the percolative behavior [96], such that the dual critical percolation threshold was found [97]. As seen in the figure, four different zones can be distinguished in the conductivity-CMF dosage plot that include two abrupt conductivity increase zones and two plateauing regions. The first sizeable increase of volume conductivity occurred in Zone I, between 0.25% and 1% CMF volume fractions, which shows the transition of the composite from insulator to semiconductor. In zone II, the conductivity-versus-CMF dosage curve plateaued until the second abrupt jump of volume conductivity occurred in zone III between 4% and 10% CMF volume fractions; this corresponds to the percolation transition zone over which the composite transfers from a semiconductor into a conductor [97, 98]. As per the definition of percolation transition zone, by increasing of CMF dosage rate above the semiconductor-to-conductor percolation transition range (4-10% Vol.), the volume conductivity is marginally increased as depicted by zone IV in the figure. In the work conducted by Wu et al. [97], with a graphite/high-density polyethylene composites, the two percolation transition zones were found at filler dosage rates of 12.29% (Vol.) and 21.79% (Vol.) respectively. This finding reveals a more effective percolative behavior of CMF compared to graphite powder.

As seen in Table 6-2, the relative standard error took greater values, relative to the neighboring points, in vicinity of 1% and 4 % CMF dosages that correspond to the turning points between the zones in Figure 6-5 where the continuously interconnected network of CMF has not yet been established. This observation is in agreement with the findings of previous works [96, 99] postulating that the electrical conductivity of different specimens

with the same conductive filler is higher before the formation of continuous conductive network, especially at the proximity of percolation threshold.

*Table 6-2. Electrical conductivity of PU-CMF coatings containing different volume fractions of CMF.*

| <b>CMF dosage rate<br/>(% Vol.)</b> | <b>Electrical Conductivity (S/cm)</b> | <b>Standard deviation</b> | <b>Relative standard error</b> |
|-------------------------------------|---------------------------------------|---------------------------|--------------------------------|
| <b>0.25</b>                         | 3.28E-03                              | 1.19E-04                  | 2.09E+00                       |
| <b>0.50</b>                         | 7.90E-02                              | 1.38E-03                  | 1.01E+00                       |
| <b>0.75</b>                         | 1.97E-01                              | 6.56E-02                  | 1.92E+01                       |
| <b>1.00</b>                         | 3.26E-01                              | 5.77E-02                  | 1.02E+01                       |
| <b>1.50</b>                         | 3.26E-01                              | 6.67E-03                  | 1.18E+00                       |
| <b>2.00</b>                         | 3.66E-01                              | 7.61E-03                  | 1.20E+00                       |
| <b>2.50</b>                         | 4.22E-01                              | 5.68E-02                  | 7.77E+00                       |
| <b>3.00</b>                         | 4.62E-01                              | 7.35E-02                  | 9.19E+00                       |
| <b>3.50</b>                         | 5.59E-01                              | 1.33E-01                  | 1.37E+01                       |
| <b>4.00</b>                         | 5.85E-01                              | 1.02E-01                  | 1.01E+01                       |
| <b>5.00</b>                         | 3.18E+00                              | 3.08E+00                  | 5.59E+01                       |
| <b>6.00</b>                         | 8.49E+00                              | 1.88E+00                  | 1.28E+01                       |
| <b>7.50</b>                         | 1.59E+01                              | 1.00E+00                  | 3.64E+00                       |
| <b>10.00</b>                        | 3.48E+01                              | 7.69E+00                  | 1.28E+01                       |
| <b>12.50</b>                        | 3.71E+01                              | 7.73E+00                  | 1.20E+01                       |
| <b>15.00</b>                        | 3.98E+01                              | 2.34E-01                  | 3.39E-01                       |
| <b>17.50</b>                        | 4.19E+01                              | 1.40E+01                  | 1.94E+01                       |
| <b>20.00</b>                        | 4.58E+01                              | 7.19E+00                  | 9.07E+00                       |

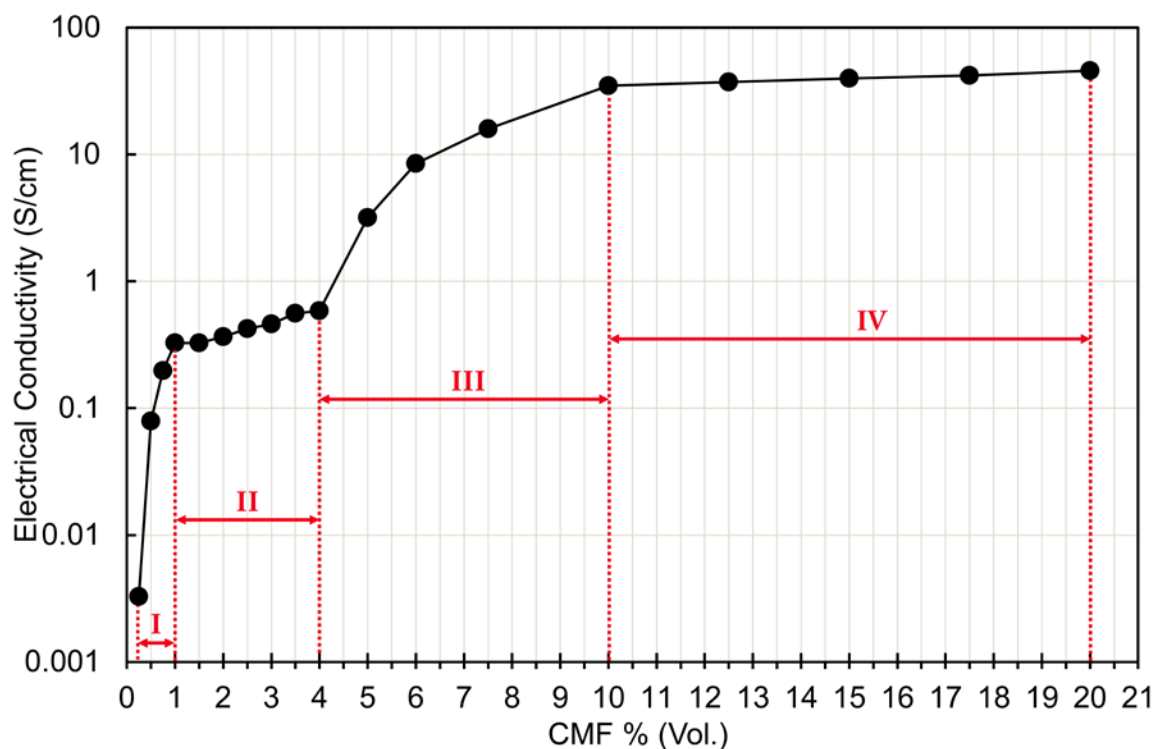


Figure 6-5. Variation of volume conductivity with CMF dosage rate in the PU-CMF composite coatings.

Figure 6-6 and Figure 6-7 show the heating capability of PU-CMF coatings on wood substrate after one minute of current application. As revealed by the results, the rise of average surface temperature increased with CMF volume fraction up to 12.5 %. Beyond 12.5% CMF dosage rate, the trend was reversed resulting in reduction of composite's heat generation capability with increase of CMF content. An abrupt jump in the surface temperature rise was observed at 1.5% CMF dosage which corresponds to the first point after the upper limit of the first percolation transition zone. The measured values exhibited a higher variation in the vicinity of each of the three turning points (1%, 4%, and 10% CMF) which correspond to the transitions between the different zones of Figure 6-5. However, because of the complicated viscoelastic behavior of the composite at filler dosages at or near the percolation transition zones [97], this behavior cannot be merely attributed to the

fluctuations of volume conductivity. Rather, the quality of the coating with respect to surface application uniformity also affects the ability of heat generation.

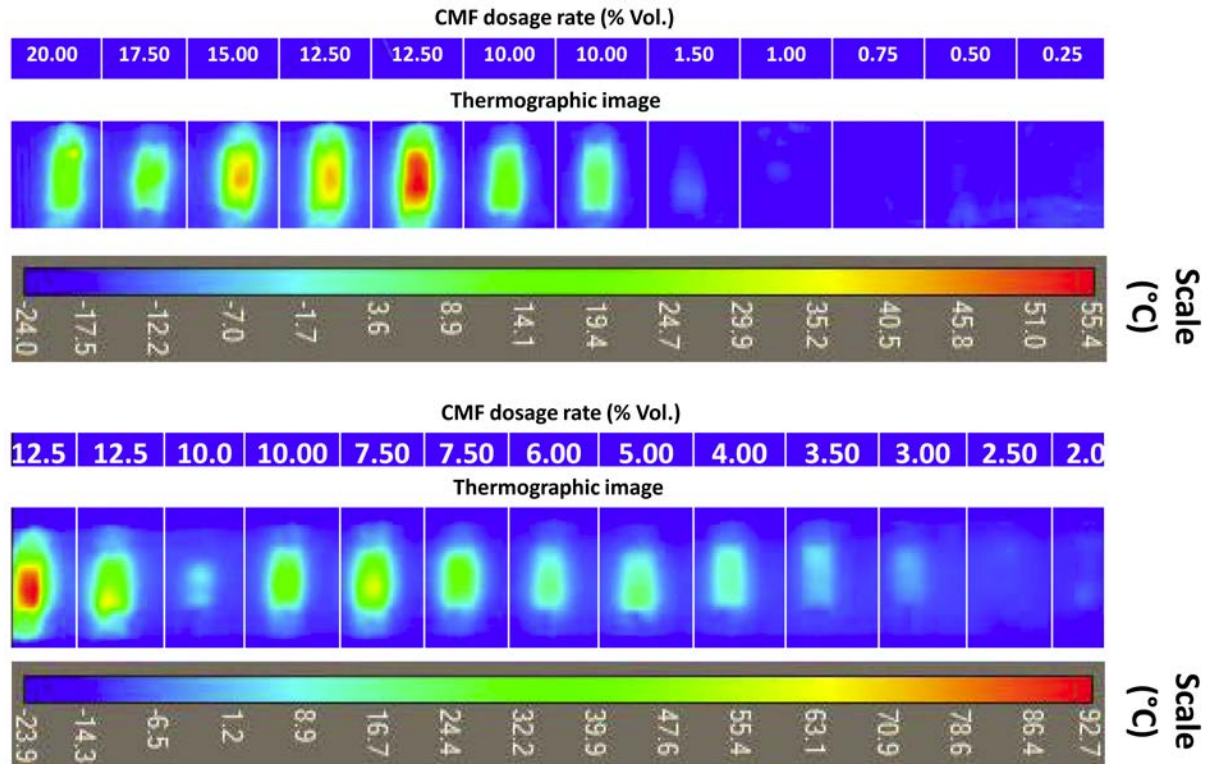


Figure 6-6. Thermal image of different CMF-content coatings on wood substrate after 1 minute of current application.

Figure 6-8 and Table 6-3 present the average temperature rise at three different durations of electric current application (1, 2, and 3 minutes) on the surface of concrete specimens coated with PU-CMF composites containing different volume fractions of the conductive filler (CMF). At all three time intervals the average surface temperature assumed an increasing trend with increase of CMF dosage rate. An abrupt jump in heat generation occurred at 7.5% CMF, Such that, after 3 minutes of electric current application, the average temperature on the surface of 7.5%-CMF specimen was ca. three times higher than the specimen coated with 6%-CMF composite, while, the difference between any two

consecutive specimens (i.e. consecutive rows in Table 6-3) at CMF contents higher than 7.5% were smaller than 40%.

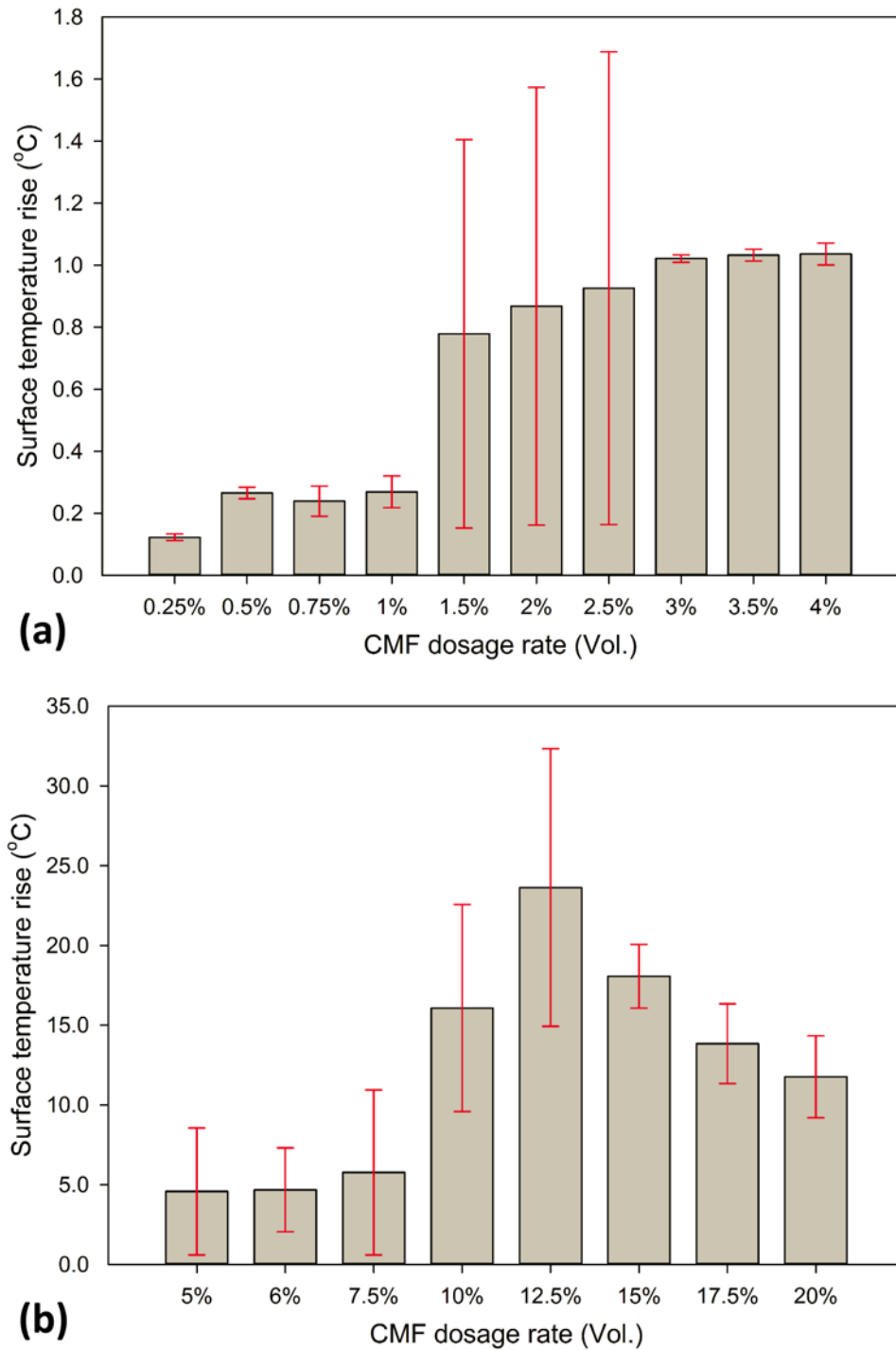


Figure 6-7. Average surface temperature rise of coatings on wood substrate at CMF dosage rates (a) below and (b) above the lower limit of second percolation transition zone after 1 minute of current application.

The continuous increase of “average surface temperature rise” with CMF dosage rate is in contradiction with the results obtained from small wood-substrate specimens (Figure 6-6 and Figure 6-7). However, the thermographic images of concrete specimens (Figure 6-9) cast a light on what appeared to be a discrepancy between the heat generation results obtained from the two experiments. As seen in Figure 6-9, with CMF dosage rates up to 12.5%, the temperature distribution on the coated surfaces between the two electrodes were almost uniform without any extreme heat concentration spots. Whereas, at 15%, 17.5%, and most significantly at 20% CMF contents, the electrical-energy-to-heat-energy conversion occurred at a small fraction of the coating, extremely increasing the temperature at some spots and leaving the majority of the surface unheated. This heat concentration is attributed to existence of high-electrical-resistivity clusters within the coating layer due to poor CMF dispersion uniformity. At high CMF contents, the composite is more susceptible to filler agglomeration and, thus, to lack of uniformity; however, this is hard to capture in small specimens like those used to obtain Figure 6-6 and Figure 6-7. As per the foregoing discussions, using the mixing and dispersion procedure of this study, the optimum CMF dosage rates with respect to resistive heating capability, is assumed to be greater than 7.5% and smaller than 15%. PU-CMF composites containing 10% and 12.5% (Vol.) conductive filler provided desirable performance with regards to both the magnitude of average temperature increase and the temperature distribution uniformity.

The amount of mass loss undergone by the PU-CMF coatings when subjected to cyclic loading are shown in Figure 6-10. Increasing CMF volume fraction from 3% to 4% resulted in smaller mass loss at 500 and 1000 loading cycles, while, this trend was reversed at 5000 and 10000 cycles with the coatings containing 4% CMF exhibiting greater mass loss.



As seen in Figure 6-10(a), there was a significant drop in the amount of coatings' mass loss at the CMF volume fraction of 5% which corresponds to the beginning of percolation transition zone (second transition zone in Figure 6-5). At CMF-dosage rates higher than 5% (Figure 6-10(b) & (c)), the loss of coatings' mass under cyclic load at all test durations was decreased with increasing the CMF volume fraction.

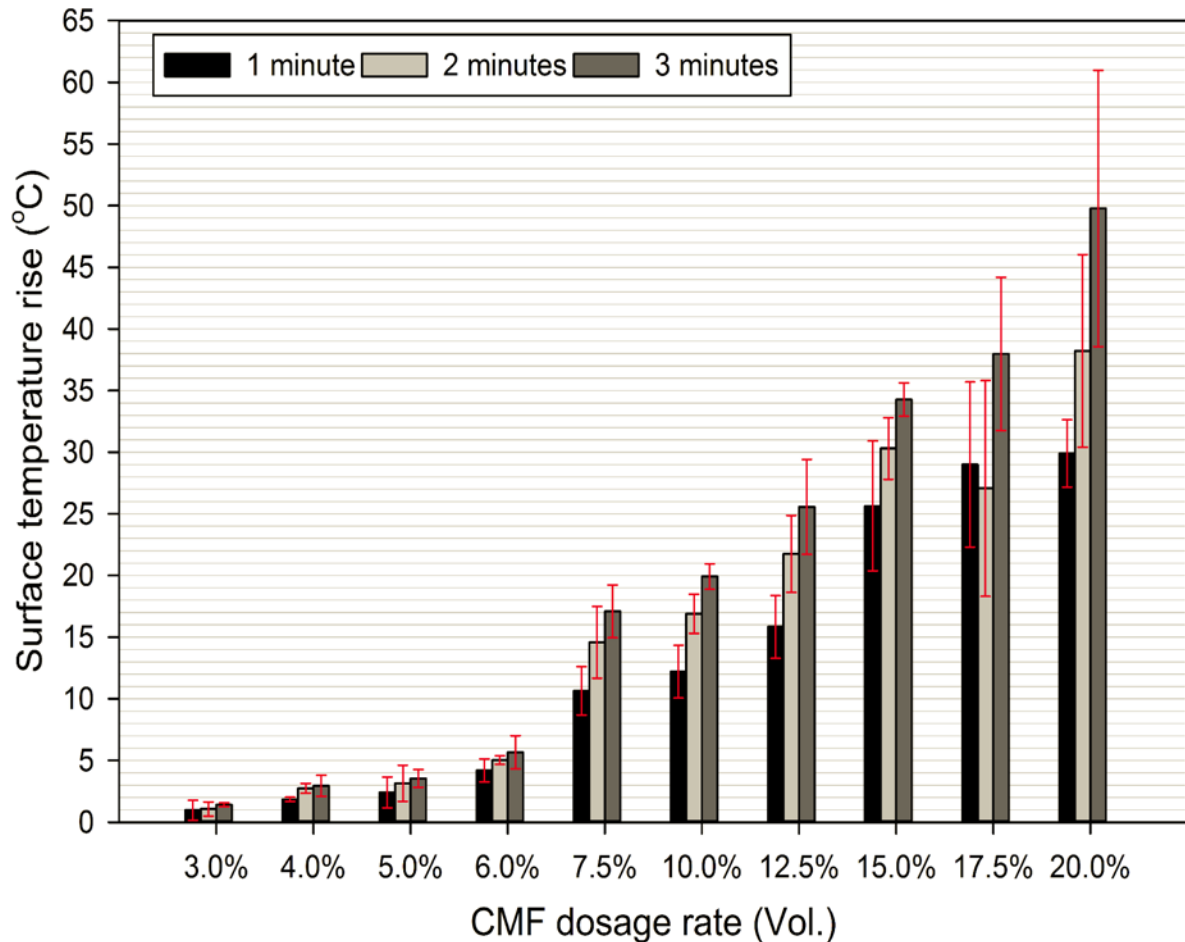


Figure 6-8. Average temperature rise on the surfaces of coated concrete specimens at different durations of electric current application.

Table 6-3. Thermography results for PU-CMF-coated concrete specimens.

| CMF dosage rate (%Vol.) | Duration (minutes) |      |                  |      |                  |      |
|-------------------------|--------------------|------|------------------|------|------------------|------|
|                         | 1                  |      | 2                |      | 3                |      |
|                         | Temperature (°C)   | S.D. | Temperature (°C) | S.D. | Temperature (°C) | S.D. |
| 3.0                     | 1.0                | 0.8  | 1.1              | 0.6  | 1.4              | 0.2  |
| 4.0                     | 1.9                | 0.2  | 2.8              | 0.4  | 3.0              | 0.9  |
| 5.0                     | 2.4                | 1.3  | 3.2              | 1.5  | 3.5              | 0.7  |
| 6.0                     | 4.2                | 0.9  | 5.0              | 0.3  | 5.7              | 1.4  |
| 7.5                     | 10.6               | 2.0  | 14.6             | 2.9  | 17.1             | 2.1  |
| 10.0                    | 12.2               | 2.1  | 16.9             | 1.6  | 19.9             | 1.0  |
| 12.5                    | 15.8               | 2.5  | 21.8             | 3.1  | 25.6             | 3.8  |
| 15.0                    | 25.6               | 5.3  | 30.3             | 2.5  | 34.3             | 1.3  |
| 17.5                    | 29.0               | 6.7  | 27.1             | 8.8  | 38.0             | 6.2  |
| 20.0                    | 29.9               | 2.7  | 38.2             | 7.8  | 49.8             | 11.2 |

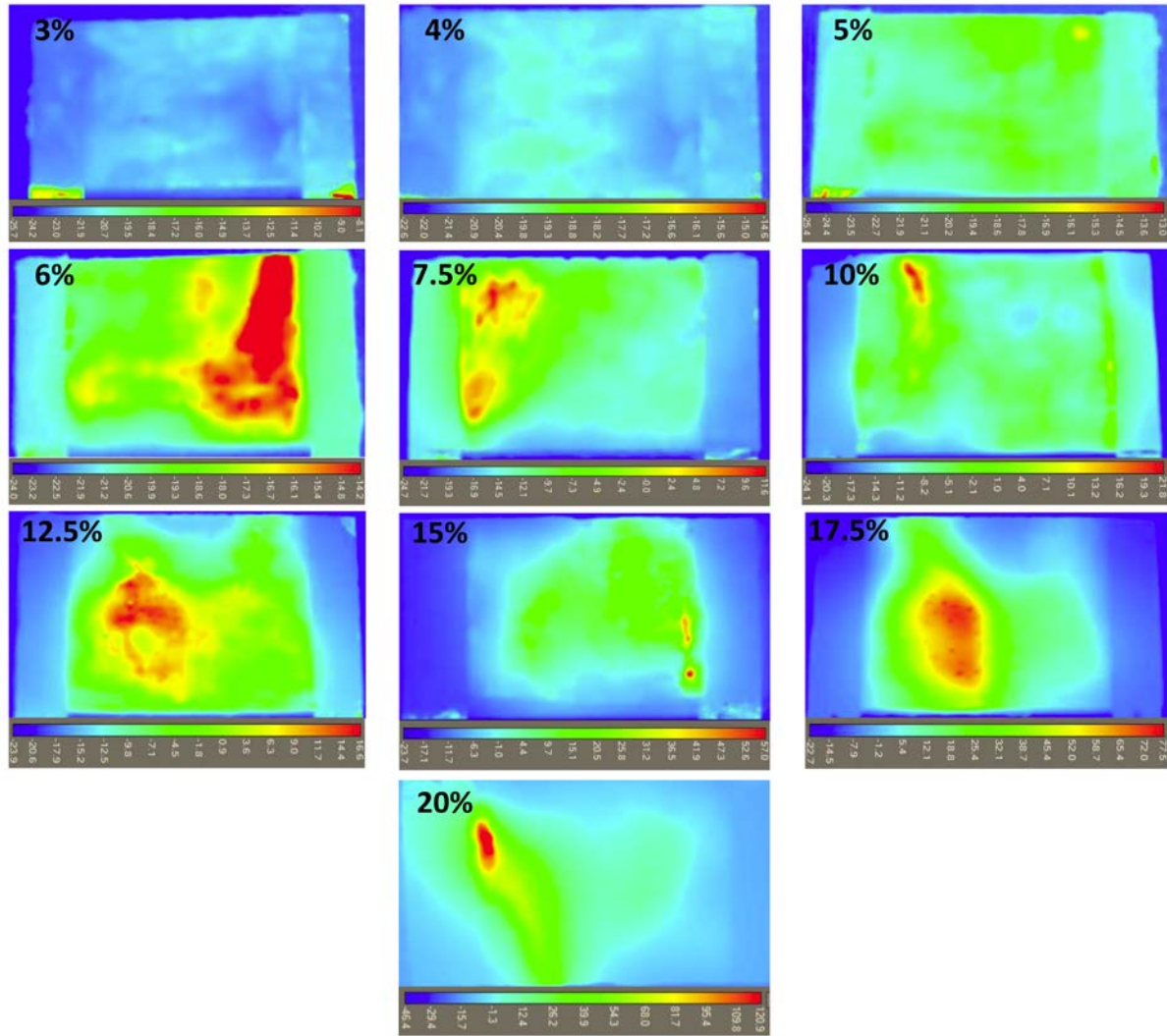
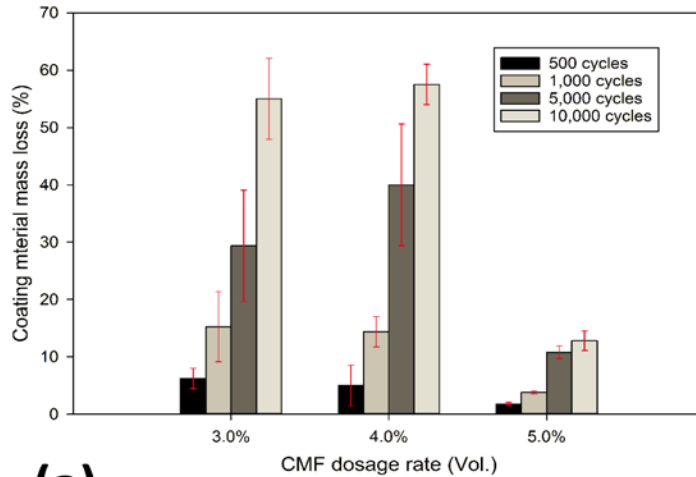
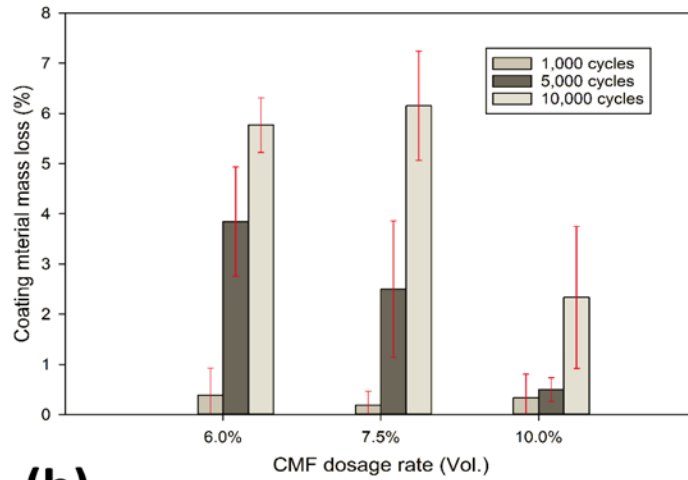


Figure 6-9. Selected infrared thermal images of concrete specimens after 3 minutes of electric current application.

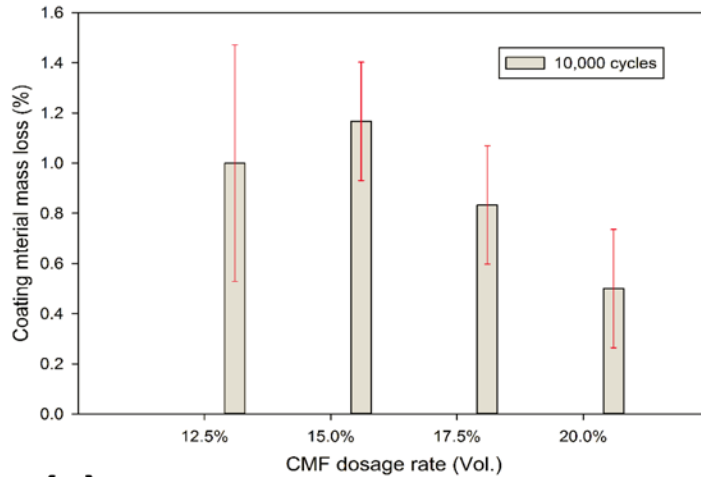
As seen in Figure 6-10(b), in the range of 6%-10% CMF content, no measurable amount of coating materials were lost at 500 loading cycles while the mass loss at 1000 cycles was also negligible. Above 10% CMF content, shown in Figure 6-10(c), the coatings lost none of their mass up to 5000 cycles of loading and a very small mass loss was observed at 10000 cycles. This observation indicates that the CMF network contributes to the strengthening of Polyurethane matrix and improves its durability.



(a)



(b)



(c)

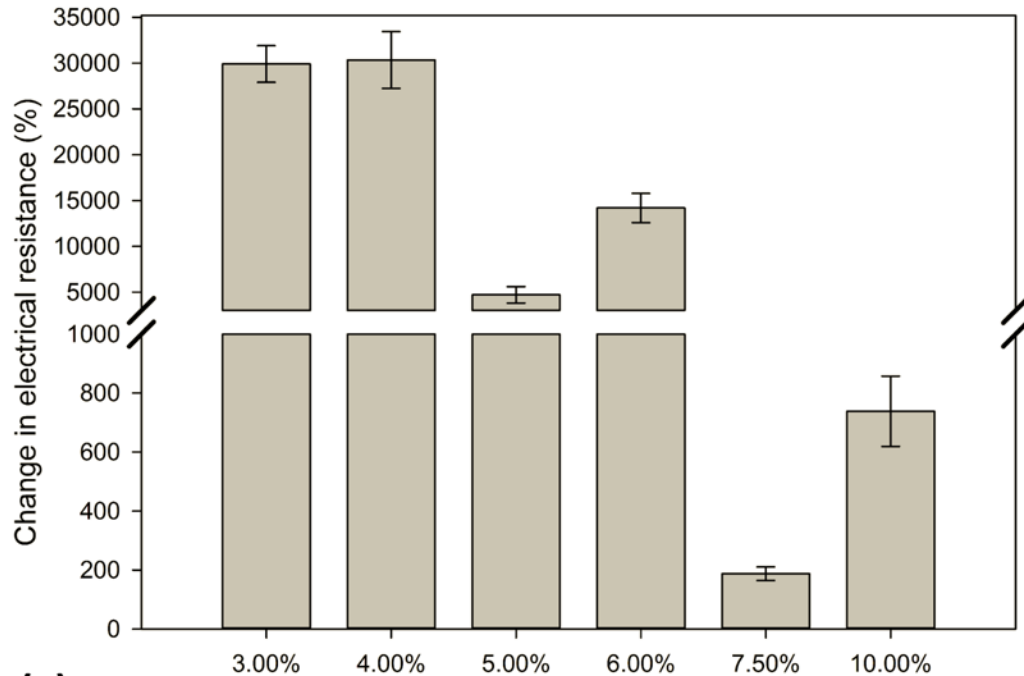
Figure 6-10. Mass loss of coatings with different CMF dosage rates. Coatings showing measurable mass loss at (a) all; (b) greater than 500; and (c) greater than 5,000 loading cycles.

The results of electrical resistance measurement on coatings before and after applying 10000 cycles of loaded wheel path, shown in Figure 6-11(a) & (b), confirmed the positive effect of CMF on durability of coatings. It was observed that up to 6% CMF dosage rate, the electrical conductivity of the coatings was severely degraded resulting in a stunning increase of electrical resistance. Increasing CMF dosage rate to higher than 6%, as seen in Figure 6-11(a), resulted in a dramatic improvement of durability and diminished the increase of resistance after loading by orders of magnitude. At 7.5% and 10% CMF contents, the electrical resistance after the cyclic loading was 3 times and ca. 9 times greater than its initial value, respectively. When CMF dosage rate was increased to values higher than 10%, virtually the percolation threshold, the electrical resistance after 10000 cycles of wheel path was even lower than its initial value resulting in negative values of resistance change in Figure 6-11(b)). Note that, the coatings containing 12.5, 15, 17.5, and 20% CMF showed a negligible amount of mass loss after 10000 load cycles (shown in Figure 6-10(c)) leaving the coating completely intact after the load application and not exerting a significant effect on the cross sectional area of the coating.

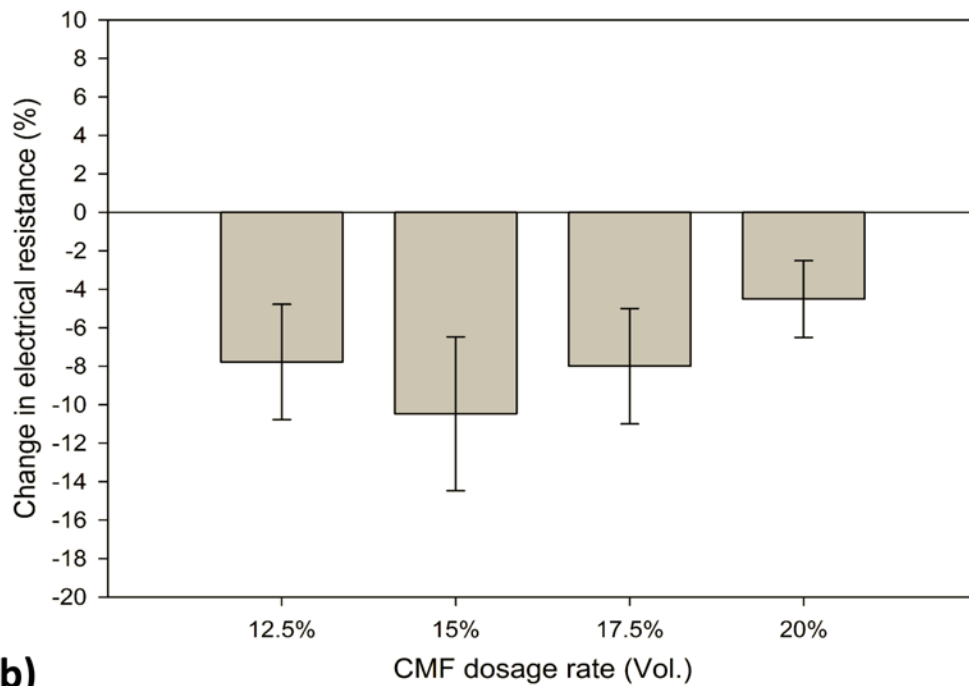
For a material with a certain volume resistivity, the electrical resistance is directly proportional to the distance between electrodes and reciprocal of the cross sectional area in the direction of current. As seen in Figure 6-12, the specimen coated with 10%-CMF coating was torn apart by cyclic wheel path and lost its electrical continuity, while, the 15%-CMF coating stayed completely intact. It is also seen in the figure, that in the durable coatings (e.g. 15%-CMF) the coating materials were to some extent compacted in the wheel path. The compaction of coating tends to bring the CMF fibers closer to each other and boost the fiber-to-fiber contact. Also, smaller spacing between fibers tends to increase the chance of electron

hopping (tunneling effect) between non-contacting fibers. The one-by-one contact between conductive fibers and the electron hopping between fibers that are not in direct contact with each other are among primary mechanisms of conduction in electrically conductive fiber-matrix composites [100,101]. Regarding that the reduction of cross sectional area above 10% CMF content was negligible (Figure 6-10(c)), its negative effect on electrical conductivity was possibly dominated by the positive effect of compaction resulting in reduction of electrical resistance in Figure 6-11(b).

The results of investigating volume resistivity variation with CMF dosage rate (0.25%-20% Vol.) captured the dual percolation transition zone at 0.25%-1% for insulator-to-semiconductor and 4-10% for semiconductor-to-conductor transitions respectively. Heating capability tests on PU-CMF composites using two types of specimens indicated that the heating efficiency of the coatings experiences significant improvement at two thresholds of 1.5% and 10% CMF, while at CMF dosage rates higher than 12.5% the small specimens showed reduction of heating ability and larger specimens showed lack of heat distribution uniformity. The durability of coatings was continuously improved by increasing the CMF volume fraction with two abrupt jumps at 5% and 12.5%. Regarding these results, CMF volume fraction greater than 10% and smaller than 15% can be identified as the desirable range for dosage rate of CMF conductive filler in the PU-CMF composite in terms of electrical conductivity, resistive heating capability, and durability.



(a)



(b)

Figure 6-11. The changes in electrical resistance of coatings after 10,000 loading cycles for (a) coatings that experienced resistance increase, and (b) coatings that experienced resistance decrease.

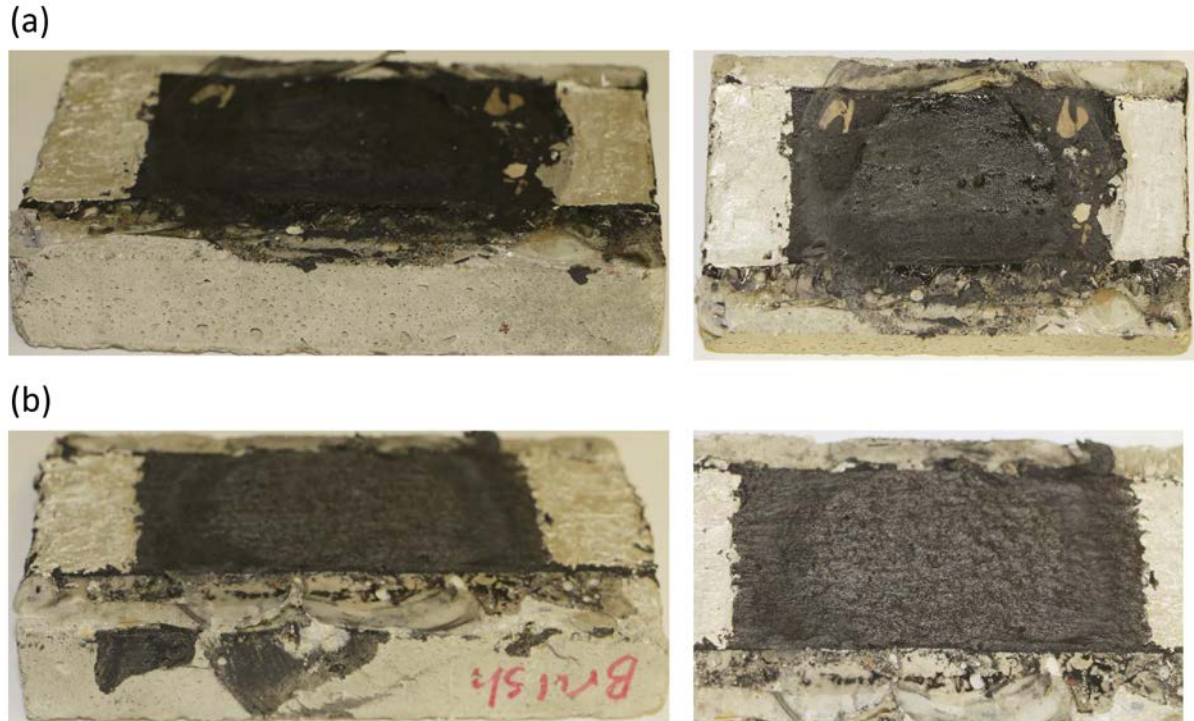


Figure 6-12. PU-CMF coatings with (a) 10%, and (b) 15% CMF dosage rates after 10,000 loading cycles.

### Conclusion

Electrically conductive composites of Polyurethane (PU) and carbon microfiber (CMF) were prepared using different volume fractions of the conductive filler (CMF) and tested for their electrical conductivity, heating capability, and durability on portland cement concrete (PCC) substrates under cyclic loaded wheel path. The electrical conductivity was evaluated in terms of percolation of microfibers within the PU matrix. Heating capability tests included investigation of the average surface temperature rise and temperature distribution over the surface area of the composite-coated specimens upon application of electric current on wood-substrate and PCC-substrate specimens. Durability of coatings on PCC-substrate was assessed in terms of coating layer's mass loss and electrical resistance change under certain cycles of loading through loaded wheel path. The main findings of the study can be summarized as the following:



- The dual percolative behavior of the CMF in PU matrix was captured in the studied range. The percolation transition zone in the 0.25% to 1% range corresponds to transition of the composite's behavior from electrical insulator to semiconductor. The composite transitioned from a semiconductor to a conductor of electricity over the CMF dosage rate range of 4-10% above which the volume conductivity did not exhibit significant improvement with the increase of CMF content.
- Increasing CMF volume fraction from 1% to 1.5% resulted in an abrupt jump in resistive heat generation. The second significant improvement of heating capability occurred at 10% CMF dosage rate. Increasing CMF content of the composite above 12.5% led to reduction of heating performance in terms of the average surface temperature rise in small wood-substrate specimens and uniformity of temperature distribution in bigger PCC-substrate specimens.
- The durability of composites continuously improved with increasing CMF volume fraction up to 20%. However, the most desirable durability properties were achieved at CMF contents higher than 10%.
- Considering all three characteristics of the coating -i.e. volume conductivity, heating capability, and durability- within the studied range of CMF volume fraction, the composites containing 12.5% CMF content exhibited more favorable properties than other coating mixtures. It can be concluded that a CMF dosage rate greater than 10% and smaller than 15% (by total volume of the composite) is likely to be the desirable range of CMF volume fraction in the PU-CMF composite studied in this research.

Regarding the desirable properties of the PU-CMF composite studied in this research, it would be timely for future studies to investigate different types of binders such as various

Polyurethane/Polyurea elastomers and Poly(methyl metacrylate) to produce more durable electrically conductive coatings for different substrates and applications. Doping PU-CMF composites with different nano- and micro-particles or fibers is a potential topic for future studies to impart additional functions, other than electrical conductivity, to this type of composites. Other applications of these composites such as sensing and electromagnetic interference shielding can be investigated in the future studies. Investigating different dispersion improvement methods to enhance the uniformity and conductivity of the PU-CMF composites is a potential topic for future works that will make a significant contribution to the existing knowledge.

### **Acknowledgements**

This paper was prepared from a study conducted at Iowa State University under Federal Aviation Administration (FAA) Air Transportation Center of Excellence Cooperative Agreement 12-C-GA-ISU for the Partnership to Enhance General Aviation Safety, Accessibility and Sustainability (PEGASAS). The authors would like to thank the current project Technical Monitor, Mr. Benjamin J. Mahaffay, and the former project Technical Monitors, Mr. Jeffrey S. Gagnon (interim), Mr. Donald Barbagallo, and Dr. Charles A. Ishee for their invaluable guidance on this study. The authors would like to express their sincere gratitude to Mr. Paul Kremer of Iowa State University, CCEE (Civil, Construction, and Environmental Engineering Department), for his extremely kind assistance with providing access to the laboratories, required trainings, and consultation in conducting the experiments. The authors immensely thank Mr. Robert F. Steffes, Iowa State University (ISU), CCEE , Portland cement concrete (PCC) Lab Manager for his significant assistance with the lab investigations. Special thanks are expressed to Zoltek for providing carbon microfiber.

Although the FAA has sponsored this project, it neither endorses nor rejects the findings of this research. The presentation of this information is in the interest of invoking comments by the technical community on the results and conclusions of the research.

### References

- [1] A. Sassani, H. Ceylan, S. Kim, K. Gopalakrishnan, A. Arabzadeh, P.C. Taylor, Factorial Study on Electrically Conductive Concrete Mix Design for Heated Pavement Systems, in: *Transp. Res. Board 96th Annu. Meet.*, Washington DC, 2017: pp. 17-05347.
- [2] A. Arabzadeh, H. Ceylan, S. Kim, K. Gopalakrishnan, A. Sassani, S. Sundararajan, P.C. Taylor, Influence of Deicing Salts on the Water-Repellency of Portland Cement Concrete Coated with Polytetrafluoroethylene and Polyetheretherketone, in: *ASCE Int. Conf. Highw. Pavements Airf. Technol.*, Philadelphia, Pennsylvania, 2017.
- [3] A. Arabzadeh, H. Ceylan, S. Kim, K. Gopalakrishnan, A. Sassani, Superhydrophobic Coatings on Asphalt Concrete Surfaces, *Transp. Res. Rec. J. Transp. Res. Board. No. 2551* (2016).
- [4] Y. Lai, Y. Liu, D. Ma, Automatically melting snow on airport cement concrete pavement with carbon fiber grille, *Cold Reg. Sci. Technol.* 103 (2014) 57–62. doi:10.1016/j.coldregions.2014.03.008.
- [5] T. Yang, Z.J. Yang, M. Singla, G. Song, Q. Li, Experimental Study on Carbon Fiber Tape-Based Deicing Technology, *J. Cold Reg. Eng.* 26 (2012) 55–70.
- [6] H. Ceylan, K. Gopalakrishnan, S. Kim, W. Cord, Heated Transportation Infrastructure Systems : Existing and Emerging Technologies, in: *Civil, Constr. Environ. Eng. Conf. Present. Proceedings.*, Iowa State University, 2014.
- [7] S. Yehia, C.Y. Tuan, Thin Conductive Concrete Overlay for Bridge Deck Deicing and Anti-Icing, *Transp. Res. Rec. J. Transp. Res. Board.* 1698 (2000) 45–53.
- [8] A. Christopher, J.E. Strong, P.A. Mosher, Effect of Deicing Salts on Metal and Organic Matter Mobilization in Roadside Soils, *Environ. Sci. Technol.* 26 (1992) 703–709. doi:10.1021/es00028a006.
- [9] M. Bäckström, S. Karlsson, L. Bäckman, L. Folkesson, B. Lind, Mobilisation of heavy metals by deicing salts in a roadside environment, *Water Res.* 38 (2004) 720–732.
- [10] M.A. Cunningham, E. Snyder, D. Yonkin, M. Ross, T. Elsen, Accumulation of deicing salts in soils in an urban environment, *Urban Ecosyst.* 11 (2008) 17–31.

- [11] D. Sanzo, S.J. Hecnar, Effects of road de-icing salt (NaCl) on larval wood frogs (*Rana sylvatica*), *Environ. Pollut.* 140 (2006) 247–256.
- [12] I. Czerniawska-Kusza, G. Kusza, M. Dużyński, Effect of deicing salts on urban soils and health status of roadside trees in the Opole Region, *Environ. Toxicol.* 19 (2004) 296–301. doi:10.1002/tox.20037.
- [13] J.R. Karraker, Nancy E., Gibbs, James P., And Vonesh, Impacts of Road Deicing Salt on the Demography of Vernal Pool-Breeding Amphibians, *Ecol. Appl.* 18 (2016) 724–734.
- [14] D.M. Ramakrishna, T. Viraraghavan, Environmental impact of chemical deicers - A review, *Water. Air. Soil Pollut.* 166 (2005) 49–63. doi:10.1007/s11270-005-8265-9.
- [15] W. Shen, H. Ceylan, K. Gopalakrishnan, S. Kim, P.C. Taylor, C.R. Rehmann, Life cycle assessment of heated apron pavement system operations, *Transp. Res. Part D Transp. Environ.* 48 (2016) 316–331. doi:10.1016/j.trd.2016.08.006.
- [16] H. Wang, C. Thakkar, X. Chen, S. Murrel, Life-cycle assessment of airport pavement design alternatives for energy and environmental impacts, *J. Clean. Prod.* 133 (2016) 163–171. doi:10.1016/j.jclepro.2016.05.090.
- [17] A. Arabzadeh, H. Ceylan, S. Kim, K. Gopalakrishnan, A. Sassani, Superhydrophobic coatings on asphalt concrete surfaces: Toward smart solutions for winter pavement maintenance, 2016. doi:10.3141/2551-02.
- [18] H. Ceylan, A. Arabzadeh, A. Sassani, S. Kim, K. Gopalakrishnan, Innovative nano-engineered asphalt concrete for ice and snow controls in pavement systems, in: 6th Eurasphalt & Eurobitume Congr., Prague, Czech Republic, 2016.
- [19] A. Arabzadeh, H. Ceylan, S. Kim, K. Gopalakrishnan, A. Sassani, S. Sundararajan, P.C. Taylor, Superhydrophobic coatings on Portland cement concrete surfaces, *Constr. Build. Mater.* 141 (2017) 393–401.
- [20] A. Arabzadeh, H. Ceylan, S. Kim, K. Gopalakrishnan, A. Sassani, Fabrication of Polytetrafluoroethylene-Coated Asphalt Concrete Biomimetic Surfaces: A Nanomaterials-Based Pavement Winter Maintenance Approach, in: *Int. Conf. Transp. Dev. 2016 Proj. Pract. Prosper. - Proc. 2016 Int. Conf. Transp. Dev.*, 2016. doi:10.1061/9780784479926.006.
- [21] C. Chang, M. Ho, G. Song, Y.-L. Mo, H. Li, A feasibility study of self-heating concrete utilizing carbon nanofiber heating elements, *Smart Mater. Struct.* 18 (2009) 127001. doi:10.1088/0964-1726/18/12/127001.
- [22] E. Heymsfield, A.B. Osweiler, R.P. Selvam, M. Kuss, Feasibility of Anti-Icing Airfield Pavements Using Conductive Concrete and Renewable Solar Energy, Fayetteville, Arkansas, 2013.

- [23] V. Piskunov, O. Volod'ko, A. Porhunov, Composite Materials for Building Heated coverings for Roads and Runways of Airdromes, *Mech. Compos. Mater.* 44 (2008) 215–220.
- [24] Z. Hou, Z. Li, J. Wang, Electrical conductivity of the carbon fiber conductive concrete, *J. Wuhan Univ. Technol. Sci. Ed.* 22 (2007) 346–349. doi:10.1007/s11595-005-2346-x.
- [25] C. Chang, M. Ho, G. Song, Y.L. Mo, H. Li, Improvement of Electrical Conductivity in Carbon Fiber-Concrete Composites using Self Consolidating Technology, in: *Earth Sp. 2010 Eng. Sci. Constr. Oper. Challenging Environ.* ASCE, 2010: pp. 3553–3558.
- [26] O. Galao, L. Bañón, F.J. Baeza, J. Carmona, P. Garcés, Highly Conductive Carbon Fiber Reinforced Concrete for Icing Prevention and Curing, *Materials (Basel)*. 9 (2016) 281. doi:10.3390/ma9040281.
- [27] J.P. Won, C.K. Kim, S.J. Lee, J.H. Lee, R.W. Kim, Thermal characteristics of a conductive cement-based composite for a snow-melting heated pavement system, *Compos. Struct.* 118 (2014) 106–111. doi:10.1016/j.compstruct.2014.07.021.
- [28] M. Sun, W. Ying, L. Bin, X. Zhang, Deicing Concrete Pavement Containing Carbon Black/Carbon Fiber Conductive Lightweight concrete Composites, in: *ICTIS 2011 Multimodal Approach to Sustain. Transp. Syst. Dev. Information, Technol. Implement.*, 2011: pp. 662–668.
- [29] W. Chen, P. Gao, Performances of Electrically Conductive Concrete with Layered Stainless Steel Fibers, *Sustain. Constr. Mater.* (2012) 163–171.
- [30] J. Wu, J. Liu, F. Yang, Three-phase composite conductive concrete for pavement deicing, *Constr. Build. Mater.* 75 (2015) 129–135. doi:10.1016/j.conbuildmat.2014.11.004.
- [31] K. Gopalakrishnan, H. Ceylan, S. Kim, S. Yang, H. Abdulla, Self-Heating Electrically Conductive Concrete for Pavement Deicing: A Revisit, in: *Transp. Res. Board 94th Annu. Meet.*, 2015: p. No. 15-4764.
- [32] J. Gomis, O. Galao, V. Gomis, E. Zornoza, P. Garcés, Self-heating and deicing conductive cement. Experimental study and modeling, *Constr. Build. Mater.* 75 (2015) 442–449. doi:10.1016/j.conbuildmat.2014.11.042.
- [33] C.Y. Tuan, *Implementation of Conductive Concrete For Deicing*, Omaha, NE, 2008.
- [34] H. Xu, D. Wang, Y. Tan, J. Zhou, M. Oeser, Investigation of design alternatives for hydronic snow melting pavement systems in China, *J. Clean. Prod.* 170 (2018) 1413–1422. doi:10.1016/j.jclepro.2017.09.262.
- [35] H. Wang, L. Liu, Z. Chen, Experimental investigation of hydronic snow melting process on the inclined pavement, *Cold Reg. Sci. Technol.* 63 (2010) 44–49.

- [36] P. Pan, S. Wu, Y. Xiao, G. Liu, A review on hydronic asphalt pavement for energy harvesting and snow melting, *Renew. Sustain. Energy Rev.* 48 (2015) 624–634. doi:10.1016/j.rser.2015.04.029.
- [37] C.Y. Tuan, Roca Spur Bridge: The Implementation of an Innovative Deicing Technology, *J. Cold Reg. Eng.* 22 (2008) 1–15. doi:10.1061/(ASCE)0887-381X(2008)22:1(1).
- [38] R. Maggenti, R. Carter, R. Meline, Development of Conductive Polyester Concrete for Bridge-Deck Cathodic Protection and Ice Control, *Transp. Res. Rec. J. Transp. Res. Board.* (1996) 61–69.
- [39] H. Abdulla, H. Ceylan, S. Kim, K. Gopalakrishnan, P.C. Taylor, Y. Turkan, System requirements for electrically conductive concrete heated pavements, *Transp. Res. Rec.* 2569 (2016) 70–79.
- [40] A. Arabzadeh, H. Ceylan, S. Kim, K. Gopalakrishnan, A. Sassani, S. Sundararajan, P.C. Taylor, Superhydrophobic coatings on Portland cement concrete surfaces, *Constr. Build. Mater.* 141 (2017). doi:10.1016/j.conbuildmat.2017.03.012.
- [41] V. Hejazi, K. Sobolev, M. Nosonovsky, From superhydrophobicity to icephobicity: forces and interaction analysis., *Sci. Rep.* 3 (2013) 2194. doi:10.1038/srep02194.
- [42] I. Flores-vivian, V. Hejazi, M.I. Kozhukhova, M. Nosonovsky, K. Sobolev, Self-Assembling Particle-Siloxane Coatings for Superhydrophobic Concrete, *ACS Appl. Mater. Interfaces.* 5 (2013) 13284–13294.
- [43] M. Nosonovsky, K. Sobolev, Superhydrophobic and icephobic concrete and construction materials, WI: University of Wisconsin–Milwaukee, 2013, 85–92.
- [44] M. Horgnies, J.J. Chen, Superhydrophobic concrete surfaces with integrated microtexture, *Cem. Concr. Compos.* 52 (2014) 81–90. doi:10.1016/j.cemconcomp.2014.05.010.
- [45] J. Orlikowski, S. Cebulski, K. Darowicki, Electrochemical investigations of conductive coatings applied as anodes in cathodic protection of reinforced concrete, *Cem. Concr. Compos.* 26 (2004) 721–728. doi:10.1016/S0958-9465(03)00105-7.
- [46] J. Xu, W. Yao, Electrochemical studies on the performance of conductive overlay material in cathodic protection of reinforced concrete, *Constr. Build. Mater.* 25 (2011) 2655–2662. doi:10.1016/j.conbuildmat.2010.12.015.
- [47] A. Cañón, P. Garcés, M.A. Climent, J. Carmona, E. Zornoza, Feasibility of electrochemical chloride extraction from structural reinforced concrete using a sprayed conductive graphite powder-cement paste as anode, *Corros. Sci.* 77 (2013) 128–134. doi:10.1016/j.corsci.2013.07.035.

- [48] M. Elsharkawy, D. Tortorella, S. Kapatral, C.M. Megaridis, Combating Frosting with Joule-Heated Liquid-Infused Superhydrophobic Coatings, *Langmuir*. 32 (2016) 4278–4288. doi:10.1021/acs.langmuir.6b00064.
- [49] P.C. Ma, N.A. Siddiqui, G. Marom, J.K. Kim, Dispersion and functionalization of carbon nanotubes for polymer-based nanocomposites: A review, *Compos. Part A Appl. Sci. Manuf.* 41 (2010) 1345–1367. doi:10.1016/j.compositesa.2010.07.003.
- [50] J.E. Mates, I.S. Bayer, J.M. Palumbo, P.J. Carroll, C.M. Megaridis, Extremely stretchable and conductive water-repellent coatings for low-cost ultra-flexible electronics, *Nat. Commun.* 6 (2015) 1–8. doi:10.1038/ncomms9874.
- [51] J.E. Mates, I.S. Bayer, M. Salerno, P.J. Carroll, Z. Jiang, L. Liu, C.M. Megaridis, Durable and flexible graphene composites based on artists' paint for conductive paper applications, *Carbon*, 87 (2015) 163–174. doi:10.1016/j.carbon.2015.01.056.
- [52] H. Chu, Z. Zhang, Y. Liu, J. Leng, Silver particles modified carbon nanotube paper/glassfiber reinforced polymer composite material for high temperature infrared stealth camouflage, *Carbon*, 98 (2016) 557–566. doi:10.1016/j.carbon.2015.11.036.
- [53] B.O. Lee, W.J. Woo, H.S. Park, H.S. Hahm, J.P. Wu, M.S. Kim, Influence of aspect ratio and skin effect on EMI shielding of coating materials fabricated with carbon nano ber/PVDF, *Carbon*, 7 (2008) 1839–1843.
- [54] L. Liu, A. Das, C.M. Megaridis, Terahertz shielding of carbon nanomaterials and their composites - A review and applications, *Carbon*, 69 (2014) 1–16. doi:10.1016/j.carbon.2013.12.021.
- [55] A. Das, H.T. Hayvaci, M.K. Tiwari, I.S. Bayer, D. Erricolo, C.M. Megaridis, Superhydrophobic and conductive carbon nanofiber/PTFE composite coatings for EMI shielding, *J. Colloid Interface Sci.* 353 (2011) 311–315. doi:10.1016/j.jcis.2010.09.017.
- [56] P. Slobodian, P. Riha, R. Benlikaya, P. Svoboda, D. Petras, A flexible multifunctional sensor based on carbon nanotube/polyurethane composite, *IEEE Sens. J.* 13 (2013) 4045–4048. doi:10.1109/JSEN.2013.2272098.
- [57] P. Slobodian, P. Riha, P. Saha, A highly-deformable composite composed of an entangled network of electrically-conductive carbon-nanotubes embedded in elastic polyurethane, *Carbon*, 50 (2012) 3446–3453. doi:10.1016/j.carbon.2012.03.008.
- [58] J.M. Engel, J. Chen, D. Bullen, C. Liu, Polyurethane rubber as a MEMS material: characterization and demonstration of an all-polymer two-axis artificial hair cell flow sensor, in: *18th IEEE Int. Conf. Micro Electro Mech. Syst.* 2005., 2005: pp. 279–282. doi:10.1109/MEMSYS.2005.1453921.

- [59] S. Laflamme, I. Pinto, H. Saleem, M. Elkashef, K. Wang, Conductive Paint-Filled Cement Paste Sensor for Accelerated Percolation, in: *Struct. Heal. Monit. Insp. Adv. Mater. Aerospace, Civ. Infrastruct.*, 2015: pp. 1–8. doi:10.1117/12.2084408.
- [60] E. Andreoli, K.S. Liao, A. Cricini, X. Zhang, R. Soffiatti, H.J. Byrne, S.A. Curran, Carbon black instead of multiwall carbon nanotubes for achieving comparable high electrical conductivities in polyurethane-based coatings, *Thin Solid Films*. 550 (2014) 558–563. doi:10.1016/j.tsf.2013.11.047.
- [61] J. Engel, J. Chen, N. Chen, S. Pandya, C. Liu, Multi-Walled Carbon Nanotube Filled Conductive Elastomers: Materials And Application to Micro Transducers, in: *IEEE MEMS*, 2006: pp. 246–249.
- [62] C.Y. Lee, J.H. Bae, T.Y. Kim, S.H. Chang, S.Y. Kim, Using silane-functionalized graphene oxides for enhancing the interfacial bonding strength of carbon/epoxy composites, *Compos. Part A Appl. Sci. Manuf.* 75 (2015) 11–17. doi:10.1016/j.compositesa.2015.04.013.
- [63] C. Su, J. Li, H. Geng, Q. Wang, Q. Chen, Fabrication of an optically transparent super-hydrophobic surface via embedding nano-silica, *Appl. Surf. Sci.* 253 (2006) 2633–2636. doi:10.1016/j.apsusc.2006.05.038.
- [64] M.K. Tiwari, I.S. Bayer, G.M. Jursich, T.M. Schutzius, C.M. Megaridis, Highly liquid-repellent, large-area, nanostructured poly(vinylidene fluoride)/poly(ethyl 2-cyanoacrylate) composite coatings: Particle filler effects, *ACS Appl. Mater. Interfaces*. 2 (2010) 1114–1119. doi:10.1021/am900894n.
- [65] I.S. Bayer, M.K. Tiwari, C.M. Megaridis, Biocompatible poly(vinylidene fluoride)/cyanoacrylate composite coatings with tunable hydrophobicity and bonding strength, *Appl. Phys. Lett.* 93 (2008) 1–4. doi:10.1063/1.3009292.
- [66] N. Vourdas, A. Tserepi, E. Gogolides, Nanotextured super-hydrophobic transparent poly(methyl methacrylate) surfaces using high-density plasma processing, *Nanotechnology*. 18 (2007) 125304. doi:10.1088/0957-4484/18/12/125304.
- [67] J. Lin, J. Zhu, D.R. Swanson, L. Milco, Cross-Linking and Physical Characteristics of a Water-Based Nonstick Hydrophobic Coating, *Langmuir*. 7463 (1996) 6676–6680.
- [68] L.D. Poulidakos, C. Papadaskalopoulou, B. Hofko, F. Gschösser, A. Cannone Falchetto, M. Bueno, M. Arraigada, J. Sousa, R. Ruiz, C. Petit, M. Loizidou, M.N. Partl, Harvesting the unexplored potential of European waste materials for road construction, *Resour. Conserv. Recycl.* 116 (2017) 32–44. doi:10.1016/j.resconrec.2016.09.008.



- [69] C. Gao, Y.Z. Jin, H. Kong, R.L.D. Whitby, S.F. Acquah, G.Y. Chen, H. Qian, A. Hartschuh, S.R.P. Silva, S. Henley, P. Fearon, H.W. Kroto, D.R.M. Walton, Polyurea-functionalized multiwalled carbon nanotubes: synthesis, morphology, and Raman spectroscopy., *J. Phys. Chem. B.* 109 (2005) 11925–32. doi:10.1021/jp051642h.
- [70] H.C. Kuan, C.C.M. Ma, W.P. Chang, S.M. Yuen, H.H. Wu, T.M. Lee, Synthesis, thermal, mechanical and rheological properties of multiwall carbon nanotube/waterborne polyurethane nanocomposite, *Compos. Sci. Technol.* 65 (2005) 1703–1710. doi:10.1016/j.compscitech.2005.02.017.
- [71] S. Rana, N. Karak, J.W. Cho, Y.H. Kim, Enhanced dispersion of carbon nanotubes in hyperbranched polyurethane and properties of nanocomposites, *Nanotechnology.* 19 (2008). doi:10.1088/0957-4484/19/49/495707.
- [72] J. Ryszkowska, M. Jurczyk-Kowalska, T. Szyborski, K.J. Kurzydłowski, Dispersion of carbon nanotubes in polyurethane matrix, *Phys. E Low-Dimensional Syst. Nanostructures.* 39 (2007) 124–127. doi:10.1016/j.physe.2007.02.003.
- [73] D.K. Chattopadhyay, K.V.S.N. Raju, Structural engineering of polyurethane coatings for high performance applications, *Prog. Polym. Sci.* 32 (2007) 352–418. doi:10.1016/j.progpolymsci.2006.05.003.
- [74] K. Golovin, M. Boban, J.M. Mabry, A. Tuteja, Designing Self-Healing Superhydrophobic Surfaces with Exceptional Mechanical Durability, *ACS Appl. Mater. Interfaces.* 9 (2017) 11212–11223. doi:10.1021/acsami.6b15491.
- [75] M.H. Irfan, Polyurethanes in the construction industry, in: *Chem. Technol. Thermosetting Polym. Constr. Appl.*, 1998: pp. 123–144.
- [76] P. Duarte, J.R. Correia, J.G. Ferreira, F. Nunes, M.R.T. Arruda, Experimental and numerical study on the effect of repairing reinforced concrete cracked beams strengthened with carbon fibre reinforced polymer laminates, *Can. J. Civ. Eng.* 41 (2014) 222–231. doi:10.1139/cjce-2013-0124.
- [77] A. Sassani, H. Ceylan, S. Kim, A. Arabzadeh, P.C. Taylor, K. Gopalakrishnan, Development of Carbon Fiber-modified Electrically Conductive Concrete for Implementation in Des Moines International Airport, *Case Stud. Constr. Mater.* 8 (2018) 277–291. doi:10.1016/j.cscm.2018.02.003.
- [78] J.M.L. Reis, R.P. Lima, S.D. Vidal, Effect of rate and temperature on the mechanical properties of epoxy BADGE reinforced with carbon nanotubes, *Compos. Struct.* (2018) 0–1. doi:10.1016/j.compstruct.2017.11.081.
- [79] G.M. Kim, B.J. Yang, G.U. Ryu, H.K. Lee, The electrically conductive carbon nanotube (CNT)/cement composites for accelerated curing and thermal cracking reduction, *Compos. Struct.* 158 (2016) 20–29. doi:10.1016/j.compstruct.2016.09.014.

- [80] G.M. Kim, B.J. Yang, K.J. Cho, E.M. Kim, H.K. Lee, Influences of CNT dispersion and pore characteristics on the electrical performance of cementitious composites, *Compos. Struct.* 164 (2017) 32–42. doi:10.1016/j.compstruct.2016.12.049.
- [81] G.M. Kim, F. Naeem, H.K. Kim, H.K. Lee, Heating and heat-dependent mechanical characteristics of CNT-embedded cementitious composites, *Compos. Struct.* 136 (2016) 162–170. doi:10.1016/j.compstruct.2015.10.010.
- [82] R.N. Howser, H.B. Dhonde, Y.L. Mo, Self-sensing of carbon nanofiber concrete columns subjected to reversed cyclic loading, *Smart Mater. Struct.* 20 (2011). doi:10.1088/0964-1726/20/8/085031.
- [83] Y. He, L. Lu, S. Jin, S. Hu, Conductive aggregate prepared using graphite and clay and its use in conductive mortar, *Constr. Build. Mater.* 53 (2014) 131–137. doi:10.1016/j.conbuildmat.2013.11.085.
- [84] J.M. Balbus, A.D. Maynard, V.L. Colvin, V. Castranova, G.P. Daston, R.A. Denison, K.L. Dreher, P.L. Goering, A.M. Goldberg, K.M. Kulinowski, N.A. Monteiro-Riviere, G. Oberdörster, G.S. Omenn, K.E. Pinkerton, K.S. Ramos, K.M. Rest, J.B. Sass, E.K. Silbergeld, B.A. Wong, Meeting report: Hazard assessment for nanoparticles-report from an interdisciplinary workshop, *Environ. Health Perspect.* 115 (2007) 1654–1659. doi:10.1289/ehp.10327.
- [85] X. Gong, L. Liu, Y. Liu, J. Leng, An electrical-heating and self-sensing shape memory polymer composite incorporated with carbon fiber felt, *Smart Mater. Struct.* 25 (2016). doi:10.1088/0964-1726/25/3/035036.
- [86] A. Ameli, P.U. Jung, C.B. Park, Electrical properties and electromagnetic interference shielding effectiveness of polypropylene/carbon fiber composite foams, *Carbon*, 60 (2013) 379–391. doi:10.1016/j.carbon.2013.04.050.
- [87] D.D. Chung, Dispersion of Short Fibers in Cement, *J. Mater. Civ. Eng.* 17 (2005) 379–383. doi:10.1061/(ASCE)0899-1561(2005)17:4(379).
- [88] J. Xiong, Z. Zheng, X. Qin, M. Li, H. Li, X. Wang, The thermal and mechanical properties of a polyurethane/multi-walled carbon nanotube composite, *Carbon*, 44 (2006) 2701–2707. doi:10.1016/j.carbon.2006.04.005.
- [89] S. Haseebuddin, K.V.S.N. Raju, D. Krishna, P.J. Reddy, M. Yaseen, Temperature dependence of viscosity of polyurethane polyol solutions: Application of rheological models, *J. Appl. Polym. Sci.* 59 (1996) 29–36. doi:10.1002/(SICI)1097-4628(19960103)59:1<29::AID-APP5>3.0.CO;2-O.
- [90] S. Velankar, S.L. Cooper, Microphase separation and rheological properties of polyurethane melts. 3. Effect of block incompatibility on the viscoelastic properties, *Macromolecules*. 33 (2000) 395–403. doi:10.1021/ma9908189.

- [91] S. Wu, L. Mo, Z. Shui, Z. Chen, Investigation of the conductivity of asphalt concrete containing conductive fillers, *Carbon*, 43 (2005) 1358–1363. doi:10.1016/j.carbon.2004.12.033.
- [92] P. Cong, P. Xu, S. Chen, Effects of carbon black on the anti aging, rheological and conductive properties of SBS/asphalt/carbon black composites, *Constr. Build. Mater.* 52 (2014) 306–313. doi:10.1016/j.conbuildmat.2013.11.061.
- [93] A. Sassani, H. Ceylan, S. Kim, K. Gopalakrishnan, A. Arabzadeh, P.C. Taylor, Influence of mix design variables on engineering properties of carbon fiber-modified electrically conductive concrete, *Constr. Build. Mater.* 152 (2017) 168–181. doi:10.1016/j.conbuildmat.2017.06.172.
- [94] S. Wen, D.D.L. Chung, The role of electronic and ionic conduction in the electrical conductivity of carbon fiber reinforced cement, *Carbon*, 44 (2006) 2130–2138. doi:10.1016/j.carbon.2006.03.013.
- [95] N. Hawkins, O. Smadi, S. Knickerbocker, A. Pike, P. Carlson, EVALUATING ALL-WEATHER PAVEMENT MARKINGS IN ILLINOIS : VOLUME 1, Research Report No. FHWA-ICT-15-018, Ames, Iowa, USA, 2015.
- [96] C.C. Chen, Y.C. Chou, Electrical-conductivity fluctuations near the percolation threshold, *Phys. Rev. Lett.* 54 (1985) 2529–2532.
- [97] G. Wu, J. Lin, Q. Zheng, M. Zhang, Correlation between percolation behavior of electricity and viscoelasticity for graphite filled high density polyethylene, *Polymer (Guildf)*. 47 (2006) 2442–2447. doi:10.1016/j.polymer.2006.02.017.
- [98] W.L. Song, M.S. Cao, M.M. Lu, J. Liu, J. Yuan, L.Z. Fan, Improved dielectric properties and highly efficient and broadened bandwidth electromagnetic attenuation of thickness-decreased carbon nanosheet/wax composites, *J. Mater. Chem. C*. 1 (2013) 1846–1854. doi:10.1039/c2tc00494a.
- [99] Y. Chekanov, R. Ohnogi, S. Asai, M. Sumita, Positive Temperature Coefficient Effect of Epoxy Resin Filled with Short Carbon Fibers, *Polym. J.* 30 (1998) 381–387. doi:10.1295/polymj.30.381.
- [100] S. Paschen, M.N. Bussac, L. Zuppiroli, E. Minder, B. Hilti, Tunnel junctions in a polymer composite, *J. Appl. Phys.* 78 (1995) 3230–3237. doi:10.1063/1.360012.
- [101] W.S. Bao, S.A. Meguid, Z.H. Zhu, G.J. Weng, Tunneling resistance and its effect on the electrical conductivity of carbon nanotube nanocomposites, *J. Appl. Phys.* 111 (2012). doi:10.1063/1.4716010.

## CHAPTER 7. CONCLUSIONS AND RECOMMENDATIONS FOR FUTURE WORK

### Summary

This study investigated the feasibility of utilizing smart materials in electrically heated pavement systems (EHPS). To this end, two general types of materials were studied: (1) portland cement-based electrically conductive concrete (ECON), and (2) polymer-based electrically conductive coating (ECOT). The focus of the study was on ECON and ECOT made with different types of carbon fibers at micrometer and millimeter scales.

The ECON portion of the study began with identifying important factors that influence the properties of carbon fiber-modified portland cement concrete. At this stage, the existing literature was surveyed to seek information on the effect of these different factors; experimental plans were pursued to cover gaps in the literature. Based on the results of initial investigations, ECON mix designs were prepared and tested at laboratory-scale to evaluate their performance when used in EHPS. After the laboratory evaluations, a real-size test section was built and tested under various levels of precipitation and freezing weather conditions at the Des Moines International airport.

Electrically conductive coating (ECOT) was studied by introducing a new combination of materials - Polyurethane doped with carbon microfiber (CMF) - for application as an electrically heated coating on Portland cement concrete surfaces. Both this material combination and the application represent, to the best of author's knowledge, novel and unprecedented approaches in the field of construction materials; the PU-CMF composite coating for any purpose has not in fact been studied for application in any other discipline. The CMF dosage rates required to achieve desirable volume conductivity, electrical heating capability, and durability in the PU-CMF composite were experimentally determined, and the

PU-CMF composite-coated Portland cement concrete electrically heated pavement was developed in proof-of-concept level.

The research presented in this dissertation has led to multiple novel findings and innovations. At each step of this study, a new finding, a new product, or a new application of a material/method has been provided. Among the main contributions of this research are:

- Finding the feasibility of using calcium nitrite solution as a conductivity-enhancing admixture in Portland cement concrete (PCC).
- Discovering age dependence of the carbon fiber percolation threshold in the PCC matrix.
- Providing a multi-composite determination of the percolation threshold of carbon fiber in the PCC matrix.
- Investigating age-dependent behavior of ECON and its performance as an electrically heated pavement system.
- Studying correlation between the properties of ECON produced at laboratory scale and at large (concrete plant) scale.
- Large-scale production of carbon fiber-modified ECON and implementation of the first ECON HPS at a U.S. Airport (probably the first in the world).
- Producing electrically conductive Polyurethane-carbon-microfiber (PU-CMF) composite coating and its application for joule heating on PCC surfaces.

## Conclusions

The major findings and conclusions corresponding to each objective of this study are:

### Identification of significant Mix Design Variables Influencing the Properties of ECON

The effects of easy-to-change mix design variables on electrical and mechanical properties of ECON related to optimized use of materials in production of ECON to achieve higher functionality, higher constructability, and lower production cost in full-scale and industrial application of ECON HPS were investigated and discussed. Influential variables were identified based on existing literature where possible and ,to fill gaps in the literature, with experimental investigation. The study was conducted using 7.2 $\mu$ m-diameter carbon fibers with different lengths as electrically conductive additive (ECA). The major conclusions obtained from this portion of the research can be summarized as:

- A calcium nitrite-based corrosion inhibitor admixture was successfully used as conductivity-enhancing agent (CEA) for improving the electrical conductivity of ECON. However, statistical analyses showed that CEA was effective in conductivity improvement only up to a fiber dosage rate of 0.87% (Vol.). CEA improved electrical conductivity and compressive strength, especially at low fiber contents. Although CEA somewhat improved flexural strength, the effect was not significant.
- The significance level of variables, in terms of asymptotic significance (P-value), varied by hydration time (age), becoming nearly steady after 7 days. It is recommended that 28-day or later age measurements be used for analyses.
- Four significant variables affecting electrical resistivity -ordered from most to least significant with respect to P-value- were fiber content, coarse-to-fine aggregate volume ratio (C/F), fiber length, and conductivity-enhancing agent (CEA) dosage.

- Compressive strength was significantly influenced by fiber content, CEA dosage, and fiber-dispersive agent (FDA) dosage.
- Two variables, C/F and FDA dosage, exhibited significant effects on flexural strength.
- Interactions between different variables resulted in coupled effects (two-way interaction) on responses.
- In addition to main effects and coupled effects of variables, ECON mix design account for practical and implementation consideration.
- Although using 12mm-long fiber (nominal aspect ratio of 1666) resulted in positive effects on the responses, the effect was only moderate relative to electrical resistivity and non-significant for strength properties, so with respect to mixing and implementation considerations 6mm-long fiber (nominal aspect ratio of 833) is recommended for ECON production.

### **The Laboratory-scale Prototype EHPS Using Carbon Fiber-Modified ECON**

The findings of the previous step were used for optimizing ECON mix design, determine optimum carbon fiber dosage rates (using the same carbon fiber types as mentioned in the previous section), and evaluating properties and ice/snow melting performance of ECON HPS at laboratory scale through a quasi long-term study. The main findings of this step are as follows:

- Measurement of the variation of electrical conductivity with fiber content in different types of cementitious composites (paste, mortar, and concrete) showed that percolation transition occurred when fiber volume dosage was between 0.25% and 1% in paste, 0.6% and 1% in mortar, and 0.5% and 0.75% in concrete.

- Electrical conductivity of ECON decreases dramatically with age up to 150 days; the rate diminishes after 150 days and becomes almost stabilized at later ages.
- Study of the effect of carbon fiber dosage on electrical conductivity of cementitious composites showed that the optimum carbon fiber volume fraction with respect to avoiding excessive fiber consumption is equal to the upper limit of the percolation transition zone. However, based on the results of quasi long-term performance evaluation of ECON HPS, using carbon fibers in a dosage rate equal to this optimum volume fraction may be insufficient in ensuring that energy consumption remains below the specification limits throughout the entire service life.
- The finite element model (FE) was found to be a viable means of evaluating the ECON HPS system design and configurations, i.e., the predicted results were similar to the experimental results. Both the FE model and the experimental results demonstrated acceptably uniform heat distribution at the slab surface.
- Energy conversion efficiency diminished from 66% at 28 days of age to 50% at 460 days. At both ages the prototype ECON heated pavement system acceptably met the power density demand for snow melting.
- Since a considerable heat flux was observed from the ECON layer toward the underlying PCC layer, an insulated ECON-PCC interface or use of PCC with low thermal conductivity (e.g. light weight concrete) is recommended to improve energy consumption efficiency.



### **Developing Carbon Fiber-modified ECON for Application in a Full-scale ECON HPS Test Section at the Des Moines International Airport**

The design and production process of an airport ECON HPS implementation was described and reported in this step. Different ECON mixtures using carbon fiber (7.2 $\mu$ m diameter and 6mm length) were prepared in the laboratory and evaluated to determine the best mix design for field implementation. The final product, produced in a concrete plant and used for constructing the test section, was compared with the laboratory samples and tested with respect to its anti-icing and de-icing performance. The key points of the study are:

- Adequacy of cementitious paste content should be maintained in a carbon fiber-reinforced ECON mix design to ensure sufficient workability.
- Replacement of portland cement with fly ash and slag cement results in higher electrical resistivity, although not providing workability advantages.
- A significant difference was observed with respect to electrical resistivity and slump between laboratory-prepared and field samples, with field samples showing electrical resistivity almost eight times higher than that of the lab samples at a 90-day age. This can be attributed to lower carbon fiber content and higher void content of the ECON prepared at large scale.
- Lower carbon fiber content in the field ECON was caused by loss of carbon fibers during mixing and fiber degradation due to excessive wear caused by aggregates.
- The highest temperature was achieved at the bottom of the ECON layer at the slab mid-span.
- Heat flux between the ECON layer and underlying PCC layer was inconsiderable.
- Heat convection at the slabs' surface is a crucial factor with respect to effective temperature on slab surface.

- The lowest temperature was observed at the slab corners in contact with adjacent regular concrete slabs.
- Electrical resistivity of the ECON layer was significantly decreased at higher temperature.
- The test section was able to generate a power density of 300-350 W/m<sup>2</sup> and effectively melt ice/snow with this amount of energy.

### **Developing a Polymer-based Electrically Conductive Coating (ECOT)**

Electrically conductive composites of Polyurethane (PU) and carbon microfiber (CMF) were prepared using different volume fractions of conductive filler (CMF) and tested for their electrical conductivity, heating capability, and durability on portland cement concrete (PCC) substrates under a loaded cyclic wheel path. The main findings of this portion of the study can be summarized as:

- The dual percolative behavior of the CMF in PU matrix was captured for the range studied. The percolation transition zone in the 0.25% to 1% range corresponds to transition of the composite's behavior from an electrical insulator to a semiconductor. The composite transitioned from a semiconductor to a conductor of electricity over a CMF dosage rate range of 4-10%, above which the volume conductivity did not exhibit significant improvement with an increase of CMF content.
- Increasing CMF volume fraction from 1% to 1.5% resulted in an abrupt jump in resistive heat generation. The second significant improvement of heating capability occurred at a 10% CMF dosage rate. Increasing CMF content of the composite above 12.5% resulted in reduction of heating performance in terms of the average surface

temperature rise in small wood-substrate specimens and uniformity of temperature distribution in larger PCC-substrate specimens.

- The durability of composites was continuously improved by increasing CMF volume fraction up to 20%. However, the most desirable durability properties were achieved at CMF contents greater than 10%.
- Considering all three characteristics of the coating: volume conductivity, heating capability, and durability, within the studied range of CMF volume fraction, the composites containing 12.5% CMF content exhibited more favorable properties than other coating mixtures. It can be concluded that a CMF dosage rate greater than 10% and smaller than 15% (by total volume of the composite) is likely to represent the most desirable range of CMF volume fraction in the PU-CMF composite studied in this research.

### **Recommendations for Future Studies**

#### **Recommendations for Studies Related to ECON**

Future studies can use the results of this study to develop an experimental plan for investigating the discussed effects with more levels of the significant variables, potentially leading to more reliable and more inclusive mathematical models for prediction of the behavior of ECON as a function of its mixture components and mixing proportions. The electrical characteristics of ECON as a function of environmental conditions can also be the subject of future studies.

A variety of admixtures and electrically conductive materials for improvement of electrical conductivity of ECON still need to be evaluated. Developing three-phase electrically conductive composites could lead to a viable method to be integrated with the

methods proposed in this study to expand the functionality of ECON beyond the levels so far achieved.

Future studies could also consider the application of recycled carbon fibers to make the production of ECON more attractive both environmentally and economically. Life cycle assessment (LCA) analyses to investigate the carbon footprint of the ECON HPS under various combinations of production and operation scenarios is also recommended. Such analyses could compare ECON HPS with hydronic systems and traditional pavement deicing methods or compare the recycled fiber-based ECON with virgin fiber-based ECON. Furthermore, optimum scenarios for production and application of each deicing method could be identified by LCA analyses.

### **Recommendations for Studies Related to ECOT**

Regarding the desirable properties of the PU-CMF composite studied in this research, it would be timely for future studies to investigate different types of binders such as various Polyurethane/Polyurea elastomers and Poly(methyl metacrylate) to produce more durable electrically conductive coatings for different substrates and applications. Doping PU-CMF composites with different nano- and micro-particles or fibers is another potential topic for future studies to impart functions other than electrical conductivity to this type of composites. Other attributes of these composites such as sensing and electromagnetic interference shielding can be investigated in future studies. Investigating different dispersion improvement methods to enhance uniformity and conductivity of PU-CMF composites is another potential topic for future work that could make a significant contribution to existing knowledge.

## REFERENCES

- [1] M.D. Joerger, F.C. Martinez, Electrical Heating of I-84 in Land Canyon, Oregon. Report No. FHWA-OR-RD06-17, Salem, OR, USA, 2006.
- [2] J.A. Zenewitz, Survey of alternatives to the use of chlorides for highway deicing, Report number FHWA-RD-77-52, 1977.
- [3] Y. Lai, Y. Liu, D. Ma, Automatically melting snow on airport cement concrete pavement with carbon fiber grille, *Cold Reg. Sci. Technol.* 103 (2014) 57–62. doi:10.1016/j.coldregions.2014.03.008.
- [4] H. Abdulla, H. Ceylan, S. Kim, K. Gopalakrishnan, P.C. Taylor, Y. Turkan, System requirements for electrically conductive concrete heated pavements, *Transp. Res. Rec. J. Transp. Res. Board.* No. 2569 (2016) 70–79.
- [5] S. Wen, D.D.L. Chung, Seebeck effect in steel fiber reinforced cement, *Cem. Concr. Res.* 30 (2000) 661–664.
- [6] N. Banthia, S. Djeridane, M. Pigeon, Electrical resistivity of carbon and steel micro-fiber reinforced cements, *Cem. Concr. Res.* 22 (1992) 804–814. doi:10.1017/CBO9781107415324.004.
- [7] S. Wen, D.D.L. Chung, Origin of the thermoelectric behavior of steel fiber cement paste, *Cem. Concr. Res.* 32 (2002) 821–823.
- [8] S. Yehia, C.Y. Tuan, Bridge Deck Deicing, in: *Transp. Conf. Proc.*, 1998: pp. 51–57.
- [9] C. Chang, M. Ho, G. Song, Y.-L. Mo, H. Li, A feasibility study of self-heating concrete utilizing carbon nanofiber heating elements, *Smart Mater. Struct.* 18 (2009) 127001. doi:10.1088/0964-1726/18/12/127001.
- [10] C.Y. Tuan, L. Nguyen, B. Chen, Conductive concrete for heating and electrical safety, WO2010059169A1, 2010.
- [11] R. McCormack, Method of making concrete electrically conductive for electromagnetic shielding purposes, US Pat. 5,346,547. (1994). <https://www.google.com/patents/US5346547> (accessed August 2, 2015).
- [12] P.J. Tumidajski, P. Xie, M. Arnott, J.J. Beaudoin, Overlay current in a conductive concrete snow melting system, *Cem. Concr. Compos.* 33 (2003) 1807–1809. doi:10.1016/S0008-8846(03)00198-4.
- [13] S. Yehia, C.Y. Tuan, D. Ferdon, B. Chen, Conductive concrete overlay for bridge deck deicing: mixture proportioning, optimization, and properties, *ACI Mater. J.* 97 (2000) 172–181.

- [14] B. Chen, K. Wu, W. Yao, Conductivity of carbon fiber reinforced cement-based composites, *Cem. Concr. Compos.* 26 (2004) 291–297. doi:10.1016/S0958-9465(02)00138-5.
- [15] S. Yehia, C.Y. Tuan, Thin Conductive Concrete Overlay for Bridge Deck Deicing and Anti-Icing, *Transp. Res. Rec. J. Transp. Res. Board.* 1698 (2000) 45–53.
- [16] X. Gong, L. Liu, Y. Liu, J. Leng, An electrical-heating and self-sensing shape memory polymer composite incorporated with carbon fiber felt, *Smart Mater. Struct.* 25 (2016). doi:10.1088/0964-1726/25/3/035036.
- [17] T. Atkins, M. Escudier, *Smart materials, A Dict. Mech. Eng.* (2013).
- [18] G. Akhras, *Smart Materials and Smart Systems for the Future, Can. Mil. J.* (2000) 25–32.
- [19] Z. SUROWIAK, *Piezoelectronic Materials on the Basis of Ferroelectric Ceramics, Mol. Quantum Acoust.* 27 (2006) 265.
- [20] C. Miclea, C. Tanasoiu, C.F. Miclea, V. Tanasoiu, Advanced electroceramic materials for electrotechnical applications, *J. Optoelectron. Adv. Mater.* 4 (2002) 51–58.
- [21] D. Talbot, *IOM3 booklet of Smart Materials, Institute of Materials, Minerals and Mining, 2003.*
- [22] M. Addington, D.L. Schodek, *Smart Materials and Technologies. For the Architecture and Design Professions, first, Elsevier, 2005.*
- [23] J. Lepart, M. Debussche, *Human Impact on Landscape Patterning: Mediterranean Examples, in: A.J. Hansen, F. di Castri (Eds.), Landsc. Boundaries. Ecol. Stud. (Analysis Synth., New York, NY, 1992: pp. 76–106.*
- [24] R.E. Hall, B. Bowerman, J. Braverman, J. Taylor, H. Todosow, *The vision of a smart city, in: 2nd Int. Life Ext. Technol. Work., Paris, France, 2000. doi:10.1017/CBO9781107415324.004.*
- [25] G. Song, V. Sethi, H.N. Li, *Vibration control of civil structures using piezoceramic smart materials: A review, Eng. Struct.* 28 (2006) 1513–1524. doi:10.1016/j.engstruct.2006.02.002.
- [26] M. Hambach, H. Moller, T. Neumann, D. Volkmer, *Carbon fibre reinforced cement-based composites as smart floor heating materials, Compos. Part B Eng.* 90 (2016) 465–470. doi:10.1016/j.compositesb.2016.01.043.
- [27] P.-W. Chen, D.D.L. Chung, *Carbon fiber reinforced concrete for smart structures capable of non-destructive flaw detection, Smart Mater. Struct.* 2 (1993) 22–30.

- [28] M.S. Konsta-Gdoutos, C.A. Aza, Self sensing carbon nanotube (CNT) and nanofiber (CNF) cementitious composites for real time damage assessment in smart structures, *Cem. Concr. Compos.* 53 (2014) 162–169. doi:10.1016/j.cemconcomp.2014.07.003.
- [29] G.M. Kim, B.J. Yang, G.U. Ryu, H.K. Lee, The electrically conductive carbon nanotube (CNT)/cement composites for accelerated curing and thermal cracking reduction, *Compos. Struct.* 158 (2016) 20–29. doi:10.1016/j.compstruct.2016.09.014.
- [30] T. Mu, L. Liu, X. Lan, Y. Liu, J. Leng, Shape memory polymers for composites, *Compos. Sci. Technol.* 160 (2018) 169–198. doi:10.1016/j.compscitech.2018.03.018.
- [31] P.-W. Chen, D.D.L. Chung, Concrete as a new strain/stress sensor, *Compos. Part B Eng.* 27B (1996) 11–23.
- [32] P. Slobodian, P. Riha, R. Benlikaya, P. Svoboda, D. Petras, A flexible multifunctional sensor based on carbon nanotube/polyurethane composite, *IEEE Sens. J.* 13 (2013) 4045–4048. doi:10.1109/JSEN.2013.2272098.
- [33] I. Kang, Y.Y. Heung, J.H. Kim, J.W. Lee, R. Gollapudi, S. Subramaniam, S. Narasimhadevara, D. Hurd, G.R. Kirikera, V. Shanov, M.J. Schulz, D. Shi, J. Boerio, S. Mall, M. Ruggles-Wren, Introduction to carbon nanotube and nanofiber smart materials, *Compos. Part B Eng.* 37 (2006) 382–394. doi:10.1016/j.compositesb.2006.02.011.
- [34] D.D.L. Chung, Cement reinforced with short carbon fibers : a multifunctional material, *Compos. Part B Eng.* 31 (2000) 511–526.
- [35] C. Chang, G. Song, D. Gao, Y.L. Mo, Temperature and mixing effects on electrical resistivity of carbon fiber enhanced concrete, *Smart Mater. Struct.* 22 (2013) 035021. doi:10.1088/0964-1726/22/3/035021.
- [36] S. Wen, D.D.L. Chung, A Comparative Study of Steel- and Carbon-Fiber Cement as Piezoresistive Strain Sensors, *Adv. Cem. Res.* 15 (2003) 119–128.
- [37] S. Wen, D.D.L. Chung, Carbon fiber-reinforced cement as a thermistor, *Cem. Concr. Res.* 29 (1999) 961–965. doi:10.1016/S0008-8846(99)00075-7.
- [38] S. Wen, D.D.L. Chung, Seebeck effect in carbon fiber-reinforced cement, *Cem. Concr. Res.* 29 (1999) 1989–1993. doi:10.1016/S0008-8846(99)00185-4.
- [39] S. Wen, D.D.L. Chung, Effect of carbon fiber grade on the electrical behavior of carbon fiber reinforced cement, *Carbon N. Y.* 39 (2001) 369–373. doi:10.1016/S0008-6223(00)00127-5.
- [40] A. Ameli, P.U. Jung, C.B. Park, Electrical properties and electromagnetic interference shielding effectiveness of polypropylene/carbon fiber composite foams, *Carbon N. Y.* 60 (2013) 379–391. doi:10.1016/j.carbon.2013.04.050.

- [41] A. Das, T.M. Schutzius, I.S. Bayer, C.M. Megaridis, Superoleophobic and conductive carbon nanofiber/fluoropolymer composite films, *Carbon N. Y.* 50 (2012) 1346–1354. doi:10.1016/j.carbon.2011.11.006.
- [42] J. Gomis, O. Galao, V. Gomis, E. Zornoza, P. Garcés, Self-heating and deicing conductive cement. Experimental study and modeling, *Constr. Build. Mater.* 75 (2015) 442–449. doi:10.1016/j.conbuildmat.2014.11.042.
- [43] M. Ho, Y. Mo, G. Song, C. Chang, Design of a conductive self-heating concrete system, Report REU 2009 – UH CIVE, Houston, Texas, 2009.
- [44] H.-M. Zhao, S.-G. Wang, Z.-M. Wu, G.-J. Che, Concrete Slab Installed with Carbon Fiber Heating Wire for Bridge Deck Deicing, *J. Transp. Eng.* 136 (2010) 500–509. doi:10.1061/(ASCE)TE.1943-5436.0000117.
- [45] C.Y. Tuan, *Concrete Technology Today: Conductive Concrete for Bridge Deck Deicing*, 1 (2004). <http://www.cement.org/for-concrete-books-learning/concrete-technology/concrete-construction/conductive-concrete> (accessed January 1, 2015).
- [46] D.D. Chung, Self-heating structural materials, *Smart Mater. Struct.* 13 (2004) 562–565. doi:10.1088/0964-1726/13/3/015.
- [47] X. Yu, E. Kwon, Carbon Nanotube Based Self-sensing Concrete for Pavement Structural Health Monitoring, Research report–Contract Number: US DOT: DTFH61-10-C-00011, Duluth, Minnesota, 2012. <http://ntl.bts.gov/lib/45000/45000/45066/3789.pdf>.
- [48] R.N. Howser, H.B. Dhonde, Y.L. Mo, Self-sensing of carbon nanofiber concrete columns subjected to reversed cyclic loading, *Smart Mater. Struct.* 20 (2011). doi:10.1088/0964-1726/20/8/085031.
- [49] S. Mingqing, L. Zhuoqiu, M. Qizhao, S. Darong, A study on thermal self-monitoring of carbon fiber reinforced concrete, *Cem. Concr. Res.* 29 (1999) 769–771.
- [50] S. When, D. Chung, Electromagnetic interference shielding reaching 70 dB in steel fiber cement, *Cem. Concr. Res.* 34 (2004) 329–332. doi:10.1016/j.cemconres.2003.08.014.
- [51] M.F.L. De Volder, S.H. Tawfick, R.H. Baughman, a J. Hart, Carbon nanotubes: present and future commercial applications., *Science*. 339 (2013) 535–9. doi:10.1126/science.1222453.
- [52] M.C. Forde, J. McCarter, H.W. Whittington, The conduction of electricity through concrete, *Mag. Concr. Res.* 33 (1981) 48–60. doi:10.1680/macr.1981.33.114.48.
- [53] R. Spragg, C. Villani, K. Snyder, D. Bentz, J.W. Bullard, J. Weiss, Factors That Influence Electrical Resistivity Measurements in Cementitious Systems, *Transp. Res. Rec. J. Transp. Res. Board.* (2013) 90–98. doi:10.3141/2342-11.



- [54] B.W. Ramme, J.J. Noegel, R.H.J. Setchell, R.F. Bischke, *Electrically Conductive Concrete and Controlled Low-Strength Materials*, 2002. doi:10.1016/j.(73).
- [55] H.F.W. Taylor, *Cement chemistry*, second, Thomas Telford Publishing, London, 1997.
- [56] P. Mehta, P. Monteiro, *Concrete: microstructure, properties, and materials*, third, McGraw-Hill, New York, 2006.
- [57] Final report of RILEM TC 205-DSC: durability of self-compacting concrete, *Mater. Struct.* 41 (2008) 225–233.
- [58] W. Lopez, J. Gonzalez, Influence of the degree of pore saturation on the resistivity of concrete and the corrosion rate of steel reinforcement, *Cem. Concr. Res.* (1993).
- [59] K. Snyder, X. Feng, B. Keen, T. Mason, Estimating the electrical conductivity of cement paste pore solutions from OH<sup>-</sup>, K<sup>+</sup> and Na<sup>+</sup> concentrations, *Cem. Concr. Res.* 33 (2003) 793–798.
- [60] E. Garboczi, D. Bentz, Modelling of the microstructure and transport properties of concrete, *Constr. Build. Mater.* 10 (1996) 293–300.
- [61] C.Y. Tuan, S. Yehia, Airfield Pavement Deicing With Conductive Concrete Overlay, in: *Civ. Eng. Fac. Proc. Present.*, 2002: p. paper 2. <http://digitalcommons.unomaha.edu/civilengfacproc/2>.
- [62] C.Y. Tuan, Roca Spur Bridge: The Implementation of an Innovative Deicing Technology, *J. Cold Reg. Eng.* 22 (2008) 1–15. doi:10.1061/(ASCE)0887-381X(2008)22:1(1).
- [63] P. Xie, P. Gu, Y. Fu, J.J. Beaudoin, *Conductive cement-based compositions*, US005447564A, 1995.
- [64] D.D.L. Chung, Electrically conductive cement-based materials, *Adv. Cem. Res.* 4 (2004) 167–176.
- [65] S. Yehia, Conductive Concrete Overlay, *Concr. Int.* 24 (2008) 56–60.
- [66] J. Wu, J. Liu, F. Yang, Study on Three-phase Composite Conductive Concrete for Pavement Deicing, in: *Transp. Res. Board 93rd Annu. Meet.*, 2014: p. No. 14-2684.
- [67] J. Wu, J. Liu, F. Yang, Three-phase composite conductive concrete for pavement deicing, *Constr. Build. Mater.* 75 (2015) 129–135. doi:10.1016/j.conbuildmat.2014.11.004.
- [68] S. Wang, S. Wen, D.D.L. Chung, Resistance heating using electrically conductive cements, *Adv. Cem. Res.* 16 (2004) 161–166. doi:10.1680/adcr.16.4.161.46662.

- [69] C.Y. Tuan, *Implementation of Conductive Concrete For Deicing*, Omaha, NE, 2008.
- [70] Federal Aviation Administration (FAA), *Standards for Specifying Construction of Airports*, FAA Advisory circular No.150/5370-10G, (2014).
- [71] J. Cao, D.D.L. Chung, Carbon fiber reinforced cement mortar improved by using acrylic dispersion as an admixture, *Cem. Concr. Res.* 31 (2001) 1633–1637. doi:10.1016/S0008-8846(01)00599-3.
- [72] B. Chen, J. Liu, Effect of fibers on expansion of concrete with a large amount of high f-CaO fly ash, *Cem. Concr. Compos.* 33 (2003) 1549–1552. doi:10.1016/S0008-8846(03)00098-X.
- [73] A. Peyvandi, P. Soroushian, A.M. Balachandra, K. Sobolev, Enhancement of the durability characteristics of concrete nanocomposite pipes with modified graphite nanoplatelets, *Constr. Build. Mater.* 47 (2013) 111–117. doi:10.1016/j.conbuildmat.2013.05.002.
- [74] E. Heymsfield, A.B. Osweiler, R.P. Selvam, M. Kuss, *Feasibility of Anti-Icing Airfield Pavements Using Conductive Concrete and Renewable Solar Energy*, Fayetteville, Arkansas, 2013.
- [75] V. Piskunov, O. Volod'ko, A. Porhunov, Composite Materials for Building Heated coverings for Roads and Runways of Airdromes, *Mech. Compos. Mater.* 44 (2008) 215–220.
- [76] J. Cao, D.D.L. Chung, Improving the dispersion of steel fibers in cement mortar by the addition of silane, *Cem. Concr. Res.* 31 (2001) 309–311. doi:10.1016/S0008-8846(00)00470-1.
- [77] Z. Hou, Z. Li, J. Wang, Electrical conductivity of the carbon fiber conductive concrete, *J. Wuhan Univ. Technol. Sci. Ed.* 22 (2007) 346–349. doi:10.1007/s11595-005-2346-x.
- [78] D. Gao, M. Sturm, Y.L. Mo, Electrical resistance of carbon-nanofiber concrete, *Smart Mater. Struct.* 20 (2011) 049501. doi:10.1088/0964-1726/20/4/049501.
- [79] S. Wen, D.D.L. Chung, Cement as a Thermoelectric Material, *J. Mater. Res.* 15 (2000) 2844–2848.
- [80] S. Wen, D.D.L. Chung, Double percolation in the electrical conduction in carbon fiber reinforced cement-based materials, *Carbon N. Y.* 45 (2007) 263–267. doi:10.1016/j.carbon.2006.09.031.
- [81] A. Pérez, M.A. Climent, P. Garcés, Electrochemical extraction of chlorides from reinforced concrete using a conductive cement paste as the anode, *Corros. Sci.* 52 (2010) 1576–1581. doi:10.1016/j.corsci.2010.01.016.

- [82] R.N. Kraus, T.R. Naik, *Testing and Evaluation of Concrete Using High- Carbon Fly Ash and Carbon Fibers*, Milwaukee, Wisconsin, 2006.
- [83] J. Carmona, P. Garcés, M.A. Climent, Efficiency of a conductive cement-based anodic system for the application of cathodic protection , cathodic prevention and electrochemical chloride extraction to control corrosion in reinforced concrete structures, *Corros. Sci.* 96 (2015) 102–111. doi:10.1016/j.corsci.2015.04.012.
- [84] X. Fu, D.D.L. Chung, Submicron-diameter-carbon-filament cement-matrix composites, *Carbon N. Y.* 36 (1998) 459–462.
- [85] J.P. Won, C.K. Kim, S.J. Lee, J.H. Lee, R.W. Kim, Thermal characteristics of a conductive cement-based composite for a snow-melting heated pavement system, *Compos. Struct.* 118 (2014) 106–111. doi:10.1016/j.compstruct.2014.07.021.
- [86] F. Javier Baeza, D.D.L. Chung, E. Zornoza, L.G. Andi3n, P. Garc3s, Triple percolation in concrete reinforced with carbon fiber, *ACI Mater. J.* 107 (2010) 396–402.
- [87] O. Galao, L. Ba3n3n, F.J. Baeza, J. Carmona, P. Garc3s, Highly Conductive Carbon Fiber Reinforced Concrete for Icing Prevention and Curing, *Materials (Basel)*. 9 (2016) 281. doi:10.3390/ma9040281.
- [88] F. Vossoughi, *Electrical Resistivity of Carbon Fiber Reinforced Concrete*, Berkeley, CA, 2004.
- [89] P. Xie, G. Ping, J.J. Beaudoin, Electrical Percolation Phenomena in Cement Composites Containing Conductive Fibers, *J. Mater. Sci.* 31 (1996) 4093–4097.
- [90] S.C. van der Marck, Calculation of percolation thresholds in high dimensions for fcc, bcc, and diamond lattices, *Int. J. Mod. Phys.* 9 (1998) 529–540. doi:10.1142/S0129183198000431.
- [91] K. Gopalakrishnan, H. Ceylan, S. Kim, S. Yang, H. Abdulla, Self-Heating Electrically Conductive Concrete for Pavement Deicing: A Revisit, in: *Transp. Res. Board 94th Annu. Meet.*, 2015: p. No. 15-4764.
- [92] O. Arioz, Effects of elevated temperatures on properties of concrete, *Fire Saf. J.* 42 (2007) 516–522. doi:10.1016/j.firesaf.2007.01.003.
- [93] C.Y. Tuan, S. Yehia, B. Chen, L. Nguyen, Heated Bridge Deck system and Materials and Method for Constructing the Same, US 6825444 B1, 2004. doi:10.1016/j.(73).
- [94] P. Keikhaei Dehdezi, *Enhancing pavements for thermal applications*, (2012). <http://theses.nottingham.ac.uk/2607/>.

- [95] J. Gao, Z. Wang, T. Zhang, L. Zhou, Dispersion of carbon fibers in cement-based composites with different mixing methods, *Constr. Build. Mater.* (2017). doi:10.1016/j.conbuildmat.2016.12.047.
- [96] D.D. Chung, Dispersion of Short Fibers in Cement, *J. Mater. Civ. Eng.* 17 (2005) 379–383. doi:10.1061/(ASCE)0899-1561(2005)17:4(379).
- [97] X. Fu, D.D.L. Chung, Effect of methylcellulose admixture on the mechanical properties of cement, *Cem. Concr. Res.* 26 (1996) 535–538. doi:10.1016/0008-8846(96)00028-2.
- [98] W.J. McCarter, S. Garvin, Dependence of electrical impedance of cement-based materials on their moisture condition, *J. Phys. D. Appl. Phys.* 22 (2000) 1773–1776. doi:10.1088/0022-3727/22/11/033.
- [99] B.J. Christensen, T. Coverdale, R.A. Olson, S.J. Ford, E.J. Garboczi, H.M. Jennings, T.O. Mason, Impedance Spectroscopy of Hydrating Cement-Based Materials: Measurement, Interpretation, and Application, *J. Am. Ceram. Soc.* 77 (1994) 2789–2804. doi:10.1111/j.1151-2916.1994.tb04507.x.
- [100] R. Polder, C. Andrade, B. Elsener, Test methods for on site measurement of resistivity of concrete, *Mater. Struct.* 33 (2000) 603–611. <http://www.springerlink.com/index/Q04244102R156584.pdf>.
- [101] F. Rajabipour, Insitu electrical sensing and material health monitoring in concrete structures, (2006).
- [102] H. Souri, I.W. Nam, H.K. Lee, Electrical properties and piezoresistive evaluation of polyurethane-based composites with carbon nano-materials, *Compos. Sci. Technol.* 121 (2015) 41–48. doi:10.1016/j.compscitech.2015.11.003.
- [103] Cao, Jingyao, D.D.L. Chung, Electric polarization and depolarization in cement-based materials, studied by apparent electrical resistance measurement, *Cem. Concr. Res.* 34 (2004) 481–485. doi:10.1016/j.cemconres.2003.09.003.
- [104] H. Li, H.G. Xiao, J. Yuan, J. Ou, Microstructure of cement mortar with nanoparticles, *Compos. Part B Eng.* 35 (2004) 185–189. doi:10.1016/S1359-8368(03)00052-0.
- [105] S. Wen, D.D.. Chung, Electric polarization in carbon fiber-reinforced cement, *Cem. Concr. Res.* 31 (2001) 141–147. doi:10.1016/S0008-8846(00)00382-3.
- [106] ASTM C 1202-12, Standard Method of Test for Surface Resistivity Indication of Concrete ' s Ability to Resist Chloride Ion Penetration, West Conshohocken, PA., 2013. doi:10.1520/C1202-12.2.

- [107] R.P. Spragg, J. Castro, T. Nantung, M. Paredes, J. Weiss, Variability Analysis of the Bulk Resistivity Measured Using Concrete Cylinders, *Adv. Civ. Eng. Mater.* 1 (2012) 104596. doi:10.1520/ACEM104596.
- [108] ASTM, C1760-12-Standard Test Method for Bulk Electrical Conductivity of Hardened Concrete, n.d.
- [109] J. Castro, R. Spragg, P. Compare, W.J. Weiss, Portland cement concrete pavement permeability performance, Purdue University, 2010.
- [110] A. Arabzadeh, H. Ceylan, S. Kim, K. Gopalakrishnan, A. Sassani, S. Sundararajan, P.C. Taylor, Influence of Deicing Salts on the Water-Repellency of Portland Cement Concrete Coated with Polytetrafluoroethylene and Polyetheretherketone, in: *ASCE Int. Conf. Highw. Pavements Airf. Technol.*, Philadelphia, Pennsylvania, 2017.
- [111] A. Arabzadeh, H. Ceylan, S. Kim, K. Gopalakrishnan, A. Sassani, Fabrication of Polytetrafluoroethylene-Coated Asphalt Concrete Biomimetic Surfaces: A Nanomaterials-Based Pavement Winter Maintenance Approach, in: *Int. Conf. Transp. Dev. 2016 Proj. Pract. Prosper. - Proc. 2016 Int. Conf. Transp. Dev.*, 2016. doi:10.1061/9780784479926.006.
- [112] A. Arabzadeh, H. Ceylan, S. Kim, K. Gopalakrishnan, A. Sassani, S. Sundararajan, P.C. Taylor, Superhydrophobic coatings on Portland cement concrete surfaces, *Constr. Build. Mater.* 141 (2017). doi:10.1016/j.conbuildmat.2017.03.012.
- [113] A. Arabzadeh, H. Ceylan, S. Kim, K. Gopalakrishnan, A. Sassani, Superhydrophobic coatings on asphalt concrete surfaces: Toward smart solutions for winter pavement maintenance, 2016. doi:10.3141/2551-02.
- [114] H. Ceylan, A. Arabzadeh, A. Sassani, S. Kim, K. Gopalakrishnan, Innovative nano-engineered asphalt concrete for ice and snow controls in pavement systems, in: *6th Eurasphalt & Eurobitume Congr.*, Prague, Czech Republic, 2016.
- [115] V. Hejazi, K. Sobolev, M. Nosonovsky, From superhydrophobicity to icephobicity: forces and interaction analysis, *Sci. Rep.* 3 (2013) 2194. doi:10.1038/srep02194.
- [116] I. Flores-vivian, V. Hejazi, M.I. Kozhukhova, M. Nosonovsky, K. Sobolev, Self-Assembling Particle-Siloxane Coatings for Superhydrophobic Concrete, *ACS Appl. Mater. Interfaces.* 5 (2013) 13284–13294.
- [117] M. Nosonovsky, K. Sobolev, Superhydrophobic and icephobic concrete and construction materials, Milwaukee, WI: University of Wisconsin–Milwaukee, 2013, 85–92.
- [118] M. Horgnies, J.J. Chen, Superhydrophobic concrete surfaces with integrated microtexture, *Cem. Concr. Compos.* 52 (2014) 81–90. doi:10.1016/j.cemconcomp.2014.05.010.

- [119] J. Orlikowski, S. Cebulski, K. Darowicki, Electrochemical investigations of conductive coatings applied as anodes in cathodic protection of reinforced concrete, *Cem. Concr. Compos.* 26 (2004) 721–728. doi:10.1016/S0958-9465(03)00105-7.
- [120] J. Xu, W. Yao, Electrochemical studies on the performance of conductive overlay material in cathodic protection of reinforced concrete, *Constr. Build. Mater.* 25 (2011) 2655–2662. doi:10.1016/j.conbuildmat.2010.12.015.
- [121] A. Cañón, P. Garcés, M.A. Climent, J. Carmona, E. Zornoza, Feasibility of electrochemical chloride extraction from structural reinforced concrete using a sprayed conductive graphite powder-cement paste as anode, *Corros. Sci.* 77 (2013) 128–134. doi:10.1016/j.corsci.2013.07.035.
- [122] M. Elsharkawy, D. Tortorella, S. Kapatral, C.M. Megaridis, Combating Frosting with Joule-Heated Liquid-Infused Superhydrophobic Coatings, *Langmuir.* 32 (2016) 4278–4288. doi:10.1021/acs.langmuir.6b00064.
- [123] P.C. Ma, N.A. Siddiqui, G. Marom, J.K. Kim, Dispersion and functionalization of carbon nanotubes for polymer-based nanocomposites: A review, *Compos. Part A Appl. Sci. Manuf.* 41 (2010) 1345–1367. doi:10.1016/j.compositesa.2010.07.003.
- [124] J.E. Mates, I.S. Bayer, J.M. Palumbo, P.J. Carroll, C.M. Megaridis, Extremely stretchable and conductive water-repellent coatings for low-cost ultra-flexible electronics, *Nat. Commun.* 6 (2015) 1–8. doi:10.1038/ncomms9874.
- [125] J.E. Mates, I.S. Bayer, M. Salerno, P.J. Carroll, Z. Jiang, L. Liu, C.M. Megaridis, Durable and flexible graphene composites based on artists' paint for conductive paper applications, *Carbon N. Y.* 87 (2015) 163–174. doi:10.1016/j.carbon.2015.01.056.
- [126] H. Chu, Z. Zhang, Y. Liu, J. Leng, Silver particles modified carbon nanotube paper/glassfiber reinforced polymer composite material for high temperature infrared stealth camouflage, *Carbon N. Y.* 98 (2016) 557–566. doi:10.1016/j.carbon.2015.11.036.
- [127] B.O. Lee, W.J. Woo, H.S. Park, H.S. Hahm, J.P. Wu, M.S. Kim, Influence of aspect ratio and skin effect on EMI shielding of coating materials fabricated with carbon nano ber/PVDF, *Carbon N. Y.* 7 (2008) 1839–1843.
- [128] L. Liu, A. Das, C.M. Megaridis, Terahertz shielding of carbon nanomaterials and their composites - A review and applications, *Carbon N. Y.* 69 (2014) 1–16. doi:10.1016/j.carbon.2013.12.021.
- [129] A. Das, H.T. Hayvaci, M.K. Tiwari, I.S. Bayer, D. Erricolo, C.M. Megaridis, Superhydrophobic and conductive carbon nanofiber/PTFE composite coatings for EMI shielding, *J. Colloid Interface Sci.* 353 (2011) 311–315. doi:10.1016/j.jcis.2010.09.017.

- [130] P. Slobodian, P. Riha, P. Saha, A highly-deformable composite composed of an entangled network of electrically-conductive carbon-nanotubes embedded in elastic polyurethane, *Carbon N. Y.* 50 (2012) 3446–3453. doi:10.1016/j.carbon.2012.03.008.
- [131] J.M. Engel, J. Chen, D. Bullen, C. Liu, Polyurethane rubber as a MEMS material: characterization and demonstration of an all-polymer two-axis artificial hair cell flow sensor, in: *18th IEEE Int. Conf. Micro Electro Mech. Syst. 2005.*, 2005: pp. 279–282. doi:10.1109/MEMSYS.2005.1453921.
- [132] S. Laflamme, I. Pinto, H. Saleem, M. Elkashef, K. Wang, Conductive Paint-Filled Cement Paste Sensor for Accelerated Percolation, in: *Struct. Heal. Monit. Insp. Adv. Mater. Aerospace, Civ. Infrastruct.*, 2015: pp. 1–8. doi:10.1117/12.2084408.
- [133] E. Andreoli, K.S. Liao, A. Cricini, X. Zhang, R. Soffiatti, H.J. Byrne, S.A. Curran, Carbon black instead of multiwall carbon nanotubes for achieving comparable high electrical conductivities in polyurethane-based coatings, *Thin Solid Films.* 550 (2014) 558–563. doi:10.1016/j.tsf.2013.11.047.
- [134] J. Engel, J. Chen, N. Chen, S. Pandya, C. Liu, Multi-Walled Carbon Nanotube Filled Conductive Elastomers: Materials And Application to Micro Transducersa, in: *IEEE MEMS*, 2006: pp. 246–249.
- [135] C.Y. Lee, J.H. Bae, T.Y. Kim, S.H. Chang, S.Y. Kim, Using silane-functionalized graphene oxides for enhancing the interfacial bonding strength of carbon/epoxy composites, *Compos. Part A Appl. Sci. Manuf.* 75 (2015) 11–17. doi:10.1016/j.compositesa.2015.04.013.
- [136] P. Duarte, J.R. Correia, J.G. Ferreira, F. Nunes, M.R.T. Arruda, Experimental and numerical study on the effect of repairing reinforced concrete cracked beams strengthened with carbon fibre reinforced polymer laminates, *Can. J. Civ. Eng.* 41 (2014) 222–231. doi:10.1139/cjce-2013-0124.
- [137] A. Sassani, H. Ceylan, S. Kim, A. Arabzadeh, P.C. Taylor, K. Gopalakrishnan, Development of Carbon Fiber-modified Electrically Conductive Concrete for Implementation in Des Moines International Airport, *Case Stud. Constr. Mater.* 8 (2018) 277–291. doi:10.1016/j.cscm.2018.02.003.
- [138] J.M.L. Reis, R.P. Lima, S.D. Vidal, Effect of rate and temperature on the mechanical properties of epoxy BADGE reinforced with carbon nanotubes, *Compos. Struct.* (2018) 0–1. doi:10.1016/j.compstruct.2017.11.081.
- [139] G.M. Kim, B.J. Yang, K.J. Cho, E.M. Kim, H.K. Lee, Influences of CNT dispersion and pore characteristics on the electrical performance of cementitious composites, *Compos. Struct.* 164 (2017) 32–42. doi:10.1016/j.compstruct.2016.12.049.
- [140] G.M. Kim, F. Naeem, H.K. Kim, H.K. Lee, Heating and heat-dependent mechanical characteristics of CNT-embedded cementitious composites, *Compos. Struct.* 136 (2016) 162–170. doi:10.1016/j.compstruct.2015.10.010.

- [141] Y. He, L. Lu, S. Jin, S. Hu, Conductive aggregate prepared using graphite and clay and its use in conductive mortar, *Constr. Build. Mater.* 53 (2014) 131–137. doi:10.1016/j.conbuildmat.2013.11.085.
- [142] J.M. Balbus, A.D. Maynard, V.L. Colvin, V. Castranova, G.P. Daston, R.A. Denison, K.L. Dreher, P.L. Goering, A.M. Goldberg, K.M. Kulinowski, N.A. Monteiro-Riviere, G. Oberdörster, G.S. Omenn, K.E. Pinkerton, K.S. Ramos, K.M. Rest, J.B. Sass, E.K. Silbergeld, B.A. Wong, Meeting report: Hazard assessment for nanoparticles-report from an interdisciplinary workshop, *Environ. Health Perspect.* 115 (2007) 1654–1659. doi:10.1289/ehp.10327.
- [143] L. Xu, R.G. Karunakaran, J. Guo, S. Yang, Transparent, superhydrophobic surfaces from one-step spin coating of hydrophobic nanoparticles, *ACS Appl. Mater. Interfaces.* 4 (2012) 1118–1125. doi:10.1021/am201750h.
- [144] R.G. Karunakaran, C.H. Lu, Z. Zhang, S. Yang, Highly transparent superhydrophobic surfaces from the coassembly of nanoparticles (??? 100 nm), *Langmuir.* 27 (2011) 4594–4602. doi:10.1021/la104067c.
- [145] A. Arabzadeh, H. Ceylan, S. Kim, K. Gopalakrishnan, A. Sassani, S. Sundararajan, P.C. Taylor, Superhydrophobic coatings on Portland cement concrete surfaces, *Constr. Build. Mater.* 141 (2017) 393–401.
- [146] M. Hikita, K. Tanaka, T. Nakamura, T. Kajiyama, A. Takahara, Super-liquid-repellent surfaces prepared by colloidal silica nanoparticles covered with fluoroalkyl groups, *Langmuir.* 21 (2005) 7299–7302. doi:10.1021/la050901r.
- [147] M. Sabzi, S.M. Mirabedini, J. Zohuriaan-Mehr, M. Atai, Surface modification of TiO<sub>2</sub> nano-particles with silane coupling agent and investigation of its effect on the properties of polyurethane composite coating, *Prog. Org. Coatings.* 65 (2009) 222–228. doi:10.1016/j.porgcoat.2008.11.006.
- [148] J. Zhang, J. Li, Y. Han, Superhydrophobic PTFE surfaces by extension, *Macromol. Rapid Commun.* 25 (2004) 1105–1108. doi:10.1002/marc.200400065.
- [149] H.J. Song, Z.Z. Zhang, X.H. Men, Superhydrophobic PEEK/PTFE composite coating, *Appl. Phys. A Mater. Sci. Process.* 91 (2008) 73–76. doi:10.1007/s00339-007-4360-7.
- [150] R. Menini, M. Farzaneh, Elaboration of Al<sub>2</sub>O<sub>3</sub>/PTFE icephobic coatings for protecting aluminum surfaces, *Surf. Coatings Technol.* 203 (2009) 1941–1946. doi:10.1016/j.surfcoat.2009.01.030.
- [151] D. Ebert, B. Bhushan, Transparent, superhydrophobic, and wear-resistant coatings on glass and polymer substrates using SiO<sub>2</sub>, ZnO, and ITO nanoparticles, *Langmuir.* 28 (2012) 11391–11399. doi:10.1021/la301479c.



- [152] C. Su, J. Li, H. Geng, Q. Wang, Q. Chen, Fabrication of an optically transparent super-hydrophobic surface via embedding nano-silica, *Appl. Surf. Sci.* 253 (2006) 2633–2636. doi:10.1016/j.apsusc.2006.05.038.
- [153] J. Bravo, L. Zhai, Z. Wu, R.E. Cohen, M.F. Rubner, Transparent superhydrophobic films based on silica nanoparticles, *Langmuir*. 23 (2007) 7293–7298. doi:10.1021/la070159q.
- [154] Z. He, M. Ma, X. Lan, F. Chen, K. Wang, H. Deng, Q. Zhang, Q. Fu, Fabrication of a transparent superamphiphobic coating with improved stability, *Soft Matter*. 7 (2011) 6435. doi:10.1039/c1sm05574g.
- [155] J.T. Han, S.Y. Kim, J.S. Woo, G.W. Lee, Transparent, conductive, and superhydrophobic films from stabilized carbon nanotube/silane sol mixture solution, *Adv. Mater.* 20 (2008) 3724–3727. doi:10.1002/adma.200800239.
- [156] S. Liu, S.S. Latthe, H. Yang, B. Liu, R. Xing, Raspberry-like superhydrophobic silica coatings with self-cleaning properties, *Ceram. Int.* 41 (2015) 11719–11725. doi:10.1016/j.ceramint.2015.05.137.
- [157] X. Deng, L. Mammen, Y. Zhao, P. Lellig, K. Mullen, C. Li, H.J. Butt, D. Vollmer, Transparent, thermally stable and mechanically robust superhydrophobic surfaces made from porous silica capsules, *Adv. Mater.* 23 (2011) 2962–2965. doi:10.1002/adma.201100410.
- [158] L. Huang, S.P. Lau, H.Y. Yang, E.S.P. Leong, S.F. Yu, S. Praver, Stable superhydrophobic surface via carbon nanotubes coated with a ZnO thin film., *J. Phys. Chem. B.* 109 (2005) 7746–7748. doi:10.1021/jp046549s.
- [159] N.L. Tarwal, P.S. Patil, Superhydrophobic and transparent ZnO thin films synthesized by spray pyrolysis technique, *Appl. Surf. Sci.* 256 (2010) 7451–7456. doi:10.1016/j.apsusc.2010.05.089.
- [160] M.K. Tiwari, I.S. Bayer, G.M. Jursich, T.M. Schutzius, C.M. Megaridis, Highly liquid-repellent, large-area, nanostructured poly(vinylidene fluoride)/poly(ethyl 2-cyanoacrylate) composite coatings: Particle filler effects, *ACS Appl. Mater. Interfaces*. 2 (2010) 1114–1119. doi:10.1021/am900894n.
- [161] I.S. Bayer, M.K. Tiwari, C.M. Megaridis, Biocompatible poly(vinylidene fluoride)/cyanoacrylate composite coatings with tunable hydrophobicity and bonding strength, *Appl. Phys. Lett.* 93 (2008) 1–4. doi:10.1063/1.3009292.
- [162] S.S. Latthe, P. Sudhagar, C. Ravidhas, A. Jennifer Christy, D. David Kirubakaran, R. Venkatesh, A. Devadoss, C. Terashima, K. Nakata, A. Fujishima, Self-cleaning and superhydrophobic CuO coating by jet-nebulizer spray pyrolysis technique, *CrystEngComm*. 17 (2015) 2624–2628. doi:10.1039/C5CE00177C.

- [163] X. Cao, A. Gao, N. Zhao, F. Yuan, C. Liu, R. Li, Surfaces wettability and morphology modulation in a fluorene derivative self-assembly system, *Appl. Surf. Sci.* 368 (2016) 97–103. doi:10.1016/j.apsusc.2016.01.248.
- [164] S. Manakasettharn, T.-H. Hsu, G. Myhre, S. Pau, J.A. Taylor, T. Krupenkin, Transparent and superhydrophobic Ta<sub>2</sub>O<sub>5</sub> nanostructured thin films, *Opt. Mater. Express.* 2 (2012) 214–221. doi:10.1364/OME.2.000214.
- [165] J.C. Zhao, F.P. Du, X.P. Zhou, W. Cui, X.M. Wang, H. Zhu, X.L. Xie, Y.W. Mai, Thermal conductive and electrical properties of polyurethane/hyperbranched poly(urea-urethane)-grafted multi-walled carbon nanotube composites, *Compos. Part B Eng.* 42 (2011) 2111–2116. doi:10.1016/j.compositesb.2011.05.005.
- [166] I.S. Gunes, G.A. Jimenez, S.C. Jana, Carbonaceous fillers for shape memory actuation of polyurethane composites by resistive heating, *Carbon*, 47 (2009) 981–997. doi:10.1016/j.carbon.2008.11.053.
- [167] S.M. Rao, *The Effectiveness of Silane and Siloxane Treatments on the Superhydrophobicity and Icephobicity of Concrete Surfaces*, University of Wisconsin Milwaukee, 2013.
- [168] X.J. Gao, H.W. Deng, Y.Z. Yang, Influence of Silane Treatment on the Freeze-Thaw Resistance of Concrete, *Adv. Mater. Res.* 250–253 (2011) 565–568. doi:10.4028/www.scientific.net/AMR.250-253.565.
- [169] K. Lin, D. Zang, X. Li, X. Geng, Superhydrophobic polytetrafluoroethylene surfaces by spray coating on porous and continuous substrates, *RSC Adv.* 6 (2016) 47096–47100. doi:10.1039/C6RA06623B.
- [170] L. Cao, D. Gao, Transparent superhydrophobic and highly oleophobic coatings, *Faraday Discuss.* 146 (2010) 13. doi:10.1039/c005270c.
- [171] O.T. de Rincon, V. Millano, M. Aboulhasan, C. Morales, J. Bravo, M. Sanchez, D. Conteras, Y. Hernandez, Evaluation of Hydrophobic Concrete Coatings in Tropical Marine Environments, *Corros. J. Sci. Eng.* 67 (2011) 115001–115001.
- [172] D. Bernat-Hunek, P. Smarzewski, Surface free energy of hydrophobic coatings of hybrid-fiber-reinforced high-performance concrete, *Mater. Technol.* 49 (2015) 895–902.
- [173] L. Calabrese, L. Bonaccorsi, A. Capri, E. Proverbio, Adhesion aspects of hydrophobic silane zeolite coatings for corrosion protection of aluminum substrate, *Prog. Org. Coatings.* 77 (2014) 1341–1350. doi:10.1016/j.porgcoat.2014.04.025.
- [174] A. Das, C.M. Megaridis, L. Liu, T. Wang, A. Biswas, Design and synthesis of superhydrophobic carbon nanofiber composite coatings for terahertz frequency shielding and attenuation, *Appl. Phys. Lett.* 98 (2011) 1–4. doi:10.1063/1.3583523.

- [175] J. Lin, J. Zhu, D.R. Swanson, L. Milco, Cross-Linking and Physical Characteristics of a Water-Based Nonstick Hydrophobic Coating, *Langmuir*. 7463 (1996) 6676–6680.
- [176] C. Prisacariu, *Polyurethane Elastomers : From Morphology to Mechanical Aspects*, Springer, Verlag/Wien, 2011. doi:10.1007/978-3-7091-0514-6.
- [177] A. Samimi, S. Zarinabadi, Application Polyurethane as Coating in Oil and Gas Pipelines, *Int. J. Sci. Eng. Investig.* 1 (2012) 43–45.
- [178] C. Gao, Y.Z. Jin, H. Kong, R.L.D. Whitby, S.F. Acquah, G.Y. Chen, H. Qian, A. Hartschuh, S.R.P. Silva, S. Henley, P. Fearon, H.W. Kroto, D.R.M. Walton, Polyurea-functionalized multiwalled carbon nanotubes: synthesis, morphology, and Raman spectroscopy., *J. Phys. Chem. B.* 109 (2005) 11925–32. doi:10.1021/jp051642h.
- [179] H. Sardon, L. Irusta, M.J. Fernández-Berridi, M. Lansalot, E. Bourgeat-Lami, Synthesis of room temperature self-curable waterborne hybrid polyurethanes functionalized with (3-aminopropyl)triethoxysilane (APTES), *Polymer (Guildf)*. 51 (2010) 5051–5057. doi:10.1016/j.polymer.2010.08.035.
- [180] M. Fir, B. Orel, A.S. Vuk, A. Vilcnik, R. Jese, V. Francetic, Corrosion studies and interfacial bonding of urea/poly(dimethylsiloxane) sol/gel hydrophobic coatings on AA 2024 aluminum alloy., *Langmuir*. 23 (2007) 5505–5514. doi:10.1021/la062976g.
- [181] K. Golovin, M. Boban, J.M. Mabry, A. Tuteja, Designing Self-Healing Superhydrophobic Surfaces with Exceptional Mechanical Durability, *ACS Appl. Mater. Interfaces*. 9 (2017) 11212–11223. doi:10.1021/acsami.6b15491.